

**Identification of novel parasitophorous  
vacuole proteins in *P. falciparum* parasites  
using BiOLD**

Identifikation neuer Proteine der parasitophoren Vakuole des  
Malaria Parasiten *P. falciparum* mittels BiOLD

Dissertation

with the aim of achieving a doctoral degree at the Faculty of Mathematics, Informatics and  
Natural Science

Department of Biology

University of Hamburg

Submitted by

**Melissa Khosh-Naucke**

Hamburg, July 2018

**1. Gutachter:** Dr. Tobias Spielmann

**2. Gutachter:** Prof. Dr. Tim-Wolf Gilberger

**Vorsitzender der Prüfungskommission:** Prof. Dr. Jörg Ganzhorn

**Datum der Disputation:** 28. September 2018

**Declaration of academic honesty**

I confirm that I composed this thesis on my own and that I did not use any other sources, means or devices than the ones listed. I did not submit this thesis for any previous examination. The written work is equivalent to the one on the electronic storage device. I agree to the publication of this thesis.

**Eidesstattliche Versicherung**

Hiermit erkläre ich an Eides statt, dass ich die vorliegende Dissertationsschrift selbst verfasst und keine anderen als die angegebenen Quellen und Hilfsmittel benutzt habe und die Arbeit von mir vorher nicht in einem anderen Prüfungsverfahren eingereicht wurde. Die eingereichte schriftliche Fassung entspricht der auf dem elektronischen Speichermedium. Ich bin damit einverstanden, dass die Doktorarbeit veröffentlicht wird.

Hamburg, the 30<sup>th</sup> of July

---

Melissa Khosh-Naucke

## **Language certificate**

I am a native speaker, have read the present PhD thesis and hereby confirm that it complies with the rules of the English language.

Hamburg, the 30<sup>th</sup> of July

---

Mateo Naucke

## Summary

Malaria pathology is caused by the asexual replication of *Plasmodium spp.* within red blood cells. Among the five *Plasmodium* species that infect humans *P. falciparum* is responsible for the severest form of malaria, still causing around 450'000 deaths annually. During their asexual development within red blood cells *P. falciparum* parasites reside within a newly created compartment – the parasitophorous vacuole (PV), which is formed through an invagination of the red blood cell membrane during the invasion process. The PV is equipped with a number of parasite proteins to serve key functions in the interaction of the parasite with its host cell. However, only a limited number of the proteins of this compartment are known to date.

In this work the BioID technique was used to systematically identify proteins of the PV compartment. BioID enables proximity-dependent biotinylation of compartment-specific proteins in living parasites based on the promiscuous biotin ligase BirA\*. Affinity purification of the biotin-tagged proteins followed by mass spectrometry can then be used to identify the proteins tagged by BirA\*.

This approach resulted in the identification of 14 putative PV proteins of which 13 were further analysed using a GFP knock in strategy. This analysis revealed 7 novel PV proteins and 3 novel proteins with a partial PV localization. For 7 of the 10 newly identified PV proteins the exact location was determined: 3 were located at the outer face of the parasite plasma membrane and 4 at the inner face of the PV membrane. Surprisingly, no new proteins soluble in the PV space were identified. In order to screen the proteins for their essentiality regarding parasite survival, it was attempted to disrupt the corresponding genes using a strategy that permits the selection of such parasites. This approach was unsuccessful for 6 of the 10 identified PV proteins, indicating that they are likely essential for parasite growth.

The identification of the novel PV proteins – especially the identification of likely essential ones – is an important step to further unravel the function of this parasite compartment. The attempt to further characterize protein function with a here generated knock side way system for the conditional inactivation of secretory proteins showed only limited success, precluding a systematic functional analysis of the candidates identified in this work using this technology. Therefore, the most promising candidate, PF3D7\_1464600 (UIS2), was further analysed using the more time intensive diCre based conditional gene knock out system. UIS2 had previously been implicated in the regulation of translation through dephosphorylation of eIF2 $\alpha$ -P in *P. berghei* liver stages. However, the here determined location of UIS2 in the PV renders such a function rather unlikely. DiCre based conditional gene knockout confirmed the essentiality of UIS2 for parasite growth. Parasites lacking UIS2 showed an arrest in ring stages. In addition, the lack of UIS2 caused an

accumulation of the PVM resident protein ETRAMP2 and the Maurer's cleft protein SBP1 within the parasite, indicating a defect in protein secretion or a general arrest of parasite functions immediately after invasion. Complementation of the UIS2 knockout cell line rescued the phenotype, while complementation with a catalytically dead mutant of the putative phosphatase domain did not. These results show that the phosphatase activity of UIS2 within the PV compartment is required for parasite survival and suggests a critical regulatory function of the dephosphorylation of proteins in this compartment for early parasite development.

This work identified a series of new PV proteins of which one, a phosphatase previously identified as UIS2, was shown to hold a critical role for parasite development very early after invasion. Characterisation of the proteins of the PV will help to understand how the malaria parasite interacts with its host cell to exploit this unique niche to foster its own development.

## Zusammenfassung

Das Krankheitsbild der Malaria wird durch die asexuelle Replikation von *Plasmodium spp.* in den Erythrozyten verursacht. Unter den fünf human pathogenen *Plasmodium* Spezies ist *P. falciparum* für die schwerste Form der Malaria verantwortlich, welche jährlich rund 450'000 Todesopfer fordert. Die intraerythrozytäre Entwicklung des Parasiten findet in der parasitophoren Vakuole (PV) statt. Die PV wird während des Invasionsprozesses des Parasiten durch Invagination der Erythrozyten Membran neu gebildet und ist mit einer Vielzahl von Parasitenproteinen ausgestattet. Diese Proteine übernehmen Schlüsselfunktionen bei der Parasiten-Wirtszell-Interaktion, sind jedoch bisher zum größten Teil unbekannt.

In dieser Arbeit wurde die BioID-Technik verwendet, um Proteine des PV-Kompartiments systematisch zu identifizieren. Durch die mutierte Biotin Ligase BirA\* ermöglicht BioID die Biotinylierung nahegelegener, Kompartiment-spezifischer Proteine in lebenden Parasiten. Zur Identifizierung dieser biotinylierten Proteine wurden die Biotin-markierten Proteine zunächst aufgereinigt und anschließend mittels Massenspektrometrie untersucht.

Dieser Ansatz führte zur Identifizierung von 14 putativen PV-Proteinen. 13 dieser Proteine wurden endogen mit GFP fusioniert und näher untersucht. Mittels Fluoreszenzmikroskopie konnte die PV-Lokalisation für 10 Proteine bestätigt werden. Hiervon zeigten 3 Kandidaten nur eine partielle PV-Lokalisation. Für 7 der 10 neu identifizierten PV-Proteine konnte die exakte Position bestimmt werden: 3 Proteine befanden sich an der äußeren Seite der parasitären Plasmamembran und 4 Proteine an der Innenseite der PV-Membran. Widererwartend wurden keine neuen löslichen PV-Proteine identifiziert. Um die Proteine zusätzlich auf ihre Bedeutung für das Überleben des Parasiten zu untersuchen, wurden die entsprechenden Gene gezielt zerstört und jene Parasiten selektioniert, welche das zerstörte Gen beinhalten. Dieser Ansatz war für 6 der 10 identifizierten PV-Proteine nicht erfolgreich. Dies lässt vermuten, dass die Proteine mit hoher Wahrscheinlichkeit essentiell für das Wachstum des Parasiten sind.

Die Identifizierung der neuartigen PV-Proteine – insbesondere die Identifizierung von wahrscheinlich essentiellen Proteinen – ist ein wichtiger Schritt, um die Funktionen dieses Parasitenkompartiments weiter zu entschlüsseln. Der Versuch, die Proteinfunktion mit einem hier generierten System für die konditionelle Inaktivierung sekretorischer Proteine weiter zu charakterisieren, zeigte nur begrenzt Erfolg und schloss eine systematische funktionelle Analyse der in dieser Arbeit identifizierten Kandidaten mit dieser Methode aus. Daher wurde der vielversprechendste Kandidat, PF3D7\_1464600 (UIS2), mit dem zeitintensiveren diCre-basierten konditionalen Gen-Knockout-System weiter analysiert. Zuvor wurde UIS2 mit der essentiellen Regulation der Translation durch Dephosphorylierung von eIF2 $\alpha$ -P in *P. berghei*-Leberstadien in Zusammenhang gebracht.

Die hier ermittelte Position von UIS2 in der PV stellt eine solche Funktion jedoch in Frage. Der diCre basierte konditionale Gen-Knockout bestätigte die essenzielle Eigenschaft von UIS2 für das Wachstum der Parasiten. Parasiten, denen UIS2 fehlte, zeigten einen Arrest in Ringstadien. Darüber hinaus führte der Verlust von UIS2 zu einer Akkumulation des PVM-Proteins ETRAMP2 sowie des Maurer's Cleft-Proteins SBP1 innerhalb des Parasiten, was einen Defekt im Proteintransport oder einen allgemeinen Stillstand der Parasitenfunktionen unmittelbar nach der Invasion vermuten lässt. Die Komplementierung der UIS2-Knockout-Zelllinie konnte das Wachstum der Parasiten wiederherstellen. Im Gegensatz dazu war die Komplementierung mit einer katalytisch inaktivierten Mutante der putativen Phosphatasedomäne dazu nicht fähig. Diese Ergebnisse zeigen, dass die Phosphataseaktivität von UIS2 innerhalb des PV-Kompartiments für das Überleben der Parasiten erforderlich ist. Dies legt eine kritische regulatorische Funktion der Dephosphorylierung von Proteinen in diesem Kompartiment für die beginnende Parasitenentwicklung nahe.

In dieser Arbeit wurden eine Reihe neuer PV-Proteine identifiziert. Darunter eine Phosphatase, die zuvor als UIS2 beschrieben wurde. UIS2 zeigte eine wichtige Rolle in der frühen Parasitenentwicklung. Die weitere Charakterisierung der PV-Proteine wird das Verständnis erweitern, wie der Malariaparasit mit seiner Wirtszelle interagiert, um diese einzigartige Nische in der PV zu nutzen und somit seine eigene Entwicklung zu fördern.

## Table of contents

<b>Summary .....</b>	<b>IV</b>
<b>Zusammenfassung .....</b>	<b>VI</b>
<b>List of abbreviations.....</b>	<b>XII</b>
<b>List of figures .....</b>	<b>XVI</b>
<b>List of tables.....</b>	<b>XVII</b>
<b>1 Introduction .....</b>	<b>1</b>
<b>1.1 Malaria – Past, Present and Future .....</b>	<b>1</b>
1.1.1 Malaria - Intervention and Control .....	2
1.1.2 Treatment and Drug Resistance.....	2
1.1.3 Vaccine Development.....	2
<b>1.2 <i>Plasmodium</i> – the Malaria causing Parasite .....</b>	<b>3</b>
1.2.1 Pathophysiology and Immunology.....	3
1.2.2 Plasmodium Life Cycle – Replication in different Hosts .....	4
1.2.2.1 Mosquito stage.....	4
1.2.2.2 Liver stage .....	5
1.2.2.3 Blood stage .....	5
1.2.3 The asexual Blood Cycle.....	6
1.2.3.1 The Host – Red Blood Cell .....	7
1.2.3.2 Invasion and Parasitophorous vacuole formation.....	7
1.2.3.3 Apical Organelles .....	9
1.2.3.4 Parasitophorous Vacuole – Interface between Parasite and Host Cell .....	9
1.2.3.4.1 Protein Composition of the PV Compartment .....	11
1.2.3.4.1.1 Early-transcribed membrane proteins (ETRAMPs).....	12
1.2.3.4.1.2 Exported protein 1 (EXP1) .....	12
1.2.3.4.1.3 Parasitophorous vacuolar protein 1 (PV1) .....	13
1.2.3.4.1.4 Plasmodium translocon of exported proteins (PTEX) .....	13
1.2.3.4.1.5 S antigen .....	14
1.2.3.4.1.6 Serine repeat antigens (SERAs) .....	14
1.2.3.4.1.7 Stomatin .....	14
1.2.3.4.1.8 Subtilisin-like serine protease 1 (SUB1) .....	14
1.2.3.5 Protein Export and Host Cell Remodelling.....	14
1.2.3.6 Egress – Leaving the Host Cell behind.....	15
<b>1.3 BioID enables Compartment-specific <i>in-vivo</i> Biotinylation .....</b>	<b>16</b>
<b>1.4 Genome Editing via Selection-Linked Integration in <i>P. falciparum</i> .....</b>	<b>17</b>
<b>1.5 Aim of this Work.....</b>	<b>18</b>

---

<b>2</b>	<b>Material and Methods</b>	<b>19</b>
2.1	<b>Material</b>	<b>19</b>
2.1.1	Antibodies	19
2.1.2	Bacterial and Plasmodium strains	20
2.1.3	Buffer, medium and stock solutions	20
2.1.4	Chemicals	25
2.1.5	Commercial Kits	27
2.1.6	DNA-and protein-ladders	27
2.1.7	Enzymes	27
2.1.7.1	Restriction enzymes	27
2.1.8	General equipment	28
2.1.8.1	Laboratory equipment	28
2.1.8.2	Glass- and plastic equipment	29
2.1.9	Oligonucleotides	30
2.1.10	Software and tools	34
2.1.11	Vectors	34
2.2	<b>Methods</b>	<b>35</b>
2.2.1	Biochemical methods	35
2.2.1.1	Immunofluorescence assay (IFA)	35
2.2.1.1.1	IFA with cells in suspension	35
2.2.1.1.2	IFA with cells on a glass slide	35
2.2.1.2	Mass spectrometry	37
2.2.1.2.1	Biotinylated protein purification	37
2.2.1.2.2	Tryptic digestion	37
2.2.1.2.3	LC-MSMS application	37
2.2.1.3	Western blot analysis	38
2.2.1.3.1	Sodium dodecyl sulfate polyacrylamide gel electrophoresis (SDS-Page)	38
2.2.1.3.2	Western blot	38
2.2.1.3.3	Detection of proteins	39
2.2.2	Cell culture methods	39
2.2.2.1	Culture of the parasite <i>P. falciparum</i>	39
2.2.2.2	Cryoconservation of <i>P. falciparum</i>	39
2.2.2.3	Endogenous GFP-tagging	40
2.2.2.4	Fluorescence-activated cell scanning (FACS) analysis	40
2.2.2.5	Generation of a conditional knockout	40
2.2.2.6	Giemsa smears	41
2.2.2.7	Life cell imaging	41
2.2.2.8	Magnetic Activated Cell Sorting (MACS)	41
2.2.2.9	Protein biotinylation	42
2.2.2.10	Saponin lysis	42

2.2.2.11	Saponin release assay.....	42
2.2.2.12	Stage specific purification with a Percoll gradient.....	43
2.2.2.13	Synchronisation of <i>P. falciparum</i> culture.....	43
2.2.2.14	Transfection of <i>P. falciparum</i> .....	43
2.2.2.14.1	Transfection of ring stages.....	43
2.2.2.14.2	Transfection of segmenters .....	44
2.2.3	Microbiological methods.....	44
2.2.3.1	Cryoconservation of bacteria .....	44
2.2.3.2	Plasmid purification.....	44
2.2.3.3	Transformation of chemo-competent bacteria .....	44
2.2.4	Molecular biological methods .....	45
2.2.4.1	Agarose gel electrophoresis .....	45
2.2.4.2	Digestion.....	45
2.2.4.3	DNA precipitation.....	45
2.2.4.4	Genomic DNA isolation.....	45
2.2.4.5	Gibson assembly .....	46
2.2.4.6	Ligation .....	46
2.2.4.7	Nucleic acid quantitation .....	46
2.2.4.8	Polymerase chain reaction (PCR).....	46
2.2.4.9	Sequencing.....	48
<b>3</b>	<b>Results .....</b>	<b>49</b>
<b>3.1</b>	<b>Construct design for BioID within the PV .....</b>	<b>49</b>
<b>3.2</b>	<b>Biotinylation of proteins (BioID) within the PV .....</b>	<b>50</b>
3.2.1	Identification of PV proteins via mass spectrometry.....	51
3.2.2	Verification of potential PV proteins.....	57
3.2.3	False positive PV proteins .....	57
3.2.3.1	Candidate PF3D7_1013300 .....	57
3.2.3.2	Candidate PF3D7_1310500 .....	59
3.2.3.3	Candidate PF3D7_1462300 .....	60
3.2.4	PV proteins with a partial PV localisation .....	61
3.2.4.1	Candidate PF3D7_0629200 .....	61
3.2.4.2	Candidate PF3D7_1123500 .....	62
3.2.4.3	Candidate PF3D7_1350500 .....	64
3.2.5	PV proteins with a PV localisation .....	65
3.2.5.1	Candidate PF3D7_0220000 .....	65
3.2.5.2	Candidate PF3D7_0731600 .....	67
3.2.5.3	Candidate PF3D7_0912400 .....	68
3.2.5.4	Candidate PF3D7_1024800 .....	69
3.2.5.5	Candidate PF3D7_1135400 .....	70
3.2.5.6	Candidate PF3D7_1226900 .....	71

---

3.2.5.7	Candidate PF3D7_1464600 .....	73
3.2.6	Generation of a knock sideway system for secretory proteins .....	74
<b>3.3</b>	<b>Functional Analysis of candidate PF3D7_1464600 UIS2.....</b>	<b>77</b>
3.3.1	Parasite viability is impaired after conditional excision of <i>uis2</i> .....	79
3.3.2	Phenotype of ring stages lacking UIS2.....	81
3.3.3	Complementation of the PF3D7_1464600 phenotype .....	82
<b>4</b>	<b>Discussion .....</b>	<b>85</b>
4.1	<b>Bioid within the PV compartment .....</b>	<b>85</b>
4.2	<b>Bioid identified true PV proteins .....</b>	<b>85</b>
4.3	<b>Analysis of essentiality with the SLI-TGD system .....</b>	<b>90</b>
4.4	<b>Difficulties in the generation of a knock sideway system for secretory proteins .....</b>	<b>92</b>
4.5	<b>Functional analysis of PF3D7_1464600 (UIS2).....</b>	<b>93</b>
4.5.1	Potential UIS2condKO-comp <sup>mut</sup> evasion mechanism .....	95
4.6	<b>Classification of UIS2 .....</b>	<b>96</b>
4.6.1	Phosphatases - potential drug targets in <i>P. falciparum</i> .....	97
<b>Literature .....</b>	<b>.....</b>	<b>XVIII</b>
<b>Appendix .....</b>	<b>.....</b>	<b>XXXIII</b>
<b>Mass spectrometry results .....</b>	<b>.....</b>	<b>XXXIII</b>
<b>Extended data for SLI-TGD, integration checks and FACS assay .....</b>	<b>.....</b>	<b>LI</b>
<b>Safety and sanitation.....</b>	<b>.....</b>	<b>LIV</b>
<b>Publications .....</b>	<b>.....</b>	<b>LV</b>
<b>Acknowledgements .....</b>	<b>.....</b>	<b>LVI</b>

**List of abbreviations**

aa	amino acids
ABA	abscisic acid
ACN	acetonitrile
ACP5	tartrate-resistant acid phosphatase 5
ACTs	artemisinin-based combination therapies
AMA	apical membrane antigen
Ape	A plasmid editor
APS	Ammonium persulfate
ATP	Adenosine triphosphate
BLAST <sup>®</sup>	Basic Local Alignment Search Tool
BSA	Bovine serum albumin
BSD	Blasticidin S
CDPK5	calcium-dependent protein kinase 5
cGMP	cyclic guanosine monophosphate
CLAG3	cytoadherence-linked asexual protein 3
ConA	Concanavalin-A
CRISPR	clustered regularly interspaced short palindromic repeats
CSP	circumsporozoite protein
CyRPA	cysteine-rich protective antigen
Da	dalton
DAPI	4',6-diamidino-2-phenylindole
DDA	data-dependent mode
DHE	Dihydroethidium
DMSO	Dimethyl sulfoxide
DNA	deoxyribonucleic acid
dNTPs	Desoxynucleotides
DRMs	detergent-resistant membranes
DTT	dithiothreitol
EBAs	erythrocyte binding antigens
EBL	erythrocyte binding-like
ECL	enhanced chemiluminescence
EDTA	Ethylenediaminetetraacetic acid
eIF2 $\alpha$	eukaryotic initiation factor 2 $\alpha$
eIF2 $\alpha$ -P	phosphorylated eukaryotic initiation factor 2 $\alpha$
EMP1	erythrocyte membrane protein 1
EPIC	exported protein-interacting complex

---

ER	endoplasmatic reticulum
ESI	electrospray-ionization
ETRAMP	early-transcribed membrane protein
EXP	exported protein
FA	formic acid
FACS	Fluorescence-activated cell scanning
FDR	false discovery rate
FNT	formate-nitrite transporter
GAP50	glideosome-associated protein 50
GDV1	gametocyte development 1
GFP	green fluorescent protein
GOI	gene of interest
GP2	Golgi Protein 2
GPI	glycosylphosphatidylinositol
GST	glutathione S-transferase
GTP	Guanosine triphosphate
HA	human influenza hemagglutinin
HEPES	4-(2-Hydroxyethyl)-1-piperazineethanesulfonicacid)
HIV	human immunodeficiency virus
HP1	heterochromatin protein 1
HPLC	high-performance liquid chromatography
HRP	horseradish peroxidase
HSP101	heat shock protein 101
HSPGs	heparin-sulfate proteoglycans
IFA	immune fluorescence assay
IMC2A	inner membrane complex protein
IPTi	intermittent preventive treatment of malaria in infants
IPTp	intermittent preventive treatment of malaria in pregnancy
iRBCs	infected RBCs
IRS	indoor residual spraying
ITNs	insecticide-treated nets
KAHRP	knob-associated histidine-rich protein
kb	kilobases
L-FABP	liver-fatty acid binding protein
LB	Lysogeny broth
M	molar
MACS	magnetic activated cell sorting

---

MAPK	mitogen-activated protein kinase
MHC	major histocompatibility complex
mM	millimolar
mRNA	messenger ribonucleic acid
MS	mass spectrometry
MSPs	merozoite surface proteins
NIF	NLI-interacting factor-like phosphatase
nM	nanomolar
NPP	new permeability pathways
<i>P.</i>	<i>Plasmodium</i>
PAGE	polyacrylamide gel electrophoresis
PBS	phosphate-buffered saline
PCR	polymerase chain reaction
PEXEL	<i>Plasmodium</i> export element
PHIST	<i>Plasmodium</i> helical interspersed subtelomeric
PKG	cGMP-dependent protein kinase
PL	phospholipase
PNEPs	PEXEL-negative exported protein
POI	protein of interest
PPM	parasite plasma membrane
PPM	metal-dependant protein phosphatase
PPP	phospho-protein phosphatases
PPs	protein phosphatases
PSAC	<i>Plasmodium</i> surface anion channel
PTEX	<i>plasmodium</i> translocon of exported proteins
PTP	protein tyrosine phosphatase
PV	parasitophorous vacuole
PV1	parasitophorous vacuolar protein 1
PV2	parasitophorous vacuolar protein 2
PVM	parasitophorous vacuole membrane
RAP	rhoptry-associated protein
RBCM	red blood cell membrane
RBCs	red blood cells
RDT	rapid diagnostic test
RhopH	rhoptry
Rhs	reticulocyte-binding like homologs
Ripr	Rh5 interacting protein

---

ROM	rhomboid protein
RON	rhoptry neck protein
rpm	rounds per minute
RPMI	Roswell Park Memorial Institute
RT	room temperature
RUSH	retention using selective hooks
SBP	streptavidin-binding peptide
SBP1	skeleton binding protein 1
SDS	Sodium dodecyl sulfate
SEP2	small exported protein 2
SERA	serine repeat antigen
SLI	selection-linked integration
SMC	seasonal malaria chemoprevention
SP	signal peptide
SR-BI	scavenger receptor BI
STEVOR	subtelomeric variable open reading frame
SUB1	subtilisin-like serine protease 1
<i>T.</i>	<i>Toxoplasma</i>
TAE	Tris-acetate-EDTA
TBS	Tris-buffered saline
TBST	Tris-buffered saline + tween
TE	Tris-EDTA
TEMED	N, N, N, N-Tetramethylethylenediamin
TGD	targeted gene disruption
TM	transmembrane
TNF $\alpha$	tumor necrosis factor $\alpha$
TRAP	thrombospondin-related anonymous protein
Trx2	thioredoxin
UIS	upregulated in infectious sporozoites
UKE	Universitätsklinikum Eppendorf
UP	unique peptide
UV	ultraviolet
WB	western blot
WHO	World Health Organisation
wt	wildtype
ZFN	zinc-finger nucleases

## List of figures

Figure 1: Countries with indigenous cases of malaria in 2000 and their status by 2016.....	1
Figure 2: Overview of the <i>Plasmodium</i> life cycle.....	4
Figure 3: Asexual blood stages in <i>P. falciparum</i> .....	6
Figure 4: Merozoite – Invasion into a new RBC.....	8
Figure 5: Formation of the PV compartment.....	10
Figure 6: Protein composition of the PV compartment.....	11
Figure 7: Steps in egress.....	16
Figure 8: The SP-GFP-BirA* construct is located in the PV.....	49
Figure 9: The SP-GFP-BirA* construct biotinylates proteins within the PV compartment.....	50
Figure 10: Candidate PF3D7_1013300.....	58
Figure 11: Candidate PF3D7_1310500.....	59
Figure 12: Candidate PF3D7_1462300.....	60
Figure 13: Candidate PF3D7_0629200.....	61
Figure 14: Candidate PF3D7_1123500.....	63
Figure 15: Candidate PF3D7_1350500.....	65
Figure 16: Candidate PF3D7_0220000.....	66
Figure 17: Candidate PF3D7_0731600.....	67
Figure 18: Candidate PF3D7_0912400.....	68
Figure 19: Candidate PF3D7_1024800.....	70
Figure 20: Candidate PF3D7_1135400.....	71
Figure 21: Candidate PF3D7_1226900.....	72
Figure 22: Candidate PF3D7_1464600.....	74
Figure 23: Theoretical model of the mislocalization into the ER.....	75
Figure 24: Rapalog induced ER-directed knock sideways.....	76
Figure 25: Conditional deletion of <i>uis2</i> encoding PF3D7_1464600.....	79
Figure 26: Parasite viability of the UIS2 conditional knockout cell line.....	80
Figure 27: Phenotype after rapalog induced excision of <i>uis2</i> .....	82
Figure 28: Complementation of the conditional <i>uis2</i> KO cell line.....	83
Figure 29: Identification of novel PV proteins.....	86
Figure xxx: Flow cytometry growth curves.....	LIII

**List of tables**

Table 1: Primary antibodies .....	19
Table 2: Secondary antibodies for IFA .....	19
Table 3: Secondary antibodies for WB .....	19
Table 4: Streptavidin conjugates .....	20
Table 5: Buffer, medium and stock solutions for agarose gel.....	20
Table 6: Buffer, medium and stock solutions for Gibson assembly .....	20
Table 7: Buffer, medium and stock solutions for Western blot .....	21
Table 8: Buffer, medium and stock solutions for mass spectrometry .....	22
Table 9: Buffer, medium and stock solutions for parasite and bacteria culture .....	22
Table 10: Restriction enzymes .....	28
Table 11: List of primers .....	30
Table 12: Vectors used as backbones for this work .....	34
Table 13: Analytical PCR conditions and pipetting scheme. ....	47
Table 14: Preparative PCR conditions and pipetting scheme. ....	47
Table 15: Results of the SP-GFP-BirA* pellet fraction after 3D7 subtraction .....	51
Table 16: Results of the SP-GFP-BirA* supernatant fraction .....	54
Table 17: Summary of all investigated candidates. ....	56
Table xviii: Mass spectrometry results for the SP-GFP-BirA* pellet fraction .....	XXXIII
Table xix: Mass spectrometry results for the 3D7 pellet fraction .....	XL
Table xx: Mass spectrometry results for the SP-GFP-BirA* supernatant fraction .....	XLV
Table xxi: Mass spectrometry results for the 3D7 supernatant fraction.....	XLVII
Table xxii: Mass spectrometry hit list for the supernatant fraction.....	L
Table xxiii: Attempts for SLI-TGD .....	LI
Table xxiv: Expected sizes for integration check PCR .....	LII

# 1 Introduction

## 1.1 Malaria – Past, Present and Future

Before the causative agent of malaria was known, it was speculated that the disease was spread by bad air (Italian: mala aria) in areas of swamps and marshland. It was only when Charles Louis Alphonse Laveran identified a parasitic protozoan in human red blood cells (RBCs) as the true cause of malaria in 1880 (Laveran, 1880), when speculations about the cause for this disease were put at rest. More than one decade later the female *Anopheles* mosquito was discovered as a vector transmitting this eukaryotic organisms of the genus *Plasmodium* (Cox, 2010; Ross, 1897).

Today the World Health Organisation (WHO) estimates nearly half of the world's population at risk of malaria. Since 2010 malaria case incidence has fallen globally. However, the decline in incidence and mortality has stalled and even reversed in some regions since 2014. The WHO report 2017 described a total of 216 million cases of malaria, an increase of 5 million cases over the previous year, whereas the number of malaria deaths was estimated at 445000, about the same number of deaths reported in 2015. Notably, pregnant women and children under the age of five are particularly at risk of malaria. Ninety per cent of the malaria cases worldwide occur within Africa, followed by South-East Asia (7%) and the East-Mediterranean Region (2%). Eighty per cent of the global malaria burden concentrates on 15 countries – all in sub-Saharan Africa, except for India (WHO, 2017).

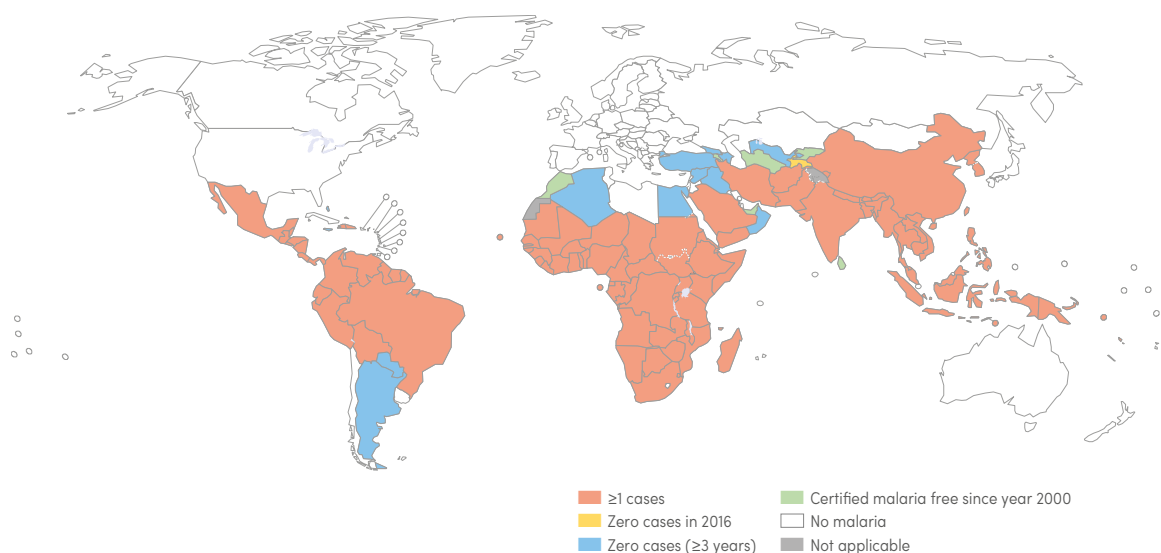


**Figure 1: Countries with indigenous cases of malaria in 2000 and their status by 2016**

Countries with zero indigenous cases over at least the past 3 consecutive years are eligible to request certification of malaria free status from the WHO. All countries in the WHO European Region reported zero indigenous cases in 2016. Kyrgyzstan and Sri Lanka were certified malaria free in 2016 (WHO, 2017).

The future aim for the fight against malaria is to prevent re-establishment of malaria in all countries that are malaria free and to reduce malaria case incidence and mortality rates globally compared to 2015. Additionally, the global target for 2030 is to eliminate malaria in at least 35 countries that show indigenous cases (red countries in Figure 1) (WHO, 2017).

### **1.1.1 Malaria - Intervention and Control**

To reach the global target to eliminate malaria by 2030 in at least 35 countries the WHO recommends different intervention and control strategies. For vector control the use of insecticide-treated nets (ITNs) and indoor residual spraying (IRS) of insecticides are the most commonly used control strategies (WHO, 2017). In sub-Saharan Africa the use of ITNs has been shown to be effective in reducing malaria case incidence rates by 50% and in reducing malaria mortality rates by 55% in children under the age of 5 (Eisele et al., 2010; Lengeler, 2004). As intervention strategies the WHO also recommends chemoprevention in high risk groups or for seasonal malaria. For pregnant women intermittent preventive treatment of malaria in pregnancy (IPTp) is frequently used, while a policy for intermittent preventive treatment of malaria in infants (IPTi) has so far not been implemented in any country. In addition, seasonal malaria chemoprevention (SMC) is now widely used for *Plasmodium falciparum* malaria control in highly seasonal transmission areas of the Sahel subregion in Africa (WHO, 2016).

### **1.1.2 Treatment and Drug Resistance**

For malaria treatment different antimalarial drugs are available that are frequently used as combination therapies. Before starting malaria treatment the WHO recommends confirming every suspected malaria case either by microscopy or by rapid diagnostic test (RDT). Once confirmed, artemisinin-based combination therapies (ACTs) are used as the gold standard for the treatment of uncomplicated malaria (WHO, 2017). For uncomplicated malaria ACTs have been estimated to reduce malaria mortality in children aged 1–23 months by 99% (range: 94–100%), and in children aged 24–59 months by 97% (range: 86–99%) (Thwing et al., 2011). Emerging parasite resistance (Ariey and Paul, 2014; Ashley et al., 2014; Delves et al., 2012; Durand and Le Bras, 2001; Haldar et al., 2018; Muller and Hyde, 2010; Wellems and Plowe, 2001) against antimalarials jeopardize the successful treatment of malaria and highlights the need for research into alternative drugs.

### **1.1.3 Vaccine Development**

An efficient malaria vaccine would be helpful in the combat against malaria. However, an efficacious malaria vaccine needs to induce strain transcending sterilizing immunity that will avert disease and interrupt transmission. Although the first malaria vaccine RTS,S

also known under the commercial name Mosquirix (developed by GlaxoSmithKline) holds some promise, a phase III trial showed only partial protection against malaria in young children with an estimated efficacy of 45.7% (Moris et al., 2018). However, the WHO recently announced that in 2018 RTS,S will be implemented as the first malaria vaccine provided to young children through routine immunization programmes in three sub-Saharan African countries (Ghana, Kenya, and Malawi) (Coelho et al., 2017). The molecular target of RTS,S is the circumsporozoite protein (CSP), which is expressed on *Plasmodium* sporozoites during the pre-erythrocyte stage. Beside vaccines against pre-erythrocytic stages (RTS,S) there are also transmission-blocking vaccines that target parasitic molecules of mosquito stages and blood stage vaccines. The most promising targets for blood stage vaccines are subunits of the invasion-related AMA1-Rh2 interaction (section 1.2.3.2) and chemically attenuated parasites that are both currently in the preclinical status and subunits of Rh5 (section 1.2.3.2) that are currently tested in clinical phase I trials (Coelho et al., 2017).

## 1.2 *Plasmodium* – the Malaria causing Parasite

Up to 200 *Plasmodium* species have been described that infect mammals, birds and reptiles. To date five *Plasmodium* species, namely *P. falciparum*, *P. malariae*, *P. ovale*, *P. vivax* and *P. knowlesi* cause malaria in humans. All *Plasmodium* species are members of the phylum *Apicomplexa*, a large group of parasitic eukaryotes that differ in their host and mode of transmission. Besides the typical cellular features of eukaryotes, these organisms contain a specialized apical complex and a secondary endosymbiont termed apicoplast. The apical complex consists of specialized secretory organelles, namely rhoptries, micronemes, exonemes and dense granules (for details see section 1.2.3.3). The apicoplast is essential for the generation of isoprenoid precursors (Yeh and DeRisi, 2011).

### 1.2.1 Pathophysiology and Immunology

The pathophysiology of malaria is closely related to the parasite species. The symptomatic part of a *Plasmodium* infection is caused by blood stage parasites. General symptoms are fever, malaise, headache, myalgia, jaundice and sometimes nausea, vomiting and diarrhoea. One typical symptom is the reoccurring fever every two days (malaria tertiana) for *P. vivax* and *P. ovale* in concordance with their 48-hour blood stage life cycle and every three days (malaria quartana) for *P. malariae* in concordance with their 72-hour blood stage cycle (Bartoloni and Zammarchi, 2012). The fever is caused by the innate immune response to the synchronous rupture of the RBCs at the end of the asexual replication cycle of the parasites. RBC rupture releases parasite antigens, glycosylphosphatidylinositol (GPI) and haemozoin into the blood stream, leading to an upregulation of the fever inducing cytokine tumor necrosis factor  $\alpha$  (TNF $\alpha$ ) and



which it develops into the so-called oocyst. Within the oocyst thousands of sporozoites are formed. The sporozoites escape from the oocyst and reach acinar cells of the salivary glands from where they will be injected with the saliva into the skin of the vertebrate host during the next blood meal. Here, the sporozoites use gliding motility to enter the blood stream by traversing endothelial cells in order to reach their destination - the liver.

#### 1.2.2.2 Liver stage

Within the liver sinusoid the sporozoites adhere to the epithelium and migrate through the endothelium and resident Kupffer cells, while forming an interaction between the sporozoite's major surface protein CSP and thrombospondin-related anonymous protein (TRAP) with highly sulphated heparin-sulfate proteoglycans (HSPGs) (Matuschewski et al., 2002a; Pinzon-Ortiz et al., 2001). The interaction and subsequent processing of CSP play central roles in activating sporozoites to switch from a migratory mode to an invasive mode (Coppi et al., 2007). During this phase, the sporozoites migrate through several hepatocytes before invading the final host hepatocyte where a parasitophorous vacuole (PV) is formed from the invaginated host cell membrane (Mota et al., 2001). It was shown that the hepatocyte EphA2 receptor and the sporozoite proteins P52 and P36 are critical for PV formation (Kaushansky et al., 2015). However, contradicting results argue for an EphA2 receptor independent invasion by either using tetraspanin CD81 and/or the scavenger receptor BI (SR-BI) (Langlois et al., 2018). Within the PV the sporozoite transforms into a trophozoite. For the transformation of sporozoites into liver stage trophozoites de-phosphorylation of the phosphorylated eukaryotic initiation factor 2 $\alpha$  (eIF2 $\alpha$ -P) is required. A process that was reported to be mediated by UIS2 (upregulated in infectious sporozoites), a member of the PP2C/PPM phosphatase family (Zhang et al., 2016). The trophozoite grows into a multinucleated schizont that generates tens of thousands of merozoites that bud off in parasite-filled vesicles (merosomes) into the sinusoid lumen (Sturm et al., 2006). For effective merozoite egress from the hepatocyte into the blood stream phospholipases (PL) that localize at the parasitophorous vacuole membrane play an important role. In *P. berghei*, a *Plasmodium* strain that infects rodents, it was shown that parasites lacking *PbPL* undergo normal liver stage development until merozoites are produced, but have a defect in egress from host hepatocytes (Burda et al., 2015). Additionally, the parasites induce a breakdown of the host cell actin cytoskeleton, leading to destabilization of the host cell plasma membrane (Burda et al., 2017). Interestingly, rupture of the merosomes happens in the lung capillaries and releases the RBC infecting form, termed merozoites, into the circulation (Baer et al., 2007).

#### 1.2.2.3 Blood stage

Merozoites target RBCs as their host cell into which they actively invade. During the invasion process the PV is formed (section 1.2.3.2). The asexual development of the

parasite in RBCs is categorized into three stages: the ring, the trophozoite and the schizont stage (Figure 3), leading to the release of up to 32 progeny merozoites that invade new RBCs (for details see section 1.2.3). A small number of schizonts carry merozoites that are committed to differentiate into sexual gametocytes (Bruce et al., 1990). To date the molecular interplay that triggers sexual commitment is partly understood. AP2-G is the master transcriptional regulator of gametocytogenesis, while heterochromatin protein 1 (HP1)-dependent silencing of *ap2-g* prevents sexual conversion in proliferating parasites (Brancucci et al., 2014). Recently the upstream regulator of sexual commitment, gametocyte development 1 (GDV1), was identified. GDV1 targets heterochromatin and triggers HP1 eviction, thereby antagonizing HP1-dependent gene silencing (Filarsky et al., 2018). Gametocytogenesis is categorized into five stages (I to V) of which only stages I and V circulate in the peripheral blood, while the gametocyte stages II-IV display homing and vascular transmigration into the host bone marrow (Aguilar et al., 2014; De Niz et al., 2018). Mature female and male stage V gametocytes are able to infect the mosquito and restart the sexual development of the parasite, causing the transmission of malaria.

### 1.2.3 The asexual Blood Cycle

A big advantage for malaria research has been the continuous *in vitro* cultivation of *P. falciparum* asexual blood stage parasites in human red blood cells (Trager and Jensen, 1976). This milestone opened the possibility to study parasite blood stage biology (Figure 3) in more detail, including particularly merozoite invasion (section 1.2.3.2) and parasite egress (section 1.2.3.6). For this advanced imaging technics (De Niz et al., 2017; Gruring and Spielmann, 2012), diverse biochemical assays or genetic modifications to study protein function (Birnbaum et al., 2017; de Koning-Ward et al., 2015; Webster and McFadden, 2014) were used.

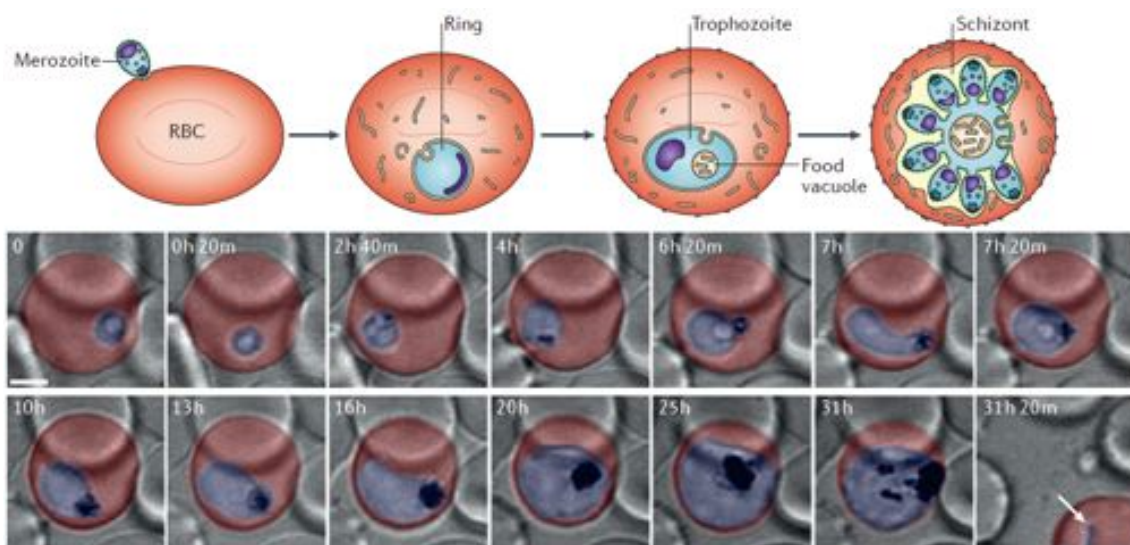


**Figure 3: Asexual blood stages in *P. falciparum***

Graphic representation of the merozoite and the three main blood stages: ring, trophozoite, and schizont (upper panel). 4D confocal microscopy images: of a parasite (blue) developing in a RBC (lower panel). The development is shown from ring stage to schizont stage; the growing black spot (2h40m to 31h) represents the degradation of haemoglobin into haemozoin within the food vacuole; the white arrow (31h 20m) indicates a freshly invaded ring; scale bar, 2  $\mu\text{m}$  (De Niz et al., 2017).

### 1.2.3.1 The Host – Red Blood Cell

RBCs are unique cells that are continuously renewed during erythropoiesis. Most *Plasmodium* species infect erythrocytes, while notably *P. vivax* is restricted to infect reticulocytes – the premature form of erythrocytes. Erythrocytes are highly derived cells that neither have a nucleus nor mitochondria, Golgi or endoplasmic reticulum (ER) but possess highly specialized properties responsible for the oxygen distribution within the body. For this purpose the cytoplasm of erythrocytes contains the oxygen-transporting metalloprotein haemoglobin, which accounts for 97% of the dry weight of RBCs (Weed et al., 1963). Haemoglobin is a major nutrient source for the parasite that digests up to 80% of the host cell's haemoglobin within the digestive vacuole where the haemoglobin is degraded and stored as the malaria pigment haemozoin (Deegan and Maegraith, 1956; Dorn et al., 1995). As a non-nucleated cell the RBC does not display class I molecules of the major histocompatibility complex (MHC) on its surface that normally present peptides from cytosolic proteins, resulting in difficulties for the host immune system to detect parasites within the RBC.

### 1.2.3.2 Invasion and Parasitophorous vacuole formation

Merozoites - the invasive form of the parasite - either released by liver merozoites (section 1.2.2.2) or by infected RBCs (iRBCs) actively penetrate RBCs. The invasion process is highly orchestrated and involves the successive secretion of apical organelles (Figure 4). Simplified, the invasion process can be divided into three main stages: 1) attachment and reorientation, which involves initial and reversible attachment of the merozoite to the RBC mediated by GPI-anchored merozoite surface proteins (MSPs) (Sanders et al., 2005). Interestingly, MSPs are also involved in complement evasion strategies as a recent study identified GPI-anchored Pf92 that downregulates complement activation by actively recruiting Factor H, protecting the parasite from complement lysis (Kennedy et al., 2016). Next, reorientation takes place to bring the invasion-relevant organelles at the apical pole of the merozoite into position for invasion (Dvorak et al., 1975). This involves wrapping of the RBC membrane around the merozoite (Dasgupta et al., 2014). In order to form the initial tight interaction, micronemes secrete adhesins, molecules involved in erythrocyte binding, such as members of the erythrocyte binding-like (EBL) family and erythrocyte binding antigens (EBAs) (Weiss et al., 2015). Rhoptry secretion of reticulocyte-binding like homologs (Rhs) initializes step 2), the formation of a

tight junction. For this process only the interaction between Rh5 and basigin (Crosnier et al., 2011; Volz et al., 2016) was shown to be essential, while the other interactors act cooperatively in tight junction formation (Lopaticki et al., 2011). Evidence suggests that during tight junction formation a pore is formed between the merozoite and the RBC through the interaction of Rh5 with Rh5 interacting protein (Ripr) (Malleret et al.) and cysteine-rich protective antigen (CyRPA), forming the tripartite Rh5-Ripr-CyRPA complex (Volz et al., 2016). Tight junction formation is completed after the high-affinity ligand-receptor interaction between the apical membrane antigen 1 (AMA1) on the merozoite surface and the rhoptry neck protein 2 (RON2) - the first parasite protein inserted into the erythrocyte membrane - is built (Besteiro et al., 2009; Tonkin et al., 2011). This tight junction facilitates step 3), the movement of the junction from the apical to the posterior pole, driven by the parasite's actin-myosin motor complex, inducing active penetration into the RBC. To enable active movement the surface coat of the merozoite has to be shed at the moving junction by proteolytic processing through proteases mainly of the rhomboid family. Successful penetration of the parasite into the RBC needs to be completed by resealing the RBC membrane at the posterior end of the invasion event, creating a new compartment – the PV – which is formed through the invagination of host cell plasma membrane and parasite lipids derived from the rhoptries. The molecular events responsible for the final resealing of the PVM are not yet clear, although it was shown that AMA1 - an essential protein for merozoite invasion – plays an either direct or indirect role in membrane resealing (Yap et al., 2014). It was also shown that the rhomboid family member ROM1 promotes proper PV modification (Vera et al., 2011).

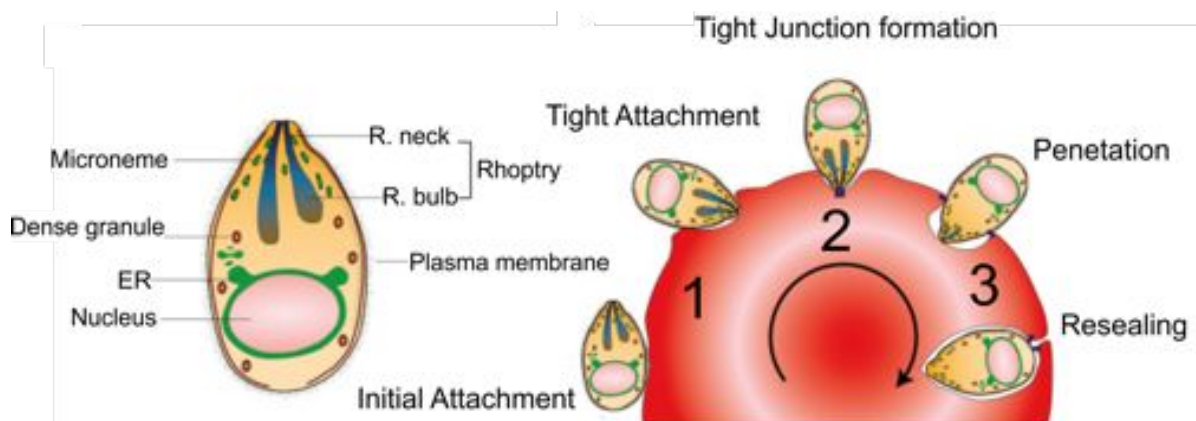


**Figure 4: Merozoite – Invasion into a new RBC**

Left) Graphic representation of a merozoite surrounded by its parasite plasma membrane, including its main organelles: ER, nucleus and the apical organelles: rhoptries, subdivided in rhoptry neck and rhoptry bulb, micronemes and dense granules. Right) Schematic representation of the invasion process: 1) initial and tight attachment, 2) tight junction formation, 3) penetration and resealing, modified from (Cowman et al., 2017).

### 1.2.3.3 Apical Organelles

Apical organelles represent a taxonomic criterion for the phylum *Apicomplexa* and are located at the apical end of the parasite (Figure 4). To date four secretory organelles were identified, namely rhoptries, micronemes, dense granules and exonemes. Just prior to egress exonemes discharge the essential subtilisin-like serine protease 1 (SUB1) (for details see section 1.2.3.6) into the PV lumen, where SUB1 mediates proteolytic maturation of downstream effector molecules that are required for successful egress from the host erythrocyte (Yeoh et al., 2007). The rhoptries are club-shaped, pairwise arranged organelles that are present in *P. falciparum* shortly before merozoite segmentation is initialized in schizonts (Bannister et al., 2000). Rhoptries are subdivided into rhoptry bulb and rhoptry neck content that are discharged independently. First, discharge of the rhoptry neck proteins of the Rh family facilitates host cell attachment and tight junction formation (section 1.2.3.2), whereas the time of discharge and the exact role of rhoptry bulb proteins remains elusive. It was shown for the rhoptry-associated protein (RAP) complex, which is situated in the rhoptry bulb, that it is required for the survival of the parasite in its new intracellular environment – the PV (Ghosh et al., 2017). Micronemes store invasion related proteins. It is believed that there are different types of micronemes, which differ from their adhesin molecule content, allowing a highly organized program of release (Healer et al., 2002). Dense granules are secretory organelles that are more distributed throughout the cell. The content of apical organelles is released by fusion with the parasite plasma membrane (PPM). In contrary to a constant release of dense granules in *Toxoplasma* throughout asexual replication (Chaturvedi et al., 1999), dense granules are released mostly just after invasion in *P. falciparum* – not contributing to initial PVM formation but rather introducing the first subset of PV and PVM proteins (Aikawa et al., 1990; Iriko et al., 2018; Morita et al., 2018).

Interestingly, most of the proteins stored in the apical organelles harbour N-terminal signal sequences, which mediate entry into the secretory pathway at the ER membrane (Lingelbach, 1993). As described in *Toxoplasma* protein trafficking to the apical complex and merozoite formation is sortilin dependent (Sloves et al., 2012). In *P. falciparum* the same results were obtained. Upon decreased expression of sortilin protein trafficking to the rhoptries, the micronemes, and the dense granules is disrupted, leading to an accumulation of apical complex proteins in the ER and the PV, while the protein export to the erythrocyte and transport through the constitutive secretory pathway remains functional (Hallee et al., 2018a).

### 1.2.3.4 Parasitophorous Vacuole – Interface between Parasite and Host Cell

As introduced in section 1.2.2.2 the PV is formed during the invasion process, presumably by invagination of the host cell plasma membrane (Ward et al., 1993). It was shown in *T.*

*gondii* that the moving junction selectively excludes host cell plasma membrane proteins on the basis of their membrane anchoring (Mordue et al., 1999). After resealing this membrane marks the boundary between parasite and RBC and is termed the parasitophorous vacuole membrane (PVM) (Figure 5). The narrow space between the two membranes surrounding the parasites, the PVM and the PPM, is called the PV lumen and has a diameter of around 50 nm (Trelka et al., 2000). In order to permit parasite survival, growth and replication within the host RBC, different parasitic proteins are transported into the PV compartment. During and just after invasion dense granules initiate the remodelling of the PV by releasing the first proteins into the PV compartment (Cowman et al., 2017) (details in section 1.2.3.4.1.8 and 1.2.3.3).

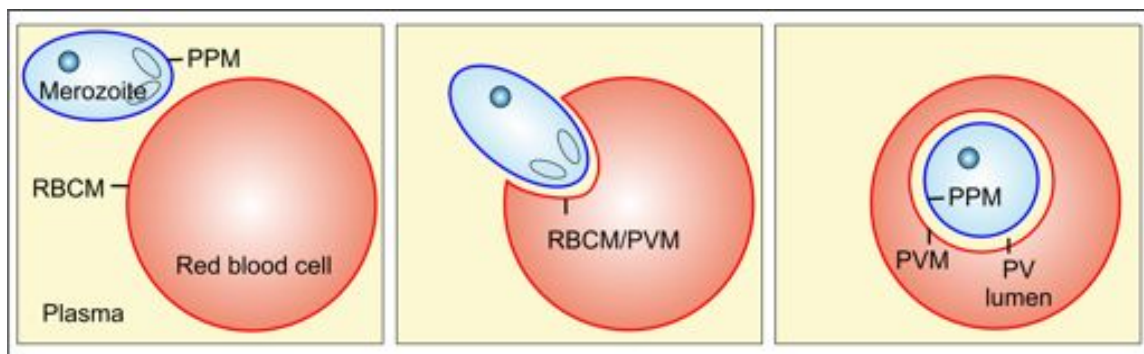


**Figure 5: Formation of the PV compartment.**

Graphic representation of a merozoite, a red blood cell and the formation of the PV compartment; PV: parasitophorous vacuole, PPM (blue): parasite plasma membrane, RBCM (red): red blood cell membrane, PVM (red): parasitophorous vacuole membrane.

Nutrient uptake is essential for the parasite and is mediated by a solute pore in the PVM that is permeable for molecules up to a size of 1400 Da (Desai et al., 1993; Desai and Rosenberg, 1997). Similar membrane permeability was identified in *T. gondii* (Schwab et al., 1994), which is mediated by the PVM proteins GRA17 and GRA23 (Gold et al., 2015). Intriguingly, *Plasmodium* EXP2 (exported protein 2) (a protein remotely related to GRA17 and GRA23) was able to rescue the phenotype of GRA17-deficient parasites, introducing EXP2 as a plausible candidate for PVM pore formation (Gold et al., 2015). To increase nutrient supply from the serum the parasite also generates new permeability pathways (NPP), including a *Plasmodium* surface anion channel (PSAC) in the RBC membrane that is composed of cytoadherence-linked asexual protein 3 (CLAG3) and other rhoptry proteins (Gupta et al., 2018; Ito et al., 2017; Nguitragool et al., 2011; Sherling et al., 2017). In addition, nutrient uptake is also mediated by cytostomes, which are host cell cytosol filled invaginations of the PPM and PVM that deliver double membrane vesicles into the food vacuole (Aikawa et al., 1966; Milani et al., 2015) as well as by the tubovesicular network that is described as PVM protrusions reaching into the host cell cytosol (Lauer et al., 1997).

The PVM has presumably also the property for the passage of waste products that might be maintained by the solute pore into the host cell cytosol and by PSAC beyond the RBC membrane. For the passage of formate and lactate across the PPM the lactate/proton symporter FNT was identified (Marchetti et al., 2015; Wu et al., 2015).

However, evidence suggests that the PVM is also a compartment to maintain homeostasis for parasite survival against the high  $K^+$  (~140 mM) and the very low  $Ca^{2+}$  concentrations (~100 nM) of the RBC cytoplasm. It was postulated that the inside-out conversion of the RBC membrane might contribute through erythrocyte plasma membrane  $Ca^{2+}$  ATPases at the RBC membrane/PVM, that pump  $Ca^{2+}$  into the PV, generating a high  $Ca^{2+}$  microenvironment in the space between the PVM and the parasite plasma membrane (Gazarini et al., 2003).

As the interface between the parasite and the host cell, the PV might also function as a signalling platform that transmits information (e.g. changing conditions within the host cell) to the parasite. A kinome analysis combined with chemical and genetic approaches identified KIN - a putative serine/threonine kinase - as a critical regulator that mediates sensing of nutrients and controls a transcriptional response based on the host nutritional status in *P. berghei* (Mancio-Silva et al., 2017).

#### 1.2.3.4.1 Protein Composition of the PV Compartment

To date a limited number of PV compartment proteins are known (Figure 6) in asexual blood stages as most PV proteins lack homologs in organisms other than *Plasmodium spp.* and do not harbour any predictable functional domains (Spielmann et al., 2012).

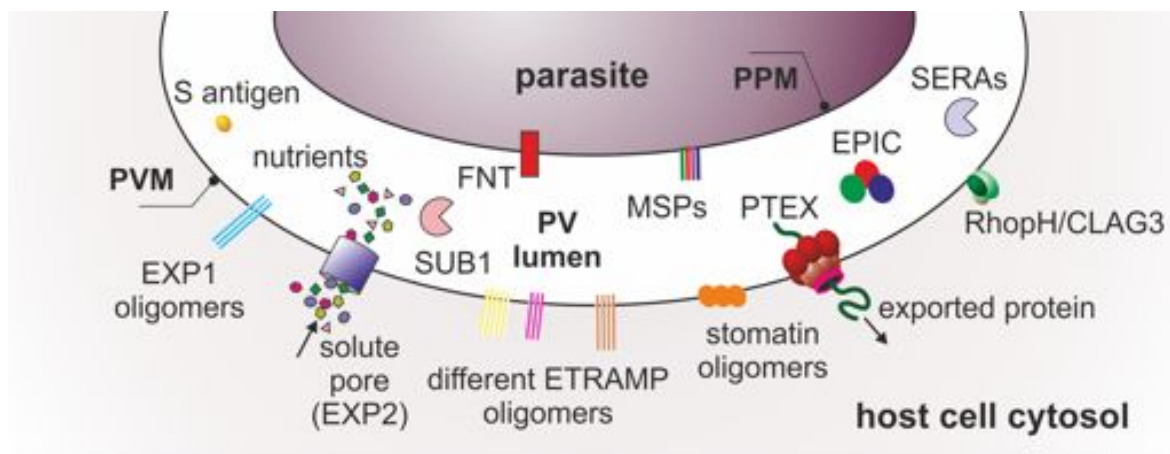


**Figure 6: Protein composition of the PV compartment**

Graphic representation of the proteins within the PV compartment; PPM: parasite plasma membrane, PV: parasitophorous vacuole, PVM: parasitophorous vacuole membrane, EXP: exported protein, ETRAMP: early-transcribed membrane protein, SUB: subtilisin-like serine protease, PTEX: *Plasmodium* translocon of exported proteins, EPIC: exported protein interacting complex, consisting of exported protein 3 (EXP3), parasitophorous vacuolar protein 1 and 2 (PV1 and PV2), RhopH: rhoptry protein complex, CLAG: cytoadherence-linked asexual protein, SERA: serine repeat antigen, MSP: merozoite surface protein, FNT: formate-nitrite transporter, modified from (Spielmann et al., 2012).

#### 1.2.3.4.1.1 Early-transcribed membrane proteins (ETRAMPs)

The family of early-transcribed membrane proteins (ETRAMPs) consists of 14 small and highly charged integral membrane proteins that are integral to the PVM (Spielmann et al., 2003). It was shown that ETRAMPs cluster in member-specific oligomeric arrays, forming a mosaic of different microdomains in the PVM with a C-terminal orientation into the host cell cytosol (Spielmann et al., 2006). Six members were exclusively observed in ring stages, four members were found in the development from ring to trophozoite and three members were not present in asexual blood stages (Spielmann et al., 2003). Notably, *etramps* are among the most highly expressed genes in asexual blood stage parasites (Le Roch et al., 2003). However, functional data for the role of ETRAMPs in the *P. falciparum* life cycle and in particular the blood stages remains elusive. Nevertheless, in the rodent malaria parasites *P. yoelii* and *P. berghei* UIS3 (34% amino acid identity with ETRAMP13) and *uis4* (orthologue of *etramp10.3*) were identified as essential members of the ETRAMP family that localize to the secretory organelles of sporozoites and the PVM of the liver stages (Kaiser et al., 2004; Matuschewski et al., 2002b; Mueller et al., 2005). For UIS3 an important interaction to mouse liver-fatty acid binding protein (L-FABP) was described (Mikolajczak et al., 2007) that might also be conserved for ETRAMP13 in *P. falciparum* liver stages and might mediate the uptake of lipids from the host cytoplasm (Sharma et al., 2008). For UIS4 it was shown that the essential *P. falciparum* orthologue ETRAMP10.3 is not the functional orthologue of UIS4 that causes an arrest in early liver stage development when depleted (Mackellar et al., 2010). In a systematic analysis 11 *etramps* were identified in *P. yoelii*, of which six genes have putative orthologues in *P. falciparum* and five *etramps* appear to be specific for rodent malaria parasites (MacKellar et al., 2011). In *P. berghei* the ETRAMP family member SEP2 (small exported protein 2) was shown to be expressed throughout the life cycle and to be released during sporozoite gliding motility (Curra et al., 2013).

#### 1.2.3.4.1.2 Exported protein 1 (EXP1)

Exported protein 1 (EXP1) was (one of) the first PVM proteins described (Simmons et al., 1987) and was reported to be stored in dense granules in merozoites (Iriko et al., 2018). It was shown that EXP1 is a negatively charged integral membrane protein of the PVM, which is presumably organized in oligomeric arrays with its N-terminus facing the PV lumen (Gunther et al., 1991; Spielmann et al., 2006). To date the exact trafficking pathway for PVM proteins remains elusive, although for EXP1 it was described that insertion into the PVM is independent of protein folding and the PTEX translocon (Tribensky et al., 2017). EXP1 is essential for parasite growth (Maier et al., 2008). Functional analysis revealed that EXP1 might function as glutathione S-transferase (GST), acting in detoxification by conjugating glutathione onto the cytotoxic haematin (Lisewski et al.,

2014). In *P. berghei* liver stages, it was shown that EXP1 interacts with host apolipoprotein H and that the interaction is important for liver stage development (Sa et al., 2017).

#### 1.2.3.4.1.3 *Parasitophorous vacuolar protein 1 (PV1)*

Parasitophorous vacuolar protein 1 (PV1) was the only PV protein identified in a systematic attempt to investigate the PV proteome (Nyalwidhe and Lingelbach, 2006) based on selective lysis of the PVM. PV1 is soluble in the PV lumen and was found in dense granules in merozoites (Morita et al., 2018). There is evidence that PV1 weakly associates with PTEX (Elsworth et al., 2016; Mesen-Ramirez et al., 2016) and it was identified as a component of the exported protein-interacting complex (EPIC) that is involved in the trafficking of virulence determinants into the host cell (Batinovic et al., 2017). An inducible knockdown of PV1 resulted in altered knob morphology on iRBCs, reduced cell rigidity and decreased binding of iRBCs to CD36 but did not substantially affect parasite viability *in vitro* (Batinovic et al., 2017). This might contradict the suggestion of PV1 to be essential for the survival of *P. falciparum* blood stages (Chu et al., 2011), although the inducible knockdown did not result in a complete depletion of PV1, leaving the possibility that residual PV1 might be sufficient to rescue a potentially essential phenotype.

#### 1.2.3.4.1.4 *Plasmodium translocon of exported proteins (PTEX)*

The *Plasmodium* translocon of exported proteins (PTEX) is a protein complex situated at the PVM that translocates proteins from the PV compartment into the host cell (Beck et al., 2014; de Koning-Ward et al., 2009; Elsworth et al., 2014). PTEX consists of 5 proteins, namely EXP2, PTEX150 and PTEX88 (that have unknown functions), thioredoxin (Trx2) and heat shock protein 101 (HSP101) (de Koning-Ward et al., 2009). However, additional proteins, like PV1, Pf113 and Hsp70-x may also associate with PTEX, albeit this interaction would likely be weaker than that of the core PTEX components and possibly more transient (Elsworth et al., 2016; Mesen-Ramirez et al., 2016). HSP101 is believed to empower translocation by its ATPase activity (de Koning-Ward et al., 2009; El Bakkouri et al., 2010). Trx2, although not fully essential for protein export, is important for parasite growth (Matthews et al., 2013), and is implicated in breaking disulphide bonds (de Koning-Ward et al., 2009). EXP2, which might be involved in forming the solute pore (Gold et al., 2015), is considered the actual pore forming entity of PTEX (Beck et al., 2014; de Koning-Ward et al., 2009; Elsworth et al., 2014). Conditional knock down studies (Beck et al., 2014; Elsworth et al., 2014) and conditional arresting of substrates in the translocon (Mesen-Ramirez et al., 2016) demonstrated translocation activity of the PTEX. Notably, EXP2, PTEX150 and HSP101 are stored in dense granules during merozoite formation, presumably to induce PVM modifications during or just after invasion (Bullen et al., 2012).

#### 1.2.3.4.1.5 *S antigen*

S-antigens are heat-stable, highly polymorphic proteins. To date the S antigen family has no known function but was found to be present in the PV lumen in late stages at the time of schizont rupture and in PV-related vesicles within the host cell cytoplasm of schizont-infected cells (Culvenor and Crewther, 1990).

#### 1.2.3.4.1.6 *Serine repeat antigens (SERAs)*

The serine repeat antigen family consists of nine putative papain-like cysteine proteases that are present within the PV lumen and are implicated in parasite egress (Arisue et al., 2007). SERA4, 5 and 6, and possibly also SERA9, are synthesized in blood stage parasites, of which the genes of SERA4, 5, and 6 could not be disrupted, indicating essential roles for the parasite (Miller et al., 2002). Indeed, recent work showed that SERA5 regulates the kinetics and efficiency of malaria parasite egress from host erythrocytes (Collins et al., 2017) and that SERA6 possesses proteolytic activity targeting the actin-binding domain of the major RBC cytoskeletal protein  $\beta$ -spectrin and that this is essential for egress (Thomas et al., 2018).

#### 1.2.3.4.1.7 *Stomatin*

Stomatin was identified as an orthologue of human band 7 stomatin and is a member of a large protein family conserved in evolution. Evidence suggests that stomatin associates with detergent-resistant membranes (DRMs) and forms oligomers. The integral membrane protein stomatin is inserted into the newly formed PVM presumably within DRMs of rhoptries (Hiller et al., 2003).

#### 1.2.3.4.1.8 *Subtilisin-like serine protease 1 (SUB1)*

The essential subtilisin-like serine protease 1 (SUB1) is stored in exonemes during merozoite formation and is discharged into the PV lumen just prior to egress (Yeoh et al., 2007). Within the exonemes SUB1 maturation is controlled by plasmepsin X (Nasamu et al., 2017). In the PV lumen SUB1 directly cleaves a number of important merozoite surface and PV proteins, including the essential merozoite surface protein complex MSP1/6/7 and members of the SERA family (Kauth et al., 2006; Koussis et al., 2009; Li et al., 2002; Silmon de Monerri et al., 2011; Yeoh et al., 2007).

### 1.2.3.5 **Protein Export and Host Cell Remodelling**

Protein export is an essential mechanism to traffic proteins beyond the PV compartment in order to induce host cell modifications (Beck et al., 2014). The exportome is predicted to account for 5-10% of all *P. falciparum* proteins (Spielmann and Gilberger, 2015). Proteins that are destined for the PV and beyond enter the secretory pathway either through a N-terminal signal peptide (SP) or through other export signals and are sorted for export by

their *Plasmodium* export element (PEXEL) with the amino acid consensus sequence RxLxE/Q/D (Hiller et al., 2004; Marti et al., 2004). However, the exportome also contains PEXEL-negative exported proteins (PNEPs) (Heiber et al., 2013). Within the ER, cleavage of the SP by signal peptidase complex and cleavage of the PEXEL motif by aspartic protease plasmepsin V (Boddey et al., 2010; Chang et al., 2008; Russo et al., 2010) takes place. The processed proteins follow the classical secretory pathway and are further trafficked to the rudimentary single membrane-bound Golgi apparatus (Struck et al., 2005). Vesicles bud from the *trans*-Golgi into different destinations e.g. retrograde transport from the Golgi back to the ER mediated by SDEL retrieval signals (Kulzer et al., 2009), to the digestive vacuole, apical organelles, mitochondria, apicoplast and to the PV compartment, where the vesicles fuse with the PPM (Deponate et al., 2012). It is thought that transmembrane (TM) proteins first end up in the PPM and that the soluble vesicle content is released into the PV lumen (Deponate et al., 2012; Gruring et al., 2012). PEXEL-positive proteins as well as PNEPs are translocated via PTEX in an unfolded state (Gehde et al., 2009; Gruring et al., 2012; Heiber et al., 2013). However, the mechanism of TM protein extraction from the PPM as well as the exact trafficking mechanism for PVM proteins are still a matter of debate (Spielmann and Gilberger, 2015).

Once in the host cell the exported proteins are trafficked further to their final destination to induce host cell modifications in the RBC cytosol, cytoskeleton or surface or in parasite induced membranous structures - the Maurer's clefts (Gruring et al., 2011) - presumably in a chaperone mediated non-vesicular manner (Gruring et al., 2012). These chaperone-protein complexes that also contain cholesterol were termed J-dots (Kulzer et al., 2012; Kulzer et al., 2010). Maurer's clefts are implicated in protein sorting as several proteins, including erythrocyte membrane protein 1 (EMP1), proteins of the subtelomeric variable open reading frame (STEVOR), members of the *Plasmodium* helical interspersed subtelomeric (PHIST) family and knob-associated histidine-rich protein (KAHRP) are detected at the Maurer's clefts before reaching their final destination - the RBC membrane (McMillan et al., 2013; Mundwiler-Pachlatko and Beck, 2013; Oberli et al., 2014; Wickham et al., 2001). In a knockout of the Maurer's cleft resident skeleton binding protein 1 (SBP1) it was shown that SBP1 is essential for EMP1 display on the RBC surface (Cooke et al., 2006). Normally, EMP1 is concentrated in parasite-induced knob structures, where the extracellular N-terminal part is implicated in cytoadhesion a major factor for parasite virulence (Hviid and Jensen, 2015; Maier et al., 2008).

#### **1.2.3.6 Egress – Leaving the Host Cell behind**

After completing their development inside the PV the progeny parasites within a segmented schizont need to egress from their host cell. Egress is an essential and highly orchestrated multistage process, including membrane permeabilization, first of the PVM

and second by cytoskeletal breakdown and rupture of the host cell membrane with the final explosive release of merozoites to invade new RBCs (Figure 7).

The master regulator of egress is cGMP-dependent protein kinase (PKG) that activates proteases and other effectors and can be inhibited by compound 1 and 2, resulting in mature schizonts unable to egress (Taylor et al., 2010). Downstream of PKG acts the calcium-dependent protein kinase 5 (CDPK5), which is expressed in invasive merozoites that also arrest as mature schizonts if CDPK5 is inactivated (Dvorin et al., 2010; Glushakova et al., 2013). However, the PVM is already permeabilized before PKG triggers PVM rupture and breakdown into multi-layered vesicles (Hale et al., 2017). The rupture of the PVM is SUB1 dependant, which is released by exonemes minutes before egress into the PV (Yeoh et al., 2007). SUB1 cleaves multiple substrates including SERA6, inducing a proteolytic cascade (Ruecker et al., 2012). However, SERA6 is not required for PVM rupture but for the disassembly of the RBC cytoskeleton by targeting and cleaving  $\beta$ -spectrin (Thomas et al., 2018). In addition SUB1-processed MSP1 has a spectrin-binding function that enables parasite egress from RBCs (Das et al., 2015). Parasite egress is not dependant on the actin-myosin motor complex (Perrin et al., 2018).

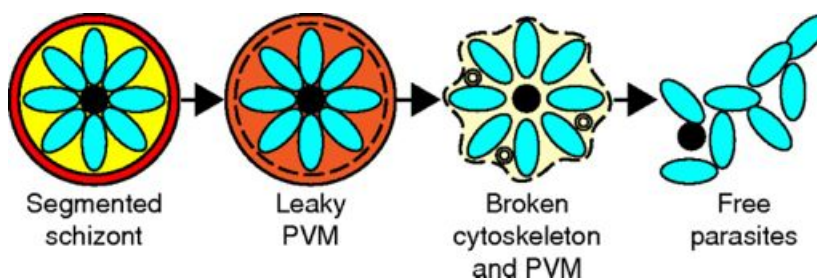


**Figure 7: Steps in egress**

Graphic model of parasite egress from the host RBC: The mature segmented schizont induces PVM permeabilization before multilamellar vesicles are formed during PVM rupture. Next, the cytoskeleton is disassembled and loses mechanical integrity. The RBC membrane becomes porous before parasites are released (Hale et al., 2017).

### 1.3 BioID enables Compartment-specific *in-vivo* Biotinylation

In order to identify the protein content of specific compartments BioID can be a method of choice. BioID makes use of the promiscuous biotin ligase BirA\* (a mutated R118G version of *Escherichia coli* BirA (Choi-Rhee et al., 2004)) that identifies proximal and interacting proteins (Roux et al., 2012). BirA\* can be fused to a bait protein that confers compartment-specific BirA\* expression and biotinylation of compartment-specific proteins over time in living cells. Simple and selective isolation of biotin-labelled proteins by conventional biotin capture methods and subsequent protein identification using mass spectrometry (MS) analysis are advantages of the method. Proteins identified by BioID represent direct as well as indirect interactors and vicinal proteins that do not physically interact with the bait protein. So far BioID has been widely used to study protein-protein associations in compartments, like among others the nuclear envelope (Kim et al., 2014),

centrosomes (Firat-Karalar et al., 2014), cell-cell junctions (Van Itallie et al., 2014) and also to identify the interplay between host and virus, like HIV (Le Sage et al., 2015) or herpes virus (Lajko et al., 2015) and in microorganisms, like *Chlamydia* (Mojica et al., 2015), *Toxoplasma* (Chen et al., 2015), *Trypanosoma* (McAllaster et al., 2015; Morriswood et al., 2013) and most recently *Plasmodium* (Kehrer et al., 2016; Khosh-Naucke et al., 2017; Schnider et al., 2018).

Improvement of the method has been made by the introduction of a smaller biotin ligase BioID2 for BioID proximity labelling that enables more-selective targeting of fusion proteins, requires less biotin supplementation, and exhibits enhanced labelling of proximate proteins (Kim et al., 2016). This study also showed that the biotinylation range of BioID2 can be modulated using flexible linkers, thus enabling application-specific adjustment of the biotin-labelling radius.

#### **1.4 Genome Editing via Selection-Linked Integration in *P. falciparum***

The *P. falciparum* genome is one of the most AT-rich genomes among eukaryotes (GC-content of *P. falciparum*: 19.34%) and is separated into 14 chromosomes, encoding about 5,300 genes (Gardner et al., 2002). Additionally, *Plasmodium* spp. have a linear mitochondrial genome and a circular genome within the apicoplast.

Genome editing in *P. falciparum* can be achieved by single crossover homologous recombination of a genome targeting region on an episomal expressed plasmid. However, single crossover homologous recombination is a rare event. The introduction of selection markers (de Koning-Ward et al., 2001; Fidock and Wellems, 1997; Mamoun et al., 1999) fuelled the development of a genetic system to study *P. falciparum* protein function that is based on the positive selection of integration events due to single crossover homologous recombination in the genome (Birnbaum et al., 2017). The selection-linked integration (SLI) system can be used to endogenously tag proteins of interest to study protein location within the parasite or to disrupt target genes of interest (SLI-TGD) to study protein essentiality for parasite growth as previously described (Crabb et al., 1997; Webster and McFadden, 2014).

The SLI system can also be used in combination with other genome editing methods e.g. for the introduction of loxP sites, flanking a gene of interest that can be recognized by Cre recombinase, which shows efficiency in *P. falciparum* and depending on the orientation of the targeting sequences either removes or inverts the region of interest (O'Neill et al., 2011). Inducibility of the system can be achieved by the use of a split Cre recombinase (diCre) that dimerizes upon the addition of a small ligand – usually rapamycin (Andenmatten et al., 2013; Jullien et al., 2007).

However, there are also genome editing systems for *P. falciparum* available that do not require insertion of target sites, like the use of Zinc-finger nucleases (ZFN) (Straimer et

al., 2012) or the use of clustered regularly interspaced short palindromic repeats (CRISPR) identified by the RNA-guided (CRISPR)-Cas9 system (Ghorbal et al., 2014; Wagner et al., 2014) that are reviewed elsewhere (Webster and McFadden, 2014).

### **1.5 Aim of this Work**

The interface between the parasite and the host cell, the PV compartment, fulfils diverse functions, like acquisition of nutrients, disposal of waste products, protein export into the host cell, maintenance of the PV milieu, and the introduction of signalling cascades. However, to date only a comparably small number of proteins of this compartment are known and only a few functions are assigned.

The aim of this thesis is to close this gap and to identify novel proteins within the PV compartment using BioID, which enables compartment-specific biotinylation and subsequent purification of target proteins from living cells. The identified proteins will be localized to validate them as true positive PV proteins and will be tested for their essentiality followed by functional analysis of selected proteins using novel genome editing methods.

## 2 Material and Methods

### 2.1 Material

Materials used in this thesis are listed below. If not noted otherwise the materials were purchased from Germany.

#### 2.1.1 Antibodies

**Table 1: Primary antibodies**

Antigen	Origin	IFA	WB	Source
Aldolase	rabbit	-	1:4000	(Nyalwidhe and Lingelbach, 2006)
ETRAMP2	rabbit	1:500	-	(Spielmann et al., 2003)
ETRAMP5	mouse	1:400	-	(Spielmann et al., 2006)
GFP-tag	mouse	1:500	1:1000	Roche, Switzerland
HA-tag	rat	1:500	1:2000	Roche, Mannheim
myc-tag	rabbit	1:200	1:500	Cell Signaling Technology, USA
SBP1	rabbit	1:1000	1:4000	(Heiber et al., 2013)

**Table 2: Secondary antibodies for IFA**

Antigen	Conjugate	Origin	Dilution	Source
Mouse	Alexa488	Goat	1:2000	Life Technologies, USA
	Alexa594	Goat		
	Alexa647	Donkey		
Rabbit	Alexa488	Donkey	1:2000	Invitrogen, Molecular Probes
	Alexa594	Donkey		
	Alexa647	Goat		Life Technologies, USA
Rat	Alexa594	Goat	1:2000	Invitrogen, Molecular Probes

**Table 3: Secondary antibodies for WB**

Antigen	Conjugate	Origin	Dilution	Source
Mouse	HRP	Goat	1:3000	Dianova, Hamburg
Rabbit		Donkey	1:2500	
Rat		Goat	1:3000	

**Table 4: Streptavidin conjugates**

Conjugate	Application	Dilution	Source
Alexa594	IFA	1:1000	Invitrogen, Molecular Probes
HRP	WB	1:5000	Thermo Scientific
Sepharose beads	Purification	100 µl slurry / 1 ml lysate	GE Healthcare life science

### 2.1.2 Bacterial and Plasmodium strains

*Escherichia coli* XL-10 Gold

Tetr  $\Delta$ (mcrA)183  $\Delta$ (mcrCB-hsdSMRmrr) 173  
endA1 supE44 thi-1 recA1 gyrA96 relA1 lac  
Hte [F'proAB lacIq Z  $\Delta$ M15 Tn10 (Tetr) Amy  
Camr]

*Plasmodium falciparum* 3D7

Clone of NF54 isolate (MRA-1000) from a  
malaria patient near the Amsterdam airport,  
Netherlands

### 2.1.3 Buffer, medium and stock solutions

**Table 5: Buffer, medium and stock solutions for agarose gel**

Agarose gel	1% agarose (w/v) in 1x TAE
6x Loading dye	40 % (v/v) Glycerol 2.5 % (w/v) Xylene cyanol 2.5 % (w/v) Bromophenol blue in dH <sub>2</sub> O
50x TAE buffer	2 M Tris base 1 M pure acetic acid 50 mM EDTA in dH <sub>2</sub> O, pH 8.5

**Table 6: Buffer, medium and stock solutions for Gibson assembly**

Assembly master mixture (1.2 ml)	320 µl 5x isothermal reaction buffer 0.64 µl 10 U/µl T5 exonuclease 20 µl 2 U/µl Phusion DNA polymerase 160 µl 40 U/ µl Taq DNA ligase ad 1.2 ml dH <sub>2</sub> O
----------------------------------	--

5x isothermal reaction buffer (6ml)	3 ml 1 M Tris-HCl, pH 7.5 150 µl 2 M MgCl <sub>2</sub> 60 µl of each 100 mM dNTP (A/C/G/T) 300µl 1M DTT 1.5 g PEG-8000 300 µl 100 mM NAD in dH <sub>2</sub> O
-------------------------------------	---

**Table 7: Buffer, medium and stock solutions for Western blot**

Ammonium persulfate (APS)	10% (w/v) in dH <sub>2</sub> O
Blocking solution for WB	5% milk powder (w/v) in PBS
Blocking solution for streptavidin-WB	5% milk powder (w/v) in TBS
Dilution buffer for streptavidin-WB	1% milk powder (w/v) in TBST
Lysis buffer for WB	4% SDS 0.5% Triton X-100 0.5 x PBS in dH <sub>2</sub> O
Saponin lysis buffer	0.03% (w/v) Saponin in DPBS
10x SDS running buffer	250 mM Tris base 1.92 M Glycine 1 % (w/v) SDS in dH <sub>2</sub> O
6 x SDS sample buffer	375 mM Tris HCl, pH 6.8 12% (w/v) SDS 60% (v/v) Glycerol 0.6 M DTT 0.06% (w/v) Bromophenol blue
Separating gel buffer	1.5 M Tris-HCl, pH 8.8
Separating gel	<u>12% gel</u> 2.5 ml separating gel buffer 4.2 ml H <sub>2</sub> O 3 ml Acrylamide (40%) 100 µl SDS (10%) 100 µl APS (10%) 4 µl TEMED  <u>10% gel</u> 2.5 ml separating gel buffer 4.7 ml dH <sub>2</sub> O 2,5 ml Acrylamide (40%) 100 µl SDS (10%) 100 µl APS (10%) 4 µl TEMED
Stacking gel buffer	1 M Tris-HCl, pH 6.8

Stacking gel	0.75 ml stacking gel buffer 4.35 ml dH <sub>2</sub> O 750 µl Acrylamide (40%) 60 µl SDS (10%) 60 µl APS (10%) 6 µl TEMED
Substrate solution for WB	0.5 ml Luminol/Enhancer Solution 0.5 ml Peroxide Solution
10x TBS	20 mM Tris-HCl 140 mM NaCl, pH 7.5
TBST	0.1% Tween-20 (v/v) in TBS
Western-transfer buffer	100 ml 10x SDS running buffer 200 ml Methanol 700 ml dH <sub>2</sub> O

**Table 8: Buffer, medium and stock solutions for mass spectrometry**

Buffer A	0.1% formic acid (FA) in HPLC-H <sub>2</sub> O
Buffer B	0.1% FA in acetonitrile (ACN)
Elution buffer	70% ACN 0.1% trifluoroacetic acid (TFA) in HPLC-H <sub>2</sub> O
LC-MS-wash buffer	0.1% TFA in HPLC-H <sub>2</sub> O
MS-lysis buffer	50 mM Tris-HCl, pH 7.4 500 mM NaCl 0.2% SDS (w/v) 2% Triton X-100 1 mM DTT
MS-wash buffer	50 mM Tris-HCl (pH 7.4) 150 mM NaCl

**Table 9: Buffer, medium and stock solutions for parasite and bacteria culture**

Ampicillin	50 mg/ml in 50 % Ethanol
Blasticidin S (BSD)	5 mg/ml BSD in medium, sterile filtered
Bodipy-TR-C5-ceramide	5 µM in 1xPBS, sterile filtered
Concanavalin-A	0.5 mg/ml in H <sub>2</sub> O
DAPI	1 µg/ml

DHE	<u>Stock solution (10x)</u> 5 mg DHE in 1 ml DMSO  <u>Working solution (1x)</u> 0.5 mg DHE in 1 ml DMSO
DSM1	<u>Stock solution (50x)</u> 187.5 mM DSM1 in DMSO  <u>Working solution (1x)</u> 100 µl DSM1 stock solution ad 5 ml 95% DMSO / 5% 1x PBS
FACS stopp Buffer	0.5 µl Glutaraldehyde in 40 ml medium
Fixing solution	2 ml 10% formaldehyde 1,5 µl 25% glutaraldehyde 500 µl 10x PBS ad 5 ml H <sub>2</sub> O
Freezing solution	37.8 g D-Sorbitol 8.1 g NaCl 350 ml Glycerol ad 1 l H <sub>2</sub> O, sterile filtered
G418 (neomycin)	50 mg/ml in medium, sterile filtered
Giemsa solution	0.42 g KH <sub>2</sub> HPO <sub>4</sub> 1.572 g Na <sub>2</sub> HPO <sub>4</sub> x 2H <sub>2</sub> O ad 1 l dH <sub>2</sub> O, pH 7.2
Glycerol freezing solution	50 % (v/v) glycerol in 1x LB medium
Hoechst 33342	<u>Stock solution (10x)</u> 4.5 mg Hoechst 33342 in 1 ml DMSO  <u>Working solution (1x)</u> 0.45 mg Hoechst 33342 in 1 ml DMSO
LB medium	<u>Stock solution</u> 10 % (w/v) NaCl 5 % (w/v) Peptone 10 % (w/v) yeast extract in dH <sub>2</sub> O, autoclaved  <u>1 x LB medium</u> 1:10 dilution of stock 1:1000 Ampicillin in dH <sub>2</sub> O

Medium for parasite culture	<p>1.587 % (w/v) RPMI 1640  12 mM NaHCO<sub>3</sub>  6 mM D-Glucose  0.5 % (v/v) Albumax II  0.2 mM Hypoxanthine  0.4 mM Gentamycin  pH 7.2, sterile filtered</p>
Percoll	<p><u>Stock solution</u>  90% (v/v) Percoll  10% (v/v) 10 x PBS</p> <p><u>80% Percoll solution</u>  89% (v/v) Percoll stock solution  11% (v/v) RPMI complete medium  4% (w/v) sorbitol, sterile filtered</p> <p><u>60% Percoll solution</u>  67% (v/v) Percoll stock solution  33% (v/v) RPMI complete medium  4% (w/v) sorbitol, sterile filtered</p> <p><u>40% Percoll solution</u>  44% (v/v) Percoll stock solution  56% (v/v) RPMI complete medium  4% (w/v) sorbitol, sterile filtered</p>
Rapalog (AP21967)	<p><u>Stock solution (20x)</u>  5 mM in ethanol</p> <p><u>Working solution (1x)</u>  1:20 dilution of stock solution  in medium, sterile filtered</p>
Synchronization solution	<p>5% (w/v) D-Sorbitol  in dH<sub>2</sub>O, sterile filtered</p>
TE buffer	<p>10 mM TrisHCl  1 mM EDTA, pH 8</p>
Thawing solution	<p>3.5% NaCl  in dH<sub>2</sub>O, sterile filtered</p>
Transfection buffer (Amaxa)	<p>90 mM Na<sub>2</sub>PO<sub>4</sub>  5 mM KCl  0.15 mM CaCl<sub>2</sub>  50 mM HEPES  pH 7.3, sterile filtered</p>

Transfection buffer (Cytomix)	120 mM KCl 150 $\mu$ M CaCl <sub>2</sub> 2 mM EGTA 5 mM MgCl <sub>2</sub> 10 mM K <sub>2</sub> HPO <sub>4</sub> /KH <sub>2</sub> PO <sub>4</sub> 25 mM HEPES, pH 7.6, sterile filtered
WR99210	<u>Stock solution</u> 20 mM in 1 ml DMSO  <u>Working solution</u> 1:1000 dilution of stock in RPMI complete medium

### 2.1.4 Chemicals

Acetic acid	Roth, Karlsruhe
Acrylamide/Bisacrylamide solution (40%)	Roth, Karlsruhe
Agar LB (Lennox)	Roth, Karlsruhe
Agarose	Invitrogen, USA
Albumax II	Gibco, Life Technologies, USA
Albumin bovine Fraction V (BSA)	Biomol, Hamburg
Ammonium persulfate (APS)	Applichem, Darmstadt
Ampicillin	Roche, Mannheim
Bacto™ Pepton	BD, USA
Bacto™ yeast extract	BD, USA
Biotin	Sigma, Steinheim
Blasticidin S (BSD)	Invitrogen, Karlsruhe
Bromophenol blue	Merck, Darmstadt
Calcium chloride (CaCl <sub>2</sub> )	Sigma, Steinheim
Concanavalin A G-250	Sigma, Steinheim
Desoxynucleotides (dNTPs)	Thermo Scientific
4',6-diamidino-2-phenylindole (DAPI)	Roche, Mannheim
Dihydroethidium (DHE)	Cayman, Ann Arbor, USA
Dimethyl sulfoxide (DMSO)	Sigma, USA
Dipotassium phosphate	Merck, Darmstadt
Disodium phosphate	Roth, Karlsruhe
1,4,-dithiothreitol (DTT)	Roche, Mannheim
DSM1	BEI resources
Ethanol	Roth, Karlsruhe

Ethidium bromide	Sigma, Steinheim
Ethylenediaminetetraacetic acid (EDTA)	Biomol, Hamburg
G418 disulfate salt	Sigma Aldrich, Steinheim
Gentamycin	Ratiopharm, Ulm
Giemsa's azure, eosin, methylene blue solution	Merck, Darmstadt
D-Glucose	Merck, Darmstadt
Dulbecco's Phosphate Buffered Saline (DPBS)	Pan Biotech, Aidenbach
Glutardialdehyd (25 %)	Roth, Karlsruhe
Glycerol	Merck, Darmstadt
Glycine	Biomol, Hamburg
Hoechst33342	Cheomdex, Switzerland
Human red blood cells Sterile, concentrate; bloodgroup O <sup>+</sup>	Blood bank, Universitätsklinikum Eppendorf (UKE), Hamburg
(4-(2-Hydroxyethyl)-1-piperazineethanesulfonicacid) (HEPES)	Roche, Mannheim
Hydrochloric acid (HCl)	Merck, Darmstadt
Hypoxanthin	Sigma, Steinheim
Isopropanol	Roth, Karlsruhe
Magnesium chloride (MgCl <sub>2</sub> )	Merck, Darmstadt
Manganese(II) chloride (MnCl <sub>2</sub> )	Merck, Darmstadt
β-Mercaptoethanol	Merck, Darmstadt
Methanol	Roth, Karlsruhe
Milk powder	Roth, Karlsruhe
Paraformaldehyde (PFA)	Polyscience, Warrington, USA
Percoll	GE Healthcare, Sweden
Phenylmethylsulfonylfluorid	Sigma Aldrich, Steinheim
Potassium chloride	Merck, Darmstadt
Protease inhibitor cocktail ("Complete Mini")	Roche, Mannheim
Rapalog (A/C Heterodimerizer AP21967)	Clontech, Mountain View, USA
Rubidium chloride	Sigma Aldrich, Steinheim
RPMI medium	Appllichem, Darmstadt
Saponin	Sigma, Steinheim
Sodium acetate	Merck, Darmstadt
Sodium bicarbonate	Sigma, Steinheim
Sodium chloride	Gerbu, Gaiberg

Sodium dihydrogen phosphate	Roth, Karlsruhe
Sodium dodecyl sulfate (SDS)	Applichem, Darmstadt
Sodium hydroxide	Merck, Darmstadt
Sorbitol	Sigma, Steinheim
N, N, N, N-Tetramethylethylenediamin (TEMED)	Merck, Darmstadt
Tris base	Roth, Karlsruhe
Tris-EDTA (TE)	Invitrogen, Karlsruhe
Triton X-100	Biomol, Hamburg
Tween-20	Sigma, Steinheim
Water for molecular biology (Ampuwa)	Fresenius Kabi, Bad Homburg
WR99210	Jacobus Pharmaceuticals, Washington, USA

### 2.1.5 Commercial Kits

Clarity™ Western ECI Substrate kit	BioRad
NucleoSpin® Gel and PCR Clean-up kit	Macherey-Nagel
NucleoSpin® Plamid	Macherey-Nagel
QIAamp DNA Mini Kit	Quiagen, Hilden
QIAGEN Plasmid Midi Kit	Quiagen, Hilden

### 2.1.6 DNA-and protein-ladders

GeneRuler™ 1 kbp ladder	
PageRuler™ prestained protein ladder	Thermo Scientific, Schwerte
PageRuler™ plus prestained protein ladder	

### 2.1.7 Enzymes

T4 DNA-ligase [3 U/μl]	NEB, Ipswich, USA
Taq DNA-ligase [40 U/μl]	NEB, Ipswich, USA
FIREPol® [5 U/μl]	Solis Biodyne, Taipei, Taiwan
Phusion® High-Fidelity [2 U/μl]	NEB, Ipswich, USA

#### 2.1.7.1 Restriction enzymes

All restriction enzymes were purchased from New England Biolabs, Ipswich, USA. Some restriction enzymes were available as high fidelity restriction enzymes that have 100% activity in CutSmart buffer.

**Table 10: Restriction enzymes**

<b>Name</b>	<b>Recognition site</b>	<b>Buffer</b>
AvrII	5'-CCTAGG-3'	Cut Smart
BglII	5'-AGATCT-3'	NEB 3.1
BamHI	5'-GGATCC-3'	NEB 3.1
BsiWI	5'-CGTACG-3'	NEB 3.1
BstEII	5'-GGTNACC-3'	NEB 3.1
DpnI	Methylated 5'-GATC-3'	Cut Smart
EcoRI	5'-GAATTC-3'	NEB 2.1
EcoNI	5'-CCTNNNNNAGG-3'	Cut Smart
KpnI	5'-GGTACC-3'	NEB 1.1
MluI	5'-ACGCGT-3'	NEB 3.1
NheI	5'-GCTACG-3'	Cut Smart
NotI	5'-GCGGCCGC-3'	NEB 3.1
PstI	5'-CTGCAG-3'	NEB 3.1
Sall	5'-CTCGAG-3'	NEB 3.1
SpeI	5'-ACTAGT-3'	Cut Smart
T5 exonuclease	5'-3' exonuclease	-
XhoI	5'-CTCGAG-3'	Cut Smart
XmaI	5'-CCCGGG-3'	Cut Smart

### 2.1.8 General equipment

The equipment used in this work belongs to or was purchased by the Bernhard-Nocht-Institute for tropical medicine.

#### 2.1.8.1 Laboratory equipment

Agarose gel chamber	BioRad, München
Analytical balance (870)	Kern
Blotting device	BioRad, München
Centrifuge (5415D)	Eppendorf, Hamburg
Centrifuge (JA-12/14)	Beckman Coulter, Krefeld
Centrifuge (Magafuge 1.0R)	Heraeus, Hannover

ChemiDoc™ XRS	Biorad
Clean bench (Sterile Guard III Advance)	Baker, Stanford, USA
Clean bench (Safe 2020)	Thermo Scientific
Flow cytometer (LSR II)	BD Biosciences, Heidelberg
Fluorescence Microscope (Axioscope 1)	Zeiss, Jena
Hemocytometer	Marienfeld, Lauda-Königshofen
Ice machine (EF 156 easy fit)	Scotsman, Venon Hills, USA
Incubator (Heracell150)	Thermo Scientific
Laboratory scale	Acculab Sartorius, Göttingen
Light Microscope (Axio Lab A1)	Zeiss, Jena
Microscope digital camera (Orca C4742-95)	Hamamatsu, Phototonics K.
Micropipettes (10/200/1000 µl)	Gilson, Middleton, USA
Microwave	Whirlpool, China
Multifuge (X3R Heraeus)	Thermo Scientific
Nanodrop 2000	Thermo Scientific
pH meter (WTW pH537)	Labotec, Wiesbaden
Pipetting aid (Pipetboy acu)	IBS, USA
Power supply (Powerpac 300)	Bio-Rad, Munich
Roller mixer (STR6)	Stuart
Thermoblock	Eppendorf, Hamburg
Thermocycler (epgradient)	Eppendorf, Hamburg
Thermomixer (5436)	Eppendorf, Hamburg
Thermomix MM	B Braun, Melsungen
Vacuum pump (BVC Contorl)	Vacuubrand
Vortexer (Genie 2)	Scientific Industries, USA
Water bath (1083)	GFL, Burgwedel
Water purification system (MilliQ)	Millipore, Bedford, USA

### 2.1.8.2 Glass- and plastic equipment

Cell culture flasks (75 cm <sup>2</sup> )	Greiner, Frickenhausen
Cell culture plates (6-well, 12-well)	Greiner, Frickenhausen
Cryotubes (1.5 ml)	Nunc, Roskilde, Denmark
Coverslip (24x65 mm)	R. Langenbrick, Emmerdingen
Disposable gloves	Kimberly-Clark, Roswell, USA
FACS-tubes	Sarstedt, Nümbrecht
Falcon tubes (15 ml, 50 ml)	Sarstedt, Nümbrecht
Filter tips (10/200/1000 µl)	Sarstedt, Nümbrecht
Eppendorf tubes (0.5 ml; 1.5 ml; 2 ml)	Sarstedt, Nümbrecht

IFA glass slide (10 well, 6.7 mm)	Thermo Scientific, USA
Leukosilk	BSN medical
Magnetic columns	Miltenyi Biotech, Bergisch Gladbach
Microscopy slides	Engelbrecht, Edermünde
Nitrocellulose membrane (0.45 µm)	GE Healthcare
Parafilm	Pechiney, Menasha, USA
Pasteur pipettes	Brand, Wertheim
PCR tubes	Sarstedt, Nümbrecht
Petri dishes (15x60/14x90 mm)	Sarstedt, Nümbrecht
Plastic pipettes (5/10/20 ml)	Sarstedt, Nümbrecht
Sterile filter (0.22 µm)	Sarstedt, Nümbrecht
Transfection cuvettes (0.2 cm)	BioRad, München

### 2.1.9 Oligonucleotides

Oligonucleotides were designed according to their purpose and purchased from Sigma Aldrich.

**Table 11: List of primers**

<b>SP-GFP-BirA*</b>	<b>5'-3'</b>
KpnI-PF08_0004_fw	GATAggtaccATGAAGAATAAACTTTCTACATTATTTTTTATTACAATTTTT CTTATTCTGATTTTTATTGATTCAGCAAAGG
PF08_0004-d1+2-linker-AvrII_rev	ATATcctaggaccggcaccggctcctgcaccagcaccggctcctgcaccagcGTTTTCACCT TCTTTTTTAATAGGG
<b>Knock-in</b>	<b>5'-3'</b>
NotI_1123500_forw	cactatagaataactcgcgccgcTAACCACATGGTGTAATCATTGTTG
1123500_AvrII_rev	GATCTTGATCTCAATCCTGAcctaggTCTATGTAATTTATGTTGTCTGAAC
NotI_1226900_forw	cactatagaataactcgcgccgcTAACCATCTAGCTGTTGTTGATAC
1226900_AvrII_rev	GATCTTGATCTCAATCCTGAcctaggATTTTCCGTAATATAATTTTGCAC
NotI_1013300_forw	cactatagaataactcgcgccgcTAACCCAACCACAAAATGTACAAGC
1013300_AvrII_rev	GATCTTGATCTCAATCCTGAcctaggTGCTGCTTTTATTTTGTTTTTATAAA AC
NotI_1464600_forw	cactatagaataactcgcgccgcTAAGAATCTCATAGAATTAATTG
1464600_AvrII_rev	GATCTTGATCTCAATCCTGAcctaggCCTTGATATTCTATTAAGGGAATC
<b>SLI</b>	<b>5'-3'</b>
NotI_0912400_forw	cactatagaataactcgcgccgcTAACCAATCACATAATTAACGAG
0912400_AvrII_rev	GATCTTGATCTCAATCCTGAcctaggTTCATCCTTTGTTTTGTGTCG
NotI_1135400_forw	CTCGgcgccgctaaAAATTTTTTCTGTTTTATTCCTAATAC
1135400_AvrII_rev	TCCTcctaggGCAAATAAATTAATTAACTC
NotI_1462300_forw	cactatagaataactcgcgccgcTAAGGATATATATTGTGCAAATGAAG
1462300_AvrII_rev	GATCTTGATCTCAATCCTGAcctaggATCCAAATATGATCTTCTCTG
NotI_1024800_forw	CTCGgcgccgcTAAGACAACCTTCACAACCAAAGATGTTG

1024800_Avrll_rev	TCCTcctaggAGAACTTAACCATGGAGCTGGTATTCC
Notl_0629200_forw	cactatagaataactcgcgccgcTAAGGATGAAGATCCAAGTGATC
0629200_Avrll_rev	GATCTTGATCTCAATCCTGAcctaggTAACAAATCTGCAAGTACC
Notl_1352500_forw	cactatagaataactcgcgccgcTAACCTGGTTTATCAAATTTTATGC
1352500_Avrll_rev	GATCTTGATCTCAATCCTGAcctaggATCCTTTTTCTTAGCAACTTTTCG
Notl_1310500_forw	cactatagaataactcgcgccgcTAACGAATTTTTTTGTAAAAATTCTATGGAG
1310500_Avrll_rev	GATCTTGATCTCAATCCTGAcctaggTTTTATTGATTCTAAAAATCCG
NeoV_Notl_1350500_	cactatagaataactcgcgccgcTAAGATCAAAGTCCCTGTCATGTAAGGG
1350500_Avrll_Neo V_rev	GATCTTGATCTCAATCCTGAcctaggTTTCTCTGGTATCTCCATAAAAGAG
SLI_0220000_frw	cactatagaataactcgcgccgcTAAGATATAGATGAAGATATAGGTGAAGAC
SLI_0220000_rev	GATCTTGATCTCAATCCTGAcctaggTTTTGATTTTTGCGTTCTACTTTTT TCGG
SLI_0731600_frw	cactatagaataactcgcgccgcTAACACAAGGTGAGTATATCGAAACAG
SLI_0731600_rev	GATCTTGATCTCAATCCTGAcctaggTTTATTTAATTCTAATTCTTGGGAC
<b>IntCheck</b>	<b>5'-3</b>
1123500_3'UTR_rev	GAAAACATTTTATAAGCCTATG
1123500_forw	CAAGTGGTACAACAGCTCCTAG
1226900_3'UTR_rev	GCTTTAATATTATGGAAGATGTG
1226900_forw	GTATGGCCATTCCATTAGC
1013300_3'UTR_rev	CATGGATACATTTTCGTATG
1013300_forw	CGAATTTGTTATATGTCTAG
1464600_3'UTR_rev	GTTACTTTATATGAAGTTATG
1464600_forw	GGATCACTAAATGATGAGG
0912400_3' UTR rev	GACATAGAAATATATTATATGC
0912400_forw	ccacttttcagATATTTTCC
1135400_3'UTR rev	GTATTTATTTATTAATGTTTTTTAAAAG
1135400 forw	CTGGGTGTATACATAATAAATTGTTATG
1462300_3'UTR_rev	GTTATGGTTAACAAAAATTTG
1462300_forw	CCATTAGATGAATTAGTATTAC
1024800_3'UTR_rev	GTATGTGTCTCTTCAGTG
1024800_forw	GCAATGAAAGCATATGCTAGCGG
0629200_3'UTR_rev	GTGATATTATGACAAAAGGG
0629200_forw	GATCGTTATGGTTTAGAAGC
1352500_3'UTR_rev	CTACTGTGTAAATCATATAG
1352500_forw	GTCAACTGGAAATACTACTG
1310500_3'UTR_rev	GATGTCCCTTTTATCTATC
1310500_forw	CACTTAAATATATAATAGTTTG
1350500_forw	GCTTTCCAAAAATGTTTAATATTGG
3'UTR_1350500_rev	CTTTAAACAAATTGTATGGGTAAATAGG
0220000_3'UTR_rev	CGCTCCAATCATTTCACTCTTCTGC
0220000_forw	GGTTTGATATTAAGGATAAGGAACC

0731600_3'UTR_rev	CATATCGAAATTTTTCTTTCTCC
0731600_frw	GTGATAACAATAGTGAAAGTATGGG
<b>SLI-TGD</b>	<b>5'-3'</b>
TGD_1464600_forw	ctatagaataactcgcgccgctaaGAACAATATAATTACGACTGTGTTG
TGD_1464600_rev	GCAGCAGCACCTCTAGCacgcgtGTGTTCAAATTAATTAAATTATCTC
TGD_1123500_forw	ctatagaataactcgcgccgctaaGGTATACATAATGATAATACG
TGD_1123500_rev	GCAGCAGCACCTCTAGCacgcgtGTTAGTTGTTTGATTATTTGG
TGD_1226900_forw	ctatagaataactcgcgccgctaaCTGAGTGCCTTGTAAGGAGG
TGD_1226900_rev	GCAGCAGCACCTCTAGCacgcgtCATTAAAGGTAATGGATTATAAAATTG
TGD_0629200_forw	ctatagaataactcgcgccgctaaATTTTCAAAAATTATTGAAATGG
TGD_0629200_rev	GCAGCAGCACCTCTAGCacgcgtCATATTCTTGCAGCTTCTAAACC
TGD_1135400_forw	CTCGcgcggccgctaaAAATTATCATCAGGAACCTCACC
TGD_1135400_rev	TCCTacgcgtTGATTTCTCTTCATTATAATTTTTTAAAAG
TGD_1024800_forw	ctatagaataactcgcgccgctaaGAGCGTGTAGAGTTAAAGTTAAAC
TGD_1024800_rev	GCAGCAGCACCTCTAGCacgcgtCTTATCTTCGTTATCTAGATCTTCTTCG
TGD_1135400_frw	ctatagaataactcgcgccgctaaAAATTTTTTCTGTTTTATTCTTAATAC
TGD_1135400_rev	GCAGCAGCACCTCTAGCacgcgtGATATCAATATTTTTTACTACAAAC
TGD_1462300_forw	ctatagaataactcgcgccgctaaAATAAACTATTTTTTTTATGTTTCC
TGD_1462300_rev	GCAGCAGCACCTCTAGCacgcgtCCCTCTCCTTCTTCGATATTTCAATTTTC
TGD_1310500_forw	ctatagaataactcgcgccgctaaAATAATAAAAAACGAATTTTTTTTG
TGD_1310500_rev	GCAGCAGCACCTCTAGCacgcgtCACTTCAACATAATTTTATTAAATTC
TGD_1013300_forw	ctatagaataactcgcgccgctaaAAAATATATAGGAAAAGAGTAC
TGD_1013300_rev	GCAGCAGCACCTCTAGCacgcgtGTATAACATCTTTTTCTTTAATTAATC
TGD_1350500_forw	ctatagaataactcgcgccgctaaAAGAGGAAGAATATCCATGTATTCTTTTATC
TGD_1350500_rev	GCAGCAGCACCTCTAGCacgcgtCTGTTTTATAAATTGAAATATTAATTTTC
TGD_0220000_forw	ctatagaataactcgcgccgctaaCGTATGTAGATAAGAAATTGAATAAAC
TGD_0220000_rev	GCAGCAGCACCTCTAGCacgcgtCGTCATTAACCTGACTTTCTCCTCC
TGD_0731600_forw	ctatagaataactcgcgccgctaaAATATTTCAATTTACGGTGTGTAGC
TGD_0731600_rev	GCAGCAGCACCTCTAGCacgcgtCCAATTTATTGAATTACTACCATAC
TGD_0912400_forw	ctatagaataactcgcgccgctaaGGCCGATGTCAAGGCGATCAAG
TGD_0912400_rev	GCAGCAGCACCTCTAGCacgcgtCGCACCATTTCTTTTATATCTGAC
<b>IntCheck TGD</b>	<b>5'-3'</b>
1464600_5'UTR_frw	GTCTACCGAGGAAAGTGAAATAGC
1464600_rev	CAATTCATCAAAAATATCATACGAG
1226900_5'UTR_frw	CATGTGTTTATATATATAAACATATG
1226900_rev	GCTGTATTTGTTAAGGCTGTTATAC
1123500_5'UTR_frw	CTATTCCTGTTTTCTCCACTTTC
1123500_rev	CCATCACCATTATTATGTCCTTGAC
0629200_5'UTR_frw	GGCGTTTACTATATTCTGTAAG
0629200_rev	GATGAAGATCGTTATTTACTCTTTC
1135400 forw	CTGTTTTATTCTTAATAC

1135400_3'UTR_rev	GTAAACGTTCTCTCTAAATAG
1024800_5'UTR_frw	GTATGTATATACCTATATATGTATG
1024800_rev	GTTGATGTTCTCTATACTCATCTTC
5'UTR_1350500_frw	CATTTTGTGGTGGTAATATGG
1350500_rev	CATTCATCAATAGATTCTTCAGTC
0220000_5'UTR_frw	CCGAAGATATTATTATTTACAATTTG
0220000_rev	CAACACTTGAGGCTACACTTTCGTCCG
0731600_5'UTR_frw	GATAGGATATAGGCTTATTGAGAAC
0731600_rev	GATCACATAATGGTACTACAGTATTGTG
1462300_5'UTR_frw	GAAAACCAACAGTAGTAAAAGC
1462300_rev	CGACATTTGAAATCCAATCATCTG
1135400_5'UTR_frw	GTTTTTCTCTCTCTCATAAC
1013300_5'UTR_frw	CATACATATATATGTATGTATATTG
1013300_rev	CGTTTTTCTAATAAATCTTGACTAACC
1310500_5'UTR_frw	CAACAAAAAAGATATGAAAATG
<b>loxP 1464600</b>	<b>5'-3'</b>
1464600TGD_loxp_frw	gaatactGCGGCCGCCGGTAAGTTGTCTTTCTATTACCCTGTAAAG
1464600TGD_loxp_rev	CTGATATTAACCTTCTGCTCACTAGTGTGTTCAAATACTTAAATTATCTC
1464600codonad_frw	GTTGAAGAAAATCCAGGTCCACCTAGGATGAACATTCTTAACCTTATTCA
1464600codonad_rev	TTTGC
1464600codonad_n	GGGTACATGGTGGTACCCCGGGACGACTAATACGGTTTAAACTGTCC
1464600_BstEII_frw	GAGCTTATAGAGAGCCTTGGTTACCAGCC
1464600_1436-1461_frw	GAACGAGTACGTTGTTGGAAAGAAG
1464600_1436-1461_rev	CTTCTTTCCAACAACGTAACGTTTC
1464600_2888-2912_frw	CGACAACAGCTCAATGGGTCGTGG
1464600_2888-2912_rev	CCACGACCCATTGAGCTGTTGTCCG
1464600_186-209_frw	GACTACCTTGACGACAAGGGAAG
1464600_1112-1234_frw	CGTAGGATACGTACGTGAGAAC
1464600_2668-2690_frw	CAGACTGGATATTCGTAGTAGG
<b>1464600 compl.</b>	<b>5'-3'</b>
compl_NMD3_frw	CGTATATCATTTTAAAGATAACTCGAGATGAACATTCTTAACCTTATTCAT
1464600_compl_TY1_rev	TTGC
1464600_compl_NMD3_frw	CCTGGTTGGTGTGCACCTCCCTAGGACGACTAATACGGTTTAAACTG
1464600_compl_NMD3_frw	CGTATATCATTTTAAAGATAACTCGAGATGAACATTCTTAACCTTATTCAT
	TTG

1464600_compl_TY 1_rev	CCTGGTTGGTGTGCACCTCCCTAGGACGACTAATACGGTTTAAACTG
1464600_BsiWI_frw	GAGAACCGTACTAGTAACGTAGG
1464600_EcoNI_rev	CCTCCTCGTCGTTCTCTTCGTCG
1464600_D554N_re v	CTTCATTGACTGTACTGTTGACTTAAGCTCGTTGAATCCCATGAAATTG TATATGTTTTGTACATTGAAGTTCTTCTCCTCCTCGAATC
1464600_D584N	GATTCAACGAGCTTAAGTCAACAGTACAGTCAATGAAGAAGTGGCACC TTGAGAACAACGCTAACTTCGTAATAAACCTTGGAGATAAC
<b>Vector-specific</b>	<b>5'-3'</b>
pARL_55_frw	ggaattgtgagcggataacaatttcacacagg
GFP_85_rev	ACCTTCACCCTCTCCACTGAC
Neo 40_rev	CGAATAGCCTCTCCACCCAAG
2xmyc-as	TAAATCTTCTTCGCTTATGAG

### 2.1.10 Software and tools

ApE (A plasmid Editor) v2.0.49

Axiovision v4.7

BLAST<sup>®</sup> Basic Local Alignment Search Tool

CorelDraw X7

Corel Photo-Paint X7

Endnote X7.2

FACS Diva v 6.1.3

FlowJo v10.0.7

Graphpad Prism Version v5.01

ImageLab Version v5.2.1

Microsoft Exel 2011

Microsoft Word 2011

PlasmoDB v24/v38

PlasmoGem

Proteome Discoverer v1.4.1.14

Signalp 3.0

TM Calculator

TMHMM Server v2.0

Zen v2.3

### 2.1.11 Vectors

**Table 12: Vectors used as backbones for this work**

Name	Resistance	Source
pARL1	WR99210	(Crabb et al., 2004)

pARL2	BSD	(Gruring et al., 2012)
pSLI-2xFKBP-GFP	WR99210/ G418	(Birnbaum et al., 2017)
pSLI-TGD-GFP	WR99210/ G418	
pARL1-SLI-TGD-loxP-3xHA	WR99210/ G418	(Mesén-Ramírez, Jakob Birnbaum unpublished)
pARL2yDHODH-Compl-Ty1	DSM1	
pSkipFlox	BSD	(Birnbaum et al., 2017)

## 2.2 Methods

### 2.2.1 Biochemical methods

#### 2.2.1.1 Immunofluorescence assay (IFA)

The first and most crucial step in IFAs is the fixation of parasites. Cells can be either fixed in suspension or on a 10 well, 6.7 mm glass slide (Thermo).

##### 2.2.1.1.1 IFA with cells in suspension

For IFAs in suspension cells were washed twice in PBS. Depending on the pellet size cells were resuspended in 0.5-1 ml of fixing solution and incubated for 30 min at RT. To remove the fixing solution cells were washed three times in PBS by centrifugation at 16000 rpm for 2 min. From this point cells can be stored in the fridge in PBS with 100 µg/ml ampicillin to prevent bacterial growth. For antibody staining an aliquot of fixated cell suspension was used and permeabilised with 0.1% Triton X-100 in PBS for 10 min at RT. Permeabilised cells were washed three times with PBS before cells were blocked with 3% BSA in PBS with 100 µg/ml ampicillin for 1 h at RT. Primary antibodies, in their respective dilution (Table 1) in 3% BSA in PBS with 100 µg/ml ampicillin, were applied on the cells (100 µL/tube) rolling over night at 4°C. For co-localisation two antibodies raised in different organisms were diluted together. The primary antibody was washed thoroughly for three times with PBS before secondary antibodies matching the organism of the primary antibody, in their respective dilution (Table 2) in 3% BSA in PBS with 100 µg/ml ampicillin and 1 µg/ml DAPI, were applied (100 µL/tube) and incubated rolling for 1 h at RT. The secondary antibody was washed thoroughly for three times for 10 min with PBS before cells were stored in the fridge in 100 µL PBS with 100 µg/ml ampicillin. For microscopic analysis one drop of the cell suspension was placed on a slide with a coverslip on top.

##### 2.2.1.1.2 IFA with cells on a glass slide

For IFAs on a glass slide two different fixation protocols were used:

1) For acetone IFAs cells were washed in PBS and adjusted to a haematocrit of 2% in PBS. A thin monolayer of the suspension was placed on the wells of the glass slide, air-dried and fixed in 100% acetone for 30 min. In a humid chamber fixated slides were rehydrated and washed with PBS to remove haemoglobin until the monolayer seemed colourless. Primary antibodies, in their respective dilution (Table 1) in 3% BSA in PBS with 100 µg/ml ampicillin, were incubated on the wells (50 µL/well) for 1 h at RT. For co-localisation two antibodies raised in different organisms were diluted together. The primary antibody was washed thoroughly for 5 times with PBS before secondary antibodies matching the organism of the primary antibody, in their respective dilution (Table 2) or Streptavidin (Table 4) in 3% BSA in PBS with 100 µg/ml ampicillin and 1 µg/ml DAPI, were applied (50 µL/well) and incubated for 1 h at RT. The secondary antibody was washed thoroughly for 5 times with PBS before slides were air-dried. Mounting medium (Dako) was added between each well and a coverslip was placed on top, which was sealed with nail polish. Slides were stored in the fridge.

2) For wet-aceton IFAs cells were washed in PBS and adjusted to a haematocrit of 2% in PBS. Cells in suspension were immobilised on glass slides coated with ConcanavalinA (ConA) (Spielmann et al., 2003) for 15 min at RT. For the coating each well (20 µL/well) was incubated with 0.5 mg/ml ConA in dH<sub>2</sub>O in a humid chamber for 30 min at 37 °C. ConA was washed several times with PBS before the cell suspension was applied. Immobilised cells were washed with PBS to remove unbound cells, tilted to remove excess liquid and fixated in 100% acetone for 30 min. In a humid chamber fixated slides were rehydrated and washed with PBS. Cells were permeabilised with 0.5% Triton X-100 in PBS for 10 min at RT and washed with PBS to remove haemoglobin until the monolayer seemed colourless. Cells were blocked with 3% BSA and 0.1% Triton X-100 in PBS for 10 min at RT. For wet-aceton IFAs primary antibody concentrations were doubled. Primary antibodies, in their respective doubled-concentration (Table 1) in 3% BSA and 0.1% Triton X-100 in PBS, were incubated on the wells (50 µL/well) for 1h at RT. For co-localisation two antibodies raised in different organisms were diluted together. The primary antibody was washed thoroughly for 5 times with PBS before secondary antibodies matching the organism of the primary antibody, in their respective dilution (Table 2) or Streptavidin (Table 4) in 3% BSA and 0.1% Triton X-100 in PBS and 1 µg/ml DAPI, were applied (50 µL/well) and incubated for 1 h at RT. The secondary antibody was washed thoroughly for 5 times with PBS before 75% glycerol in PBS with 100 µg/ml ampicillin was added between each well and a coverslip was placed on top, which was sealed with nail polish. Slides were stored in the fridge.

IFAs were imaged on a fluorescence microscopy Zeiss Axioscope M1 with a 63x and 100x/1,4 numerical aperture oil immersion lens.

### 2.2.1.2 Mass spectrometry

Proteins can be identified from mass spectrometry data. Large-scale cell culture (50-100 ml/sample) with a high parasitemia (5-10%) was used in order to get sufficient amounts of protein. Biotinylated proteins (section 2.2.1.2.1) were purified with streptavidin-coated beads and digested with trypsin in centrifuge filters. Peptides were desalted and applied for LC-MSMS measurement. Samples were ionized and separated according to their mass-to-charge ratio. Peptides with a unique mass-to-charge ratio were correlated to known data from PlasmoDBv24 (April 2015).

#### 2.2.1.2.1 Biotinylated protein purification

Biotinylated proteins were enriched with Streptavidin Sepharose™ High Performance beads (GE Healthcare). First, the bead slurry was equilibrated and washed three times with MS-lysis buffer under mild centrifugation (2 min at 1600 rpm). Approximately, 100 µl of equilibrated bead slurry was used for 1 ml of lysate. During constant rolling at 4 °C over night biotinylated proteins non-covalently bound to the streptavidin-coated beads. Notably, streptavidin and biotin have the strongest non-covalent biological interaction known. Beads were washed thoroughly under constant rolling at RT, three times with lysis buffer, two times with *Ampuwa*® H<sub>2</sub>O and three times with MS-wash buffer.

#### 2.2.1.2.2 Tryptic digestion

For tryptic digestion the beads were redissolved in 6 M urea transferred into centrifuge filters Amicon Ultra (Merck) for filter-aided sample preparation (Wisniewski et al., 2009). The following steps were done on the filter, using centrifugation to remove buffers. The proteins adsorbed to the beads were washed twice with 6 M Urea and reduced in 100 mM DTT/100 mM ammonium bicarbonate (Sigma Aldrich) for 15 min at 56 °C. Thereafter acetylation was performed with 300 mM iodacetamid (Sigma-Aldrich) in 100 mM ammonium bicarbonate for 30 min at room temperature. Proteins were digested with 0.5 µg trypsin (Promega) over night at 37 °C in 100 mM ammonium bicarbonate (Sigma Aldrich). Tryptic peptides were desalted with reversed phase columns (Poro Oligo R3).

#### 2.2.1.2.3 LC-MSMS application

Tryptic peptides were separated on a nano-ultra-pressure-liquid-chromatography system (UltiMate 3000 Rapid Separation liquid chromatography system, Dionex, Thermo Scientific) coupled online via electrospray-ionization (ESI) to a tandem mass spectrometer (Orbitrap QExactive, Thermo Scientific). The samples were loaded with a flowrate of 5 µl/min onto a trapping column (Acclaim PepMap µ-precolumn, C18, 300 µm × 5 mm, 5 µm, 100 Å, Thermo Scientific) in buffer A (0.1% formic acid (FA) in HPLC-H<sub>2</sub>O). The trapping column was washed firstly for 5 min with 2% buffer B (0.1% FA in acetonitrile (ACN)) at a flowrate of 5 µL/min and subsequently the peptides were eluted onto the

separation reversed phase C18 column (Acclaim PepMap 100, 75  $\mu\text{m}$   $\times$  250 mm, 2  $\mu\text{m}$ , 100  $\text{\AA}$ ; Thermo Scientific) at a flowrate of 200 nL/ $\mu\text{m}$  with a binary buffer system of buffer A and buffer B. The peptides were eluted with a gradient of 2–30% buffer B over 35 min followed by 30–70% buffer B over 10 min, resulting in 75 min gradients, respectively.

Mass spectrometric analysis was performed in positive ion mode and was programmed to acquire fragment spectra in data-dependent mode (DDA). The full scan spectra were acquired with the orbitrap mass analyser with resolution of 70,000 FWHM at  $m/z$  200 on MS level over a  $m/z$  range from 400 to 1300 (maximum injection time: 100 ms and AGC target:  $3e^6$ ). The fragmentation was carried out with a HCD collision energy of 28% and an intensity threshold of  $1e^5$  and an isolation width 2.0  $m/z$ . Only precursors with charge states between +2 and +4 and the most intense precursors were selected for fragmentation. The top intense ions were isolated to a target value of  $4e^4$  with a maximum injection time of 250 ms (Top5) and detected in the orbitrap with a resolution 17,500 of FWHM at  $m/z$  120.

The raw data were processed with the software Proteome Discoverer, v1.4.1.14 (Thermo Scientific) using the following parameters: FDR < 0.01 at the level of proteins, peptides and modifications; precursor mass tolerance 10 ppm and fragment mass tolerance 0.02 Da. Up to 2 missed cleavages were allowed for protease digestion. Enzyme specificity was set to trypsin, and the search included N-acetylation of protein, deamidation of asparagine, glutamine, biotinylation of lysine and oxidation of methionine as dynamic modifications and cysteine carbamidomethylation as a fixed modification. Searches were performed against the *Plasmodium falciparum* 3D7 PlasmoDBv24 (Aurrecochea et al., 2009) FASTA database (April 2015).

### **2.2.1.3 Western blot analysis**

#### **2.2.1.3.1 Sodium dodecyl sulfate polyacrylamide gel electrophoresis (SDS-Page)**

SDS-Page is a method to separate proteins according to their molecular weight. SDS is responsible for a negative net charge by covering the intrinsic charge of each protein. Unfolded, negatively charged proteins migrate in the direction of the anode allowing the separation by mass. For denaturation of tertiary and secondary structure DTT, a reducing agent to break disulphide bonds, is present in the SDS sample buffer. In addition, the protein samples were also heat denaturated (85  $^{\circ}\text{C}$ , 5 min). Samples (supernatant and pellet fractions) were loaded together with a prestained protein marker into pockets of 10 and 12% polyacrylamide gels. For separation gels were applied to an electric field (150 V, 44 mA for 60-90 min) in SDS running buffer.

#### **2.2.1.3.2 Western blot**

Proteins separated by SDS-Page were transferred on a nitrocellulose membrane for

further analysis. As SDS is responsible for a negative net charge the correct assembly of the blotting process in the direction of the anode is crucial. The polyacrylamide gel was layered on a nitrocellulose membrane in a blotting device. Three layers of Whatman filter papers and a sponge compressed the polyacrylamide gel and the nitrocellulose membrane from both sides. The assembly was done under wet conditions avoiding air bubbles. The blotting process was accomplished in transfer buffer in a tank blotting chamber at 4 °C (100 V, 500 mA) for 70 min.

#### 2.2.1.3.3 Detection of proteins

For immune-detection after protein transfer the nitrocellulose membrane was blocked in 5% skim milk in PBS and for streptavidin blots in 5% skim milk in TBS for 1 h at RT. For immune-detection primary and secondary antibodies were diluted in 5% skim milk in PBS according to (Table 1 and Table 3). Primary antibodies were applied over night at 4 °C and washed thoroughly with PBS afterwards. Next, horseradish peroxidase (HRP) conjugated secondary antibodies were applied for several hours at RT and washed thoroughly with PBS. For streptavidin-detection of biotinylated proteins HRP-conjugated streptavidin (Table 4) was applied in Dilution buffer (1% skim milk in TBST). The Clarity™ Western ECL Substrate (Bio Rad) kit was used for detection and the chemiluminescence signal recorded using a Chemi Doc XRS imaging system (Bio-Rad). Images were processed with Image Lab Software 5.2 (Bio-Rad).

## 2.2.2 Cell culture methods

### 2.2.2.1 Culture of the parasite *P. falciparum*

*P. falciparum* blood stage parasites were continuously cultured in human O<sup>+</sup> erythrocytes (UKE) with a haematocrit of 5% described in (Trager and Jensen, 1976). Transgenic and 3D7 wildtype parasites were cultured in petri dishes using RPMI 1640 medium containing 0.5% AlbuMAX (Invitrogen). A box containing the petri dishes was fumigated with (5% O<sub>2</sub>, 5% CO<sub>2</sub>, 90% N<sub>2</sub>) and incubated at 37 °C. Transgenic parasites were selected with 4 nM WR99210, 2 µg/ml blasticidin S or 0.9 µg DSM1. Integrants were selected with 400 µg/ml G418.

### 2.2.2.2 Cryoconservation of *P. falciparum*

To stock *P. falciparum* parasites cryoconservation is the method of choice. During the freezing process it is crucial to prevent damage from water crystallization through an adequate freezing solution. A pelleted parasite culture preferably containing a majority of ring stage parasites, as this stage is able to survive the freezing process, was resuspended in 1 ml of freezing solution. The suspension was transferred into a cryo tube (Nunc) and stored at -80 °C or in liquid nitrogen. Thawing of a cryo-stabilate is possible

with an adequate thawing solution. Cryo tubes were placed in a 37 °C water until thawed. The suspension was transferred into an Eppendorf tube and centrifuged. The supernatant was discarded and the pellet resuspended in 1 ml of thawing solution. The parasites were washed once in medium and cultured in the desired volume. Fresh blood was added to adjust the haematocrit to 5%.

### 2.2.2.3 Endogenous GFP-tagging

Initially, integration was done conventionally via on- and off-drug cycling with parasites harbouring the episomal plasmid (for genes PF3D7\_1464600, PF3D7\_1123500, PF3D7\_1013300, PF3D7\_1226900). The corresponding plasmids were obtained by cloning of the 737–1184 bp long C-terminal target regions into pARL-GFP (Crabb et al., 2004) without a promoter using *NotI* and *AvrII* (see section 2.1.9). All other integrants were obtained using selection-linked integration (SLI) as described in (Birnbaum et al., 2017). Cloning of the 599–1027 bp long C-terminal targeting regions into *NotI* and *AvrII* digested pSLI-2×FKBP-GFP (Birnbaum et al., 2017) via Gibson assembly generated the corresponding plasmids. For targeted-gene-disruption (TGD) 300–363 bp long N-terminal targeting regions (starting with a stop codon) were PCR amplified (see section 2.1.9) and cloned *NotI/MluI* into pSLI-TGD (Birnbaum et al., 2017) via Gibson assembly. Correct integration of the plasmid into the genome was checked for all integrants via PCR using two vector- and two candidate-specific primers as previously described (Birnbaum et al., 2017).

### 2.2.2.4 Fluorescence-activated cell scanning (FACS) analysis

FACS analysis was used to determine the parasitemia for growth assays. Initially, the parasitemia of a synchronized culture was adjusted to either 0.01% (long term survival) or 0.1%. Cultures were split into a control 2 ml dish and a rapalog treated (250 nM) 2 ml dish. Medium was changed every second day or cells were diluted when a parasitemia of 2% was exceeded. For FACS analysis 20 µl of a 5% haematocrit cell culture was stained in a flow cytometry tube with 80 µl staining solution containing 0.45 µg Hoechst 33342 (staining the nuclei) and 0.5 µg DHE (staining DNA and RNA in viable cells after conversion into Ethidium). The mix was incubated for 20 min in the dark. The staining reaction was stopped and parasites were inactivated by adding 400 µl of FACS stop solution. Samples were measured at the LSRII and data was analysed with FlowJo. The FACS assay is based on a previous publication (Malleret et al., 2011).

### 2.2.2.5 Generation of a conditional knockout

To further analyse likely essential proteins (PF3D7\_1464600) a cell line containing a TGD of the endogenous GOI followed by a re-codonized (Genescript) but floxed version of the

gene was generated within the vector pARL1-SLI-TGD-loxP-3xHA (Mesén-Ramírez and Jakob Birnbaum unpublished).

For TGD a 401 bp long region (starting with a stop codon) in the N-terminal part of the gene of interest was PCR amplified (section 2.1.9) and cloned *NotI/MluI* into pARL1-SLI-TGD-loxP-3xHA via Gibson assembly (section 2.2.4.5). The re-codonized version of PF3D7\_1464600 (Genescript) was PCR amplified (section 2.1.9) without a stop codon and cloned *AvrII/XmaI* into pARL1-SLI-TGD-loxP-3xHA via Gibson assembly (section 2.2.4.5).

For rapalog-induced excision of the re-codonized version a second plasmid pSkipFlox with two parts of the Cre recombinase was transfected. Upon the addition of rapalog (250 nM) the dimerization of the two parts of the Cre recombinase induced the excision of the loxp flanked region, resulting in a knockout cell line.

Complementation cell lines were generated via transfection of pARL2yDHODH-Compl-Ty1 (Paolo Mesén-Ramírez and Jakob Birnbaum unpublished) that contained the re-codonized version of PF3D7\_1464600. D554N and D584N mutations were inserted via PCR and subsequent Gibson assembly (section 2.2.4.5) into the *BSWI* and *EcoNI* restriction sites.

#### **2.2.2.6 Giemsa smears**

Thin blood smears were fixated with methanol on a glass slide and subsequently stained with Giemsa for at least 10 min. Parasitemia was determined under a light microscope Axio Lab A1. Pictures were taken with the Axio Cam ERc5s and the Zeiss Zen software.

#### **2.2.2.7 Life cell imaging**

Proteins tagged endogenously or episomally with GFP, mCherry or mScarlett were analysed on a fluorescence microscopy Zeiss AxioScope M1 equipped with a 63x/1.4 and a 100x/1.4 numerical aperture oil immersion lens. To visualise membranes sphingolipids were stained with 50 µl of a 5 µM Bodipy-TR-C5-ceramide solution and washed once in medium (Gruring and Spielmann, 2012). To visualise nuclei cells were stained with 1 µg/ml DAPI for 10 min at RT and washed once with medium. A drop of cells was placed on a glass slide with a coverslip on top and imaged in medium at RT. Pictures were taken with a Hamamatsu Orca C4742-95 and the Zeiss Axiovision software. Images were processed in Corel PHOTO-PAINT X7.

#### **2.2.2.8 Magnetic Activated Cell Sorting (MACS)**

For the separation of late stage parasites from rings and uninfected RBCs magnetic activated cell sorting (MACS) can be applied. However, late stage parasites can be purified in a magnetic field due to their magnetic haemozoin content and do not need to be activated with magnetic beads. For this purpose MACS CS columns (Miltenyi) were

used according to the manufacturer's protocol. Before the cell culture suspension was applied, columns were equilibrated with medium twice. Columns were washed thoroughly with medium until no residual RBCs were visible in the flow through. Columns were removed from the magnetic field and late stage parasites were eluted in medium and further processed.

#### **2.2.2.9 Protein biotinylation**

Protein biotinylation (Roux et al., 2012) was induced by the addition of 500  $\mu$ M biotin to the culture medium of transgenic parasite lines expressing SP-GFP-BirA\* or 3D7 wildtype as a control. After 20 h incubation cells were harvested with a parasitemia of 5-10%. Late stage parasites were either purified with MACS (for mass spectrometry) or Percoll (for Western blot analysis) and were further processed.

#### **2.2.2.10 Saponin lysis**

Saponin is a detergent that selectively lyses the RBC and the PVM membrane, whereas the PPM is less susceptible due to a different lipid composition (Benting et al., 1994). To eliminate haemoglobin from parasite extracts or to separate the soluble RBC and PV content from the parasite saponin lysis was performed. Cells from a desired culture volume were harvested and washed with PBS. One cell pellet volume of PBS remained in order to keep the cell pellet in suspension. 10 pellet volumes of freshly prepared 0.03 % saponin were added to the suspension, resuspended and incubated on ice for 10 minutes. Lysates were centrifuged for 5 minutes at 16000 rpm. The remaining pellets contained intact parasites within the RBC/PV membranes, whereas the supernatant contained haemoglobin, soluble RBC and PV proteins. For some experiments supernatants were harvested, protease inhibitor cocktail was added and frozen at  $-20^{\circ}\text{C}$ . In this case parasites were enriched via Percoll (section 2.2.2.12) or MACS (section 2.2.2.8) to reduce the haemoglobin content prior to saponin lysis. The remaining pellet was washed thoroughly with DPBS until the supernatant was clear of any residual haemoglobin. Intact parasite pellets were lysed with appropriate amounts of lysis buffer added with complete protease inhibitor cocktail. Extracts were frozen at  $-20^{\circ}\text{C}$  for Western blot or  $-80^{\circ}\text{C}$  for mass spectrometry analysis.

#### **2.2.2.11 Saponin release assay**

In order to test the solubility of proteins within the PV a selective lysis of the RBCM and the PVM was performed during live cell imaging. For this purpose cells were prepared for life cell imaging (section 2.2.2.7) and once under the microscope 0.03 - 0.3% saponin was carefully applied between the slide and the coverslip to avoid movement of the cells. Cells were observed until selective lysis took place. Pictures were taken before and shortly after

saponin lysis. To take pictures a Hamamatsu Orca C4742-95 and the Zeiss Axiovision software were used. Images were processed in Corel PHOTO-PAINT X7.

#### **2.2.2.12 Stage specific purification with a Percoll gradient**

A Percoll gradient was used to purify trophozoite and schizonts from uninfected RBCs and ring stages. For gradient generation equal volumes of 80%, 60% and 40% Percoll solution were carefully layered. The pelleted parasite culture was layered on the top of the gradient without disturbing the Percoll phases. Centrifugation (5 min at 2500 rpm) caused the separation into four different phases. The highest phase contained merozoites and debris, while the two middle ones contained schizonts (middle-high) and trophozoites (middle-low). The pellet contained uninfected RBCs and ring stages. For Western blot analysis trophozoites and schizonts were enriched to overcome the problem of haemoglobin in the supernatant after saponin lysis. Enriched late stage parasites were washed to remove residual Percoll and further processed. Each Percoll layer can be used to separate the desired stage specific population. In order to purify schizonts the pelleted parasite culture was layered on the top of a 60% Percoll phase resulting in a single schizont phase after centrifugation. Whereas the pellet fraction contained uninfected RBCs, ring stages and trophozoites.

#### **2.2.2.13 Synchronisation of *P. falciparum* culture**

Synchronization of parasites (Lambros and Vanderberg, 1979) was performed with five pellet volumes of 5% D-sorbitol in dH<sub>2</sub>O for at least 10 min at 37 °C. Late stage parasites are sensitive to sorbitol treatment, whereas ring stages survive. Sorbitol treated cultures were washed once in medium and were further cultivated. Another way to synchronize parasites can be achieved through the re-cultivation of Percoll purified segmenters (section 2.2.2.12).

#### **2.2.2.14 Transfection of *P. falciparum***

For parasite transfection two different electroporation protocols were used:

##### **2.2.2.14.1 Transfection of ring stages**

For the transfection of ring stages (Wu et al., 1995) 100 µg of DNA in 15 µl TE buffer were resuspended in 385 µl cytomix. The dissolved DNA was mixed with 250 µl of pelleted, synchronized ring stage parasites with a parasitemia of 5-10% and transferred into an electroporation cuvette (2 mm, BioRad). Electroporation was performed with a Gene Pulser Xcell (350 V, 50 µF, ∞ Ω) and the electroporated cell suspension was further cultivated. The medium was changed daily for 5 days and the selection drug was added after 24 h.

#### 2.2.2.14.2 Transfection of segmenters

The transfection of segmenters described in (Moon et al., 2013) is more efficient compared to the transfection of ring stages and reduced the time until transgenic cell lines were generated. Synchronized segmenters were purified with 60% Percoll (section 2.2.2.12), washed once in medium and were resuspended in 90 µl transfection buffer and mixed with 50 µg of DNA in 10 µl TE buffer. The DNA-segmenter suspension was transferred into an electroporation cuvette (2 mm, BioRad) and electroporated with the Nucleofector II AAD-1001N, program U-033 from the Amaxa system. Electroporated segmenters were transferred in prewarmed (37 °C) tubes containing 250 µl uninfected RBC in 500 µl medium. The tube was incubated for 30 min at 37 °C under rigorous shaking before the suspension was further cultivated. The medium was changed daily for 5 days and the selection drug was added after 24 h.

### 2.2.3 Microbiological methods

#### 2.2.3.1 Cryoconservation of bacteria

To stock bacteria cryoconservation is the method of choice. During the freezing process it is crucial to prevent damage from water crystallization. Therefore, 50% glycerol was added to the bacteria suspension. Bacteria were stored at -80 °C.

#### 2.2.3.2 Plasmid purification

Small amounts (80 ng/µl) of purified plasmids are needed for sequencing. For this purpose plasmid mini-preparations (<25 µg DNA) were performed with the NucleoSpin Plasmid Kit (Macherey Nagel) according to the manufacturer's protocol.

For parasite transfection higher plasmid concentrations (50-100 µg/transfection) were acquired with the Plasmid Midi Kit (QIAGEN) according to the manufacturer's protocol. Plasmid DNA was dissolved in 200 µl TE-buffer and quantified with a Nanodrop. 50-100 µg plasmid DNA was precipitated for parasite transfection.

#### 2.2.3.3 Transformation of chemo-competent bacteria

Prior to transformation the *E. coli* strain XL10 Gold was made competent with a sterile filtered calcium chloride solution (CaCl<sub>2</sub>) (Hanahan, 1983).

For transformation 100 µl of the chemo-competent *E. coli* was thawed on ice and mixed with 5 µl plasmid DNA generated in a ligation reaction. The suspension was incubated on ice for 20 min, heat shocked at 42 °C for 40 s and put back on ice for 1-3 min. The suspension was plated on a preheated LB agar plate containing ampicillin as a selection marker and incubated at 37 °C over night.

## 2.2.4 Molecular biological methods

### 2.2.4.1 Agarose gel electrophoresis

The agarose gel electrophoresis is a method to separate molecules according to their molecular weight. DNA naturally occurs negatively charged, so the DNA is forced to move in the direction of the anode in an electrical field. Each sample was pre-mixed with loading dye before application on the gel. The DNA fragments were compared to a standardized 1 Kb DNA ladder to determine their size. For detection ethidium bromide was added into the 1% agarose gel. Ethidium bromide intercalates into the DNA, which can therefore be visualized under UV light. The gel was analysed with the gel imaging system ChemiDoc™ XRS (Biorad) and the ImageLab software.

### 2.2.4.2 Digestion

For subsequent cloning procedures preparative DNA digestion is necessary. Restriction enzymes (section 2.1.7.1) were chosen according to their required restriction site recognized to linearize plasmid DNA or to digest PCR products to generate sticky ends for successful ligation. *DpnI* was used to eliminate plasmid DNA as it targets only methylated restriction sites commonly found in plasmid DNA. For each restriction enzyme the appropriate buffer was used. The digestion mix was incubated for 3 h at 37 °C.

#### Digestion mix

5µl plasmid DNA

1µl of each enzyme

5µl 10x Buffer

Ad 50µl *Ampuwa*® H<sub>2</sub>O

### 2.2.4.3 DNA precipitation

For parasite transfection a volume containing 50-100 µg plasmid DNA was precipitated with 1/10 volume of sodium acetate 3 M, pH 5.0 and three volumes of absolute ethanol. For adequate precipitation DNA was stored overnight at -20 °C. Subsequently, plasmid DNA was washed with 70% ethanol and dissolved in 10-15 µl TE-buffer.

### 2.2.4.4 Genomic DNA isolation

3D7 wild type genomic DNA was used as a template to amplify the homology regions for selection-linked integration as well as for targeted gene disruption. Isolation of genomic DNA from transgenic parasite lines is crucial to verify correct integration or excision. For this purpose the QIAamp DNA Mini Kit was used according to the manufacturer's protocol.

#### 2.2.4.5 Gibson assembly

In a Gibson assembly reaction (Gibson, 2009) up to 6 fragments can be ligated. In contrast to conventional ligation no sticky ends are required as correct and efficient ligation is maintained by overlaps of 15 - 80 bp generated during PCR amplification between insert and plasmid DNA. Equimolar amounts of linear plasmid DNA and insert were added to the Gibson assembly mix and incubated at 50 °C for 60 min.

#### 2.2.4.6 Ligation

DNA ligation is an enzymatically-catalysed process to join linear DNA strands by the formation of a phosphodiester bond. As an ATP-dependent process it is crucial to use freshly aliquoted ligase buffer. Digested PCR products and plasmids were joined by the DNA ligase from bacteriophage T4 (T4 ligase). The ligation mix was incubated for 1h at RT.

#### Ligation mix

7 µl Insert

1 µl Plamid DNA

1 µl 10x T4 ligase buffer

1 µl T4 DNA ligase

#### 2.2.4.7 Nucleic acid quantitation

The measurement of DNA concentrations and the assessment of its purity is an important step for downstream analysis. Nucleic acid quantitation was conducted with the Nanodrop 2000c. 1 µl of sample volume was pipetted onto an optical measurement surface and 1 µl of the corresponding buffer was used to blank. The spectrometer exposes the sample to ultra violet light. Due to the light absorbing characteristics of nucleic acids the light that passes through the sample measured by a photo-detector determines the nucleic acid concentration. With this method nucleic acid contamination with other molecules can also be detected. Therefore, the ratio of the absorbance at 260 and 280 nm ( $A_{260/280}$ ) provides the information about the purity of nucleic acids. For pure DNA the ratio of absorbance is defined by  $A_{260/280} = 1.8$ .

#### 2.2.4.8 Polymerase chain reaction (PCR)

Specific DNA fragments can be amplified in a polymerase chain reaction (PCR). Design of a unique forward and reverse primer defines the specificity of the fragments. A polymerase can amplify the template DNA flanked by the two primers resulting in an exponential increase of the fragment in each cyclic reaction consisting of denaturation, annealing and extension. The denaturation step creates single stranded DNA to which the primers can anneal to during the annealing step. During extension the polymerase

rebuilds double stranded DNA identical to the template DNA using the primer as a starting point. The annealing temperature depends on the primer melting temperature. Optimal annealing temperatures were identified with the TM calculator (NEB). Elongation times were adjusted according to the expected size of the PCR product.

For analytical PCRs (colony screens, integration checks, excision checks) FIREPol® DNA Polymerase (Solis Biodyne) was used (Table 13).

**Table 13: Analytical PCR conditions and pipetting scheme.**

Cycle number	Denature	Anneal	Extend
1	2 min, 95 °C	-	-
2-30	30 s, 95 °C	30 s, 50-68 °C	1 min per kb, 72 °C
31	-	-	10 min, 72 °C

Reagent	Volume [µl]
Ampuwa® H <sub>2</sub> O	6.4
10x FIREPol Buffer	1
MgCl <sub>2</sub> (25 mM)	0.6
Primer frw (10 µM)	0.4
Primer rev (10 µM)	0.4
dNTPs (2 mM)	1
Template	0.1
FIREPol®	0.1

For preparative PCRs the Phusion® High-Fidelity DNA Polymerase (NEB) was used (Table 14). Correct fragment size was analysed on an agarose gel and the PCR product was purified with the NucleoSpin® Gel and PCR Clean-up kit (Macherey-Nagel) for downstream analysis (e.g. ligation, Gibson assembly, digestion).

**Table 14: Preparative PCR conditions and pipetting scheme.**

Cycle number	Denature	Anneal	Extend
1	30 s, 98 °C	-	-
2-30	10 s, 98 °C	30 s, 45-72 °C	30 s per kb, 72 °C
31	-	-	5 min, 72 °C

Reagent	Volume [ $\mu$ l]
Ampuwa <sup>®</sup> H <sub>2</sub> O	30.4
5x Phusion Buffer	10
Primer frw (10 $\mu$ M)	2
Primer rev (10 $\mu$ M)	2
dNTPs (2 mM)	5
Template	0.3
Phusion <sup>®</sup>	0.3

#### 2.2.4.9 Sequencing

For sequencing the single tube sequencing barcode economy run service from Seqlab (Sequence Laboratories Göttingen) was used. Samples were sent according to the requirements of Seqlab.

#### Sequencing mix

80 ng/ $\mu$ l Plasmid DNA

3  $\mu$ l Primer (10  $\mu$ M)

ad 15  $\mu$ l Ampuwa<sup>®</sup> H<sub>2</sub>O

The results were aligned to the vector and sequences designed in ApE and checked manually comparing the expected sequence to the given sequencing peaks. Mutations within the sequences were evaluated for their severity.

### 3 Results

#### 3.1 Construct design for BioID within the PV

The aim of the thesis was to identify new PV proteins. In order to carry out BioID and to biotinylate PV proteins, the promiscuous biotin ligase BirA\* (Roux et al., 2012) needed to be transported into the PV compartment. The PV is the default destination for proteins in *P. falciparum* that have a signal peptide (SP) but do not contain other trafficking motives (such as e.g. SDEL, KDEL, PEXEL etc.) (Waller et al., 2000). Taking this into account, a construct was designed where the PF3D7\_0830400 signal peptide (Heiber et al., 2013) that mediates entry into the secretory pathway was N-terminally fused to BirA\*. A GFP-tag was added at the N-terminus of BirA\* to track the construct in the parasite. The resulting construct was episomally expressed (under a *crt*-promotor) and termed SP-GFP-BirA\* (Figure 8A). The region of PF3D7\_0830400 used as a signal peptide comprised amino acids 1-60, including a predicted cleavage site of the SP between amino acid 25 and 26 (SignalP 3.0). It was previously shown that the GFP-tagged first 60 amino acids of PF3D7\_0830400 were trafficked into the PV compartment (Blancke Soares, 2016). In concordance, live cell microscopy of SP-GFP-BirA\* containing cells showed a fluorescence pattern in the parasite periphery, surrounding the parasite, typical for a PV localisation (Figure 8B).

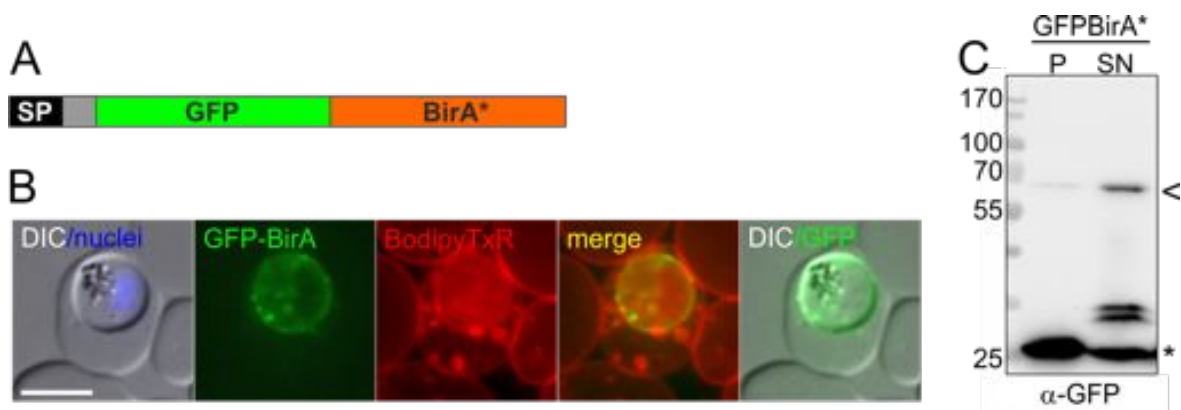


**Figure 8: The SP-GFP-BirA\* construct is located in the PV.**

A) Schematic of the SP-GFP-BirA\* construct. SP: signal peptide; grey area: 35 amino acids left after the SP to serve as a linker before GFP. B) Life cell images of a Bodipy-TX-ceramide stained parasite expressing the SP-GFP-BirA\* construct (GFP-BirA). Merge indicates overlay of green and red channels; DIC: differential interference contrast; nuclei were stained with DAPI; size bar: 5  $\mu$ m. C) Western blot of SP-GFP-BirA\* expressing parasites separated into saponin supernatant (SN, including the PV content) and pellet (P, including the parasite content with the PPM and PVM) after isolation of infected RBCs through Percoll. The blot was probed with anti-GFP. Arrowhead, fusion construct (predicted size after in silico cleavage of the SP: 72 kDa); asterisk, GFP alone (degradation product of the fusion protein).

To determine the solubility of the construct, the supernatant as well as the pellet fraction of saponin lysed parasites were analysed in a Western blot (Figure 8C). Here, the majority

of the fusion construct molecules were seen in the supernatant fraction, which contains the soluble PV content. Both fractions, but in particular the pellet fraction, also showed a prominent band of ~27 kDa, which correlates in size of the GFP-tag alone, indicating degradation of the fusion protein. The dominant GFP-sized degradation product in the parasite pellet fraction is typical for constructs internalised into the food vacuole where degradation to the stable GFP core takes place (Boddey et al., 2016). Overall these data indicate that BirA\* was indeed trafficked into the PV and is at least partially soluble in this compartment.

### 3.2 Biotinylation of proteins (BioID) within the PV

In order to test whether BirA\* was functional and biotinylated proteins of the parasite, biotin was visualised by red-fluorescent streptavidin in an immuno- and streptavidin-fluorescence assay (Figure 9A). A streptavidin signal was detected in the parasite periphery and co-localised with the GFP signal of SP-GFP-BirA\*, as well as with the PVM marker ETRAMP5, indicating that biotinylation occurred within the PV compartment. In a streptavidin western blot analysis, the supernatant (soluble PV proteins) and pellet (PV proteins attached to the PVM or PPM) fractions from SP-GFP-BirA\* and 3D7 wild type parasites grown in the absence and presence of biotin were compared (Figure 9B).

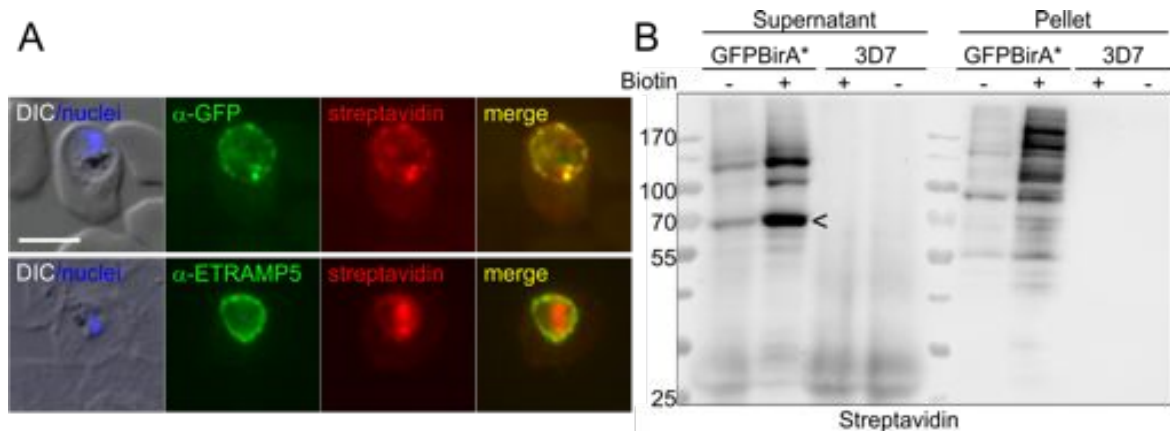


**Figure 9: The SP-GFP-BirA\* construct biotinylates proteins within the PV compartment**

A) Immune fluorescence assay (IFA) of SP-GFP-BirA\* expressing parasites grown in the presence of biotin show co-localization of biotinylated protein (detected using streptavidin) with GFP-BirA\* (upper panel) and ETRAMP5 (lower panel). Merge indicates overlay of green and red channels; DIC: differential interference contrast; nuclei were stained with DAPI; size bar: 5 μm. B) Western blot of saponin supernatant and pellet from parental (3D7) and SP-GFP-BirA\* expressing parasites in the presence and absence of biotin. Biotinylation of proteins was visualized by streptavidin-HRP. Probable, self-biotinylated SP-GFP-BirA\* is indicated with an arrowhead.

As expected, the 3D7 wild type control showed no biotinylation, while the SP-GFP-BirA\* cell line showed biotinylation even in the absence of additional biotin (Figure 9B). This is likely due to fact that the culture medium contains trace amounts of biotin. In the presence of biotin both the supernatant as well as the pellet fraction showed biotinylated proteins. The supernatant showed a weaker signal with fewer bands, one of them likely

corresponding to the self-biotinylated SP-GFP-BirA\* (arrowhead). The pellet showed diverse and prominent bands, indicating biotinylation of different PV proteins.

### 3.2.1 Identification of PV proteins via mass spectrometry

For the identification of PV proteins via mass spectrometry (MS) asynchronous SP-GFP-BirA\* (positive control) and 3D7 wild type (negative control) parasites were grown in the presence of biotin. After 20 hours biotin incubation, trophozoite and schizont stage parasites were enriched via magnetic purification using MACs columns and treated with saponin to release the parasites from the host cell content (mainly consisting of haemoglobin) and to separate the soluble PV proteins (supernatant fraction) and the proteins attached to the PVM and PPM (pellet fraction). Streptavidin beads were used to enrich biotinylated proteins in both fractions for LC-MSMS analysis. For MS-data analysis only proteins that were identified by at least two unique peptides were included (see appendix: Table xviii, Table xix, Table xxi and Table xxii). For the identification of potential PV proteins in the pellet fraction the negative control (Table xix) was subtracted from the positive control (Table xviii) (i.e. any protein detected in the control was removed from the positive list), resulting in the hit list containing potential PV proteins (Table 15). In agreement with the comparably large number of bands of the streptavidin Western blot analysis (Figure 9B) the MS of the pellet fraction resulted in a large number of proteins meeting the threshold (77 proteins in Table 15).

**Table 15: Results of the SP-GFP-BirA\* pellet fraction after 3D7 subtraction**

SP: signal peptide, TMD: transmembrane domain, ED: export domain, UP: unique peptides.

#	SP	TMD	ED	Accession	Description	# UP
1	no	no	no	PF3D7_1149000	antigen 332, DBL-like protein (Pf332)	40
2	yes	no	no	PF3D7_1436300	translocon component PTEX150 (PTEX150)	23
3	yes	no	no	PF3D7_1464600	phosphatase, putative	17
4	yes	yes	no	PF3D7_1420700	surface protein P113 (P113)	10
5	yes	yes	no	PF3D7_1116800	heat shock protein 101, chaperone protein ClpB2 (HSP101)	7
6	yes	no	no	PF3D7_1471100	exported protein 2 (EXP2)	6
7	no	no	no	PF3D7_1312700	probable protein, unknown function	6
8	yes	no	no	PF3D7_1129100	parasitophorous vacuolar protein 1 (PV1)	5
9	no	yes	yes	PF3D7_0730900	EMP1-trafficking protein (PTP4)	5
10	no	yes	no	PF3D7_1452500	SNARE protein, putative (BET1)	5
11	no	yes	yes	PF3D7_1016400	serine/threonine protein kinase, FIKK family (FIKK10.1)	4
12	no	no	no	PF3D7_0507100	60S ribosomal protein L4 (RPL4)	4
13	no	yes	PNEP	PF3D7_0801000	Plasmodium exported protein (PHISTc), unknown function	4
14	no	yes	PNEP	PF3D7_1334500	MSP7-like protein (MSRP6)	3
15	yes	no	no	PF3D7_1108600	endoplasmic reticulum-resident calcium binding protein (ERC)	3
16	no	no	no	PF3D7_1229500	T-complex protein 1, gamma subunit, putative	3
17	no	no	no	PF3D7_0212300	peptide chain release factor subunit 1, putative	3
18	no	no	no	PF3D7_1129200	26S proteasome regulatory subunit RPN7, putative (RPN7)	3

19	no	no	no	PF3D7_0915400	6-phosphofructokinase (PFK9)	3
20	no	no	no	PF3D7_1212700	eukaryotic translation initiation factor 3 subunit 10, putative	2
21	no	no	no	PF3D7_0307200	60S ribosomal protein L7, putative	2
22	yes	yes	yes	PF3D7_0501200	parasite-infected erythrocyte surface protein (PIESP2)	2
23	no	no	no	PF3D7_0728000	eukaryotic translation initiation factor 2 alpha subunit, putative	2
24	yes	yes	yes	PF3D7_1108700	heat shock protein DnaJ homologue Pfj2	2
25	yes	no	no	PF3D7_0302200	cytoadherence linked asexual protein 3.2 (CLAG3.2)	2
26	yes	no	no	PF3D7_0302500	cytoadherence linked asexual protein 3.1 (CLAG3.1)	2
27	yes	yes	no	PF3D7_0918000	secreted acid phosphatase (GAP50)	2
28	yes	no	no	PF3D7_1420400	glycine--tRNA ligase (GlyRS)	2
29	yes	yes	no	PF3D7_1322000	adenosine-diphosphatase, putative	2
30	no	no	no	PF3D7_1107300	polyadenylate-binding protein-interacting protein 1, putative (PAIP1)	2
31	no	no	no	PF3D7_1011800	PRE-binding protein (PREBP)	2
32	no	no	no	PF3D7_1334200	chaperone binding protein, putative	2
33	no	no	no	PF3D7_1015800	ribonucleotide reductase small subunit, putative	2
34	no	no	no	PF3D7_1409800	RNA binding protein Bruno, putative (HoBo)	2
35	yes	yes	no	PF3D7_1116700	cathepsin C, homolog,dipeptidyl aminopeptidase 1 (DPAP1)	2
36	yes	yes	no	PF3D7_1123500	conserved Plasmodium protein, unknown function	2
37	yes	yes	no	PF3D7_0629200	DnaJ protein, putative	2
38	no	no	no	PF3D7_1311900	vacuolar ATP synthase subunit a (vapA)	2
39	no	no	no	PF3D7_1426100	basic transcription factor 3b, putative	2
40	no	no	no	PF3D7_1302800	40S ribosomal protein S7, putative	2
41	no	no	no	PF3D7_0418200	golgi organization and biogenesis factor, putative	2
42	no	no	no	PF3D7_1136300	tudor staphylococcal nuclease (TSN)	2
43	no	no	no	PF3D7_1304500	small heat shock protein, putative	2
44	no	no	no	PF3D7_1206200	eukaryotic translation initiation factor 3 subunit 8, putative	2
45	no	no	no	PF3D7_1424100	60S ribosomal protein L5, putative	2
46	no	no	no	PF3D7_1109900	60S ribosomal protein L36 (RPL36)	2
47	yes	yes	no	PF3D7_1352500	thioredoxin-related protein, putative	2
48	yes	yes	no	PF3D7_1462300	conserved Plasmodium protein, unknown function	2
49	yes	yes	no	PF3D7_0912400	conserved Plasmodium protein, unknown function	2
50	no	no	no	PF3D7_1132200	TCP-1/cpn60 chaperonin family, putative	2
51	yes	yes	no	PF3D7_1104400	conserved protein, unknown function	2
52	no	yes	no	PF3D7_1037300	ADP/ATP transporter on adenylate translocase (ADT)	2
53	no	no	yes	PF3D7_0424600	Plasmodium exported protein (PHISTb), unknown function	2
54	no	no	no	PF3D7_1338200	60S ribosomal protein L6-2, putative	2
55	yes	no	no	PF3D7_1135400	conserved Plasmodium protein, unknown function	2
56	no	no	no	PF3D7_1323100	60S ribosomal protein L6, putative	2
57	no	no	no	PF3D7_0919000	nucleosome assembly protein (NAPS)	2
58	yes	yes	no	PF3D7_0935800	cytoadherence linked asexual protein 9 (CLAG9)	2
59	yes	yes	no	PF3D7_1024800	conserved Plasmodium protein, unknown function	8
60	yes	no	no	PF3D7_1035300	glutamate-rich protein (GLURP)	7
61	yes	no	yes	PF3D7_1201000	Plasmodium exported protein (PHISTb), unknown function	4
62	no	yes	no	PF3D7_0220000	liver stage antigen 3 (LSA3)	3

63	yes	no	no	PF3D7_1105600	translocon component PTEX88 (PTEX88)	3
64	yes	yes	no	PF3D7_0532100	early transcribed membrane protein 5 (ETRAMP5)	2
65	yes	yes	no	PF3D7_1033200	early transcribed membrane protein 10.2 (ETRAMP10.2)	2
66	no	yes	no	PF3D7_1353200	membrane associated histidine-rich protein (MAHRP2)	2
67	yes	yes	no	PF3D7_1310500	conserved protein, unknown function	2
68	yes	no	no	PF3D7_1345100	thioredoxin 2 (TRX2)	2
69	yes	yes	yes	PF3D7_1001400	alpha/beta hydrolase, putative	2
70	yes	no	no	PF3D7_1226900	conserved Plasmodium protein, unknown function	2
71	no	yes	no	PF3D7_0922100	ubiquitin-like protein, putative	2
72	no	no	no	PF3D7_1219100	clathrin heavy chain, putative	2
73	no	no	no	PF3D7_1340600	RNA lariat debranching enzyme, putative (DBR1)	2
74	yes	no	no	PF3D7_0731600	acyl-CoA synthetase (ACS5)	2
75	yes	yes	no	PF3D7_1013300	conserved Plasmodium protein, unknown function	2
76	prob	no	no	PF3D7_1360800	falcilysin (FLN)	2
77	yes	yes	yes	PF3D7_0721100	conserved Plasmodium protein, unknown function	2

	Exported proteins
	Contaminants
	PV Candidates
	PV proteins

This included: ten known PV proteins such as the five PTEX components that are known to be located at the inner face of the PVM (de Koning-Ward et al., 2009), P113 that was previously pulled down with PTEX (Elsworth et al., 2016; Mesen-Ramirez et al., 2016) and is located on the PPM (Sanders et al., 2005), as well as two ETRAMPs which are found integral to the PVM (Spielmann et al., 2003) and PV1, the single confirmed PV protein found in the only other systematic attempt to identify PV proteins (Nyalwidhe and Lingelbach, 2006), 15 exported proteins, that were either identified by their PEXEL motif (Hiller et al., 2004; Marti et al., 2004) (including FIKK 10.1 (Jones et al., 2016), the Maurer's cleft protein PIESP2 (Dietz et al., 2014), different members of the PHIST protein family (Sargeant et al., 2006)) or known PEXEL-negative exported proteins (PNEPs) (including Pf332 (Nilsson et al., 2012), MSRP6 (Heiber et al., 2013), MAHRP2 a component of Maurer's cleft tethers (Pachlatko et al., 2010), CLAG 3.1 and 3.2 that have recently been implicated in the formation of the plasmodial surface anion channel (PSAC) (Desai, 2012)), a large number (38 proteins) of PV unrelated proteins most of them likely contaminants but also many ER proteins that are likely biotinylated during SP-GFP-BirA\* trafficking and 13 potentially novel PV proteins (Table 17). Twelve of the 13 potential PV proteins contained a predicted signal peptide (SignalP3.0), a likely prerequisite for PV proteins.

Next the BioID hits of the supernatant fraction (Table xx), consisting of the soluble PV content, were investigated. After 3D7 (Table xxi) subtraction (threshold: unique

peptides $\geq$ 2) the supernatant fraction contained fewer hits than the pellet fraction (16 proteins, Table xxii) with MSP9 (Weber et al., 1988), SERA9 (Miller et al., 2002), and UIS2 (Khosh-Naucke et al., 2017) as the only known PV proteins. As the supernatant of both, the 3D7 control and the SP-GFP-BirA\* sample should - due to the saponin lysis - be both enriched for soluble PV proteins per se, the subtraction of the 3D7 sample may have removed some true positives. Therefore the MS hits of the SP-GFP-BirA\* sample were also analysed without 3D7 subtraction, resulting in a hit list with 46 proteins (Table 16), which included two additional known PV proteins such as PV1 and SERA5 (Collins et al., 2017). Interestingly, analysis of the entire supernatant hit list, including also the proteins identified by only one unique peptide, revealed that the SP-GFP-BirA\* supernatant fraction contained another additional 5 known PV proteins ETRAMP5 and ETRAMP10.1, EXP3 (Batinovic et al., 2017; Khosh-Naucke et al., 2017) and the PTEX components PTEX 150 and 88. However, as these proteins are not soluble, this indicates that they were carried over from the pellet fraction. Nevertheless, this may indicate that true positives of novel PV proteins could be present in low abundance in this fraction. One such candidate was analysed (PF3D7\_1350500 identified by one unique peptide, see section 3.2.4.3 and Table xx in red or Table 17 highlighted in grey).

**Table 16: Results of the SP-GFP-BirA\* supernatant fraction**

All accession numbers marked with an asterisk (\*) would have been removed if the 3D7 supernatant fraction had been subtracted, UP: unique peptide.

#	Accession	Description	# UP
1	PF3D7_1016300*	glycophorin binding protein (GBP)	17
2	PF3D7_0801000*	Plasmodium exported protein (PHISTc), unknown function	17
3	PF3D7_0500800*	mature parasite-infected erythrocyte surface antigen,erythrocyte membrane protein 2 (MESA)	10
4	PF3D7_0730900	EMP1-trafficking protein (PTP4)	8
5	PF3D7_1201000	Plasmodium exported protein (PHISTb), unknown function	7
6	PF3D7_1357000*	elongation factor 1-alpha	7
7	PF3D7_0608800*	ornithine aminotransferase (OAT)	6
8	PF3D7_0922200*	S-adenosylmethionine synthetase (SAMS)	6
9	PF3D7_1149000	antigen 332, DBL-like protein (Pf332)	6
10	PF3D7_1129100*	parasitophorous vacuolar protein 1 (PV1)	5
11	PF3D7_0207600*	serine repeat antigen 5 (SERA5)	5
12	PF3D7_1311800*	M1-family alanyl aminopeptidase (M1AAP)	5
13	PF3D7_1444800*	fructose-bisphosphate aldolase (FBPA)	5
14	PF3D7_1462800*	glyceraldehyde-3-phosphate dehydrogenase (GAPDH)	5
15	PF3D7_1229400*	macrophage migration inhibitory factor (MIF)	4
16	PF3D7_1229500	T-complex protein 1, gamma subunit, putative	4
17	PF3D7_0626800*	pyruvate kinase (PyrK)	4
18	PF3D7_1120100*	phosphoglycerate mutase, putative (PGM1)	4
19	PF3D7_0708400*	heat shock protein 90 (HSP90)	4
20	PF3D7_1246200*	actin I (ACT1)	4
21	PF3D7_1451100*	elongation factor 2	4
22	PF3D7_0818200*	14-3-3 protein (14-3-3I)	3

23	PF3D7_0922500*	phosphoglycerate kinase (PGK)	3
24	PF3D7_1228600	merozoite surface protein 9 (MSP9)	3
25	PF3D7_1124600*	ethanolamine kinase (EK)	2
26	PF3D7_1117700*	GTP-binding nuclear protein RAN/TC4 (RAN)	2
27	PF3D7_0831700	heat shock protein 70 (HSP70-x)	2
28	PF3D7_1343000*	phosphoethanolamine N-methyltransferase (PMT)	2
29	PF3D7_1015900*	enolase (ENO)	2
30	PF3D7_0935900*	ring-exported protein 1 (REX1)	2
31	PF3D7_1012400*	hypoxanthine-guanine phosphoribosyltransferase (HGPRT)	2
32	PF3D7_0524000*	karyopherin beta (KASbeta)	2
33	PF3D7_1008700*	tubulin beta chain	2
34	PF3D7_1222300	endoplasmic, putative (GRP94)	2
35	PF3D7_1454400	aminopeptidase P (APP)	2
36	PF3D7_0902800	serine repeat antigen 9 (SERA9)	2
37	PF3D7_0511800*	inositol-3-phosphate synthase (INO1)	2
38	PF3D7_1253000*	gametocyte erythrocyte cytosolic protein (GECO)	2
39	PF3D7_1012600*	GMP synthetase (GMPS)	2
40	PF3D7_1116700*	cathepsin C, homolog, dipeptidyl aminopeptidase 1 (DPAP1)	2
41	PF3D7_1302100	gamete antigen 27/25 (Pfg27)	2
42	PF3D7_0520900*	S-adenosyl-L-homocysteine hydrolase (SAHH)	2
43	PF3D7_1109900*	60S ribosomal protein L36 (RPL36)	2
44	PF3D7_0320900*	histone H2A variant, putative (H2A.Z)	2
45	PF3D7_1464600	phosphatase, putative	2
46	PF3D7_1424100	60S ribosomal protein L5, putative	2

	Exported proteins
	Contaminants
	PV proteins

**Table 17: Summary of all investigated candidates.**

Accession #	PlasmoDB	# UP	TM (#)	MW [kDa]	PV Location	SLI-TGD	TGD homology region [bp of gene intact]	GOI sequence length [bp]	TGD [% of gene intact]	Plasmo Gem <i>P.berghei</i>	piggybag <i>P.falciparum</i>
PF3D7_0220000	liver stage antigen 3	3	2	176	positive	important for growth	774	4677	16,55	no orthologue for PbANKA	dispensable
PF3D7_0629200	DnaJ protein, putative	2	-	45	partial	important for growth	354	1143	30,97	slow	dispensable
PF3D7_0731600	acyl-CoA synthetase	2	-	93	positive	not essential	435	2436	17,86	dispensable	dispensable
PF3D7_0912400	alkaline phosphatase, putative	2	1	53	positive	not essential	438	1341	32,66	NA	dispensable
PF3D7_1013300	conserved Plasmodium protein, unknown function	2	1	75	negative	important for growth	309	1887	16,38	NA	dispensable
PF3D7_1024800	conserved Plasmodium protein, unknown function (EXP3)	2	1	171	positive	not essential	393	4395	8,94	NA	dispensable
PF3D7_1123500	conserved Plasmodium protein, unknown function (GP2)	2	2	154	partial	not essential	471	4011	11,74	NA	dispensable
PF3D7_1135400	conserved Plasmodium protein, unknown function	2	-	29	positive	not essential/important for growth	540/282	738	73,17/38,21	no orthologue for PbANKA	dispensable
PF3D7_1226900	conserved Plasmodium protein, unknown function (PV2)	2	-	57	positive	important for growth	393	1488	26,41	dispensable	dispensable
PF3D7_1310500	conserved protein, unknown function	2	1	24	negative	important for growth	303	618	49,03	dispensable	essential
PF3D7_1350500	conserved Plasmodium protein, unknown function	1	-	134	partial	important for growth	408	3435	11,88	essential	essential
PF3D7_1352500	thioredoxin-related protein, putative	2	1	24	not tagable	-	-	-	-	NA	essential
PF3D7_1462300	conserved Plasmodium protein, unknown function	2	3	161	negative	important for growth	369	4074	9,06	NA	essential
PF3D7_1464600	serine/threonine protein phosphatase UIS2, putative	17	-	170	positive	important for growth	426	4329	9,84	essential	dispensable

### 3.2.2 Verification of potential PV proteins

From the mass spectrometry hit lists, 14 proteins that seemed to be most likely candidates for the identification of novel PV proteins were selected for further analysis (Table 17). The criteria for inclusion were: the presence of a predicted signal peptide (SignalP3.0) (13 proteins), a likely prerequisite for PV proteins or a N-terminal transmembrane domain. All candidates were chosen from the pellet fraction, except for PF3D7\_1350500, which derived from the supernatant hit list.

For localisation of the candidate proteins the corresponding genes were endogenously tagged with the sequence encoding a green fluorescent protein (GFP-tag), either through conventional drug cycling or using the SLI-system (Birnbaum et al., 2017). For eventual downstream analysis the integration vectors also consisted of an additional 2xFKBP between the homology region and the GFP-tag. C-terminal homology regions of 599 - 1027 base pairs were chosen as targeting regions. Correct integration was demonstrated by an integration check PCR where the 5' and 3' plasmid/genome junctions as well as the absence of parasites with the unmodified locus in the population were verified (Birnbaum et al., 2017). All expected sizes for integration check PCRs are listed in the appendix in Table xxiv.

Integration of the plasmid resulting in a C-terminally GFP-tagged protein was successful for all but one of the 14 candidates. Candidate PF3D7\_1352500, annotated as a putative thioredoxin-related protein, appeared to be refractory to C-terminal tagging with GFP. Attempts to tag PF3D7\_1352500 with a small epitope tag (HA) were equally unsuccessful, suggesting that any C-terminal tag is detrimental for the function of this protein.

### 3.2.3 False positive PV proteins

Proteins with no fluorescence signal observed in the PV (or a PV signal derived from a degradation product) were considered as false positives. Knowing the location of these proteins may still be of use in other contexts and the location of these proteins were therefore still carefully recorded. These false positive proteins are presented in the following sections (3.2.3.1 - 3.2.3.3).

#### 3.2.3.1 Candidate PF3D7\_1013300

PF3D7\_1013300 (predicted molecular weight of 75 kDa) is annotated as conserved *Plasmodium* protein of unknown function in PlasmoDB ([www.plasmodb.org](http://www.plasmodb.org)) and contains a predicted N-terminal signal peptide (SignalP3.0) and a single transmembrane domain (according to TMHMM) close to its C-terminal end (amino acid 595 - 617 from 628 in total) (Figure 10A). An integration cell line resulting in a 2xFKBP-GFP tagged PF3D7\_1013300 expressed from the endogenous locus was successfully established (Figure 10B and Table xxiv) using conventional drug cycling (performed by Johanna Becker (Becker,

2016)). Fluorescence microscopy with this cell line revealed that PF3D7\_1013300 was expressed in all parasite stages (Figure 10C). In trophozoites and schizonts a prominent ER signal in addition to a faint PV signal was detected, whereas ring stages showed a weaker and more diffuse staining in the parasite periphery. Western blot analysis (Figure 10D) showed the full-length protein (~130 kDa), concordant with the presence of a predicted transmembrane domain, in the saponin pellet fraction. In contrast the supernatant contained only degradation products. A saponin-release assay (Figure 10E, see section 2.2.2.11) with live parasites showed that the fluorescence signal around the parasite vanished after permeabilization of the PVM, suggesting that the faint PV signal derived from the soluble degradation products (asterisks) in the PV. Hence, PF3D7\_1013300 needs to be categorized as a false-positive PV candidate as the PV signal derived from a potentially non-physiological degradation product. Notably, for this candidate SLI-TGD (deleting ~83% of the gene) did not result in a cell line, indicating the protein to be likely essential for parasite growth (Table 17 and Table xxiii).

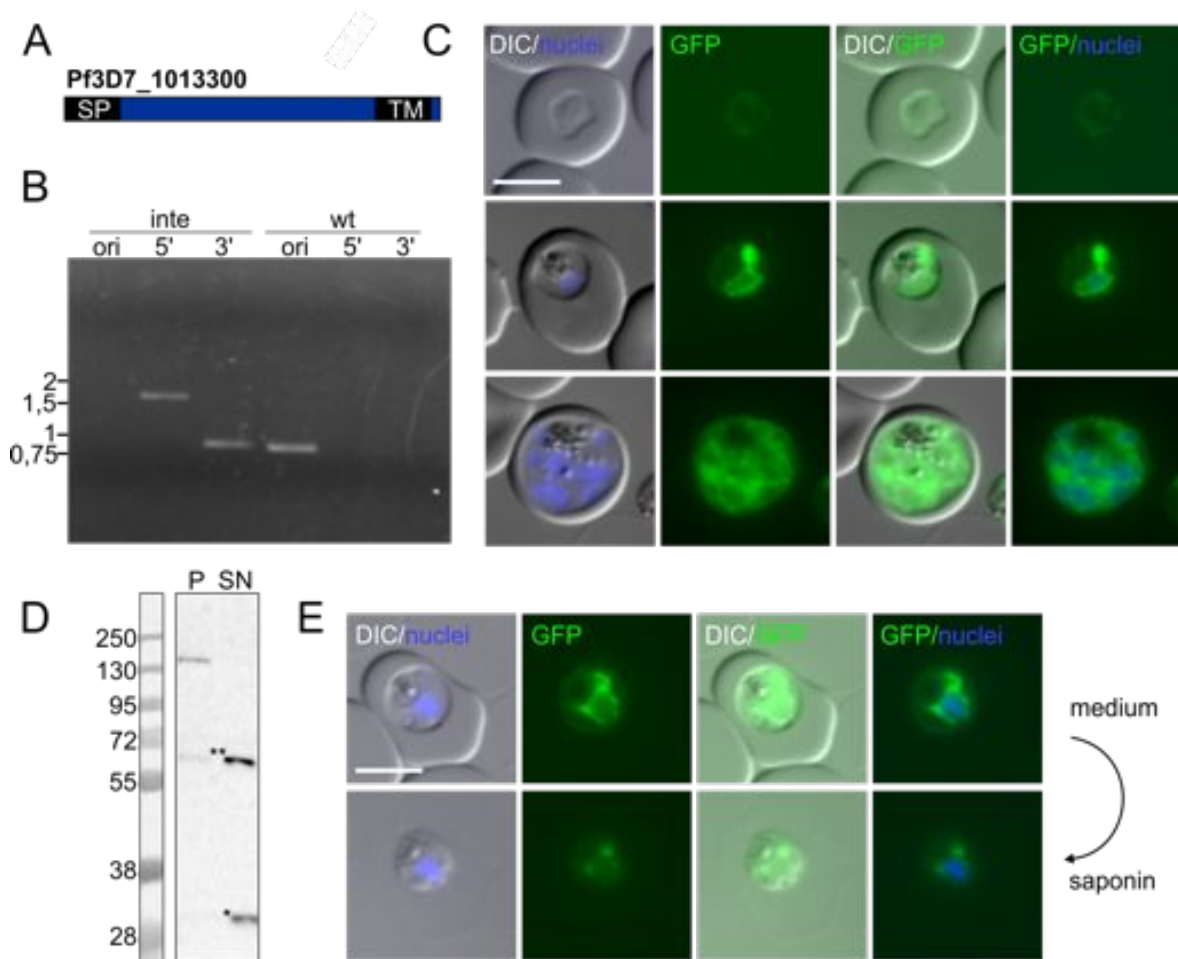


**Figure 10: Candidate PF3D7\_1013300.**

A) Schematic of PF3D7\_1013300 (SP: signal peptide; TM: transmembrane domain). B) Agarose gel with integration check PCR, confirming integration of the GFP-tagging-plasmid into the genome (inte, corresponding integration parasite line; wt, 3D7 parental line; ori, original locus; 5', PCR detection of 5' integration; 3', detection of 3' integration; the marker is indicated in kbp. C) Fluorescence microscopy images of live parasites showing a ring stage (top), a trophozoite stage

(middle) and a schizont stage parasite (bottom); DIC: differential interference contrast; nuclei were stained with DAPI; size bar: 5  $\mu$ m. D) Western blot probed with anti-GFP from parasite extracts derived from saponin supernatant (SN) and pellet (P) fractions after isolation of infected RBC by Percoll (the marker is indicated in kDa); degradation products in the Western blot: GFP alone (\*) and 2xFKBP-GFP(\*\*). E) Live saponin lysis, showing the same parasite before (upper panel) and after saponin lysis (lower panel); DIC: differential interference contrast; nuclei were stained with DAPI; size bar: 5  $\mu$ m.

### 3.2.3.2 Candidate PF3D7\_1310500

Candidate PF3D7\_1310500 (predicted molecular weight of 24 kDa) is annotated as conserved *Plasmodium* protein of unknown function in PlasmoDB and contains a predicted N-terminal signal peptide and a single transmembrane domain close to its C-terminal end (amino acid 153 - 175 from 205 in total) (Figure 11A). Correct integration of the 2xFKBP-GFP SLI-plasmid into the endogenous locus of PF3D7\_1310500 was confirmed in an integration check PCR (Figure 11B and Table xxiv). Western blot analysis showed the 2xFKBP-GFP-tagged full-length protein (~79 kDa) to be present in the pellet fraction, concordant to the N-terminal transmembrane domain. Additionally, degradation products of 2xFKBP-GFP (~55 kDa) in the pellet as well as GFP-tag alone (~27 kDa) in the pellet and supernatant fraction were visible (Figure 11C). In live cell microscopy the GFP signal of PF3D7\_1310500 was found around the parasite's nucleus, typical for an ER localisation (Figure 11D) and was categorized as a false positive candidate. Notably, for this candidate SLI-TGD (deleting ~50% of the gene) did not result in a cell line, indicating the protein to be likely essential for parasite growth (Table 17 and Table xxiii).

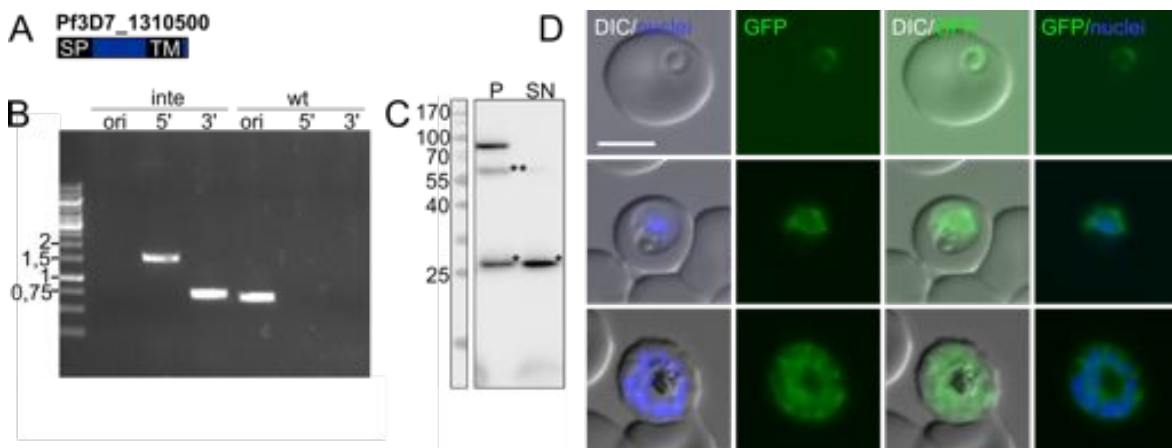


**Figure 11: Candidate PF3D7\_1310500.**

A) Schematic of Pf3D7\_1310500 (SP: signal peptide; TM: transmembrane domain). B) Agarose gel with integration check PCR, confirming integration of the GFP-tagging-plasmid into the genome (inte, corresponding integration parasite line; wt, 3D7 parental line; ori, original locus; 5', PCR detection of 5' integration; 3', detection of 3' integration; the marker is indicated in kbp. C) Western blot probed with anti-GFP from parasite extracts derived from saponin supernatant (SN) and pellet (P) fractions after isolation of infected RBC by Percoll (the marker is indicated in kDa); degradation products in the Western blot: GFP alone (\*) and 2xFKBP-GFP(\*\*). D) Live cell microscopy images of the endogenously GFP-tagged PF3D7\_1310500 showing a ring stage (top), a trophozoite stage (middle) and a schizont stage parasite (bottom); DIC: differential interference contrast; nuclei were stained with DAPI; size bar: 5  $\mu$ m.

### 3.2.3.3 Candidate PF3D7\_1462300

Candidate PF3D7\_1462300 (predicted molecular weight of 161 kDa) was annotated as conserved *Plasmodium* protein of unknown function to the time of MS analysis (April 2015) in PlasmoDBv24. In the meantime the annotation has been changed to a putative GTP-binding protein (PlasmoDBv38). PF3D7\_1462300 contains a predicted N-terminal signal peptide and three transmembrane domains in close proximity to its C-terminal end (amino acid 1155 - 1178, 1185 - 1204 and 1224 - 1246 from 1357 in total) (Figure 12A). Correct integration of the 2xFKBP-GFP SLI-plasmid into the endogenous locus of PF3D7\_1462300 was confirmed in an integration check PCR (Figure 12B and Table xxiv). Western blot analysis showed the 2xFKBP-GFP-tagged full-length protein (~216 kDa) to be present in the pellet fraction, concordant to the three N-terminal transmembrane domains (Figure 12C). The tagged protein was seen in distinct foci in schizont stage parasites (Figure 12D bottom panel) that may represent apical organelles or a location in structures of the secretory pathway such as the ER or Golgi. Interestingly, two weak foci per cell were detected in ring stages (Figure 12B top panel). These localisation results indicate that this candidate does not show a staining typical for the PV and was categorized as false positive. Notably, for this candidate SLI-TGD (deleting ~90% of the gene) did not result in a cell line, indicating the protein to be likely essential for parasite growth (Table 17 and Table xxiii).

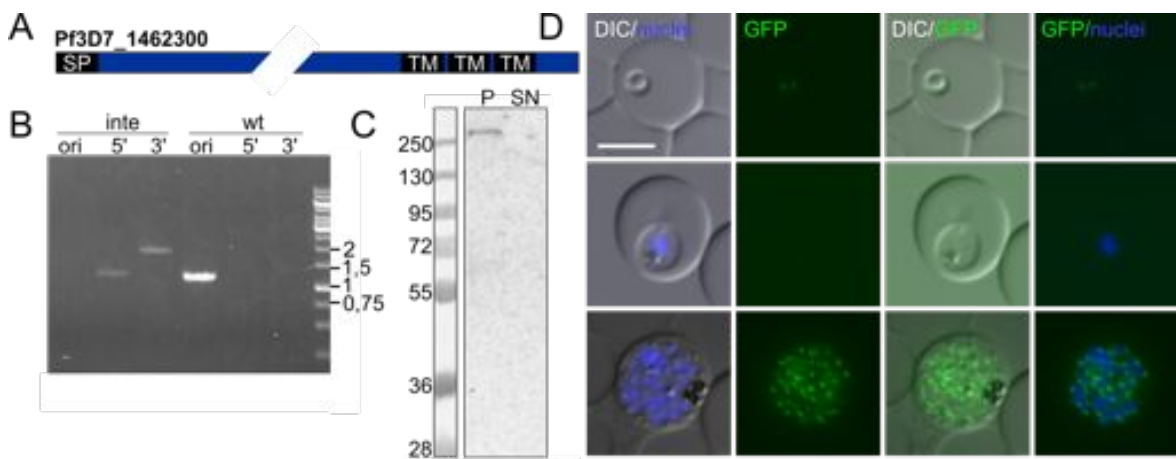


**Figure 12: Candidate PF3D7\_1462300.**

A) Schematic view of PF3D7\_1462300 (SP: signal peptide; TM: transmembrane domain). B) Agarose gel with integration check PCR, confirming integration of the GFP-tagging-plasmid into the genome (inte, corresponding integration parasite line; wt, 3D7 parental line; ori, original locus; 5', PCR detection of 5' integration; 3', detection of 3' integration; the marker is indicated in kbp). C) Western blot probed with anti-GFP from parasite extracts derived from saponin supernatant (SN) and pellet (P) fractions after isolation of infected RBC by Percoll (the marker is indicated in kDa). D) Live cell microscopy images of the endogenously GFP-tagged PF3D7\_1462300 showing a ring stage (top), a trophozoite stage (middle) and a schizont stage parasite (bottom); DIC: differential interference contrast; nuclei were stained with DAPI; size bar: 5 μm.

### 3.2.4 PV proteins with a partial PV localisation

Proteins with a fluorescence signal typical for the PV compartment but additional prominent fluorescence signal elsewhere were categorized as partial PV candidates. These candidates are presented in the following sections (3.2.4.1 - 3.2.4.3).

#### 3.2.4.1 Candidate PF3D7\_0629200

Candidate PF3D7\_0629200 (predicted molecular weight of 45 kDa) contains a predicted N-terminal signal peptide and is annotated as a putative DnaJ domain protein (Figure 13A). Endogenous tagging of PF3D7\_0629200 was performed via the SLI system (Birnbaum et al., 2017) and was confirmed in an integration check PCR (Figure 13B and Table xxiv).

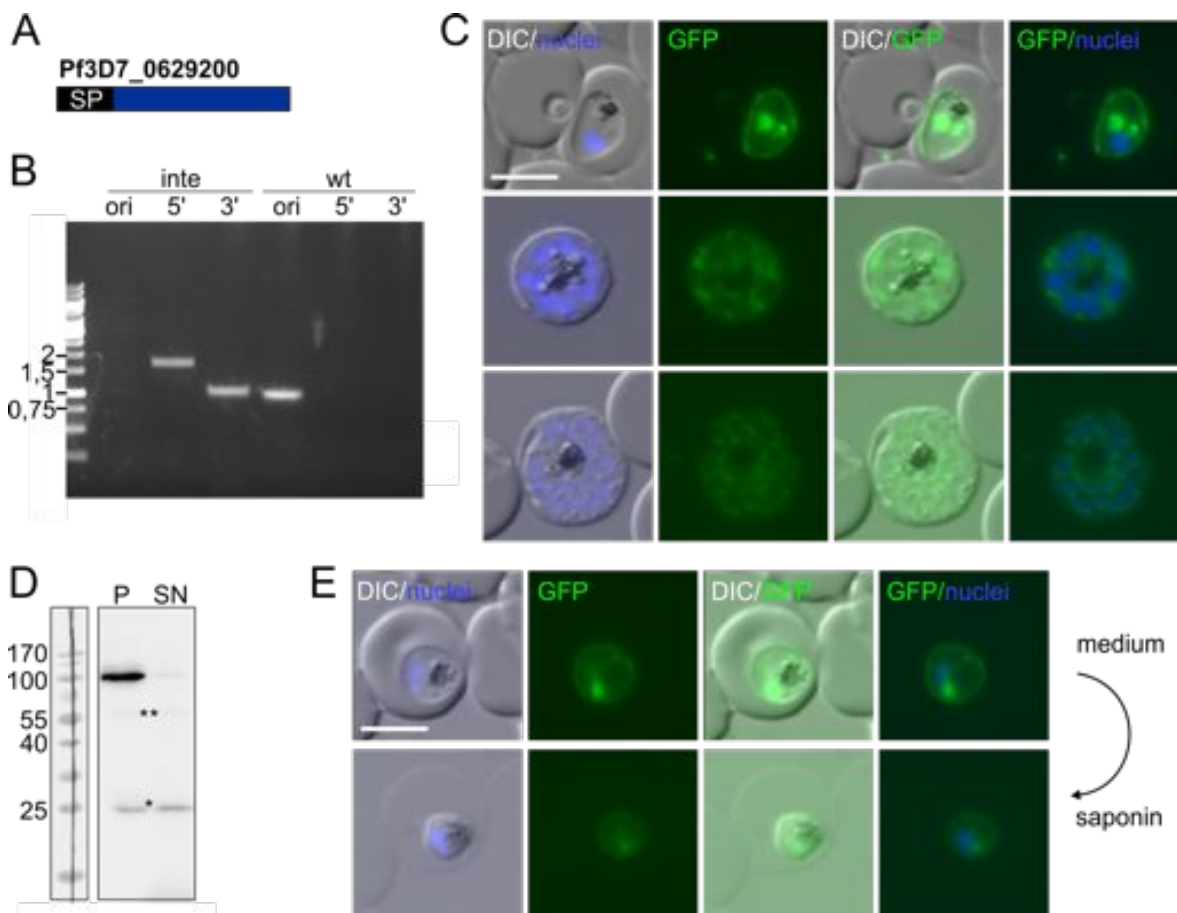


**Figure 13: Candidate PF3D7\_0629200.**

A) Schematic of PF3D7\_0629200 (SP: signal peptide). B) Agarose gel with integration check PCR, confirming integration of the GFP-tagging-plasmid into the genome (inte, corresponding integration parasite line; wt, 3D7 parental line; ori, original locus; 5', PCR detection of 5' integration; 3', detection of 3' integration; the marker is indicated in kbp). C) Live cell microscopy images of the endogenously GFP-tagged PF3D7\_0629200 showing a ring and a trophozoite stage (top) and two schizont stage parasites (middle and bottom); DIC: differential interference contrast; nuclei were stained with DAPI; size bar: 5  $\mu$ m. D) Western blot probed with anti-GFP from parasite extracts derived from saponin supernatant (SN) and pellet (P) fractions after isolation of infected RBC by Percoll (the marker is indicated in kDa); degradation products in the Western blot: GFP alone (\*) and 2xFKBP-GFP(\*\*). E) Life saponin lysis, showing the same parasite before (upper panel) and

after saponin lysis (lower panel); DIC: differential interference contrast; nuclei were stained with DAPI; size bar: 5  $\mu$ m.

The GFP-tagged DnaJ protein was not present in ring stages but was detectable in trophozoites where it showed a signal in the parasite periphery, consistent with a PV location. In addition pronounced foci in close proximity to the nucleus were detected, suggesting that some protein remained in the secretory pathway. In later stage parasites, only the parasite-internal staining of the candidate remained (Figure 13C). Despite the lack of transmembrane domains, the fusion protein (~100 kDa) was found in the pellet fraction after saponin lysis of parasites as judged by Western blot analysis (Figure 6D). In the soluble fraction only a weak signal of degradation products was detected (Figure 13D). However, saponin lysis of living parasites showed that the staining around the parasite was unaffected by lysis of the PVM (Figure 13E), which demonstrated that the degradation products were not the reason for the signal in the PV. PF3D7\_0629200 is therefore likely a protein found within the parasite and peripherally attached at the outer face of the PPM or the inner face of the PVM. Notably, for this candidate several attempts of SLI-TGD (deleting ~69% of the gene) were not successful, indicating the protein to be likely essential for parasite growth (Table 17 and Table xxiii).

#### 3.2.4.2 Candidate PF3D7\_1123500

Candidate PF3D7\_1123500 (predicted molecular weight of 154 kDa) is annotated as conserved *Plasmodium* protein of unknown function in PlasmoDB and contains a predicted N-terminal signal peptide and two transmembrane domains close to its C-terminal end (amino acid 1223 - 1245 and 1300 - 1319 from 1336 in total) (Figure 14A). The endogenous 2xFKBP-GFP integration cell line was generated via conventional drug cycling (performed by Johanna Becker (Becker, 2016)) and correct genomic modification was confirmed in an integration check PCR (Figure 14B and Table xxiv). PF3D7\_1123500 showed a faint fluorescence signal at the parasite periphery and additional prominent foci within the parasite throughout all asexual blood stages (Figure 14C). In accordance with two predicted transmembrane domains, this protein (~209 kDa) was found in the pellet fraction after saponin lysis (Figure 7D). Minor degradation (or physiologically processed) products were also detected by Western blot (Figure 14D). As all these products were found in the pellet fraction the possibility that the PV signal is derived from a clipped off fragment released into the PV is excluded and this interpretation was also confirmed by a saponin release assay (Figure 14E). Interestingly, in some free merozoites a peripheral staining was detected, indicating that this protein may be integral to the PPM, as at this stage the PVM is not present anymore (Figure 14F).

Candidate PF3D7\_1123500 is not essential for parasite growth as a SLI-TGD cell line disrupting ~90% of the gene was generated and confirmed by integration check PCR

(Figure 14G, Table 17 and Table xxiv). Notably, the integration cell line still contained cells with the original locus, indicating a cell population that had not or not correctly integrated the episomal SLI-TGD plasmid. The GFP-tagged SLI-TGD product still comprises the N-terminal signal peptide but no transmembrane domains. In agreement with this, the SLI-TGD product (~47 kDa) was found in the supernatant fraction as judged by Western blot analysis (Figure 14H).

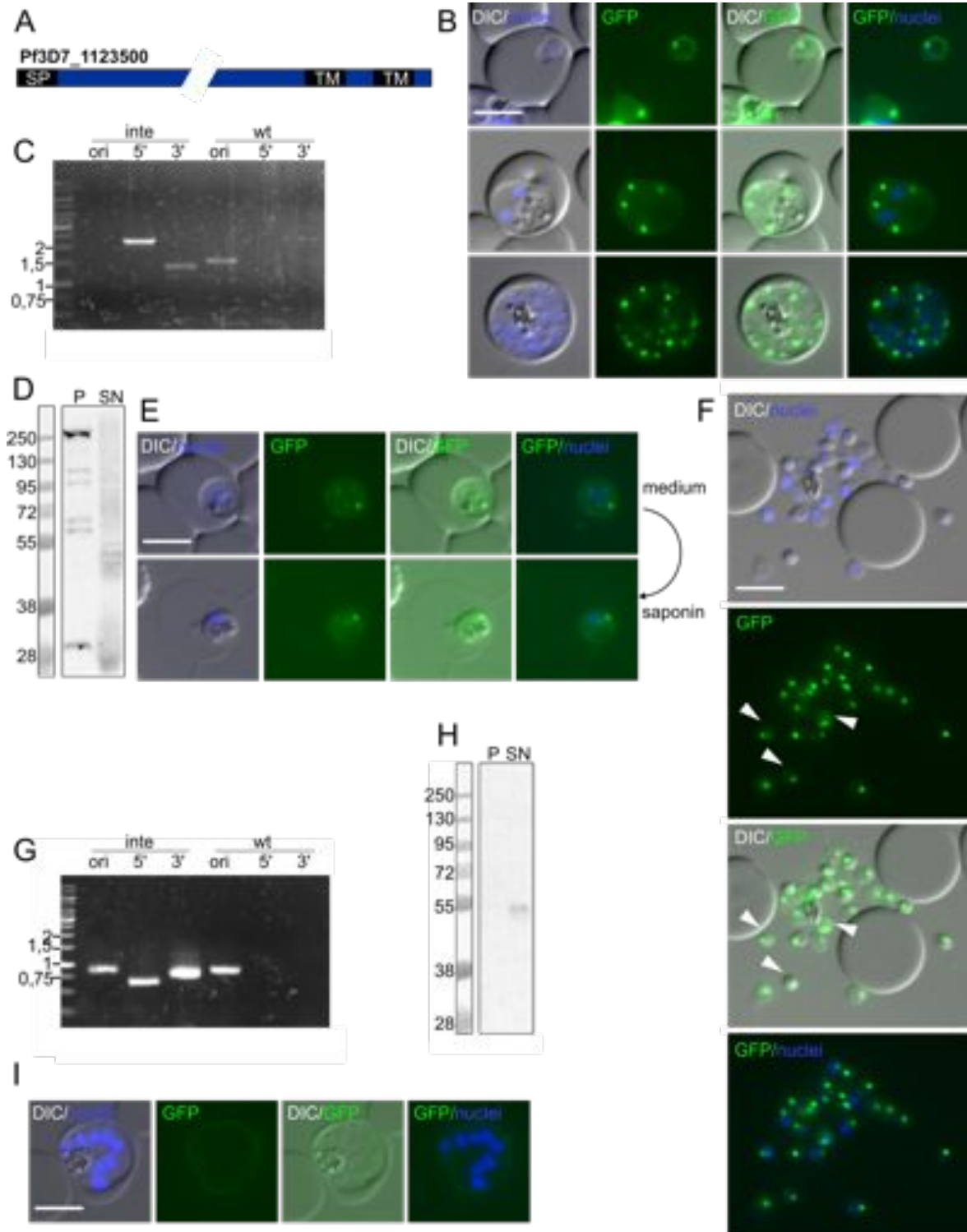


Figure 14: Candidate PF3D7\_1123500.

A) Schematic of PF3D7\_1123500 (SP: signal peptide; TM: transmembrane domain). C+G) Agarose gel with integration check PCR, confirming integration of the GFP-tagging-plasmid into the genome (inte, corresponding integration parasite line; wt, 3D7 parental line; ori, original locus; 5', PCR detection of 5' integration; 3', detection of 3' integration; the marker is indicated in kbp. B+F+I) Live cell microscopy images of the endogenously GFP-tagged PF3D7\_1123500 showing C) a ring and a trophozoite stage (top), late trophozoite (middle) and a schizont stage parasite (bottom) F) free merozoites and I) a schizont containing the SLI-TGD fusion protein; DIC: differential interference contrast; nuclei were stained with DAPI; size bar: 5  $\mu$ m. D+H) Western blot probed with anti-GFP from parasite extracts derived from saponin supernatant (SN) and pellet (P) fractions after isolation of infected RBC by Percoll (the marker is indicated in kDa); degradation product in the Western blot: GFP alone (\*). E) Life saponin lysis showing the same parasite before (upper panel) and after saponin lysis (lower panel); DIC: differential interference contrast; nuclei were stained with DAPI; size bar: 5  $\mu$ m.

Live cell microscopy with this TGD cell line confirmed a faint presence of the truncated PF3D7\_1123500 in the parasite periphery, in accordance with the Western blot result suggesting solubility of the truncation product in the PV (Figure 14I).

#### 3.2.4.3 Candidate PF3D7\_1350500

Candidate PF3D7\_1350500 (predicted molecular weight of 134 kDa) is annotated as conserved *Plasmodium* protein of unknown function in PlasmoDB and contains a predicted N-terminal signal peptide (Figure 15A) and was the only candidate selected from the supernatant fraction analysed by mass spectrometry. Endogenous 2xFKBP-GFP tagging of the candidate was done via the SLI method and the correct integration confirmed by integration check PCR (Figure 15B and Table xxiv). Notably, the integration cell line still contained cells, comprising the original locus, indicating a cell population that had not or not correctly integrated the episomal SLI plasmid. Western blot analysis showed that the full-length fusion protein (~189 kDa) is present in the pellet fraction, which was unexpected as the candidate derived from the supernatant fraction. However, in the supernatant fraction a degradation product (asterisks) was visible (Figure 15C) that might potentially also be a physiologically processed product. In live cell microscopy the protein showed a faint GFP-signal in the parasite periphery as well as in the parasite cytosol in trophozoites. A faint GFP signal was also detectable in ring stages (Figure 15D). Due to a lack of transmembrane domains the protein is most likely a peripheral membrane protein either of the PPM or PVM. In late schizonts, a single focus per nucleus was evident in addition to the cytoplasmic signal, suggesting a secretory pathway location or presence in apical organelles (Figure 15D bottom panel). Due to the lack of a PV signal in late stages, the exact position of this protein on either the PPM or PVM could not be assessed. In principle it cannot be excluded that the peripheral staining might be due to the degradation product that was present in the supernatant fraction of the Western blot or might arise from integration in a different genomic locus, conferring neomycin resistance. However, PF3D7\_1350500 was categorized as a partial PV protein unless proven differently.

Notably, six attempts to generate a SLI-TGD cell line failed (deleting ~83% of the gene), indicating that the gene PF3D7\_1350500 is likely essential for parasite growth (Table 17 and Table xxiii). Interestingly, during normal cell culture, the 2xFKBP-GFP tagged PF3D7\_1350500 cell line seemed to grow significantly slower compared to other cell lines. A preliminary experiment comparing the growth of cell line expressing 2xFKBP-GFP tagged PF3D7\_1350500 from the endogenous locus against 3D7 over 5 consecutive days (starting with synchronized parasites with a parasitemia of 0.1%) confirmed that already the C-terminal tag has a negative effect on the growth of the parasites (Figure 15E).

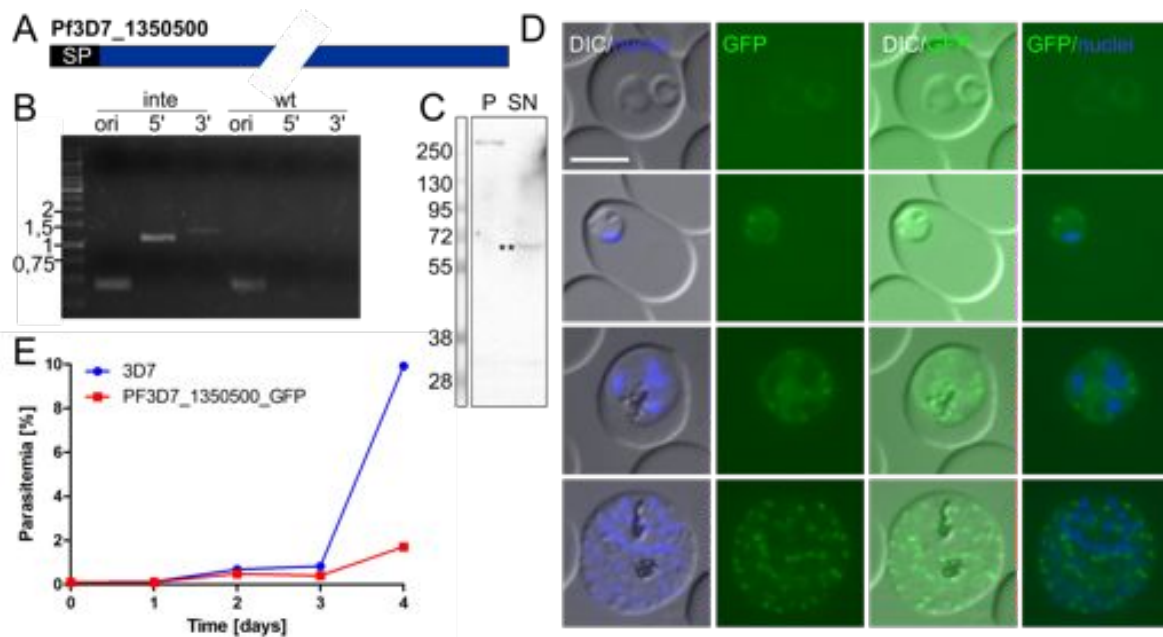


**Figure 15: Candidate PF3D7\_1350500.**

A) Schematic of PF3D7\_1350500 (SP: signal peptide). B) Agarose gel with integration check PCR, confirming integration of the GFP-tagging-plasmid into the genome (inte, corresponding integration parasite line; wt, 3D7 parental line; ori, original locus; 5', PCR detection of 5' integration; 3', detection of 3' integration; the marker is indicated in kbp. C) Western blot probed with anti-GFP from parasite extracts derived from saponin supernatant (SN) and pellet (P) fractions after isolation of infected RBC by Percoll (the marker is indicated in kDa); degradation product in the Western blot: 2xFKBP-GFP(\*\*). D) Live cell microscopy images of the endogenously GFP-tagged PF3D7\_1350500 showing a ring (top), two trophozoite stages (middle) and a schizont stage parasite (bottom); DIC: differential interference contrast; nuclei were stained with DAPI; size bar: 5  $\mu$ m. E) Growth curves comparing the parasitemia of PF3D7\_1350500-2xFKBP-GFP against 3D7 wildtype parasites on 5 consecutive days (n=1).

### 3.2.5 PV proteins with a PV localisation

Proteins with a major or even exclusive fluorescence signal around the parasite were categorized as PV proteins (including outer PPM face, PV lumen and inner face of PVM) and are presented in following sections (3.2.5.1 - 3.2.5.7)

#### 3.2.5.1 Candidate PF3D7\_0220000

Candidate PF3D7\_0220000 (predicted molecular weight of 176 kDa) is annotated as liver stage antigen 3 in PlasmoDB and contains two predicted transmembrane domains one

close to the N-terminus that may also be a signal peptide and one close to the C-terminal end (amino acid 45 - 64 and 1434 - 1456 from 1558 in total) (Figure 16A). Endogenous 2xFKBP-GFP tagging of the candidate was done via the SLI method and the correct modification was confirmed by integration check PCR (Figure 16B and Table xxiv). Western blot analysis showed the full length 2xFKBP-GFP tagged protein (~231 kDa) as well as degradation (or physiologically processed) products in the pellet fraction after saponin treatment, as expected for a transmembrane protein (Figure 16C). Live cell images of the PF3D7\_0220000-2xFKBP-GFP parasites showed a GFP signal in the parasite periphery in all asexual blood stages (Figure 16D), indicating that PF3D7\_0220000 is present within the PV compartment. The staining varied from a smooth distribution around the parasites and occasional distinct foci that appeared to be situated in the periphery or on the outer rim of the peripheral staining (Figure 9D). Occasionally, foci were also observed outside of the parasite in the host cell. In free merozoites one distinct focus per nucleus was detected, indicating presence in apical organelles or a location in the secretory pathway. Notably, the generation of a SLI-TGD cell line failed (deleting ~83% of the gene) (Table 17 and Table xxiii). This was unexpected, as this protein is known to be not essential (Maier et al., 2008).

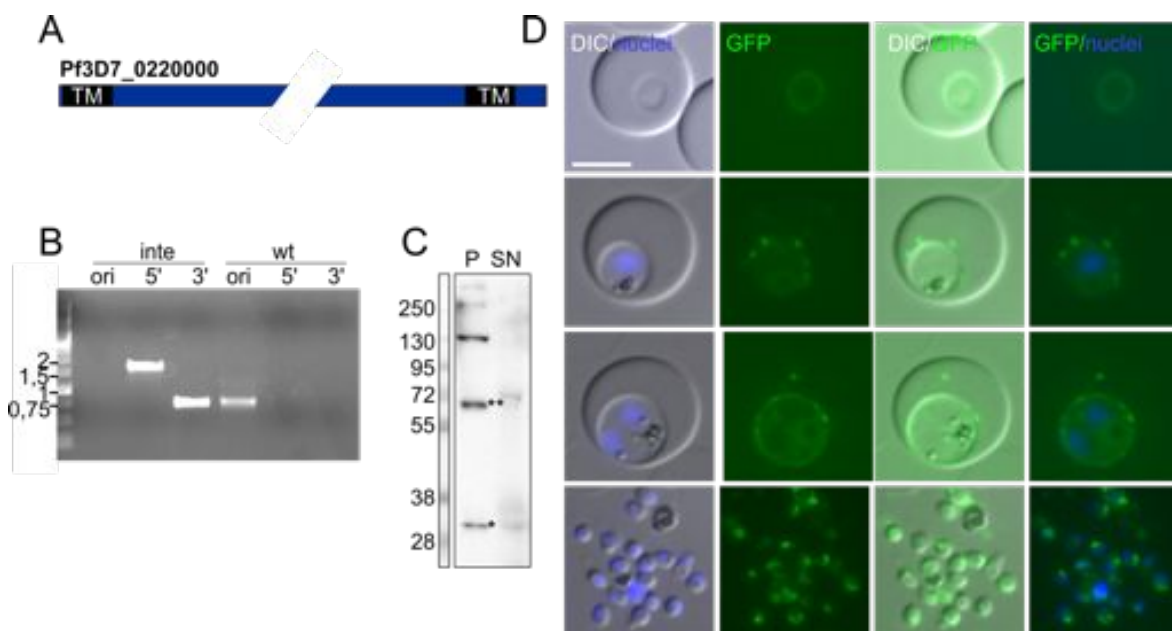


**Figure 16: Candidate PF3D7\_0220000.**

A) Schematic of PF3D7\_0220000 (TM: transmembrane domain). B) Agarose gel with integration check PCR, confirming integration of the GFP-tagging-plasmid into the genome (inte, corresponding integration parasite line; wt, 3D7 parental line; ori, original locus; 5', PCR detection of 5' integration; 3', detection of 3' integration; the marker is indicated in kbp. C) Western blot probed with anti-GFP from parasite extracts derived from saponin supernatant (SN) and pellet (P) fractions after isolation of infected RBC by Percoll (the marker is indicated in kDa); degradation products in the Western blot: GFP alone (\*) and 2xFKBP-GFP (\*\*). D) Live cell microscopy images of PF3D7\_0220000-2xFKBP-GFP parasites, showing a ring (top), a trophozoite stage (top middle), a late trophozoite (bottom middle) and free merozoites (bottom); DIC: differential interference contrast; nuclei were stained with DAPI; size bar: 5 µm.

### 3.2.5.2 Candidate PF3D7\_0731600

Candidate PF3D7\_0731600 (predicted molecular weight of 93 kDa) is annotated as acyl-CoA synthetase in PlasmoDB and contains a predicted N-terminal signal peptide (Figure 17A). Endogenous tagging of PF3D7\_0731600 with 2xFKBP-GFP was performed with the SLI method and correct integration of the corresponding plasmid was confirmed by integration check PCR (Figure 17B and Table xxiv). Western blot analysis with protein extracts of the PF3D7\_0731600-2xFKBP-GFP cell line detected the full-length fusion protein (~148 kDa) in the pellet fraction. Additionally, degradation products were visible in the pellet and in the supernatant fraction (Figure 17C).

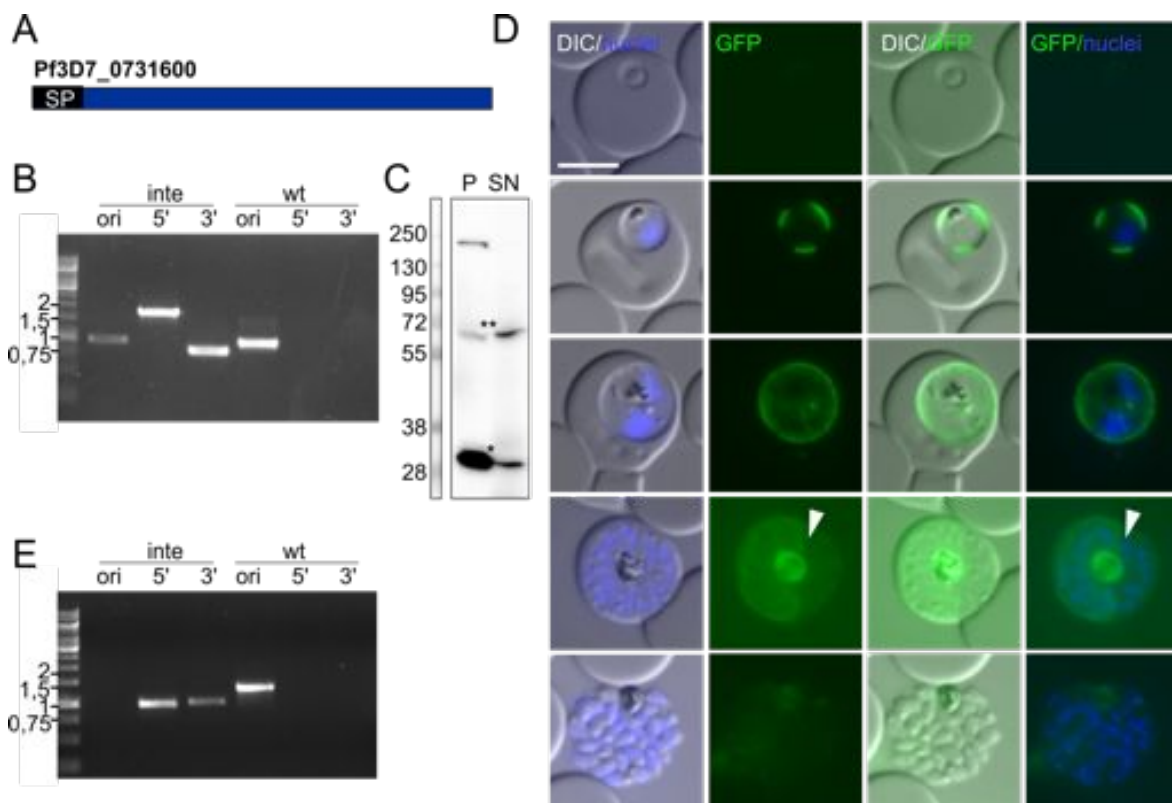


**Figure 17: Candidate PF3D7\_0731600.**

A) Schematic of Pf3D7\_0731600 (SP: signal peptide). B+E) Agarose gel with integration check PCR, confirming integration of the GFP-tagging-plasmid into the genome (inte, corresponding integration parasite line; wt, 3D7 parental line; ori, original locus; 5', PCR detection of 5' integration; 3', detection of 3' integration; the marker is indicated in kbp). C) Western blot probed with anti-GFP from parasite extracts derived from saponin supernatant (SN) and pellet (P) fractions after isolation of infected RBC by Percoll (the marker is indicated in kDa); degradation products in the Western blot: GFP alone (\*) and 2xFKBP-GFP(\*\*). D) Live cell microscopy images of PF3D7\_0731600-2xFKBP-GFP parasites, showing a ring (top), two trophozoite stages (middle), a schizont stage parasite and free merozoites (bottom); DIC: differential interference contrast; nuclei were stained with DAPI; size bar: 5  $\mu$ m.

Live cell microscopy showed a prominent staining, either evenly distributed or in patches in the parasite periphery typical for a presence within the PV compartment of trophozoites (Figure 10D). The GFP signal was absent in ring stages. With maturation of the parasite the GFP signal became more diffuse and accumulated in the food vacuole although it was

still also visible in the parasite periphery in segmented schizonts but not around individual merozoites (white arrow, Figure 17D). This finding indicated that PF3D7\_0731600 is a peripheral membrane protein of the PVM. In free merozoites no GFP signal was detectable (Figure 17D). A gene disruption cell line (~18% of the residual gene remaining) via SLI-TGD was successfully raised and confirmed by integration check PCR, indicating that candidate PF3D7\_0731600 is not essential for parasite growth (Figure 17E, Table 17 and Table xxiv).

### 3.2.5.3 Candidate PF3D7\_0912400

Candidate PF3D7\_0912400 (predicted molecular weight of 53 kDa) is annotated as a putative alkaline phosphatase and contains a predicted N-terminal signal peptide and a transmembrane domain close to its C-terminal end (amino acid 405 - 427 from 446 in total) (Figure 18A). Endogenous tagging of PF3D7\_0912400 with 2xFKBP-GFP was performed with the SLI method and correct integration of the corresponding plasmid into the genome (inte, corresponding integration parasite line; wt, 3D7 parental line; ori, original locus; 5', PCR detection of 5' integration; 3', detection of 3' integration; the marker is indicated in kbp). C) Western blot probed with anti-GFP from parasite extracts derived from saponin supernatant (SN) and pellet (P) fractions after isolation of infected RBC by Percoll (the marker is indicated in kDa); hashes indicate antibody independent reaction of ECL with haemoglobin dimer and trimer. D) Live cell

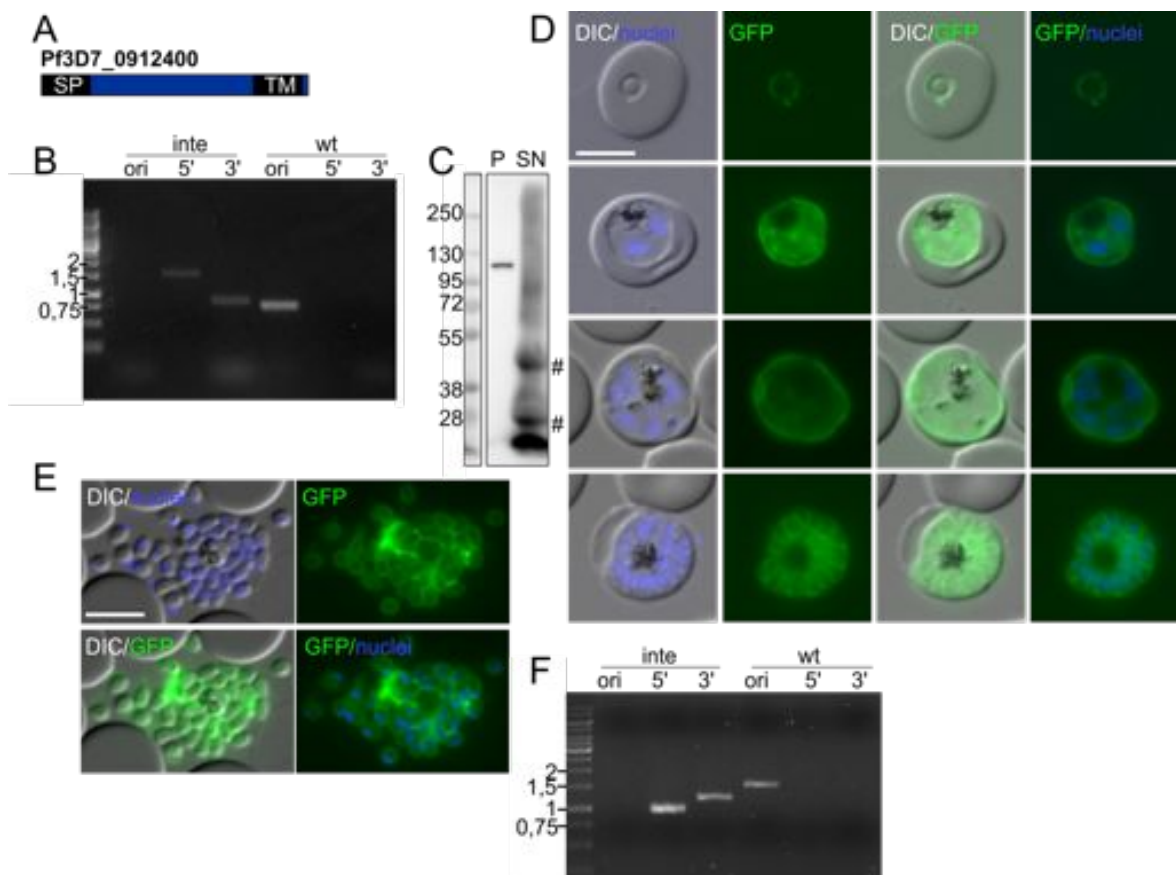


**Figure 18: Candidate PF3D7\_0912400.**

A) Schematic of PF3D7\_0912400 (SP: signal peptide; TM: transmembrane domain). B+F) Agarose gel with integration check PCR, confirming integration of the GFP-tagging-plasmid into the genome (inte, corresponding integration parasite line; wt, 3D7 parental line; ori, original locus; 5', PCR detection of 5' integration; 3', detection of 3' integration; the marker is indicated in kbp). C) Western blot probed with anti-GFP from parasite extracts derived from saponin supernatant (SN) and pellet (P) fractions after isolation of infected RBC by Percoll (the marker is indicated in kDa); hashes indicate antibody independent reaction of ECL with haemoglobin dimer and trimer. D) Live cell

microscopy images of the endogenously 2xFKBP-GFP-tagged PF3D7\_0912400 parasites, showing a ring stage (top) a trophozoite and a late trophozoite (middle) and a schizont stage parasite (bottom) E) free merozoites; DIC: differential interference contrast; nuclei were stained with DAPI; size bar: 5  $\mu$ m.

In accordance with its predicted transmembrane domain, PF3D7\_0912400-2xFKBP-GFP was present in the pellet fraction after saponin lysis as judged by Western analysis of the knock-in parasites (Figure 18C). Immunofluorescence microscopy with the PF3D7\_0912400-2xFKBP-GFP showed a staining around the parasite typical for a location within the PV compartment in all asexual blood stages. In late schizonts the staining surrounded individual merozoites (Figure 11D), suggesting a PPM location. This was confirmed in released merozoites where the protein was found around each extraerythrocytic parasite (Figure 18E). A SLI-TGD cell line disrupting ~67% of the gene was successfully generated and confirmed by integration check PCR (Figure 18F and Table xxiv), demonstrating that candidate PF3D7\_0912400 is not essential for parasite growth (Table 17 and Table xxiv).

#### **3.2.5.4 Candidate PF3D7\_1024800**

Candidate PF3D7\_1024800 (predicted molecular weight of 171 kDa) was annotated as conserved *Plasmodium* protein of unknown function at the time of MS analysis (PlasmoDB v24). In the meantime the annotation was changed to exported protein 3 (Batinovic et al., 2017). PF3D7\_1024800 contains a predicted N-terminal signal peptide and a transmembrane domain close to its C-terminal end (amino acid 1405 - 1427 from 1464 in total) (Figure 19A). The integration cell line containing an endogenous 2xFKBP-GFP-tag was generated via the SLI method by Paolo Mesén-Ramírez and was confirmed by integration check PCR (Figure 19B and Table xxiv). Beside the full-length fusion protein (~226 kDa) also smaller degradation (or physiologically processed) products were detected by Western analysis (Figure 19C). Fluorescence microscopy showed that the GFP-tagged PF3D7\_1024800 was present in all asexual blood stages but towards the end of the cycle lost the peripheral signal that indicated presence within the PV compartment for a more uniform staining within the parasite cytosol (Figure 19D), potentially due to processed fragments containing GFP that were detected by the Western analysis. In late schizonts a single focus per nucleus was evident in addition to the cytoplasmic signal, suggesting a secretory pathway location or presence in apical organelles (Figure 19D bottom panel). Due to the lack of a PV signal in late stages, the exact position of this protein in the PV could not be assessed. A disruption of this gene using SLI-TGD was successfully established (~9% of the residual gene remaining), indicating that EXP3 is not important for parasite growth (Figure 19E, Table 17 and Table xxiv).

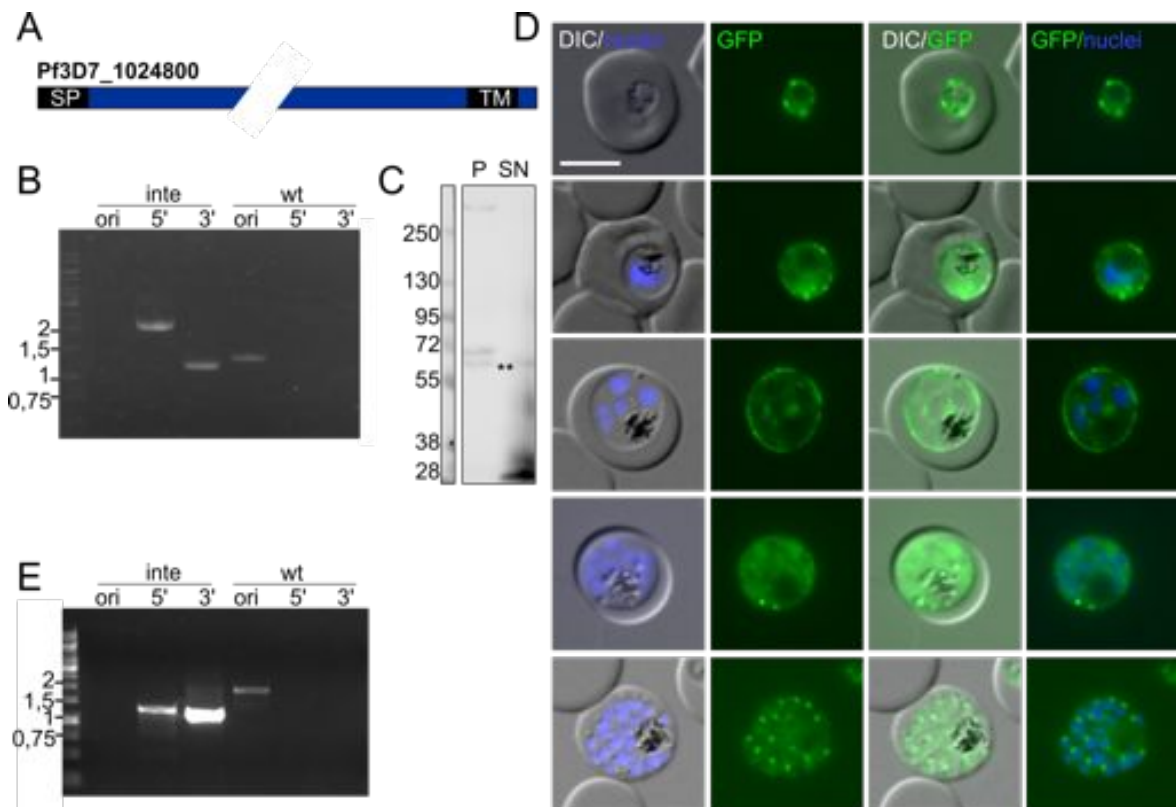


**Figure 19: Candidate PF3D7\_1024800.**

A) Schematic of PF3D7\_1024800 (SP: signal peptide; TM: transmembrane domain). B+E) Agarose gel with integration check PCR, confirming integration of the GFP-tagging-plasmid into the genome (inte, corresponding integration parasite line; wt, 3D7 parental line; ori, original locus; 5', PCR detection of 5' integration; 3', detection of 3' integration; the marker is indicated in kbp. C) Western blot probed with anti-GFP from parasite extracts derived from saponin supernatant (SN) and pellet (P) fractions after isolation of infected RBC by Percoll (the marker is indicated in kDa); degradation product in the Western blot: 2xFKBP-GFP(\*\*). D) Live cell microscopy images of the endogenously GFP-tagged PF3D7\_1024800 showing (from top to bottom) a ring, a trophozoite, a late trophozoite and two schizont stages; DIC: differential interference contrast; nuclei were stained with DAPI; size bar: 5  $\mu$ m.

### 3.2.5.5 Candidate PF3D7\_1135400

Candidate PF3D7\_1135400 (predicted molecular weight of 28 kDa) is annotated as a conserved *Plasmodium* protein of unknown function in PlasmoDB and contains a predicted N-terminal signal peptide (SignalP3.0) (Figure 20A). The integration cell line containing an endogenous 2xFKBP-GFP-tag fused to the gene encoding PF3D7\_1135400 was generated via SLI and correct integration was confirmed by integration check PCR (both performed by Paolo Mesén-Ramírez) (Figure 20B and Table xxiv). Although transmembrane domains are absent the 2xFKBP-GFP-tagged fusion protein (~83 kDa) was found in the pellet fraction in western blot analysis, indicating membrane association (Figure 20C). Fluorescence microscopy showed that the GFP-tagged protein was found in the parasite periphery typical for a PV location and in the parasite cytosol and that the protein was expressed in all asexual blood stages (Figure 13C). In late schizonts the signal was still prominent around the entire group of forming merozoites, indicating a PVM location. However, there was also more dispersed signal

between forming merozoites, potentially indicating limited release from the membrane. No signal was detected in released merozoites (Figure 20D).

Taken together, candidate PF3D7\_1135400 is likely a peripheral membrane protein of the PVM from where it is partially released before rupture. Interestingly, the attempt to perform SLI-TGD of Paolo Mesén-Ramírez was successful, although the target homology region was chosen in a way that ~73% of the gene was still intact. Another attempt with a shorter targeting region leading to a deletion of more than 60% of the gene, including parts of the region encoding the predicted thioesterase domain, did not succeed in 6 attempts (Table xxiii). It is therefore possible that the N-terminal 73% of this gene are still sufficient for function, but that shorter deletions are not and that PF3D7\_1135400 is important for parasite growth (Table 17, Table xxiii and Table xxiv).

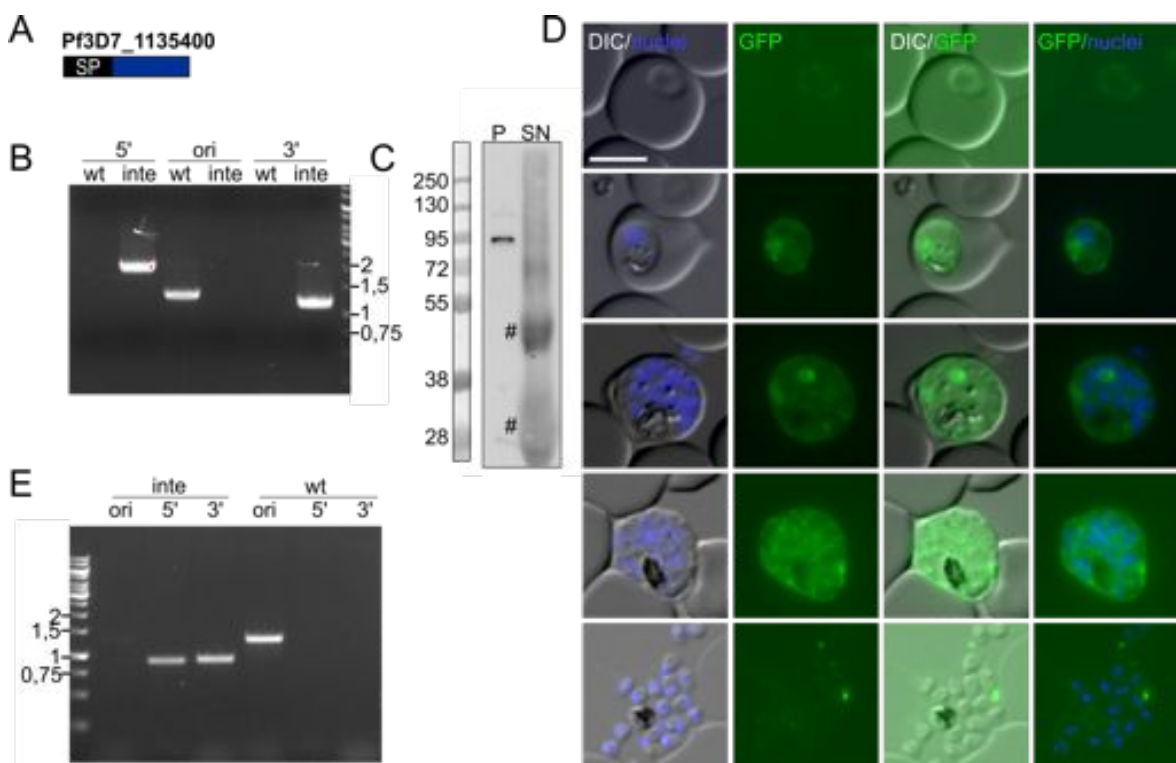


**Figure 20: Candidate PF3D7\_1135400.**

A) Schematic of PF3D7\_1135400 (SP: signal peptide). B+E) Agarose gel with integration check PCR, confirming integration of the GFP-tagging-plasmid into the genome (inte, corresponding integration parasite line; wt, 3D7 parental line; ori, original locus; 5', PCR detection of 5' integration; 3', detection of 3' integration; the marker is indicated in kbp. C) Western blot probed with anti-GFP from parasite extracts derived from saponin supernatant (SN) and pellet (P) fractions after isolation of infected RBC by Percoll (the marker is indicated in kDa); hashes indicate antibody independent reaction of ECL with haemoglobin dimer and trimer. D) Live cell microscopy images of the endogenously GFP-tagged PF3D7\_1135400 showing (from top to bottom) a ring, a trophozoite, two schizont stages and free merozoites; DIC: differential interference contrast; nuclei were stained with DAPI; size bar: 5 µm.

### 3.2.5.6 Candidate PF3D7\_1226900

Candidate PF3D7\_1226900 (predicted molecular weight of 57 kDa) was annotated as conserved Plasmodium protein of unknown function to the time of MS analysis in

PlasmoDBv24. In the meantime the annotation was changed to parasitophorous vacuolar protein 2 (Batinovic et al., 2017). PF3D7\_1226900 contains a predicted N-terminal signal peptide (Figure 21A). The endogenously 2xFKBP-GFP tagged integration cell line was generated via conventional drug cycling (performed by Johanna Becker (Becker, 2016)) and correct integration was confirmed by integration check PCR (Figure 21B and Table xxiv).

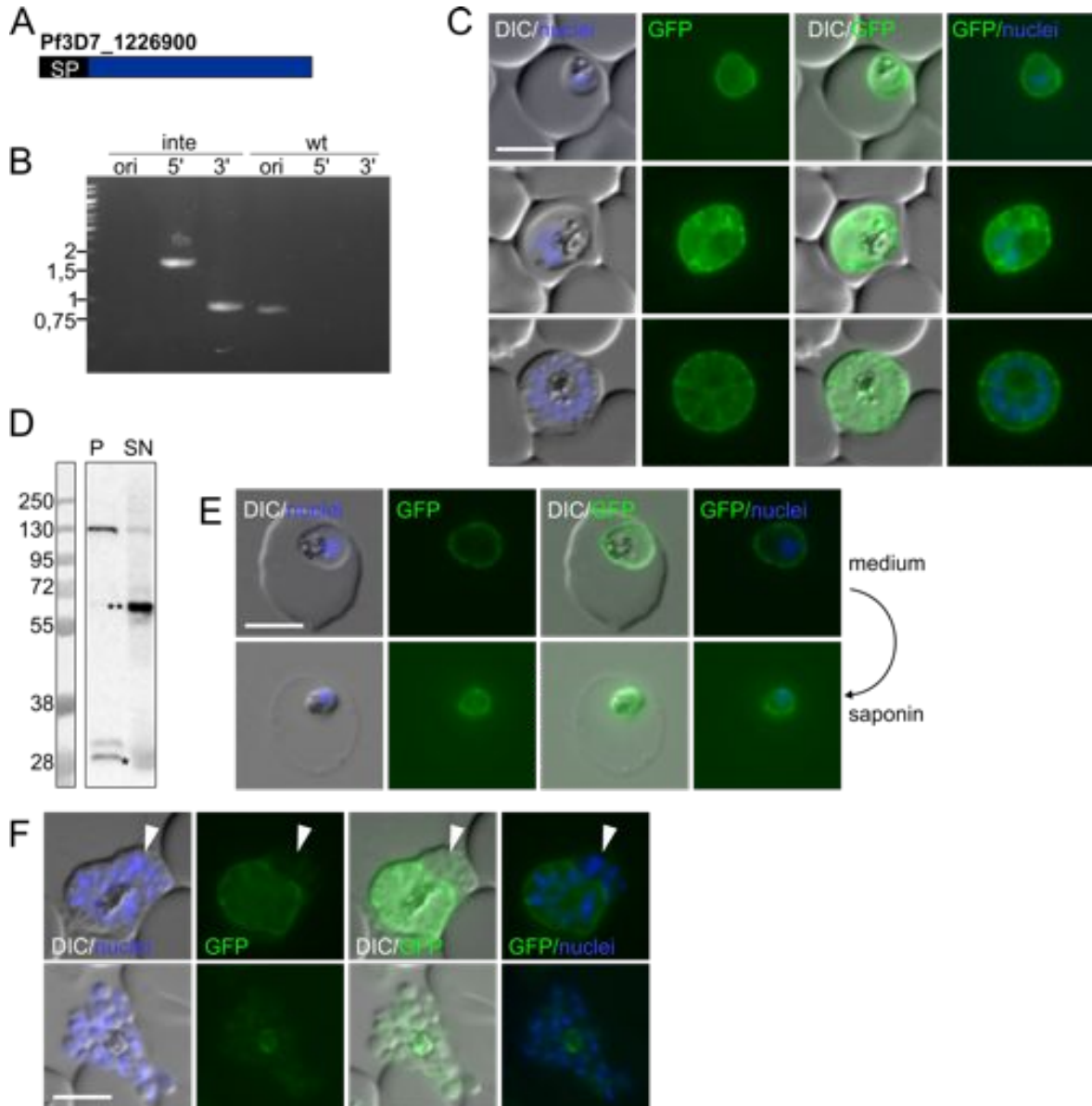


**Figure 21: Candidate PF3D7\_1226900.**

A) Schematic of PF3D7\_1226900 (SP: signal peptide). B) Agarose gel with integration check PCR, confirming integration of the GFP-tagging-plasmid into the genome (inte, corresponding integration parasite line; wt, 3D7 parental line; ori, original locus; 5', PCR detection of 5' integration; 3', detection of 3' integration; the marker is indicated in kbp. C+F) Live cell microscopy images of the endogenously GFP-tagged PF3D7\_1226900 showing a trophozoite stage (top), late trophozoite (middle) and a schizont stage parasite (bottom) F) a schizont (upper panel) and free merozoites (lower panel); DIC: differential interference contrast; nuclei were stained with DAPI; size bar: 5  $\mu$ m. D) Western blot probed with anti-GFP from parasite extracts derived from saponin supernatant (SN) and pellet (P) fractions after isolation of infected RBC by Percoll (the marker is indicated in

kDa); degradation products in the Western blot: GFP alone (\*) and 2xFKBP-GFP(\*\*). E) Life saponin lysis, showing the same parasite before (upper panel) and after saponin lysis (lower panel); DIC: differential interference contrast; nuclei were stained with DAPI; size bar: 5  $\mu$ m.

Life cell microscopy of the integration cell line showed a prominent staining in the parasite periphery throughout all asexual blood stages (Figure 21C), indicating a location within the PV compartment. Western blot analysis showed the full-length protein (~112 kDa) in the pellet fraction and a prominent degradation band in the saponin supernatant (Figure 21D). However, release of the PV content in a saponin release assay did not abolish the signal in the parasite periphery (Figure 21E), clearly showing that the signal around the parasite derives from the full-length protein. In late stages merozoites were observed that had already been partially released but, in contrast to the merozoites in the remainder of the schizont, were not surrounded by GFP signal (arrowheads Figure 21F upper panel). As the released merozoites are surrounded by PPM, this indicates that these proteins were associated with the PVM. In agreement with this, no fluorescence was observed with fully released merozoites (Figure 21F bottom panel). Notably, for this candidate the generation of a SLI-TGD cell line (deleting ~73% of the gene) was unsuccessful, indicating that this protein is likely essential for growth (Table 17 and Table xxiii).

#### **3.2.5.7 Candidate PF3D7\_1464600**

Candidate PF3D7\_1464600 (predicted molecular weight of 170 kDa) is annotated as a putative serine/threonine protein phosphatase UIS2 and contains besides metallo-dependant phosphatase domains (GeneDB) a predicted N-terminal signal peptide (Figure 22A). The integration cell line to endogenously tag UIS2 with 2xFKBP-GFP was generated via conventional drug cycling (performed by Johanna Becker (Becker, 2016)) and correct integration was confirmed by integration check PCR (Figure 22B and Table xxiv). Interestingly, the fusion protein (~225 kDa) was detected in the pellet fraction in Western blot analysis, indicating membrane association (Figure 22C). Life cell microscopy images with this cell line showed fluorescence around the parasites in all blood stages, either evenly distributed or sometimes with gaps (Figure 22D). This is consistent with a location of UIS2 in the PV compartment. In late stages merozoites were observed that had already been partially released but, in contrast to the merozoites in the remainder of the schizont, were not surrounded by GFP signal (arrowheads Figure 22E bottom panel). As the released merozoites are surrounded by PPM, this indicates that UIS2 was associated with the PVM. In agreement with this, no fluorescence was observed with fully released merozoites (Figure 22E upper panel). Notably, for this candidate several attempts of SLI-TGD (deleting ~90% of the gene) did not result in a cell line, indicating that the protein is likely essential for parasite growth (Table 17 and Table xxiii).

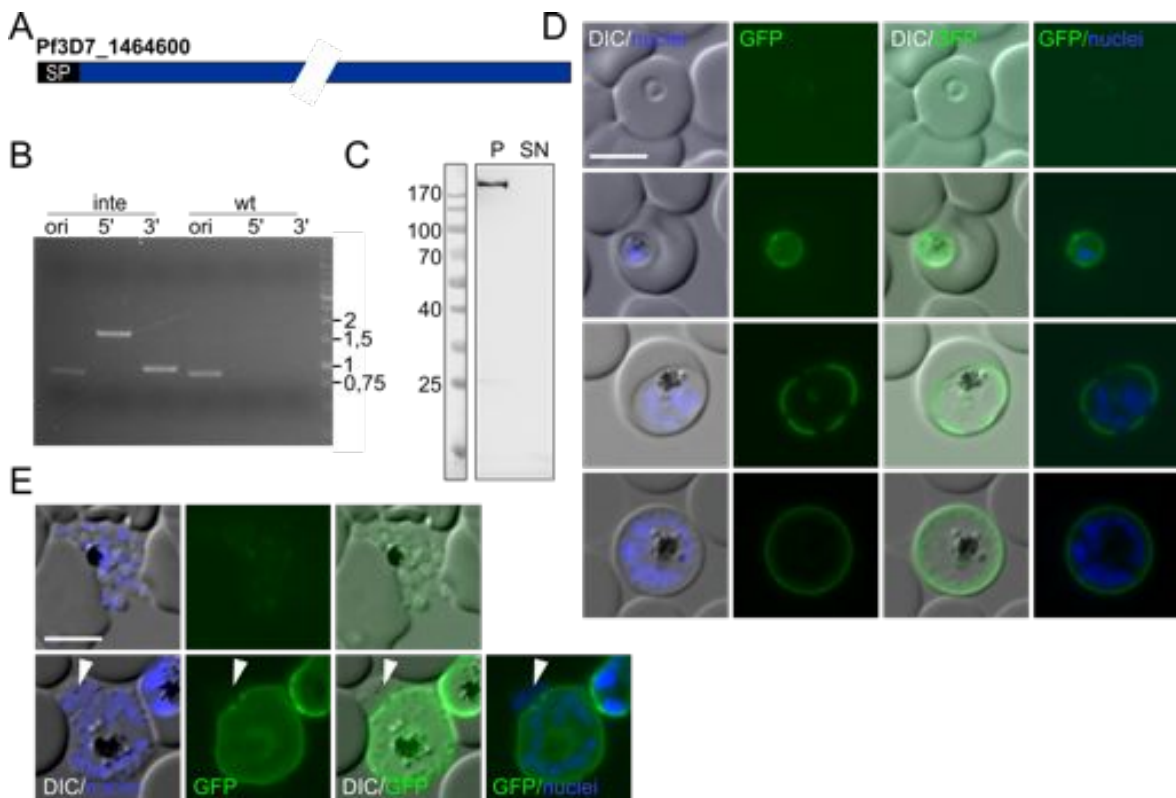


**Figure 22: Candidate PF3D7\_1464600.**

A) Schematic of PF3D7\_1464600 (SP: signal peptide). B) Agarose gel with integration check PCR, confirming integration of the GFP-tagging-plasmid into the genome (inte, corresponding integration parasite line; wt, 3D7 parental line; ori, original locus; 5', PCR detection of 5' integration; 3', detection of 3' integration; the marker is indicated in kbp. C+F) Live cell microscopy images of the endogenously 2xFKBP-GFP-tagged PF3D7\_1464600 showing a ring stage (top) trophozoite stage (upper middle), late trophozoite (lower middle) and a schizont stage parasite (bottom) F) free merozoites (upper panel) and a schizont (lower panel); DIC: differential interference contrast; nuclei were stained with DAPI; size bar: 5  $\mu$ m. D) Western blot probed with anti-GFP from parasite extracts derived from saponin supernatant (SN) and pellet (P) fractions after isolation of infected RBC by Percoll (the marker is indicated in kDa).

### 3.2.6 Generation of a knock sideway system for secretory proteins

For the functional characterization of proteins in *P. falciparum* the knock sideway system has been useful (Birnbaum et al., 2017). This system is based on the induced mislocalization of the target protein to remove it from its site of action. So far this had been restricted to proteins accessible in the parasite cytoplasm and in the nucleus (Birnbaum et al., 2017). The mislocalization of proteins within the secretory pathway, including proteins of the PV compartment, has not been feasible due to a lack of suitable mislocalizers. To overcome this problem, an ER-mislocalizer was generated by fusing a FRB domain to the mScarlett-SDEL ER marker (generated by Jakob Birnbaum). The SDEL has previously been shown to be an effective ER retention signal in *P. falciparum* (Kulzer et al., 2009). In theory the 2xFKBP-GFP-tagged protein of interest (POI) would be retained in the ER upon the addition of rapalog, which induces the dimerization to the ER-located mislocalizer (Figure 23). A similar approach was successfully used to synchronize protein transport in

the secretory pathway to analyse and visualize intracellular trafficking, although this system (termed 'RUSH' for retention using selective hooks) was based on a different pair of conditionally interacting domains (Boncompain and Perez, 2012).

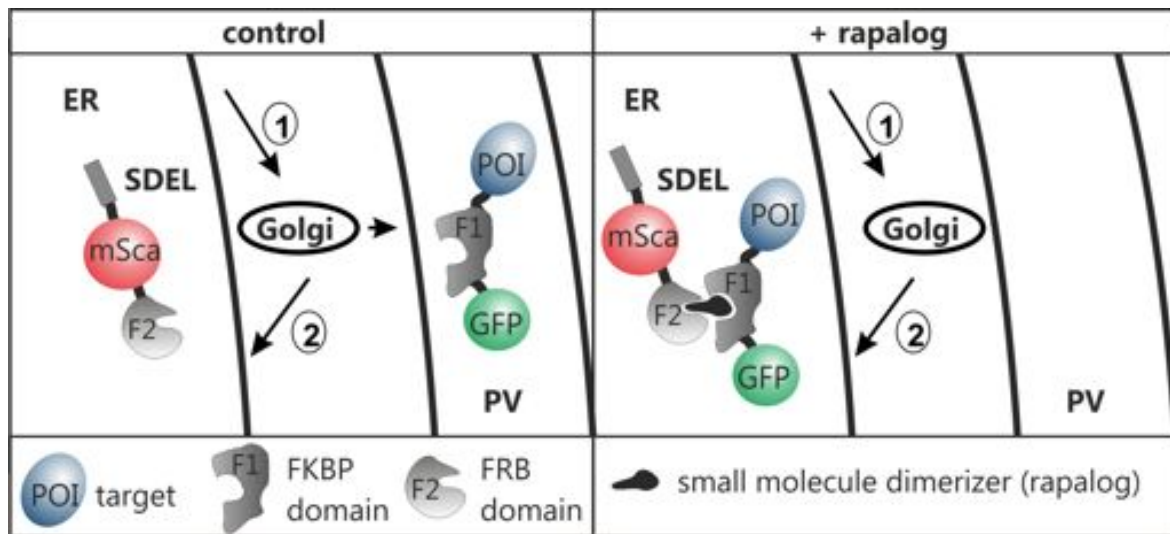


**Figure 23: Theoretical model of the mislocalization into the ER**

The FRB-mScarlet-SDEL mislocalizer is present within the ER due to the SDEL retention signal that mediates retrograde transport for proteins that escaped to the Golgi (1) from the Golgi back to the ER (2). The FKBP-tagged protein of interest (POI) is normally trafficked to the PV compartment. Upon the addition of rapalog the POI dimerizes with the mislocalizer either in the ER or in the Golgi, which results in a retrograde transport of the dimerization complex back into the ER (2) and effective mislocalization.

Here, four candidates, namely PF3D7\_0629200 (section 3.3.2.1), PF3D7\_0912400 (section 3.3.3.3), PF3D7\_1123500 (section 3.3.2.2) and PF3D7\_1464600 (section 3.3.3.7) were transfected with the generated ER-mislocalizer to test whether a conditional protein inactivation system is possible for secretory proteins using this approach.

For PF3D7\_0629200 it was difficult to determine to which extend mislocalization had occurred after addition of rapalog, as a prominent ER signal was present in trophozoites of the control and the rapalog-treated cells (Figure 24A). Interestingly, for the PF3D7\_0629200 cell line rapalog treatment had a negative growth effect on day 4 post addition of rapalog (Figure 24A).

For the PPM protein PF3D7\_0912400 partial mislocalization (i.e. retention in the ER) was observed in trophozoites. In later stages the ER seemed to be dragged to the parasite periphery and the POI changed from an evenly distributed staining of the PPM (compare also to Figure 18D) to distinct fluorescent patches in the parasite periphery that seemed to be attached to the ER (Figure 24B). The growth curve for this candidate showed a small difference in parasitemia (Figure 24B), which is presumably due to a small difference in the starting parasitemia and should be neglected. Hence, the addition of rapalog had no negative effect on parasite viability, which is in agreement with the TGD data (Table 17).

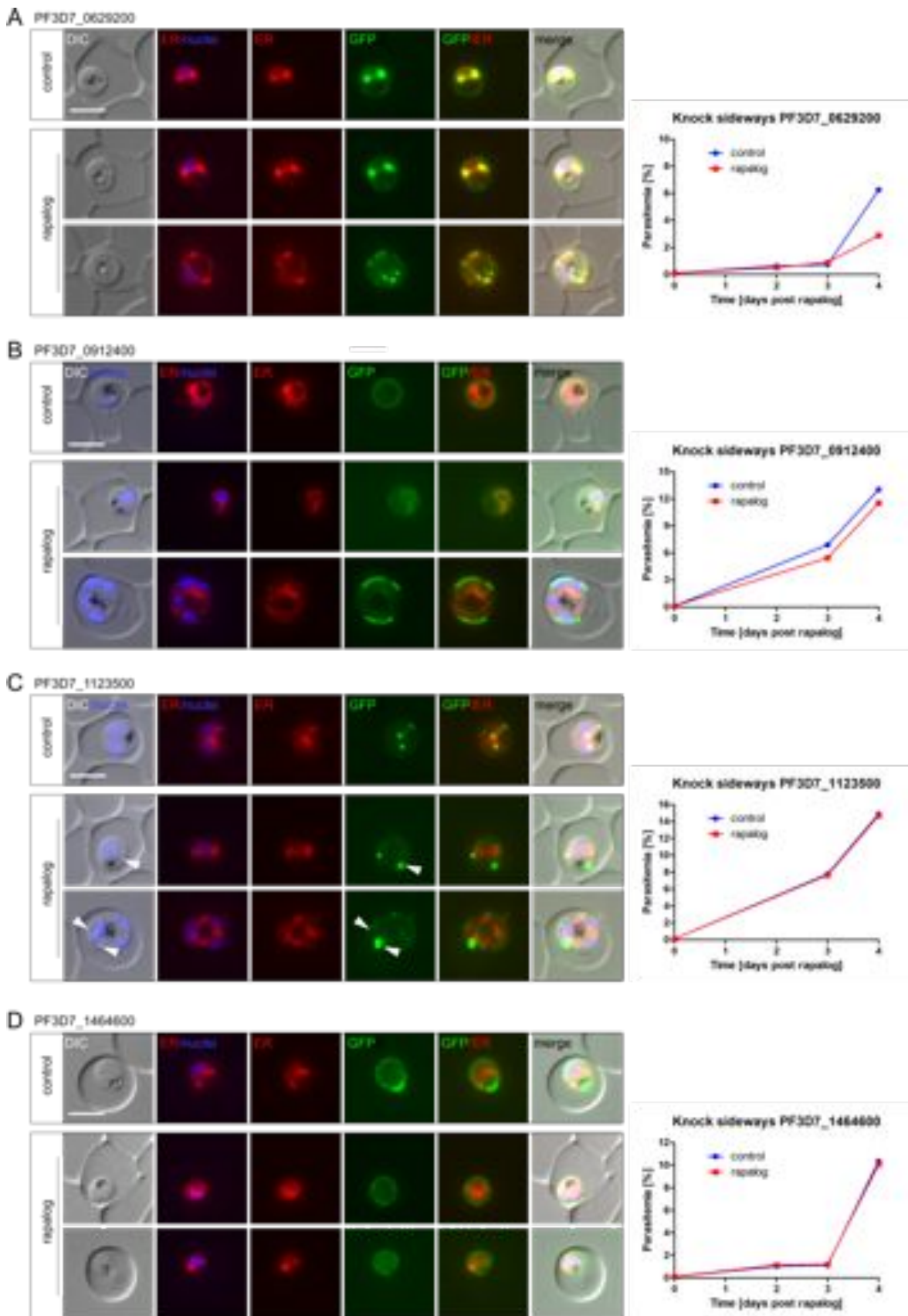


**Figure 24: Rapalog induced ER-directed knock sideways.**

Fluorescence microscopy images of ER-directed knock sideways and flow cytometry growth curves, comparing the parasitemia in the culture where rapalog-induced mislocalization of the protein of interest (POI) was induced compared to the control on 5 consecutive days for A) PF3D7\_0629200 (n=2, see Appendix Figure xxx), B) PF3D7\_0912400 (n=1), C) PF3D7\_1123500 (n=1) (white

arrows indicate vesicle-like structures) and D) PF3D7\_1464600 (n=1); DIC: differential interference contrast; ER: mScarlet-tagged mislocalizer; nuclei were stained with DAPI; GFP: GFP-tagged POI; merge indicates overlay of all presented channels; size bar: 5  $\mu$ m. All cell lines were transfected with the ER mislocalizer. Control and rapalog treated cells were imaged one day post rapalog

The partial PV protein PF3D7\_1123500, presumably also associated with the PPM (Figure 14F), showed no co-localization between the ER-mislocalizer after addition of rapalog and the GFP signal of the POI after induction of the knock sideways, although a different location of the distinct foci within the parasite was observed (Figure 24C). Compared to the control cells (see also section 3.2.4.2) the rapalog treated cells presented their foci exclusively (13 of 13 investigated cells) at the parasite periphery in vesicle-like structures (white arrows). In concordance with the TGD data, the mislocalization upon the addition of rapalog had no effect on parasite viability (Figure 24C). Hence, in this case the knock sideways was clearly ineffective.

The PVM associated protein PF3D7\_1464600 (UIS2) seemed to be completely unaffected by the rapalog-induced mislocalization and no co-localization or a change in the pattern of the GFP signal was observed (Figure 24D). In agreement, rapalog treatment did not affect parasite viability in a growth assay (Figure 24D), although this protein was found to be essential for parasite survival (section 3.2.5.7 and 3.3).

In all four tested cell lines the mislocalizer showed a typical ER staining. However, the investigated POI were not or only inefficiently mislocalized and this approach was therefore not used for large-scale functional analysis of the newly identified proteins. Further optimisation is needed to make this system a viable option for conditional protein inactivation in *P. falciparum* parasites.

### 3.3 Functional Analysis of candidate PF3D7\_1464600 UIS2

Candidate PF3D7\_1464600 is annotated as the putative serine/threonine protein phosphatase UIS2 and was here discovered to be a PV protein attached to the PVM (section 3.3.3.7). UIS2 has previously been described as a unique phosphatase of the PP2C/PPM (metal-dependent protein phosphatase) family that is required for liver stage development by presumably interacting with the phosphorylated eukaryotic initiation factor 2 $\alpha$  (eIF2 $\alpha$ -P) in *P. berghei* (Zhang et al., 2016). In the same publication several attempts to generate an UIS2 knock out cell line for *P. berghei* blood stages failed. In accordance with these findings SLI-TGD did not result in a gene deletion cell line, indicating that the protein is likely essential for parasite growth (section 3.2.5.7). To verify this finding and to further characterize the function of PF3D7\_1464600, a conditional knockout cell line was generated. For this, a plasmid was designed that after integration truncated the gene encoding PF3D7\_1464600 but at the same time provided a HA-tagged, floxed and recodonized version of the gene that by virtue of a T2A skip peptide was expressed from

the same locus to rescue the disrupted gene (Figure 25A modified locus). An inducible split Cre recombinase (diCre) that can be activated through addition of rapalog (Andenmatten et al., 2013; Birnbaum et al., 2017; Jullien et al., 2007) can then be used to excise the floxed active copy of *uis2* to assess the phenotype of parasites without this gene (Figure 25A excised locus). For all subsequent experiments diCre-mediated gene excision was induced through addition of rapalog in synchronized ring stage parasites.

First the generation of the integration cell line (Figure 1A, 'modified locus') was verified by integration check PCR (Figure 25B and Table xxiv). Upon addition of rapalog excision of the active PF3D7\_1464600 version was induced, resulting in a gene deletion cell line as was demonstrated in a PCR specific for the excised and the modified genomic locus (Figure 25C). This also showed that excision is already detectable on day 1 post rapalog and on day 2 post rapalog a prominent band representing the excised locus was detected while the modified locus was difficult to detect, suggesting rapid and efficient excision (Figure 25C). As expected, the control cells preserved the modified locus on both days. Taken together the PCR confirmed that the complete excision of the functional *uis2* gene is possible within one asexual growth cycle.

On the protein level the *uis2* gene deletion was verified by immune fluorescence assay and Western blot analysis on day 2 post rapalog. On day 2 post rapalog *uis2* excised ring stages are present that left residual UIS2 protein associated with the PVM during egress. Immune fluorescence images showed that the HA-tagged recodonized PF3D7\_1464600 is present in the control but absent in the rapalog treated cells due to *uis2* gene excision and the consequent lack of UIS2 in the second life cycle (Figure 25D). In agreement, anti-HA Western blot analysis detected only a faint band in the extract of the rapalog treated cells compared to a prominent band in the control (Figure 25E), confirming loss of the protein. Although probing the same samples for aldolase revealed that there was also less overall protein in the extracts of the parasites grown with rapalog (likely due to the negative impact of loss of UIS2 on growth, see below), UIS2 was proportionally less abundant in the rapalog-treated extracts compared to the untreated control extracts.

In general the presented data leads to the conclusion that the *uis2* gene excision is rapid and takes place within the first asexual cycle after rapalog addition, while residual UIS2 protein remains associated with the PVM until new merozoite progeny start into the next round of propagation in new red blood cells, leaving the PVM behind during egress. The experimental configuration to obtain matched cultures with and without UIS2 at their PVM summarizes the presented data and was used for all further assays (sections 3.3.1, 3.3.2 and 3.3.3) (Figure 25F).

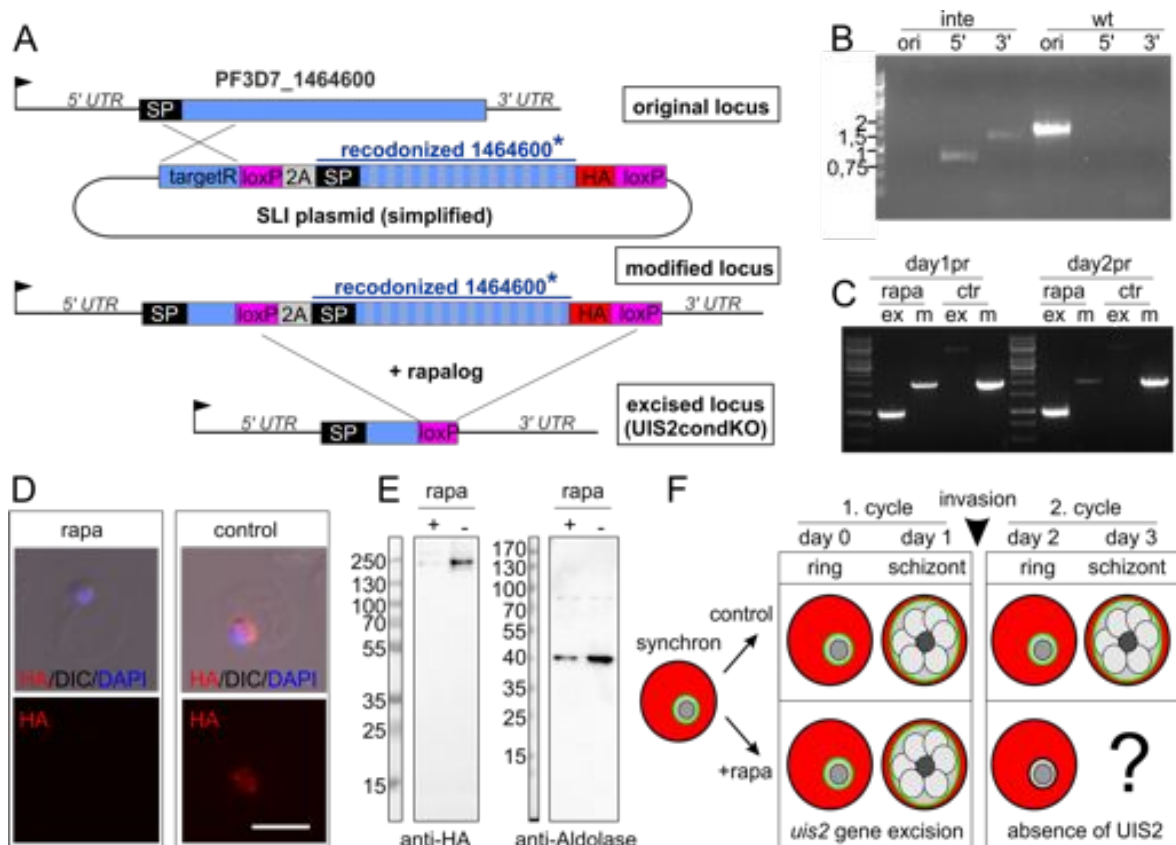


**Figure 25: Conditional deletion of *uis2* encoding PF3D7\_1464600**

A) Schematic for the generation of a conditional knockout cell line (UIS2condKO) targeting PF3D7\_1464600 and subsequent excision upon the addition of rapalog; UTR: untranslated region; SP: signal peptide; 2A: skip peptide; arrow: endogenous *uis2* promoter. B) Agarose gel with integration check PCR, confirming integration of the construct into the genome, modifying the *uis2* locus to enable excision of the functional copy of *uis2*. (inte, integration parasite line; wt, 3D7 parental line; ori, original locus; 5', PCR detection of 5' integration; 3', detection of 3' integration; the marker is indicated in kbp. C) Agarose gel with PCR to confirm loss of functional copy of *uis2* after addition of rapalog on day 1 and 2; rapa: on rapalog, ctr: control, ex: excised locus, m: modified locus. D) Anti-HA (HA) probed IFA in suspension with cells harvested on day 2 post rapalog; nuclei were stained with DAPI; DIC: differential interference contrast; size bar: 5 μm. E) Western blot probed with anti-HA and anti-Aldolase with protein extracts generated on day 2 post rapalog from the UIS2condKO cell line (minus: control; plus: rapalog). F) Overview of the experimental setup for matched cultures, harbouring diCre induced *uis2* excision and control cells: synchronized ring stages are either treated with rapalog or left untreated as control cells, rapalog induces the excision of *uis2* in the first cycle while the previously expressed UIS2 remains in association with the PVM (green), the event of invasion (black arrow) into the second cycle marks the loss of UIS2 together with the old PVM during egress. No new UIS2 is replenished, as the *uis2* gene was excised in the previous cycle.

### 3.3.1 Parasite viability is impaired after conditional excision of *uis2*

After demonstrating effective excision of the functional *uis2* gene and the lack of UIS2 on day 2 post rapalog (section 3.3) it was next tested if this affected viability of the parasites. This was done using our standard FACS assay (Birnbbaum et al., 2017) that measures parasite growth over five consecutive days, comparing the same culture split into one serving as control and one grown in the presence of rapalog (Figure 25F). The resulting growth curves showed similar parasitemia until day 3 post addition of rapalog but failure of the rapalog-treated cells to expand on day 4 post rapalog addition, whereas the control

expanded at a typical rate (Figure 26A). This indicated that during the first cycle, while *uis2* was being excised, parasite growth was unaffected but that in the new cycle, when parasites invaded new red blood cells and started a cycle without UIS2 in the PVM, growth was inhibited.

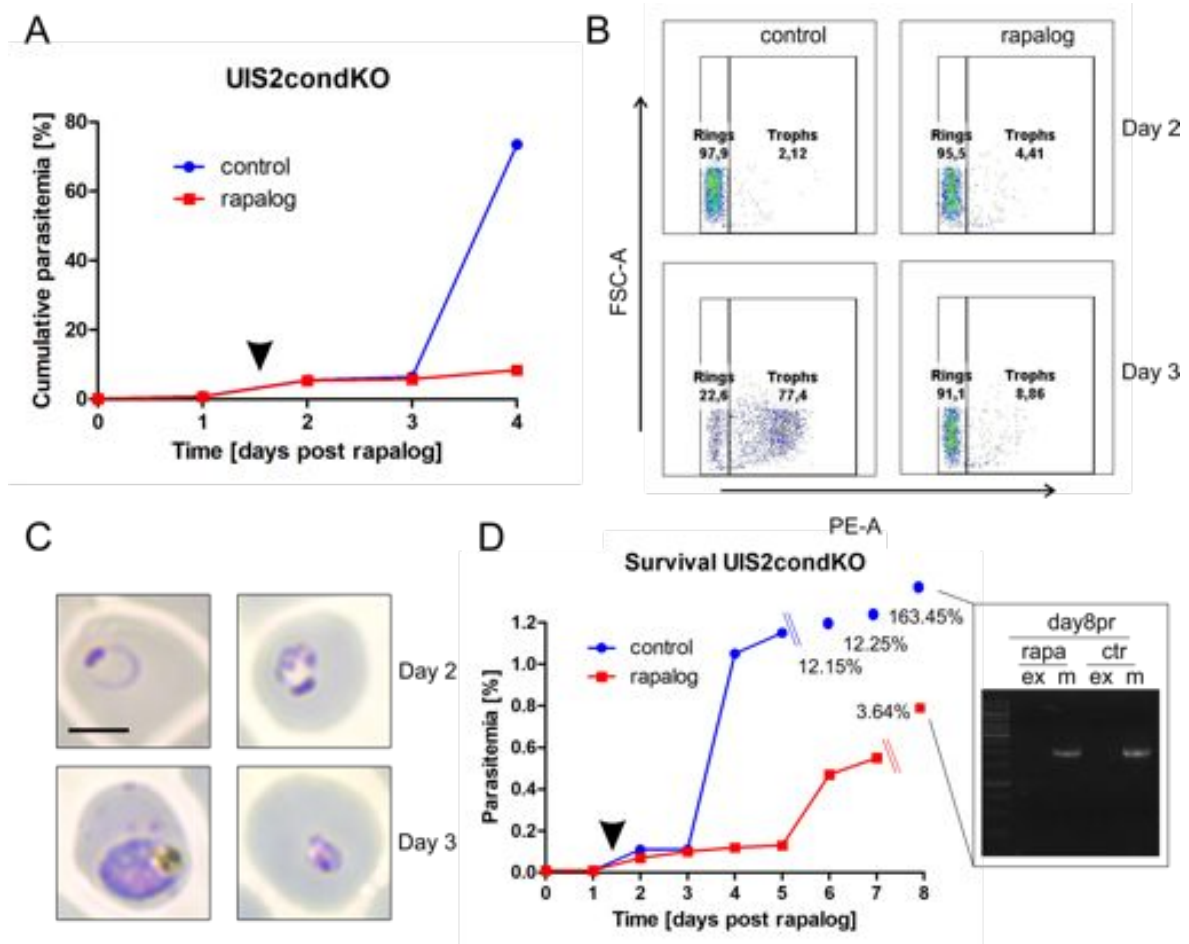


**Figure 26: Parasite viability of the UIS2 conditional knockout cell line**

A) Representative growth curve comparing the parasitemia of the control and rapalog-treated UIS2condKO cell line on 5 consecutive days, black arrow marks invasion into the second cycle and loss of UIS2 (one of  $n=8$  independent experiments (Figure xxx)). B) Exemplary dot plots for the whole control and rapalog-induced knockout parasite population on day 2 and 3 gated in order to differentiate between ring stage and trophozoites/late stage parasites; x-axis: PE-A represents DHE staining; y-axis: FSC-A = forward scatter. C) Giemsa smears of control and UIS2 knockout cultures on day 2 and 3 post rapalog. D) Representative growth curve comparing the parasitemia of the UIS2condKO cell line in the presence and absence of rapalog for 8 days post rapalog, black arrow marks invasion into the second cycle and loss of UIS2 (one of  $n=3$  independent experiments), gDNA was isolated on day 8 post rapalog and the genomic status was checked via PCR; rapa: on rapalog, ctr: control, ex: excised locus, m: modified locus.

The failure of the rapalog-treated cells to expand without UIS2 during the second round of replication in red blood cells was examined in further detail in the flow cytometry assay. Interestingly, FACS dot plots of whole parasite populations showed that parasite development was impaired already on day 3. This was evident from the fact that the control cell population developed normally from 97,9% rings on day 2 to 77,4%

trophozoites on day 3 (Figure 26B). In comparison the rapalog-treated parasite population showed a ring stage arrest evident from the fact that from the 95,5% rings on day 2 91,1% remained in the ring stage on day 3, indicating that they did not develop further in their live cycle (Figure 26B). Giemsa smears of the parasite cultures confirmed this finding: in the rapalog-treated culture small ring-like parasites dominated on day 3, suggesting that the parasites had not developed further from day 2, whereas the control cells developed normally from rings (day 2) to trophozoites (day 3) (Figure 26C). These results indicate that parasites lacking UIS2 arrested in ring stages, resulting in a lethal phenotype.

A long-term survival assay of the control and rapalog-treated cultures confirmed the lethal phenotype of the knock out, although a small cell population kept growing and gained a parasitemia of almost 4% on day 8 (Figure 26D). A PCR, specific for the excised and the intact genomic locus, demonstrated that the remaining cell population in the rapalog-treated culture contained exclusively the unexcised genomic locus. This finding confirms once more the essential function of UIS2 for parasite viability.

### **3.3.2 Phenotype of ring stages lacking UIS2**

The data in section 3.3.1 indicated that loss of UIS2 led to an arrest of parasite development already in ring stages. In order to determine the cause of the loss of viability, ring stage parasites were examined by live cell microscopy (Figure 27A). No obvious differences were detected between the parasites without UIS2 and the controls with UIS2 using DIC microscopy and fluorescence microscopy for bodipy membrane staining (Figure 27A). To further investigate the phenotype of the parasites without UIS2, SBP1 (skeleton-binding protein 1), an integral membrane protein of the Maurer's clefts (Blisnick et al., 2000) and ETRAMP2, an integral membrane protein of the PVM (Spielmann et al., 2003) were localised using immune fluorescence assays (IFAs) in the UIS2condKO cell line. Interestingly, SBP1 and ETRAMP2 showed marked differences in location between the cells with and without UIS2. While SBP1 was correctly trafficked to the Maurer's clefts in the control (as evident by dots in the RBC cytosol), the rapalog-treated cells lacking UIS2 were not able to traffic SBP1 to the Maurer's clefts but SBP1 remained within the parasite (Figure 27B). The trafficking of ETRAMP2 was similarly affected: the control cells displayed normal ETRAMP2 staining around the parasites, typical for the PVM, whereas the cells lacking UIS2 did not show ETRAMP2 around the parasite but this protein was also observed within the parasite (Figure 27C). UIS2 had previously been implicated in translational control (Zhang et al., 2016), however, the detection of both, SBP1 and ETRAMP2 (albeit incorrectly trafficked), indicated that transcription and translation were presumably not impaired. Taken together, the phenotype indicates either a general block

in trafficking of secretory proteins or a general developmental delay in the cells lacking UIS2 that led to an indirect inhibition of secretory trafficking.

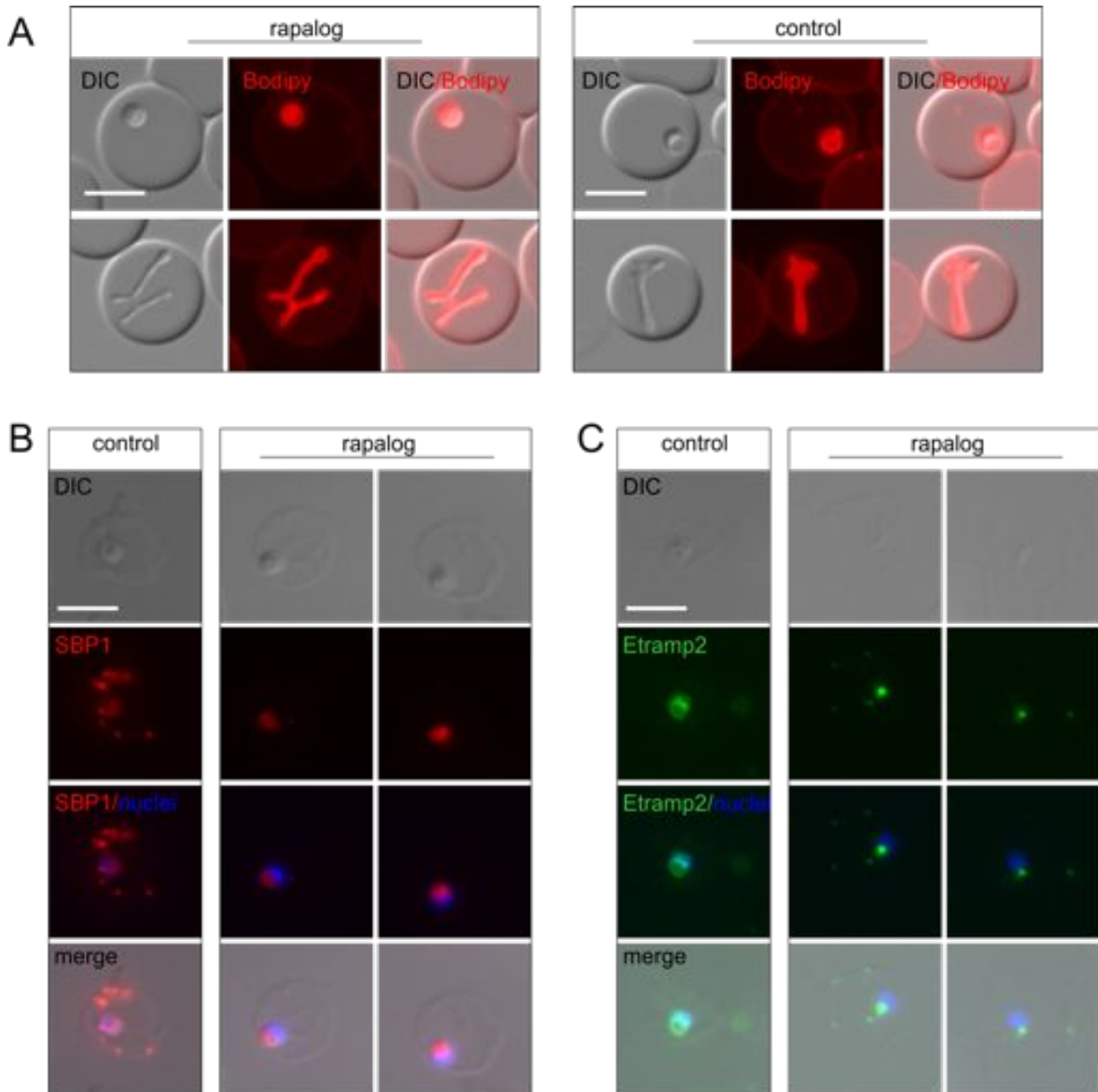


**Figure 27: Phenotype after rapalog induced excision of *uis2*.**

A) Live cell microscopy images of the control and rapalog-induced *UIS2*condKO cell line on day 2 post rapalog; membranes were stained with Bodipy-TX-ceramide, DIC: differential interference contrast B) Fluorescence images of suspension IFA on day 2 after addition of rapalog probed with anti-SBP1 antibodies in cells with (control) or without (rapalog) *UIS2*. C) Fluorescence images of wet acetone IFA of day 2 parasites probed with ETRAMP2 in cells with (control) or without (rapalog) *UIS2*. DIC: differential interference contrast; nuclei were stained with DAPI; merge indicates overlay of all presented channels; size bar: 5  $\mu$ m.

### 3.3.3 Complementation of the PF3D7\_1464600 phenotype

To confirm that the effects observed after *UIS2* loss were indeed specific complementation of the conditional knock out was carried out. Two different constructs were used. One construct expressed wild type *UIS2* to test whether the lethal phenotype induced by loss of *UIS2* can be rescued (Figure 28A). The other complementation construct was designed to express *UIS2* with two point mutation that are known to impair

the predicted phosphatase function of UIS2 by destroying metal coordination in Ser/Thr phosphoprotein phosphatases (PPases) (Zhuo et al., 1994). The corresponding point mutations D554N and D586N were inserted in the catalytic core domain and resulted in the amino acid switch from the negatively charged aspartic acid (D) into the structurally similar but uncharged asparagine (N). Both constructs (wild type and catalytic site mutant) were under the control of the NMD3 promoter that shows a similar expression profile to the promoter of PF3D7\_1464600 (Le Roch et al., 2003). The complementation plasmids were transfected into the conditional UIS2 knock out parasites, resulting in the two cell lines UIS2condKO-comp<sup>wt</sup> and UIS2condKO-comp<sup>mut</sup>.

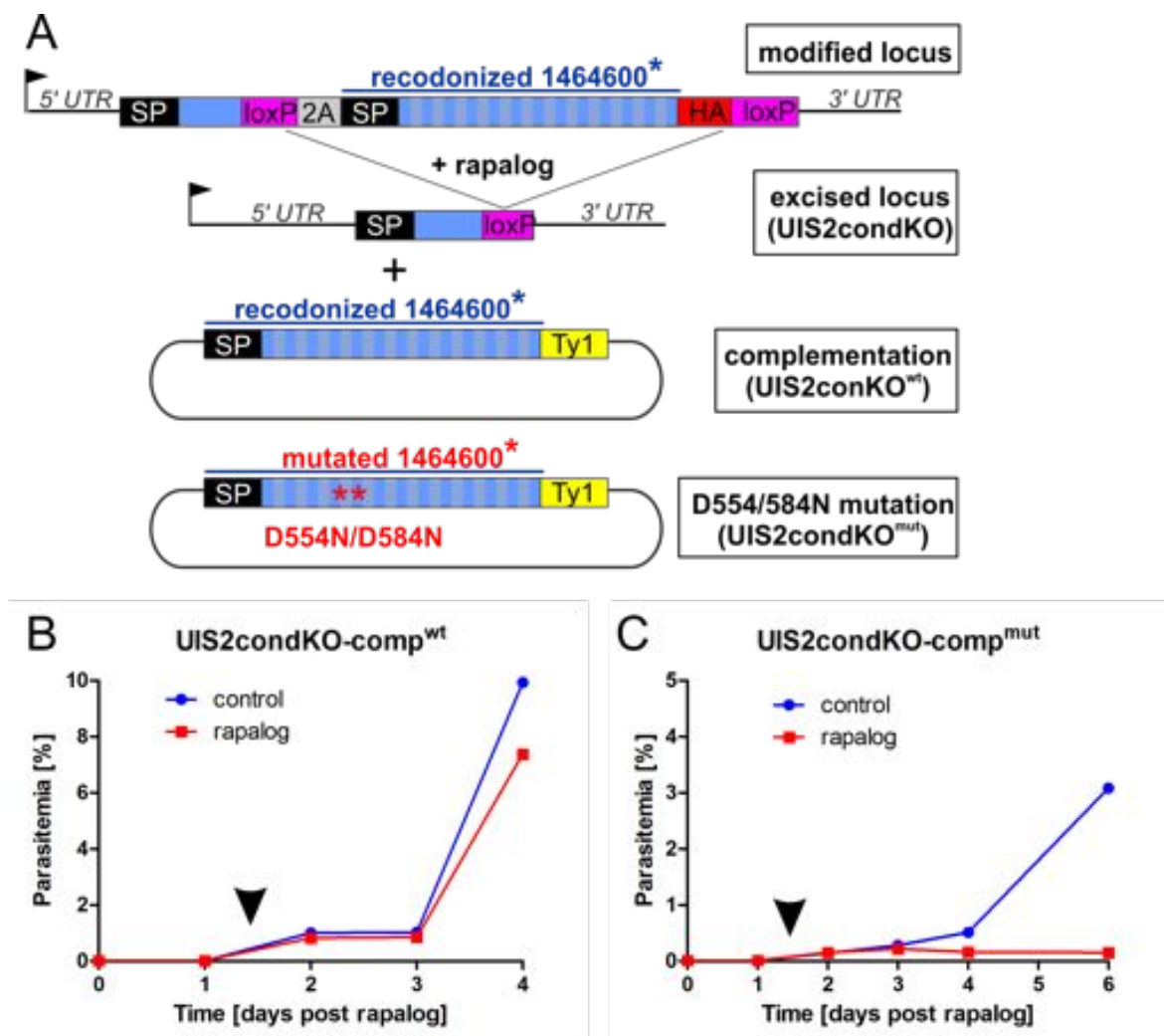


**Figure 28: Complementation of the conditional *uis2* KO cell line**

A) Schematic for the complementation of the UIS2condKO cell line resulting in UIS2condKO-comp<sup>wt</sup> (complementation) and UIS2condKO-comp<sup>mut</sup> (mutation). B) Representative growth curve of UIS2condKO-comp<sup>wt</sup> (one of n=4 independent experiments (Figure xxx)), showing the parasitemia assessed by flow cytometry on 5 consecutive days in the presence and absence (control) of rapalog, black arrow marks invasion into the second cycle and loss of UIS2 C) Representative growth curve of UIS2condKO-comp<sup>mut</sup> (one of n=2 independent experiments (Figure xxx)) showing the parasitemia assessed by flow cytometry on 7 consecutive days in the presence and absence (control) of rapalog (note that day 5 was not measured), black arrow marks invasion into the second cycle and loss of UIS2.

To test the complementation capacity of the two constructs, the endogenous floxed *uis2* locus was excised by adding rapalog and parasite growth was measured by flow cytometry. The growth curves of the UIS2condKO-comp<sup>wt</sup> showed no significant difference between rapalog and control cells (Figure 28B), indicating that the functional impairment caused by loss of UIS2 can be reverted by the wild type complementation construct. In contrast, the complementation with the UIS2 that harboured the mutated phosphatase domain already showed impaired growth of the cells before excision of the gene encoding the endogenously expressed UIS2 (Figure 28C). This indicated either poor expression of the complementation construct or a dominant negative effect of this construct. However, addition of rapalog to excise the functional copy of *uis2* aggravated the growth phenotype (note that the growth assay was prolonged to more clearly reveal the growth difference), indicating that the mutated extra copy of UIS2 in UIS2condKO-comp<sup>mut</sup> had no complementing capacity (Figure 28C). Unfortunately, the UIS2condKO-comp<sup>mut</sup> parasites quickly adapted in an unknown way to the dominant negative effect, resulting in a cell line growing at typical rates, likely through the strong selection, based on the growth impairment. The UIS2condKO-comp<sup>mut</sup> cell line was also not affected by addition of rapalog, suggesting selection of profoundly rearranged parasites to circumvent the impeding effects of the introduced genetic modifications. The capacity of the parasites to do this was already demonstrated by the long-term growth assay carried out with the uncomplemented conditional *uis2* knock out cell line (compare Figure 26D). Taken together, the complementation data demonstrate that the effect of the *uis2* knockout is specific, that the activity of the phosphatase domain is critical for the function of UIS2 and that expression of the phosphatase dead mutant likely has a dominant negative effect on parasite growth.

## 4 Discussion

### 4.1 BiOID within the PV compartment

BiOID was used to identify compartment-specific proteins within the PV. Biotinylated proteins were enriched with streptavidin-coated beads. Subsequent mass spectrometry identified among known PV proteins a number of exported proteins that were presumably biotinylated within the PV on their way into the host cell cytosol. Nevertheless, unspecific binding of abundant proteins to the beads is also likely as some proteins identified by mass spectrometry analysis were likely contaminants. However, it is also possible that a number of these likely contaminants (mostly ER and Golgi proteins) were biotinylated en route of the SP-GFP-BirA\* from the ER to the PV (Tonkin et al., 2006a) and were therefore not included in the 3D7 negative control for subtraction. In order to subtract the en route biotinylated proteins the use of a different negative control e.g. SP-GFP-BirA\*-SDEL that cycles within the ER and Golgi pathway is possible. For both the 3D7 and the SP-GFP-BirA\*-SDEL control cells it is difficult to obtain matching cultures that consist of the same stages and are therefore comparable. To circumvent this problem the SP-GFP-BirA\* expressing parasites can be split into two cultures: one can be treated with Brefeldin A that induces retrograde transport from the Golgi back to the ER as a negative control and can be subtracted from the matching SP-GFP-BirA\* culture. However, this has the disadvantage of putting the culture into non-physiological conditions.

### 4.2 BiOID identified true PV proteins

Manual analysis of the mass spectrometry hit list, taking into consideration the presence of signal peptides, transmembrane domains and export domains resulted in 14 potential PV candidates. Localization studies revealed that the potential candidates could be categorized into three false positive proteins (3.3.1.1 – 3.3.1.3), three candidates with a partial PV localization (3.3.2.1 - 3.3.2.3) and seven proteins with a major PV localization (section 3.3.3.1 – 3.3.3.7). All proteins are summarized in Figure 29 except one protein that was refractory to C-terminal tagging.

Interestingly, two (PF3D7\_1013300 and PF3D7\_1310500) of three false positive PV candidates (section 3.2.3) showed a typical ER staining. In addition, the MS data set consisted of several ER proteins among the likely contaminants. This might be due to biotinylation of ER-resident proteins by the BirA\* fusion protein along its trafficking route into the PV (Tonkin et al., 2006a). This might also be the case for PF3D7\_1013300 and PF3D7\_1310500.

Candidate PF3D7\_0629200 annotated as a DnaJ protein was categorized as a partial PV protein (section 3.2.4.1) as it showed foci close to the nucleus and GFP-staining within the PV compartment. However, an exact location within the PV compartment could not be

assigned. In order to determine the exact location within the PV compartment, as well as the exact location within the parasite for this likely essential protein, further experiments are needed. PF3D7\_0629200 was implicated to contain a predicted apicoplast-targeting signal (Zuegge et al., 2001). The described location of the apicoplast as a small extension on the ER (Tonkin et al., 2006b) fits to the observed location near the nucleus. Further experiments are also needed to clarify if PF3D7\_0629200 has beside a dual location also a dual function or if one of the two locations might be due to incorrect trafficking favoured by the 2xFKBP-GFP tag. However, incorrect trafficking seems to be unlikely as this candidate was identified to be likely essential for parasite growth and incorrect trafficking might also be detrimental for the parasite. It is possible that PF3D7\_0629200 functions as a chaperone or a chaperone-related protein due to its annotation as a putative DnaJ protein.

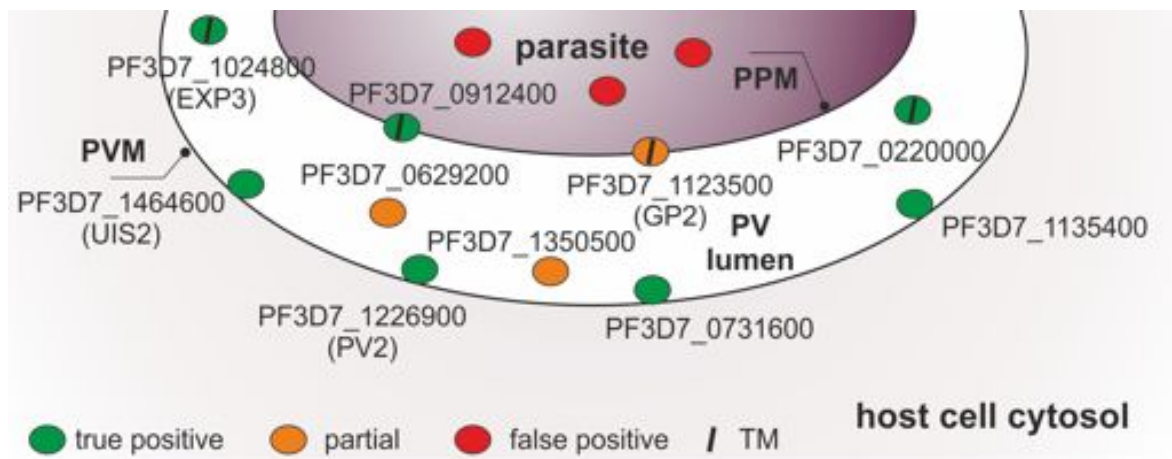


**Figure 29: Identification of novel PV proteins**

Graphic representation of the proteins identified within the PV compartment; green: true positive PV proteins, orange: PV proteins with a partial PV localization and red: false positives within the parasite (PF3D7\_1462300, PF3D7\_1013300 and PF3D7\_1310500), TM: transmembrane domain. Localization studies revealed a localization either at the PPM: parasite plasma membrane or PVM: parasitophorous vacuole membrane. Proteins displayed within the PV lumen could not be assigned to a definite position. Graph modified from (Spielmann et al., 2012).

Candidate PF3D7\_1123500 categorized here as a PV protein with partial PV localization and distinct foci within the parasite (section 3.2.4.2) was recently identified as a Golgi protein thereafter named Golgi Protein 2, GP2 (Hallee et al., 2018b). Interestingly, in a similar BiID approach in *P. berghei* (Schnider et al., 2018) the orthologue PBANKA\_0924800 was identified as a potential PV protein but then was similarly found to localize in a single focus per parasite in developing and free blood stage merozoites, also indicating a secretory pathway location. Nevertheless, the appearance of GP2 in two independent BiID approaches that identified new PV proteins (Khosh-Naucke et al., 2017; Schnider et al., 2018) might either indicate a dual location of GP2 with the majority of protein within the Golgi, transient cycling of GP2 from the Golgi to the PV in small

quantities that it might not always be evident by live cell imaging of the parasites expressing the GFP-tagged protein or that in both studies BirA\* tagged the protein while passing through the Golgi. Further studies are needed to confirm the dual role of PF3D7\_1123500 in the Golgi and in the PV. As PF3D7\_1123500 is dispensable for the parasite ((Hallee et al., 2018b) and section 3.2.4.1) it needs also to be considered that the 2xFKBP-GFP tag caused incorrect trafficking and therefore a signal within the PV.

PF3D7\_1350500 was the only protein that was selected from the supernatant fraction. Nevertheless, Western blot analysis showed that this protein was present in the pellet fraction, while the supernatant fraction contained either a physiologically processed or a degradation product. Although this protein was categorized as a partial PV protein it cannot be excluded that the fluorescence that was observed in the parasite periphery during live cell microscopy resulted from a potential degradation product. Further experiments are required to test whether this location is due to a degradation product or is due to the full-length protein. In this thesis a saponin-release assay was developed to show this (2.2.2.11). However, this assay could not determine the exact location as the fluorescent signal of PF3D7\_1350500-2xFKBP-GFP was too faint for this assay. It therefore remains unclear, if this protein is a true PV protein.

PF3D7\_0220000, known as liver stage antigen 3 (LSA3), contains 2 hydrophobic regions that are both predicted to be TMs although the N-terminal region likely represents a SP. LSA3 was shown to localize within the PV compartment, although an exact localization could not be determined (section 3.2.5.1). However, the two transmembrane domains within the protein indicate integral membrane localization. Despite the here-described localization within the PV, LSA3 has been reported to have a PEXEL motif at position (89-93 of the amino acid sequence) and is therefore predicted to be an exported protein (Maier et al., 2008; Morita et al., 2017). However, export of LSA3 has never been shown, but LSA3 has recently been localized to dense granules in schizont blood stage parasites via immune fluorescence assays and electron microscopy and to the PV of ring stages (Morita et al., 2017). However, in the before-mentioned study the protein has not been localized in other stages. The localization of LSA3 in dense granules is consistent with our observation of one distinct LSA3-2xFKBP-GFP focus per nucleus in free merozoites that is in agreement with a presence in apical organelles. It needs to be taken into consideration that LSA3 might be inhibited in its export due to the 2xFKBP-GFP tag, resulting in an accumulation of LSA3 within the PV. In this case LSA3-2xFKBP-GFP would not be properly trafficked but erroneously be found at the PV and in this case would not be essential for parasite survival as previously reported (Maier et al., 2008), at odds with our findings via SLI-TGD suggesting an essential role of LSA3 in parasite survival. However, in the Maier study it is not clear at which point the gene disruption was induced.

It is possible that in their gene disruption the functional part of the protein remained, which might have been destroyed in our approach. Further experiments e.g. conditional knockout of LSA3 are needed to elucidate the essentiality of this candidate. LSA3 is also expressed in liver stages and sporozoites and has been localized within the PV of liver-stage schizonts in chimpanzee's liver cells (Daubersies et al., 2000) and was implicated as a promising vaccine candidate in various studies (Aidoo et al., 2000; Daubersies et al., 2000; Prieur and Druilhe, 2009; Toure-Balde et al., 2009).

PF3D7\_0731600 is annotated as an acyl-CoA synthetase (ACS) and was presented in this work as a true PV protein associated with the PVM (section 3.2.5.2). In general acyl-CoA synthetases are housekeeping genes that catalyse the activation of fatty acids to acyl-CoA. This metabolic process was shown to be important for the survival of *Plasmodium* species (Beaumelle and Vial, 1988a, b; Vial et al., 2003). However, PF3D7\_0731600 that is encoded by the *acs5* gene was here found not to be essential for parasite survival as a TGD cell line was successfully raised. In *P. falciparum* an unusually high number (relative to other *Plasmodium* species and other organisms) of 13 ACS homologs were identified that are present in a subtelomeric location (Bethke et al., 2006). This might indicate redundancy of some of the ACS homologs or differential functionalization of ACSs that do not play a pivotal role for the parasite. As PF3D7\_0731600 is located at the PVM a role in scavenging fatty acids from the extracellular milieu might be possible, which would allow the parasite to bypass energy-expensive de novo synthesis (Mi-Ichi et al., 2006; Vial et al., 2003).

The putative alkaline phosphatase PF3D7\_0912400 was identified as a true PV protein of the PPM (section 3.2.5.3). The function of the dispensable protein remains unknown. However, as an annotated phosphatase it can be assumed that the protein carries out dephosphorylation events.

PF3D7\_1024800 (section 3.2.5.4) and PF3D7\_1226900 (section 3.2.5.6) were both identified as true PV proteins, whereas PF3D7\_1226900 could be assigned as a protein associated with the PVM. For PF3D7\_1024800 the *P. berghei* orthologue PBANKA\_0509000 showed a similar localization (Schnider et al., 2018). Both candidates (PF3D7\_1226900 and PF3D7\_1024800) were also identified together with PV1 to interact with an epitope tagged minimal construct of *PfEMP1* (*PfEMP1B*) (Batinovic et al., 2017). The three interaction partners of the PV-resident *PfEMP1B*, PV1, PF3D7\_1226900 thereafter named parasitophorous vacuolar protein-2 (PV2) and PF3D7\_1024800 thereafter named exported protein-3 (EXP3) were postulated to form an exported protein-interacting complex (EPIC), suggesting a possible role for EPIC in preparing exported proteins for export through PTEX. Batinovic et al. also produced inducible knockdown lines of the three EPIC components PV1, PV2 and EXP3 using the *glmS* riboswitch

system. Knockdown of the EPIC proteins did not affect parasite viability but in the PV1 knockdown *PfEMP1* trafficking. In concordance with their findings a TGD cell line was obtained for EXP3. In conflict, no TGD cell line could be established for PV2 (further discussed in section 4.3).

Notably, also PF3D7\_0629200 and PF3D7\_1135400 were among the proteins identified in the mass spectrometry analysis of *PfEMP1B* parasites. Interestingly, mass spectrometry analysis of EXP3-HA interacting proteins also identified PF3D7\_1135400 and UIS2. One explanation for the high congruence of identified proteins between the Batinovic study and the here discovered PV proteins might be the amino acid sequence here chosen for fusion with GFP-BirA\* to target this construct to the PV: this sequence consisted of a signal peptide and 35 further amino acids of the PEXEL-negative exported protein PF3D7\_0830400 (Heiber et al., 2013). As BirA\* identifies proximal proteins and interaction partners it cannot be excluded that the 35 N-terminal amino acids of PF3D7\_0830400 might mediate interaction with export-related proteins, like PV2 and EXP3. It was shown that the domain 1 in PF3D7\_0830400, a region present within the 35 N-terminal amino acids, comprises relevant export information and is necessary for efficient export (Blancke Soares, 2016). Another explanation for the overlap of the here identified PV proteins with the proteins identified in the *PfEMP1B* interactome (Batinovic et al) might be that the PV is so narrow that the same proteins get identified due to spatial limitations and a limited protein composition of the compartment itself (Trelka et al., 2000).

PF3D7\_1135400 was identified as a true PV protein that is peripheral to the PVM (section 3.2.5.5). Beside the appearance in the mass spectrometry analysis of EXP3-HA interacting proteins (Batinovic et al., 2017), PF3D7\_1135400 was also pulled down in an immunoprecipitation of EXP2 (Mesen-Ramirez et al., 2016). Both publications support the finding of a localisation within the PV compartment. In order to resolve the contradicting results concerning the essentiality of this protein in this work (a targeted gene disruptions leaving 73% of the gene still intact was successful whereas a disruption removing more than 60% of the gene failed, section 3.2.5.5 Table 17 and Table xxiii) and to elucidate a possible function of the predicted thioesterase domain (that would have been disrupted in the unsuccessful attempts) more experiments are needed. One possibility to achieve this would be to use the diCre based gene elimination used in this thesis for UIS2.

PF3D7\_1464600 (UIS2) was identified as a true PV protein associated with the PVM. Functional analysis of this essential candidate are presented in section 3.3 and discussed in detail in section 4.5.

In general it should be noted that it cannot be excluded that in some cases the 2xFKBP-GFP tag had a negative influence on correct protein trafficking and therefore correct

protein localization in the dispensable proteins. For essential proteins this is unlikely, as incorrect targeting would have abolished function and the corresponding 2xFKBP-GFP tagged POI expressing cell line would not have been obtained.

### 4.3 Analysis of essentiality with the SLI-TGD system

The SLI-TGD system gives a good indication for the essentiality of parasite proteins as demonstrated in a previous study where essentiality of a POI interest when determined by other methods correlated well with the SLI-TGD result, i.e., dispensable genes could be disrupted whereas essential genes were refractory to disruption (Birnbaum et al., 2017). In addition SLI-TGD has the advantage of a fast and effective selection via G418 for TGD cell lines over previous TGD approaches that have been time consuming. Nevertheless, there are disadvantages of this system: only TGDs of non-essential genes are obtained and can be further analysed for function, whereas no cell lines arise from TGDs for essential genes. This also raises the problem that in the case a cell line is not obtained, it is not fully clear if failure to obtain the line was indeed due to essentiality of the targeted gene or other factors, for instance refractoriness of the locus for recombination. To avoid other reasons for failure to obtain TGDs, for instance unwanted and unnoticed general culture conditions affecting parasite viability in an independent way, these experiments were always done in at least 3 independent occasions, each in technical duplicates.

In awareness of the limitation of the SLI-TGD approach, the outcome of the TGDs was categorized into not essential and likely important for growth. Among the 13 investigated candidates the TGD results indicated that 8 candidates were likely important for growth and 4 candidates were not essential. The here-identified proportion between essential and dispensable proteins correlates well with the proportion determined by a genome-wide study of gene functions in *P. berghei* (Gomes et al., 2015) and is higher than in a previous TGD analysis in *P. falciparum* (Birnbaum et al., 2017). For one candidate, namely PF3D7\_1135400, a TGD cell line was generated with a targeting region of 540 base pairs, leading into a disruption of approximately 26% of the gene, while all attempts to generate a TGD with a smaller targeting region (282 base pairs), resulting in a 61% gene deletion remained unsuccessful. In the latter a thioesterase domain would have been deleted that remained intact in the other approach where only 26% of the gene was removed. This finding demonstrates that targeting regions for the SLI-TGD system need to be carefully chosen in compliance with 1) the size of the targeting region, 2) domains within the gene and 3) the overall gene size. It was shown that the length of the targeting region influences the time for integration and that targeting regions should be at least 200 base pairs (Birnbaum et al., 2017) but possibly the size of the region needs to exceed 400 bp to be reliable which for small genes such as PF3D7\_1135400 is problematic. Important

domains within the gene should not be included in the targeting region as the remaining part of the gene may in some cases retain partial or full functionality. In general targeting regions containing introns are favourable as they enlarge the targeting region without decreasing the overall gene deletion, although it is also not clear if the higher AT content in the introns may again negatively affect proper target recognition or affinity, thereby reducing efficiency.

Comparison of the TGD outcome with high throughput phenotypic analysis for *P. falciparum* (Zhang et al., 2018) and *P. berghei* (Gomes et al., 2015) revealed that the TGD data for two candidates, namely PF3D7\_0731600 and PF3D7\_1350500, were congruent to the data from both high throughput phenotypic analysis. The comparably small congruence was mostly due to the fact that for eight candidates no data from the high throughput analysis of *P. berghei* were available. Two candidates, namely PF3D7\_0220000 and PF3D7\_1135400, had no orthologue in *P. berghei*, whereas the other six were not included in the database and were therefore not assigned. Comparison of the TGD data with the high throughput phenotypic analysis for *P. falciparum* that was performed using saturation mutagenesis revealed congruence for seven candidates. Intriguingly, saturation mutagenesis did not indicate essentiality of PF3D7\_1464600 (UIS2), a protein for which a crucial function was here clearly shown by conditional knock out (3.3), and this was confirmed in the high throughput functional screen in *P. berghei*. However, PF3D7\_1226900 (PV2) was assigned as dispensable in both phenotypic analyses, whereas several attempts did not result in a TGD cell line for this candidate, which would indicate an essential function. In a different approach it was shown that the knockdown of PV2 using of the *glmS* riboswitch system did not affect parasite viability (Batinovic et al., 2017). Similarly, PF3D7\_0220000, which was in this work categorized as likely important for growth but was assigned as dispensable in the phenotypic analysis for *P. falciparum* was successfully disrupted in a previous publication (Maier et al., 2008), indicating that SLI-TGD did not always accurately predict essentiality.

In general all likely essential genes comprise a link for potential drug targets and should be analysed further, independent of their cellular location. First, essentiality of the gene or the gene product should be verified with an appropriate inducible knockout or knockdown system that can also be used for functional analysis. For PF3D7\_1464600 (UIS2) (section 3.3) a conditional knock out cell line was generated that excises the functional version of the gene using the diCre system (Andenmatten et al., 2013; Birnbaum et al., 2017; Collins et al., 2013), while only the disrupted endogenous copy remained. However, also other systems are available to study protein functionality and these might also be suitable for conditional gene and protein inactivation (de Koning-Ward et al., 2015; Ganesan et al., 2016; Webster and McFadden, 2014).

#### **4.4 Difficulties in the generation of a knock sideway system for secretory proteins**

The attempt to generate a knock sideway system for secretory proteins to inducibly mislocalize PV proteins and prevent them from reaching their site of action has to be regarded as mostly unsuccessful. In 3 of 4 cases at least a partial mislocalization was observed, although a reliable, effective and complete mislocalization into the ER that would be important for routine use could not be achieved. A similar approach was used to successfully synchronize protein transport in the secretory pathway to analyse and visualize intracellular trafficking (Boncompain and Perez, 2012). Their developed secretory assay was named RUSH (retention using selective hooks) and was based on the interaction between the streptavidin-binding peptide (SBP) and streptavidin in the mislocalizer (in this system termed 'hook') instead of the rapalog-induced dimerization of FRB and FKBP. The binding of streptavidin to the SBP is induced in the absence and released in the presence of biotin.

Difficulties of the rapalog-induced FRB and FKBP system might be due to sterical hindrance of the 2xFKBP, which are positioned between the POI and the GFP. It was shown that the addition of 2xFKBP at the C-terminal end of the protein improved mislocalization efficiency (Birnbaum et al., 2017). Therefore, it might be useful to re-evaluate the system with the additional C-terminal 2xFKBP resulting in the 2xFKBP-GFP-2xFKBP sandwich plasmid (Birnbaum et al., 2017). This would also enhance the mislocalization, as four mislocalizers instead of two would now bind the POI.

Life cell microscopy images showed a typical ER staining pattern of the ER mislocalizer throughout the asexual life cycle. It is expected that the majority of the ER mislocalizer is present within the ER lumen. Small amounts that escape from the ER into the Golgi lumen are transported back to the ER via the SDEL receptor. As the mislocalizer resides within the ER or Golgi lumen the reversed mislocalization to the PPM observed in PF3D7\_0912400 and partially in PF3D7\_1123500 is difficult to explain from a topological point of view. However, it is possible that the mislocalizer is dragged along with the POI, causing an aberrant mislocalization. It is also possible that the POI-mislocalizer complex caused an accumulation on its trafficking route in-between the POI site of action and the ER lumen, where the ER mislocalizer normally resides. As expected (in alignment with the TGD data section 3.2.4.2 and 3.2.5.3) the growth assays for the dispensable proteins PF3D7\_1123500 and PF3D7\_0912400 did not affect parasite viability.

Intriguingly, PF3D7\_1464600 did not show any mislocalization, indicating a position of the 2xFKBP that does not face the lumen of the ER and Golgi. However, the lack of transmembrane domains within this secretory protein implies the presence within the ER lumen. In conclusion, the immunity of this protein for mislocalization might be either due to

a sterical unfavourable position of the 2xFKBP or due to the presence of the fusion protein in an unfolded state that would prevent the dimerization of FRB and FKBP upon the addition of rapalog. In concordance, also the growth curve of PF3D7\_1464600 did not show an effect on parasite viability, although the protein was shown to be essential for parasite survival (section 3.2.5.7 and 3.3).

The mislocalization of the likely essential partial PV candidate (section 3.2.4.1) PF3D7\_0629200 slightly reduced the parasitemia compared to control cells on day four. The mislocalization for this protein was only partial, indicating that the remaining protein was still able to function at its site of action. The observed growth phenotype might indeed indicate an essential role for PF3D7\_0629200 for parasite viability, although the significance of the growth phenotype needs to be assessed in further experiments. Supportingly, in *P. berghei*, the growth phenotype of parasites lacking PF3D7\_0629200 was annotated as slow growing (Gomes et al., 2015).

#### 4.5 Functional analysis of PF3D7\_1464600 (UIS2)

The conditional *uis2* knockout cell line was generated to characterise the function of this protein in asexual blood stages. Induction of the conditional *uis2* knockout cell line resulted in an arrest of ring stages, presumably at a very early stage immediately after invasion. Interestingly, this finding is comparable with the data generated by Zhang and colleagues where knockout of *uis2* resulted in a developmental arrest of invaded sporozoites in liver stages. The sporozoites were not able to transform into trophozoites and continue liver stage development (Zhang et al., 2016). They explained their findings with the possible role of UIS2 to dephosphorylate eIF2 $\alpha$ -P that is only present in its phosphorylated state in salivary gland sporozoites where it leads to an inhibition of translation and subsequent accumulation of stalled mRNAs into granules (Zhang et al., 2010). Notably, UIS2 is the only phosphatase among the 30 *uis* genes (Matuschewski et al., 2002b). In order to demonstrate the interaction between UIS2 and eIF2 $\alpha$ -P, Zhang and colleagues showed that the UIS2 N-terminus stably bound to eIF2 $\alpha$ -P but not to non-phosphorylated eIF2 $\alpha$  *in vitro*. Further, they showed by co-immunoprecipitation that UIS2 from lysates of *P. berghei* blood stage parasites also associated with recombinant GST-PfeIF2 $\alpha$ . Additionally they showed that the UIS2 phosphatase domain was able to dephosphorylate eIF2 $\alpha$ -P *in vitro* and that EDTA and Cd<sup>2+</sup>, which are inhibitors of the PP2C/PPM family, inhibited its phosphatase activity. Furthermore, the phosphatase displayed a strong preference for Mn<sup>2+</sup> over Mg<sup>2+</sup>, indicating that UIS2 is a true member of PP2C/PPM family (Zhang et al., 2016). Altogether, these data indicate that UIS2 is a phosphatase of the PP2C/PPM family that binds and dephosphorylates eIF2 $\alpha$ -P. However, our localisation studies of UIS2 revealed a location associated with the luminal face of the PVM in asexual blood stages, which makes dephosphorylation of cytosolic

eIF2 $\alpha$ -P as a physiological function of UIS2 unlikely from a spatial point of view. Interestingly, localisation of *Pb*UIS2 recently also revealed an association with the PVM in *P. berghei* liver stages (Schnider et al., 2018). Taken together, the PVM location in blood as well as liver stages questions the spatial interaction of UIS2 and eIF2 $\alpha$ -P *in vivo* and needs to be re-evaluated in further experiments. One theoretical possibility would be that UIS2 is internalised via the cytostome. However, even in that case it would be unclear how this protein could reach eIF2 $\alpha$ . Cytostomes form out of PPM and the PVM, resulting in double membraned vesicular structures containing the PVM as the inner membrane (Aikawa et al., 1966; Francis et al., 1997). UIS2 therefore would be shielded from the parasite cytosol by the outer membrane formed from the PPM. While it is not fully resolved how cytostomes deliver their content to the digestive vacuole (Milani et al., 2015), dissolving of the outer membrane before they reach the digestive vacuole to the parasite does not seem very likely. However, no such vesicle-like structures were observed in fluorescence microscope images of GFP tagged UIS2, indicating that the described scenario is unlikely. Interestingly, eIF2 $\alpha$  was also present in the BirA\* specific pellet proteome and categorized as a likely contaminant. This might indicate that eIF2 $\alpha$  could also be present within the PV compartment. Therefore, it would be interesting to endogenously tag eIF2 $\alpha$  in the conditional *uis2* knockout cell line in order to co-localize UIS2 and eIF2 $\alpha$ -P and to see if eIF2 $\alpha$  remains in the phosphorylated state upon *uis2* gene excision.

In eukaryotic cells less phosphatases are present compared to kinases, reflecting the in generally less discriminating substrate selectivity of phosphatases compared to kinases. Therefore, selection of a substrate might be mainly triggered by the presence of a phosphate rather than a specific protein structure, raising some doubts about the high substrate specificity between UIS2 and eIF2 $\alpha$ -P. Furthermore, phenotypic analysis of UIS2 lacking ring stages showed that the translation of SBP1 and ETRAMP2 are not affected, arguing against an interplay between UIS2 and eIF2 $\alpha$ -P that would have caused an inhibition of translation. However, it should be noted that the exact expression levels of these proteins were not determined. This may be achievable using Western analysis, but due to the very early arrest of the *uis2* knockout parasites, assessing differences in protein abundance would likely be confounded by small differences in development stages. It is also to consider that the lack of functional UIS2 may have impaired PVM integrity. In *P. yoelii* infected liver stages it was shown that the lack of a PVM induces apoptosis and that the parasites are rapidly cleared by the host cell (Kaushansky et al., 2013). Due to the diffraction limit the difference between PPM and PVM cannot be assessed by live cell microscopy, as the diameter of the PV lumen is only around 50 nm (Trelka et al., 2000). Electron microscopy would be needed to assess the integrity of the PVM in the *uis2* KO parasites. However, with this approach smaller breaches of the PVM

might be missed, as EM sections provide only a small slice of a cell. Furthermore preparation artefacts, a common problem of EM that often varies considerably in extent between different samples, may confound such an analysis. A further possibility would be to express a soluble fluorescent marker in the PV to assess for release of this marker into the host cell, which would indicate a PVM breach. However, if this marker is similarly affected as SBP1 and ETRAMP2, this analysis would not be possible.

Whatever has caused the observed phenotype on the cellular level – on the molecular level the phenotype is presumably caused by the dephosphorylation of downstream substrates. It was here shown that the mutation of the UIS2 phosphatase domain into a catalytically dead mutant led to a dominant negative effect already in the control cell line that also expressed a wild type copy of *uis2*. The effect for the cells that exclusively expressed the catalytically dead mutant due to the rapalog-induced excision of wild type *uis2* was even more profound, as no increase in parasitemia was observed in the corresponding growth assays. This finding underlines that the lethal phenotype is not due to structural absence of the protein but rather due to its missing dephosphorylation activity. Nevertheless, the different compartmentalization of UIS2 and eIF2 $\alpha$ -P raise the question of the true phosphatase target. The association with the PVM – a position at the boundary between parasite and host cell makes the UIS2 dephosphorylation activity predestined to induce downstream signalling cascades that are yet to be identified. For the identification of downstream signalling cascades it would be interesting to map the phosphorylation status in cells lacking UIS2 compared to control cells in a phosphoproteome. For the substrate identification alone, co-immunoprecipitation or a UIS2-specific BioID may already be sufficient should the target(s) remain associated with UIS2.

#### 4.5.1 Potential UIS2condKO-comp<sup>mut</sup> evasion mechanism

UIS2condKO-comp<sup>mut</sup> is the complementation with a catalytically dead mutant, leading to a disadvantage in growth already for the control cell line and a full growth arrest in the *uis2* knockout parasites (section 3.3.3 Figure 28C). Unfortunately, the parasites quickly adapted due to the unfavourable selection pressure, resulting in normal growth rates of the *uis2* knockout cell line comparable to the control. One possible scenario is the single crossover homologous recombination of the recodonized *uis2* version on the episomal plasmid with the floxed endogenously integrated recodonized *uis2* copy. Both sequences are identical except for the two inserted point mutations D554N and D584N, resulting in a C-terminal homology region of 3745 bp. Integration of the C-terminal homology region of the episomal plasmid, carrying the catalytically dead mutant would on the one hand result in the elimination of the catalytically dead mutant, but on the other hand would result in a loss of the HA-tag and a loss of neomycin resistance in the endogenous genomic locus.

To prevent this scenario, the parasites were continuously kept on neomycin. In addition, the parasites would presumably also lose the ability to excise the recodonized version due to a loss of the C-terminal loxP site, which is consistent with the observed insensitivity to rapalog-induced diCre activity. Western blot analysis confirmed the presence of similar amounts of HA-tagged UIS2 in the presence and absence of rapalog in UIS2condKO-comp<sup>mut</sup> parasites, indicating inadequate excision of the gene, although the above-described scenario would have eliminated the HA-tag. The exact reason for loss of the capacity to excise *uis2* would require further analyses such as specific PCRs to assess whether the locus was changed and if pSkipFlox (the plasmid providing diCre) is still present as well as IFA to test whether all cells still express the HA-tagged version of UIS2. Although the mechanism of evasion is at present unclear, it may be advisable to either avoid sequence homology through use of a differently recodonized version of the complementation construct or to use the original sequence that was destroyed with the first integration event. However, the second possibility may also not be advisable as the original N-terminal homology sequence is still present under the endogenous promoter, which could provide a recombination site that would restore expression of the entire molecule, although this protein would then carry the mutations that were introduced.

#### 4.6 Classification of UIS2

Protein phosphorylation in *Plasmodium* parasites is accomplished by approximately 80 protein kinases (Ward et al., 2004), while approximately 30 protein phosphatases (PPs) are responsible for the reverse reaction - the dephosphorylation. In a bioinformatics screen for *P. falciparum* 27 putative PPs were identified. This comprised proteins belonging to the four major established PP families, namely the PPP group, (phospho-protein phosphatases), the PPM/PP2C group, the PTP superfamily (protein tyrosine phosphatase) and the NIF group (NLI interacting factor-like phosphatase), plus 7 sequences that were predicted to dephosphorylate "non-protein" substrates (Wilkes and Doerig, 2008). Wilkes and Doerig constructed Neighbour-Net phylogenetic trees to position these sequences relative to PPs from other organisms representing all major eukaryotic phyla except Cercozoans. They found profound divergences between the phosphatome of malaria parasites and those of representative organisms from all major eukaryotic phyla, indicating considerable phylogenetic distance between Apicomplexa and other Eukaryotes. Some *P. falciparum* PPs were present in clades lacking human homologues. Interestingly, UIS2 was not categorized in a distinct cluster but neighbored with tartrate-resistant acid phosphatase and acid phosphatase.

In a genome wide *in silico* analysis of the *P. falciparum* phosphatome UIS2 was categorized together with PF3D7\_0918000 in the MPP\_ACP5 family (Pandey et al., 2014). Human tartrate-resistant acid phosphatase 5 (ACP5) is known to remove the

mannose 6-phosphate recognition marker from lysosomal proteins presumably in a pre-lysosomal compartment as well as in lysosomes (Sun et al., 2008). PF3D7\_0918000 is annotated as glideosome-associated protein 50 (GAP50), secreted acid phosphatase (PlasmoDB) and is involved in protein anchoring in the inner membrane complex of *P. falciparum* (Bosch et al., 2012).

Interestingly, both publications (Pandey et al., 2014; Wilkes and Doerig, 2008) did not group UIS2 into the PPM/PP2C family but a recent publication did so (Zhang et al., 2016). The PPM/PP2C family consists of highly diverse and evolutionarily recent Mg<sup>2+</sup> or Mn<sup>2+</sup>-dependent serine/threonine phosphatases that comprise regulatory domains in C- or N-terminal extensions. However, the catalytic core domains that contribute to metal coordination are highly conserved throughout the family. In this thesis, the same mutations that were identified to destroy metal coordination, leading to a catalytically dead mutant in the bacteriophage  $\lambda$  Ser/Thr protein phosphatase (Zhuo et al., 1994) also caused an inactivation of UIS2. It was shown that UIS2 has a preference for Mn<sup>2+</sup> and Mg<sup>2+</sup>, which are required for PP2C activity. Classification as a PP2C member was validated by the fact that EDTA and Cd<sup>2+</sup> inhibit phosphatase activity (Zhang et al., 2016). However, UIS2 lacks a canonical PP2C catalytic domain and shows high similarity to purple acid phosphatases (Kaida et al., 2010). In *T. gondii* two orthologues of UIS2 exist, namely acid phosphatase (TGME49\_228160) and inner membrane complex protein IMC2A (TGME49\_228170), both tandemly localized on chromosome X, suggesting a duplication event (Yang and Arrizabalaga, 2017).

Major functions of PPM/PP2C phosphatases are to regulate mainly stress responses, but also cell differentiation, growth, survival, apoptosis, and metabolism (Lu and Wang, 2008). In plants - that contain a greatly expanded PPM/PP2C family (Xue et al., 2008) - PP2Cs are negative regulators of abscisic acid (ABA) signalling, of stress-induced MAPK pathways and of receptor kinase signalling (Schweighofer et al., 2004). Interestingly, a recent study showed that within the ABA signalling pathway PP2C phosphatases are required to control seed dormancy (Nee et al., 2017).

Altogether, the different classifications of UIS2 give no conclusion about functionality, but show the diversity of phosphatases and their possible functions in different cellular processes. For UIS2 further functional analyses as well as substrate identification might clarify the actual situation of how this protein can be classified in relation to known PPs.

#### **4.6.1 Phosphatases - potential drug targets in *P. falciparum*.**

The lethal phenotype of the conditional *uis2* knockout presented here for *P. falciparum* blood stages as well as for liver stages (Zhang et al., 2016) raises the question of protein phosphatases (PPs) and UIS2 in particular as potential malaria drug targets. In general the most challenging problem for selective pharmacological inhibition is the low intrinsic

PPs substrate specificity.

At present no direct inhibitor for UIS2 is available, although salubrinal – a selective inhibitor of cellular complexes that dephosphorylate eIF2 $\alpha$  – was identified in a screen for small molecules that protect cells from ER stress (Boyce et al., 2005). However, salubrinal is not PP specific as it also blocks eIF2 $\alpha$  dephosphorylation mediated by a herpes simplex virus protein and inhibits viral replication. Furthermore, it needs to be assessed which substrates UIS2 dephosphorylates under physiological conditions.

For members of the PP2C family also broad inhibitors like, EDTA and Cd<sup>2+</sup> are known: both target metal coordination, while Cd<sup>2+</sup> targets the M1 metal ion binding site (Pan et al., 2013) and EDTA M2 (Pan et al., 2015). However, these family members are insensitive to inhibition by okadaic acid or microcystin that both target primarily PPs of the PP1 and PP2A family (Shi, 2009). Interestingly, in *P. falciparum* general phosphatase inhibition was achieved by adding PhosSTOP™ phosphatase inhibitor tablets (Roche) to 3D7 parasites, resulting in a severe growth inhibition. PhosSTOP™ inhibits acid and alkaline phosphatases, as well as serine/threonine (PP1, PP2A, and PP2B) and tyrosine protein phosphatases.

In conclusion, UIS2 as well as members of the PPM/PP2C family and phosphatases in general present an interesting group for the discovery of novel targets in search for novel anti-malarials.

## Literature

- Aguilar, R., Magallon-Tejada, A., Achtman, A.H., Moraleda, C., Joice, R., Cistero, P., Li Wai Suen, C.S., Nhabomba, A., Macete, E., Mueller, I., Marti, M., Alonso, P.L., Menendez, C., Schofield, L., Mayor, A., 2014. Molecular evidence for the localization of *Plasmodium falciparum* immature gametocytes in bone marrow. *Blood* 123, 959-966.
- Aidoo, M., Lalvani, A., Gilbert, S.C., Hu, J.T., Daubersies, P., Hurt, N., Whittle, H.C., Druihle, P., Hill, A.V., 2000. Cytotoxic T-lymphocyte epitopes for HLA-B53 and other HLA types in the malaria vaccine candidate liver-stage antigen 3. *Infection and immunity* 68, 227-232.
- Aikawa, M., Hepler, P.K., Huff, C.G., Sprinz, H., 1966. The feeding mechanism of avian malarial parasites. *The Journal of cell biology* 28, 355-373.
- Aikawa, M., Torii, M., Sjolander, A., Berzins, K., Perlmann, P., Miller, L.H., 1990. Pf155/RESA antigen is localized in dense granules of *Plasmodium falciparum* merozoites. *Experimental parasitology* 71, 326-329.
- Andenmatten, N., Egarter, S., Jackson, A.J., Jullien, N., Herman, J.P., Meissner, M., 2013. Conditional genome engineering in *Toxoplasma gondii* uncovers alternative invasion mechanisms. *Nature methods* 10, 125-127.
- Ariey, F., Paul, R.E., 2014. Antimalarial resistance: is vivax left behind? *The Lancet. Infectious diseases* 14, 908-909.
- Arisue, N., Hirai, M., Arai, M., Matsuoka, H., Horii, T., 2007. Phylogeny and evolution of the SERA multigene family in the genus *Plasmodium*. *Journal of molecular evolution* 65, 82-91.
- Ashley, E.A., Dhorda, M., Fairhurst, R.M., Amaratunga, C., Lim, P., Suon, S., Sreng, S., Anderson, J.M., Mao, S., Sam, B., Sopha, C., Chuor, C.M., Nguon, C., Sovannaroeth, S., Pukrittayakamee, S., Jittamala, P., Chotivanich, K., Chutasmit, K., Suchatsoonthorn, C., Runcharoen, R., Hien, T.T., Thuy-Nhien, N.T., Thanh, N.V., Phu, N.H., Htut, Y., Han, K.T., Aye, K.H., Mokuolu, O.A., Olaosebikan, R.R., Folaranmi, O.O., Mayxay, M., Khanthavong, M., Hongvanthong, B., Newton, P.N., Onyamboko, M.A., Fanello, C.I., Tshefu, A.K., Mishra, N., Valecha, N., Phyo, A.P., Nosten, F., Yi, P., Tripura, R., Borrmann, S., Bashraheil, M., Peshu, J., Faiz, M.A., Ghose, A., Hossain, M.A., Samad, R., Rahman, M.R., Hasan, M.M., Islam, A., Miotto, O., Amato, R., MacInnis, B., Stalker, J., Kwiatkowski, D.P., Bozdech, Z., Jeeyapant, A., Cheah, P.Y., Sakulthaew, T., Chalk, J., Intharabut, B., Silamut, K., Lee, S.J., Vihokhern, B., Kunasol, C., Imwong, M., Tarning, J., Taylor, W.J., Yeung, S., Woodrow, C.J., Flegg, J.A., Das, D., Smith, J., Venkatesan, M., Plowe, C.V., Stepniewska, K., Guerin, P.J., Dondorp, A.M., Day, N.P., White, N.J., Tracking Resistance to Artemisinin, C., 2014. Spread of artemisinin resistance in *Plasmodium falciparum* malaria. *The New England journal of medicine* 371, 411-423.
- Aurrecoechea, C., Brestelli, J., Brunk, B.P., Dommer, J., Fischer, S., Gajria, B., Gao, X., Gingle, A., Grant, G., Harb, O.S., Heiges, M., Innamorato, F., Iodice, J., Kissinger, J.C., Kraemer, E., Li, W., Miller, J.A., Nayak, V., Pennington, C., Pinney, D.F., Roos, D.S., Ross, C., Stoeckert, C.J., Jr., Treatman, C., Wang, H., 2009. PlasmoDB: a functional genomic database for malaria parasites. *Nucleic acids research* 37, D539-543.
- Baer, K., Klotz, C., Kappe, S.H., Schnieder, T., Frevort, U., 2007. Release of hepatic *Plasmodium yoelii* merozoites into the pulmonary microvasculature. *PLoS pathogens* 3, e171.
- Bannister, L.H., Hopkins, J.M., Fowler, R.E., Krishna, S., Mitchell, G.H., 2000. Ultrastructure of rhoptry development in *Plasmodium falciparum* erythrocytic schizonts. *Parasitology* 121 ( Pt 3), 273-287.
- Bartoloni, A., Zammarchi, L., 2012. Clinical aspects of uncomplicated and severe malaria. *Mediterranean journal of hematology and infectious diseases* 4, e2012026.
- Batinovic, S., McHugh, E., Chisholm, S.A., Matthews, K., Liu, B., Dumont, L., Charnaud, S.C., Schneider, M.P., Gilson, P.R., de Koning-Ward, T.F., Dixon, M.W.A., Tilley, L., 2017. An exported protein-interacting complex involved in the trafficking of virulence determinants in *Plasmodium*-infected erythrocytes. *Nature communications* 8, 16044.

- Beaumelle, B.D., Vial, H.J., 1988a. Acyl-CoA synthetase activity in Plasmodium knowlesi-infected erythrocytes displays peculiar substrate specificities. *Biochimica et biophysica acta* 958, 1-9.
- Beaumelle, B.D., Vial, H.J., 1988b. Correlation of the efficiency of fatty acid derivatives in suppressing Plasmodium falciparum growth in culture with their inhibitory effect on acyl-CoA synthetase activity. *Molecular and biochemical parasitology* 28, 39-42.
- Beck, J.R., Muralidharan, V., Oksman, A., Goldberg, D.E., 2014. PTEX component HSP101 mediates export of diverse malaria effectors into host erythrocytes. *Nature* 511, 592-595.
- Becker, J., 2016. Identification of new parasitophorous vacuole proteins in the human malaria parasite Plasmodium falciparum, *Molecular Biotechnology*. RWTH Aachen, Aachen.
- Benting, J., Mattei, D., Lingelbach, K., 1994. Brefeldin A inhibits transport of the glycoporphin-binding protein from Plasmodium falciparum into the host erythrocyte. *The Biochemical journal* 300 ( Pt 3), 821-826.
- Besteiro, S., Michelin, A., Poncet, J., Dubremetz, J.F., Lebrun, M., 2009. Export of a Toxoplasma gondii rhoptry neck protein complex at the host cell membrane to form the moving junction during invasion. *PLoS pathogens* 5, e1000309.
- Bethke, L.L., Zilversmit, M., Nielsen, K., Daily, J., Volkman, S.K., Ndiaye, D., Lozovsky, E.R., Hartl, D.L., Wirth, D.F., 2006. Duplication, gene conversion, and genetic diversity in the species-specific acyl-CoA synthetase gene family of Plasmodium falciparum. *Molecular and biochemical parasitology* 150, 10-24.
- Birnbaum, J., Flemming, S., Reichard, N., Soares, A.B., Mesen-Ramirez, P., Jonscher, E., Bergmann, B., Spielmann, T., 2017. A genetic system to study Plasmodium falciparum protein function. *Nature methods* 14, 450-456.
- Blancke Soares, A., 2016. Identification of trafficking determinants in novel PNEPs of the human malaria parasite Plasmodium falciparum, *Department of Biology*. University of Hamburg, Hamburg.
- Blisnick, T., Morales Betoulle, M.E., Barale, J.C., Uzureau, P., Berry, L., Desroses, S., Fujioka, H., Mattei, D., Braun Breton, C., 2000. Pfsbp1, a Maurer's cleft Plasmodium falciparum protein, is associated with the erythrocyte skeleton. *Molecular and biochemical parasitology* 111, 107-121.
- Boddey, J.A., Hodder, A.N., Gunther, S., Gilson, P.R., Patsiouras, H., Kapp, E.A., Pearce, J.A., de Koning-Ward, T.F., Simpson, R.J., Crabb, B.S., Cowman, A.F., 2010. An aspartyl protease directs malaria effector proteins to the host cell. *Nature* 463, 627-631.
- Boddey, J.A., O'Neill, M.T., Lopaticki, S., Carvalho, T.G., Hodder, A.N., Nebl, T., Wawra, S., van West, P., Ebrahimzadeh, Z., Richard, D., Flemming, S., Spielmann, T., Przyborski, J., Babon, J.J., Cowman, A.F., 2016. Export of malaria proteins requires co-translational processing of the PEXEL motif independent of phosphatidylinositol-3-phosphate binding. *Nature communications* 7, 10470.
- Boncompain, G., Perez, F., 2012. Synchronizing protein transport in the secretory pathway. *Current protocols in cell biology* Chapter 15, Unit 15 19.
- Bosch, J., Paige, M.H., Vaidya, A.B., Bergman, L.W., Hol, W.G., 2012. Crystal structure of GAP50, the anchor of the invasion machinery in the inner membrane complex of Plasmodium falciparum. *Journal of structural biology* 178, 61-73.
- Boyce, M., Bryant, K.F., Jousse, C., Long, K., Harding, H.P., Scheuner, D., Kaufman, R.J., Ma, D., Coen, D.M., Ron, D., Yuan, J., 2005. A selective inhibitor of eIF2alpha dephosphorylation protects cells from ER stress. *Science* 307, 935-939.
- Brancucci, N.M.B., Bertschi, N.L., Zhu, L., Niederwieser, I., Chin, W.H., Wampfler, R., Freymond, C., Rottmann, M., Felger, I., Bozdech, Z., Voss, T.S., 2014. Heterochromatin protein 1 secures survival and transmission of malaria parasites. *Cell host & microbe* 16, 165-176.
- Bruce, M.C., Alano, P., Duthie, S., Carter, R., 1990. Commitment of the malaria parasite Plasmodium falciparum to sexual and asexual development. *Parasitology* 100 Pt 2, 191-200.

- Bullen, H.E., Charnaud, S.C., Kalanon, M., Riglar, D.T., Dekiwadia, C., Kangwanrangsang, N., Torii, M., Tsuboi, T., Baum, J., Ralph, S.A., Cowman, A.F., de Koning-Ward, T.F., Crabb, B.S., Gilson, P.R., 2012. Biosynthesis, localization, and macromolecular arrangement of the Plasmodium falciparum translocon of exported proteins (PTEX). *The Journal of biological chemistry* 287, 7871-7884.
- Burda, P.C., Caldelari, R., Heussler, V.T., 2017. Manipulation of the Host Cell Membrane during Plasmodium Liver Stage Egress. *mBio* 8.
- Burda, P.C., Roelli, M.A., Schaffner, M., Khan, S.M., Janse, C.J., Heussler, V.T., 2015. A Plasmodium phospholipase is involved in disruption of the liver stage parasitophorous vacuole membrane. *PLoS pathogens* 11, e1004760.
- Chang, H.H., Falick, A.M., Carlton, P.M., Sedat, J.W., DeRisi, J.L., Marletta, M.A., 2008. N-terminal processing of proteins exported by malaria parasites. *Molecular and biochemical parasitology* 160, 107-115.
- Chaturvedi, S., Qi, H., Coleman, D., Rodriguez, A., Hanson, P.I., Striepen, B., Roos, D.S., Joiner, K.A., 1999. Constitutive calcium-independent release of Toxoplasma gondii dense granules occurs through the NSF/SNAP/SNARE/Rab machinery. *The Journal of biological chemistry* 274, 2424-2431.
- Chen, A.L., Kim, E.W., Toh, J.Y., Vashisht, A.A., Rashoff, A.Q., Van, C., Huang, A.S., Moon, A.S., Bell, H.N., Bentolila, L.A., Wohlschlegel, J.A., Bradley, P.J., 2015. Novel components of the Toxoplasma inner membrane complex revealed by BioID. *mBio* 6, e02357-02314.
- Choi-Rhee, E., Schulman, H., Cronan, J.E., 2004. Promiscuous protein biotinylation by Escherichia coli biotin protein ligase. *Protein science : a publication of the Protein Society* 13, 3043-3050.
- Chu, T., Lingelbach, K., Przyborski, J.M., 2011. Genetic evidence strongly support an essential role for PfPV1 in intra-erythrocytic growth of P. falciparum. *PloS one* 6, e18396.
- Coelho, C.H., Doritchamou, J.Y.A., Zaidi, I., Duffy, P.E., 2017. Advances in malaria vaccine development: report from the 2017 malaria vaccine symposium. *NPJ vaccines* 2, 34.
- Collins, C.R., Das, S., Wong, E.H., Andenmatten, N., Stallmach, R., Hackett, F., Herman, J.P., Muller, S., Meissner, M., Blackman, M.J., 2013. Robust inducible Cre recombinase activity in the human malaria parasite Plasmodium falciparum enables efficient gene deletion within a single asexual erythrocytic growth cycle. *Molecular microbiology* 88, 687-701.
- Collins, C.R., Hackett, F., Atid, J., Tan, M.S.Y., Blackman, M.J., 2017. The Plasmodium falciparum pseudoprotease SERA5 regulates the kinetics and efficiency of malaria parasite egress from host erythrocytes. *PLoS pathogens* 13, e1006453.
- Cooke, B.M., Buckingham, D.W., Glenister, F.K., Fernandez, K.M., Bannister, L.H., Marti, M., Mohandas, N., Coppel, R.L., 2006. A Maurer's cleft-associated protein is essential for expression of the major malaria virulence antigen on the surface of infected red blood cells. *The Journal of cell biology* 172, 899-908.
- Coppi, A., Tewari, R., Bishop, J.R., Bennett, B.L., Lawrence, R., Esko, J.D., Billker, O., Sinnis, P., 2007. Heparan sulfate proteoglycans provide a signal to Plasmodium sporozoites to stop migrating and productively invade host cells. *Cell host & microbe* 2, 316-327.
- Cowman, A.F., Berry, D., Baum, J., 2012. The cellular and molecular basis for malaria parasite invasion of the human red blood cell. *The Journal of cell biology* 198, 961-971.
- Cowman, A.F., Tonkin, C.J., Tham, W.H., Duraisingh, M.T., 2017. The Molecular Basis of Erythrocyte Invasion by Malaria Parasites. *Cell host & microbe* 22, 232-245.
- Cox, F.E., 2010. History of the discovery of the malaria parasites and their vectors. *Parasites & vectors* 3, 5.
- Crabb, B.S., Cooke, B.M., Reeder, J.C., Waller, R.F., Caruana, S.R., Davern, K.M., Wickham, M.E., Brown, G.V., Coppel, R.L., Cowman, A.F., 1997. Targeted gene disruption shows that knobs enable malaria-infected red cells to cytoadhere under physiological shear stress. *Cell* 89, 287-296.

- Crabb, B.S., Rug, M., Gilberger, T.W., Thompson, J.K., Triglia, T., Maier, A.G., Cowman, A.F., 2004. Transfection of the human malaria parasite *Plasmodium falciparum*. *Methods in molecular biology* 270, 263-276.
- Crosnier, C., Bustamante, L.Y., Bartholdson, S.J., Bei, A.K., Theron, M., Uchikawa, M., Mboup, S., Ndir, O., Kwiatkowski, D.P., Duraisingh, M.T., Rayner, J.C., Wright, G.J., 2011. Basigin is a receptor essential for erythrocyte invasion by *Plasmodium falciparum*. *Nature* 480, 534-537.
- Culvenor, J.G., Crewther, P.E., 1990. S-antigen localization in the erythrocytic stages of *Plasmodium falciparum*. *The Journal of protozoology* 37, 59-65.
- Curra, C., Di Luca, M., Picci, L., de Sousa Silva Gomes dos Santos, C., Siden-Kiamos, I., Pace, T., Ponzi, M., 2013. The ETRAMP family member SEP2 is expressed throughout *Plasmodium berghei* life cycle and is released during sporozoite gliding motility. *PLoS one* 8, e67238.
- Das, S., Hertrich, N., Perrin, A.J., Withers-Martinez, C., Collins, C.R., Jones, M.L., Watermeyer, J.M., Fobes, E.T., Martin, S.R., Saibil, H.R., Wright, G.J., Treeck, M., Epp, C., Blackman, M.J., 2015. Processing of *Plasmodium falciparum* Merozoite Surface Protein MSP1 Activates a Spectrin-Binding Function Enabling Parasite Egress from RBCs. *Cell host & microbe* 18, 433-444.
- Dasgupta, S., Auth, T., Gov, N.S., Satchwell, T.J., Hanssen, E., Zuccala, E.S., Riglar, D.T., Toye, A.M., Betz, T., Baum, J., Gompper, G., 2014. Membrane-wrapping contributions to malaria parasite invasion of the human erythrocyte. *Biophysical journal* 107, 43-54.
- Daubersies, P., Thomas, A.W., Millet, P., Brahimi, K., Langermans, J.A., Ollomo, B., BenMohamed, L., Slierendregt, B., Eling, W., Van Belkum, A., Dubreuil, G., Meis, J.F., Guerin-Marchand, C., Cayphas, S., Cohen, J., Gras-Masse, H., Druilhe, P., 2000. Protection against *Plasmodium falciparum* malaria in chimpanzees by immunization with the conserved pre-erythrocytic liver-stage antigen 3. *Nature medicine* 6, 1258-1263.
- de Koning-Ward, T.F., Gilson, P.R., Boddey, J.A., Rug, M., Smith, B.J., Papenfuss, A.T., Sanders, P.R., Lundie, R.J., Maier, A.G., Cowman, A.F., Crabb, B.S., 2009. A newly discovered protein export machine in malaria parasites. *Nature* 459, 945-949.
- de Koning-Ward, T.F., Gilson, P.R., Crabb, B.S., 2015. Advances in molecular genetic systems in malaria. *Nature reviews. Microbiology* 13, 373-387.
- de Koning-Ward, T.F., Waters, A.P., Crabb, B.S., 2001. Puromycin-N-acetyltransferase as a selectable marker for use in *Plasmodium falciparum*. *Molecular and biochemical parasitology* 117, 155-160.
- De Niz, M., Burda, P.C., Kaiser, G., Del Portillo, H.A., Spielmann, T., Frischknecht, F., Heussler, V.T., 2017. Progress in imaging methods: insights gained into *Plasmodium* biology. *Nature reviews. Microbiology* 15, 37-54.
- De Niz, M., Meibalan, E., Mejia, P., Ma, S., Brancucci, N.M.B., Agop-Nersesian, C., Mandt, R., Ngotho, P., Hughes, K.R., Waters, A.P., Huttenhower, C., Mitchell, J.R., Martinelli, R., Frischknecht, F., Seydel, K.B., Taylor, T., Milner, D., Heussler, V.T., Marti, M., 2018. *Plasmodium* gametocytes display homing and vascular transmigration in the host bone marrow. *Science advances* 4, eaat3775.
- Deegan, T., Maegraith, B.G., 1956. Studies on the nature of malarial pigment (haemozoin). I. The pigment of the simian species, *Plasmodium knowlesi* and *P. Cynomolgi*. *Annals of tropical medicine and parasitology* 50, 194-211.
- Del Portillo, H.A., Ferrer, M., Brugat, T., Martin-Jaular, L., Langhorne, J., Lacerda, M.V., 2012. The role of the spleen in malaria. *Cellular microbiology* 14, 343-355.
- Delves, M., Plouffe, D., Scheurer, C., Meister, S., Wittlin, S., Winzeler, E.A., Sinden, R.E., Leroy, D., 2012. The activities of current antimalarial drugs on the life cycle stages of *Plasmodium*: a comparative study with human and rodent parasites. *PLoS medicine* 9, e1001169.
- Deponte, M., Hoppe, H.C., Lee, M.C., Maier, A.G., Richard, D., Rug, M., Spielmann, T., Przyborski, J.M., 2012. Wherever I may roam: protein and membrane trafficking in *P. falciparum*-infected red blood cells. *Molecular and biochemical parasitology* 186, 95-116.

- Desai, S.A., 2012. Ion and nutrient uptake by malaria parasite-infected erythrocytes. *Cellular microbiology* 14, 1003-1009.
- Desai, S.A., Krogstad, D.J., McCleskey, E.W., 1993. A nutrient-permeable channel on the intraerythrocytic malaria parasite. *Nature* 362, 643-646.
- Desai, S.A., Rosenberg, R.L., 1997. Pore size of the malaria parasite's nutrient channel. *Proceedings of the National Academy of Sciences of the United States of America* 94, 2045-2049.
- Dietz, O., Rusch, S., Brand, F., Mundwiler-Pachlatko, E., Gaida, A., Voss, T., Beck, H.P., 2014. Characterization of the small exported Plasmodium falciparum membrane protein SEMP1. *PloS one* 9, e103272.
- Dorn, A., Stoffel, R., Matile, H., Bubendorf, A., Ridley, R.G., 1995. Malarial haemozoin/beta-haematin supports haem polymerization in the absence of protein. *Nature* 374, 269-271.
- Durand, R., Le Bras, J., 2001. [Plasmodium falciparum: point mutations of pcfrt and chloroquine susceptibility]. *Annales pharmaceutiques francaises* 59, 312-318.
- Dvorak, J.A., Miller, L.H., Whitehouse, W.C., Shiroishi, T., 1975. Invasion of erythrocytes by malaria merozoites. *Science* 187, 748-750.
- Dvorin, J.D., Martyn, D.C., Patel, S.D., Grimley, J.S., Collins, C.R., Hopp, C.S., Bright, A.T., Westenberger, S., Winzeler, E., Blackman, M.J., Baker, D.A., Wandless, T.J., Duraisingh, M.T., 2010. A plant-like kinase in Plasmodium falciparum regulates parasite egress from erythrocytes. *Science* 328, 910-912.
- Eisele, T.P., Larsen, D., Steketee, R.W., 2010. Protective efficacy of interventions for preventing malaria mortality in children in Plasmodium falciparum endemic areas. *International journal of epidemiology* 39 Suppl 1, i88-101.
- El Bakkouri, M., Pow, A., Mulichak, A., Cheung, K.L., Artz, J.D., Amani, M., Fell, S., de Koning-Ward, T.F., Goodman, C.D., McFadden, G.I., Ortega, J., Hui, R., Houry, W.A., 2010. The Clp chaperones and proteases of the human malaria parasite Plasmodium falciparum. *Journal of molecular biology* 404, 456-477.
- Elsworth, B., Matthews, K., Nie, C.Q., Kalanon, M., Charnaud, S.C., Sanders, P.R., Chisholm, S.A., Counihan, N.A., Shaw, P.J., Pino, P., Chan, J.A., Azevedo, M.F., Rogerson, S.J., Beeson, J.G., Crabb, B.S., Gilson, P.R., de Koning-Ward, T.F., 2014. PTEX is an essential nexus for protein export in malaria parasites. *Nature* 511, 587-591.
- Elsworth, B., Sanders, P.R., Nebl, T., Batinovic, S., Kalanon, M., Nie, C.Q., Charnaud, S.C., Bullen, H.E., de Koning Ward, T.F., Tilley, L., Crabb, B.S., Gilson, P.R., 2016. Proteomic analysis reveals novel proteins associated with the Plasmodium protein exporter PTEX and a loss of complex stability upon truncation of the core PTEX component, PTEX150. *Cellular microbiology* 18, 1551-1569.
- Fidock, D.A., Wellems, T.E., 1997. Transformation with human dihydrofolate reductase renders malaria parasites insensitive to WR99210 but does not affect the intrinsic activity of proguanil. *Proceedings of the National Academy of Sciences of the United States of America* 94, 10931-10936.
- Filarsky, M., Fraschka, S.A., Niederwieser, I., Brancucci, N.M.B., Carrington, E., Carrio, E., Moes, S., Jenoe, P., Bartfai, R., Voss, T.S., 2018. GDV1 induces sexual commitment of malaria parasites by antagonizing HP1-dependent gene silencing. *Science* 359, 1259-1263.
- Firat-Karalar, E.N., Rauniyar, N., Yates, J.R., 3rd, Stearns, T., 2014. Proximity interactions among centrosome components identify regulators of centriole duplication. *Current biology : CB* 24, 664-670.
- Francis, S.E., Sullivan, D.J., Jr., Goldberg, D.E., 1997. Hemoglobin metabolism in the malaria parasite Plasmodium falciparum. *Annual review of microbiology* 51, 97-123.
- Ganesan, S.M., Falla, A., Goldfless, S.J., Nasamu, A.S., Niles, J.C., 2016. Synthetic RNA-protein modules integrated with native translation mechanisms to control gene expression in malaria parasites. *Nature communications* 7, 10727.
- Gardner, M.J., Hall, N., Fung, E., White, O., Berriman, M., Hyman, R.W., Carlton, J.M., Pain, A., Nelson, K.E., Bowman, S., Paulsen, I.T., James, K., Eisen, J.A., Rutherford, K., Salzberg, S.L., Craig, A., Kyes, S., Chan, M.S., Nene, V., Shallom, S.J., Suh, B.,

- Peterson, J., Angiuoli, S., Perteau, M., Allen, J., Selengut, J., Haft, D., Mather, M.W., Vaidya, A.B., Martin, D.M., Fairlamb, A.H., Fraunholz, M.J., Roos, D.S., Ralph, S.A., McFadden, G.I., Cummings, L.M., Subramanian, G.M., Mungall, C., Venter, J.C., Carucci, D.J., Hoffman, S.L., Newbold, C., Davis, R.W., Fraser, C.M., Barrell, B., 2002. Genome sequence of the human malaria parasite *Plasmodium falciparum*. *Nature* 419, 498-511.
- Gazarini, M.L., Thomas, A.P., Pozzan, T., Garcia, C.R., 2003. Calcium signaling in a low calcium environment: how the intracellular malaria parasite solves the problem. *The Journal of cell biology* 161, 103-110.
- Gehde, N., Hinrichs, C., Montilla, I., Charpian, S., Lingelbach, K., Przyborski, J.M., 2009. Protein unfolding is an essential requirement for transport across the parasitophorous vacuolar membrane of *Plasmodium falciparum*. *Molecular microbiology* 71, 613-628.
- Ghorbal, M., Gorman, M., Macpherson, C.R., Martins, R.M., Scherf, A., Lopez-Rubio, J.J., 2014. Genome editing in the human malaria parasite *Plasmodium falciparum* using the CRISPR-Cas9 system. *Nature biotechnology* 32, 819-821.
- Ghosh, S., Kennedy, K., Sanders, P., Matthews, K., Ralph, S.A., Counihan, N.A., de Koning-Ward, T.F., 2017. The *Plasmodium* rhoptry associated protein complex is important for parasitophorous vacuole membrane structure and intraerythrocytic parasite growth. *Cellular microbiology* 19.
- Gibson, D.G., 2009. Synthesis of DNA fragments in yeast by one-step assembly of overlapping oligonucleotides. *Nucleic acids research* 37, 6984-6990.
- Glushakova, S., Lizunov, V., Blank, P.S., Melikov, K., Humphrey, G., Zimmerberg, J., 2013. Cytoplasmic free Ca<sup>2+</sup> is essential for multiple steps in malaria parasite egress from infected erythrocytes. *Malaria journal* 12, 41.
- Gold, D.A., Kaplan, A.D., Lis, A., Bett, G.C., Rosowski, E.E., Cirelli, K.M., Bougdour, A., Sidik, S.M., Beck, J.R., Lourido, S., Egea, P.F., Bradley, P.J., Hakimi, M.A., Rasmusson, R.L., Saeij, J.P., 2015. The *Toxoplasma* Dense Granule Proteins GRA17 and GRA23 Mediate the Movement of Small Molecules between the Host and the Parasitophorous Vacuole. *Cell host & microbe* 17, 642-652.
- Gomes, A.R., Bushell, E., Schwach, F., Girling, G., Anar, B., Quail, M.A., Herd, C., Pfander, C., Modrzynska, K., Rayner, J.C., Billker, O., 2015. A genome-scale vector resource enables high-throughput reverse genetic screening in a malaria parasite. *Cell host & microbe* 17, 404-413.
- Gruring, C., Heiber, A., Kruse, F., Flemming, S., Franci, G., Colombo, S.F., Fasana, E., Schoeler, H., Borgese, N., Stunnenberg, H.G., Przyborski, J.M., Gilberger, T.W., Spielmann, T., 2012. Uncovering common principles in protein export of malaria parasites. *Cell host & microbe* 12, 717-729.
- Gruring, C., Heiber, A., Kruse, F., Ungefehr, J., Gilberger, T.W., Spielmann, T., 2011. Development and host cell modifications of *Plasmodium falciparum* blood stages in four dimensions. *Nature communications* 2, 165.
- Gruring, C., Spielmann, T., 2012. Imaging of live malaria blood stage parasites. *Methods in enzymology* 506, 81-92.
- Gunther, K., Tummler, M., Arnold, H.H., Ridley, R., Goman, M., Scaife, J.G., Lingelbach, K., 1991. An exported protein of *Plasmodium falciparum* is synthesized as an integral membrane protein. *Molecular and biochemical parasitology* 46, 149-157.
- Gupta, A., Balabaskaran-Nina, P., Nguiragool, W., Saggi, G.S., Schureck, M.A., Desai, S.A., 2018. CLAG3 Self-Associates in Malaria Parasites and Quantitatively Determines Nutrient Uptake Channels at the Host Membrane. *mBio* 9.
- Haldar, K., Bhattacharjee, S., Safeukui, I., 2018. Drug resistance in *Plasmodium*. *Nature reviews. Microbiology* 16, 156-170.
- Hale, V.L., Watermeyer, J.M., Hackett, F., Vizcay-Barrena, G., van Ooij, C., Thomas, J.A., Spink, M.C., Harkiolaki, M., Duke, E., Fleck, R.A., Blackman, M.J., Saibil, H.R., 2017. Parasitophorous vacuole poration precedes its rupture and rapid host erythrocyte cytoskeleton collapse in *Plasmodium falciparum* egress. *Proceedings of the National Academy of Sciences of the United States of America* 114, 3439-3444.

- Hallee, S., Counihan, N.A., Matthews, K., de Koning-Ward, T.F., Richard, D., 2018a. The malaria parasite *Plasmodium falciparum* Sortilin is essential for merozoite formation and apical complex biogenesis. *Cellular microbiology*, e12844.
- Hallee, S., Theriault, C., Gagnon, D., Kehrer, J., Frischknecht, F., Mair, G.R., Richard, D., 2018b. Identification of a Golgi apparatus protein complex important for the asexual erythrocytic cycle of the malaria parasite *Plasmodium falciparum*. *Cellular microbiology*, e12843.
- Hanahan, D., 1983. Studies on transformation of *Escherichia coli* with plasmids. *Journal of molecular biology* 166, 557-580.
- Healer, J., Crawford, S., Ralph, S., McFadden, G., Cowman, A.F., 2002. Independent translocation of two micronemal proteins in developing *Plasmodium falciparum* merozoites. *Infection and immunity* 70, 5751-5758.
- Heiber, A., Kruse, F., Pick, C., Gruring, C., Flemming, S., Oberli, A., Schoeler, H., Retzlaff, S., Mesen-Ramirez, P., Hiss, J.A., Kadekoppala, M., Hecht, L., Holder, A.A., Gilberger, T.W., Spielmann, T., 2013. Identification of new PNEPs indicates a substantial non-PEXEL exportome and underpins common features in *Plasmodium falciparum* protein export. *PLoS pathogens* 9, e1003546.
- Hiller, N.L., Akompong, T., Morrow, J.S., Holder, A.A., Haldar, K., 2003. Identification of a stomatin orthologue in vacuoles induced in human erythrocytes by malaria parasites. A role for microbial raft proteins in apicomplexan vacuole biogenesis. *The Journal of biological chemistry* 278, 48413-48421.
- Hiller, N.L., Bhattacharjee, S., van Ooij, C., Liolios, K., Harrison, T., Lopez-Estrano, C., Haldar, K., 2004. A host-targeting signal in virulence proteins reveals a secretome in malarial infection. *Science* 306, 1934-1937.
- Hviid, L., Jensen, A.T., 2015. PfEMP1 - A Parasite Protein Family of Key Importance in *Plasmodium falciparum* Malaria Immunity and Pathogenesis. *Advances in parasitology* 88, 51-84.
- Iriko, H., Ishino, T., Otsuki, H., Ito, D., Tachibana, M., Torii, M., Tsuboi, T., 2018. *Plasmodium falciparum* Exported Protein 1 is localized to dense granules in merozoites. *Parasitology international* 67, 637-639.
- Ito, D., Schureck, M.A., Desai, S.A., 2017. An essential dual-function complex mediates erythrocyte invasion and channel-mediated nutrient uptake in malaria parasites. *eLife* 6.
- Jones, M.L., Das, S., Belda, H., Collins, C.R., Blackman, M.J., Treeck, M., 2016. A versatile strategy for rapid conditional genome engineering using loxP sites in a small synthetic intron in *Plasmodium falciparum*. *Scientific reports* 6, 21800.
- Jullien, N., Goddard, I., Selmi-Ruby, S., Fina, J.L., Cremer, H., Herman, J.P., 2007. Conditional transgenesis using Dimerizable Cre (DiCre). *PloS one* 2, e1355.
- Kaida, R., Serada, S., Norioka, N., Norioka, S., Neumetzler, L., Pauly, M., Sampedro, J., Zarra, I., Hayashi, T., Kaneko, T.S., 2010. Potential role for purple acid phosphatase in the dephosphorylation of wall proteins in tobacco cells. *Plant physiology* 153, 603-610.
- Kaiser, K., Matuschewski, K., Camargo, N., Ross, J., Kappe, S.H., 2004. Differential transcriptome profiling identifies *Plasmodium* genes encoding pre-erythrocytic stage-specific proteins. *Molecular microbiology* 51, 1221-1232.
- Kaushansky, A., Douglass, A.N., Arang, N., Vigdorovich, V., Dambrauskas, N., Kain, H.S., Austin, L.S., Sather, D.N., Kappe, S.H., 2015. Malaria parasites target the hepatocyte receptor EphA2 for successful host infection. *Science* 350, 1089-1092.
- Kaushansky, A., Metzger, P.G., Douglass, A.N., Mikolajczak, S.A., Lakshmanan, V., Kain, H.S., Kappe, S.H., 2013. Malaria parasite liver stages render host hepatocytes susceptible to mitochondria-initiated apoptosis. *Cell death & disease* 4, e762.
- Kauth, C.W., Woehlbier, U., Kern, M., Mekonnen, Z., Lutz, R., Mucke, N., Langowski, J., Bujard, H., 2006. Interactions between merozoite surface proteins 1, 6, and 7 of the malaria parasite *Plasmodium falciparum*. *The Journal of biological chemistry* 281, 31517-31527.
- Kehrer, J., Frischknecht, F., Mair, G.R., 2016. Proteomic Analysis of the *Plasmodium berghei* Gametocyte Egressome and Vesicular bioID of Osmiophilic Body Proteins

- Identifies Merozoite TRAP-like Protein (MTRAP) as an Essential Factor for Parasite Transmission. *Molecular & cellular proteomics : MCP* 15, 2852-2862.
- Kennedy, A.T., Schmidt, C.Q., Thompson, J.K., Weiss, G.E., Taechalerpaisarn, T., Gilson, P.R., Barlow, P.N., Crabb, B.S., Cowman, A.F., Tham, W.H., 2016. Recruitment of Factor H as a Novel Complement Evasion Strategy for Blood-Stage Plasmodium falciparum Infection. *Journal of immunology* 196, 1239-1248.
- Khosh-Naucke, M., Becker, J., Mesen-Ramirez, P., Kiani, P., Birnbaum, J., Frohlike, U., Jonscher, E., Schluter, H., Spielmann, T., 2017. Identification of novel parasitophorous vacuole proteins in *P. falciparum* parasites using BiOLD. *International journal of medical microbiology : IJMM*.
- Kim, D.I., Birendra, K.C., Zhu, W., Motamedchaboki, K., Doye, V., Roux, K.J., 2014. Probing nuclear pore complex architecture with proximity-dependent biotinylation. *Proceedings of the National Academy of Sciences of the United States of America* 111, E2453-2461.
- Kim, D.I., Jensen, S.C., Noble, K.A., Kc, B., Roux, K.H., Motamedchaboki, K., Roux, K.J., 2016. An improved smaller biotin ligase for BiOLD proximity labeling. *Molecular biology of the cell* 27, 1188-1196.
- Koussis, K., Withers-Martinez, C., Yeoh, S., Child, M., Hackett, F., Knuepfer, E., Juliano, L., Woehlbier, U., Bujard, H., Blackman, M.J., 2009. A multifunctional serine protease primes the malaria parasite for red blood cell invasion. *The EMBO journal* 28, 725-735.
- Kulzer, S., Charnaud, S., Dagan, T., Riedel, J., Mandal, P., Pesce, E.R., Blatch, G.L., Crabb, B.S., Gilson, P.R., Przyborski, J.M., 2012. Plasmodium falciparum-encoded exported hsp70/hsp40 chaperone/co-chaperone complexes within the host erythrocyte. *Cellular microbiology* 14, 1784-1795.
- Kulzer, S., Gehde, N., Przyborski, J.M., 2009. Return to sender: use of Plasmodium ER retrieval sequences to study protein transport in the infected erythrocyte and predict putative ER protein families. *Parasitology research* 104, 1535-1541.
- Kulzer, S., Rug, M., Brinkmann, K., Cannon, P., Cowman, A., Lingelbach, K., Blatch, G.L., Maier, A.G., Przyborski, J.M., 2010. Parasite-encoded Hsp40 proteins define novel mobile structures in the cytosol of the *P. falciparum*-infected erythrocyte. *Cellular microbiology* 12, 1398-1420.
- Lajko, M., Haddad, A.F., Robinson, C.A., Connolly, S.A., 2015. Using proximity biotinylation to detect herpesvirus entry glycoprotein interactions: Limitations for integral membrane glycoproteins. *Journal of virological methods* 221, 81-89.
- Lambros, C., Vanderberg, J.P., 1979. Synchronization of Plasmodium falciparum erythrocytic stages in culture. *The Journal of parasitology* 65, 418-420.
- Langlois, A.C., Marinach, C., Manzoni, G., Silvie, O., 2018. Plasmodium sporozoites can invade hepatocytic cells independently of the Ephrin receptor A2. *PloS one* 13, e0200032.
- Lauer, S.A., Rathod, P.K., Ghori, N., Haldar, K., 1997. A membrane network for nutrient import in red cells infected with the malaria parasite. *Science* 276, 1122-1125.
- Laveran, C.L.A., 1880. Drawings of *P. falciparum*, Personal Notebook.
- Le Roch, K.G., Zhou, Y., Blair, P.L., Grainger, M., Moch, J.K., Haynes, J.D., De La Vega, P., Holder, A.A., Batalov, S., Carucci, D.J., Winzeler, E.A., 2003. Discovery of gene function by expression profiling of the malaria parasite life cycle. *Science* 301, 1503-1508.
- Le Sage, V., Cinti, A., Valiente-Echeverria, F., Moulard, A.J., 2015. Proteomic analysis of HIV-1 Gag interacting partners using proximity-dependent biotinylation. *Virology journal* 12, 138.
- Lengeler, C., 2004. Insecticide-treated bed nets and curtains for preventing malaria. *The Cochrane database of systematic reviews*, CD000363.
- Li, J., Matsuoka, H., Mitamura, T., Horii, T., 2002. Characterization of proteases involved in the processing of Plasmodium falciparum serine repeat antigen (SERA). *Molecular and biochemical parasitology* 120, 177-186.
- Lingelbach, K.R., 1993. Plasmodium falciparum: a molecular view of protein transport from the parasite into the host erythrocyte. *Experimental parasitology* 76, 318-327.
- Lisewski, A.M., Quiros, J.P., Ng, C.L., Adikesavan, A.K., Miura, K., Putluri, N., Eastman, R.T., Scanfeld, D., Regenbogen, S.J., Altenhofen, L., Llinas, M., Sreekumar, A., Long, C.,

- Fidock, D.A., Lichtarge, O., 2014. Supergenomic network compression and the discovery of EXP1 as a glutathione transferase inhibited by artesunate. *Cell* 158, 916-928.
- Lopaticki, S., Maier, A.G., Thompson, J., Wilson, D.W., Tham, W.H., Triglia, T., Gout, A., Speed, T.P., Beeson, J.G., Healer, J., Cowman, A.F., 2011. Reticulocyte and erythrocyte binding-like proteins function cooperatively in invasion of human erythrocytes by malaria parasites. *Infection and immunity* 79, 1107-1117.
- Lu, G., Wang, Y., 2008. Functional diversity of mammalian type 2C protein phosphatase isoforms: new tales from an old family. *Clinical and experimental pharmacology & physiology* 35, 107-112.
- Mackellar, D.C., O'Neill, M.T., Aly, A.S., Sacchi, J.B., Jr., Cowman, A.F., Kappe, S.H., 2010. Plasmodium falciparum PF10\_0164 (ETRAMP10.3) is an essential parasitophorous vacuole and exported protein in blood stages. *Eukaryotic cell* 9, 784-794.
- MacKellar, D.C., Vaughan, A.M., Aly, A.S., DeLeon, S., Kappe, S.H., 2011. A systematic analysis of the early transcribed membrane protein family throughout the life cycle of Plasmodium yoelii. *Cellular microbiology* 13, 1755-1767.
- Maier, A.G., Rug, M., O'Neill, M.T., Brown, M., Chakravorty, S., Szeszak, T., Chesson, J., Wu, Y., Hughes, K., Coppel, R.L., Newbold, C., Beeson, J.G., Craig, A., Crabb, B.S., Cowman, A.F., 2008. Exported proteins required for virulence and rigidity of Plasmodium falciparum-infected human erythrocytes. *Cell* 134, 48-61.
- Malleret, B., Claser, C., Ong, A.S., Suwanarusk, R., Sriprawat, K., Howland, S.W., Russell, B., Nosten, F., Renia, L., 2011. A rapid and robust tri-color flow cytometry assay for monitoring malaria parasite development. *Scientific reports* 1, 118.
- Mamoun, C.B., Gluzman, I.Y., Goyard, S., Beverley, S.M., Goldberg, D.E., 1999. A set of independent selectable markers for transfection of the human malaria parasite Plasmodium falciparum. *Proceedings of the National Academy of Sciences of the United States of America* 96, 8716-8720.
- Mancio-Silva, L., Slavic, K., Grilo Ruivo, M.T., Grosso, A.R., Modrzynska, K.K., Vera, I.M., Sales-Dias, J., Gomes, A.R., MacPherson, C.R., Crozet, P., Adamo, M., Baena-Gonzalez, E., Tewari, R., Llinas, M., Billker, O., Mota, M.M., 2017. Nutrient sensing modulates malaria parasite virulence. *Nature* 547, 213-216.
- Maneerattanasak, S., Gosi, P., Krudsood, S., Chimma, P., Tongshoob, J., Mahakunkijcharoen, Y., Sukasem, C., Imwong, M., Snounou, G., Khusmith, S., 2017. Molecular and immunological analyses of confirmed Plasmodium vivax relapse episodes. *Malaria journal* 16, 228.
- Marchetti, R.V., Lehane, A.M., Shafik, S.H., Winterberg, M., Martin, R.E., Kirk, K., 2015. A lactate and formate transporter in the intraerythrocytic malaria parasite, Plasmodium falciparum. *Nature communications* 6, 6721.
- Marti, M., Good, R.T., Rug, M., Knuepfer, E., Cowman, A.F., 2004. Targeting malaria virulence and remodeling proteins to the host erythrocyte. *Science* 306, 1930-1933.
- Matthews, K., Kalanon, M., Chisholm, S.A., Sturm, A., Goodman, C.D., Dixon, M.W., Sanders, P.R., Nebl, T., Fraser, F., Haase, S., McFadden, G.I., Gilson, P.R., Crabb, B.S., de Koning-Ward, T.F., 2013. The Plasmodium translocon of exported proteins (PTEX) component thioredoxin-2 is important for maintaining normal blood-stage growth. *Molecular microbiology* 89, 1167-1186.
- Matuschewski, K., Nunes, A.C., Nussenzweig, V., Menard, R., 2002a. Plasmodium sporozoite invasion into insect and mammalian cells is directed by the same dual binding system. *The EMBO journal* 21, 1597-1606.
- Matuschewski, K., Ross, J., Brown, S.M., Kaiser, K., Nussenzweig, V., Kappe, S.H., 2002b. Infectivity-associated changes in the transcriptional repertoire of the malaria parasite sporozoite stage. *The Journal of biological chemistry* 277, 41948-41953.
- Mbengue, B., Niang, B., Niang, M.S., Varela, M.L., Fall, B., Fall, M.M., Diallo, R.N., Diatta, B., Gowda, D.C., Dieye, A., Perraut, R., 2016. Inflammatory cytokine and humoral responses to Plasmodium falciparum glycosylphosphatidylinositols correlates with malaria immunity and pathogenesis. *Immunity, inflammation and disease* 4, 24-34.
- McAllaster, M.R., Ikeda, K.N., Lozano-Nunez, A., Anrather, D., Unterwurzacher, V., Gossenreiter, T., Perry, J.A., Crickley, R., Mercadante, C.J., Vaughan, S., de Graffenried,

- C.L., 2015. Proteomic identification of novel cytoskeletal proteins associated with TbPLK, an essential regulator of cell morphogenesis in *Trypanosoma brucei*. *Molecular biology of the cell* 26, 3013-3029.
- McMillan, P.J., Millet, C., Batinovic, S., Maiorca, M., Hanssen, E., Kenny, S., Muhle, R.A., Melcher, M., Fidock, D.A., Smith, J.D., Dixon, M.W., Tilley, L., 2013. Spatial and temporal mapping of the PfEMP1 export pathway in *Plasmodium falciparum*. *Cellular microbiology* 15, 1401-1418.
- Mesen-Ramirez, P., Reinsch, F., Blancke Soares, A., Bergmann, B., Ullrich, A.K., Tenzer, S., Spielmann, T., 2016. Stable Translocation Intermediates Jam Global Protein Export in *Plasmodium falciparum* Parasites and Link the PTEX Component EXP2 with Translocation Activity. *PLoS pathogens* 12, e1005618.
- Mi-Ichi, F., Kita, K., Mitamura, T., 2006. Intraerythrocytic *Plasmodium falciparum* utilize a broad range of serum-derived fatty acids with limited modification for their growth. *Parasitology* 133, 399-410.
- Mikolajczak, S.A., Jacobs-Lorena, V., MacKellar, D.C., Camargo, N., Kappe, S.H., 2007. L-FABP is a critical host factor for successful malaria liver stage development. *International journal for parasitology* 37, 483-489.
- Milani, K.J., Schneider, T.G., Taraschi, T.F., 2015. Defining the morphology and mechanism of the hemoglobin transport pathway in *Plasmodium falciparum*-infected erythrocytes. *Eukaryotic cell* 14, 415-426.
- Miller, S.K., Good, R.T., Drew, D.R., Delorenzi, M., Sanders, P.R., Hodder, A.N., Speed, T.P., Cowman, A.F., de Koning-Ward, T.F., Crabb, B.S., 2002. A subset of *Plasmodium falciparum* SERA genes are expressed and appear to play an important role in the erythrocytic cycle. *The Journal of biological chemistry* 277, 47524-47532.
- Milner, D.A., Jr., Lee, J.J., Frantzreb, C., Whitten, R.O., Kamiza, S., Carr, R.A., Pradham, A., Factor, R.E., Playforth, K., Liomba, G., Dzamalala, C., Seydel, K.B., Molyneux, M.E., Taylor, T.E., 2015. Quantitative Assessment of Multiorgan Sequestration of Parasites in Fatal Pediatric Cerebral Malaria. *The Journal of infectious diseases* 212, 1317-1321.
- Mojica, S.A., Hovis, K.M., Frieman, M.B., Tran, B., Hsia, R.C., Ravel, J., Jenkins-Houk, C., Wilson, K.L., Bavoil, P.M., 2015. SINC, a type III secreted protein of *Chlamydia psittaci*, targets the inner nuclear membrane of infected cells and uninfected neighbors. *Molecular biology of the cell* 26, 1918-1934.
- Moon, R.W., Hall, J., Rangkuti, F., Ho, Y.S., Almond, N., Mitchell, G.H., Pain, A., Holder, A.A., Blackman, M.J., 2013. Adaptation of the genetically tractable malaria pathogen *Plasmodium knowlesi* to continuous culture in human erythrocytes. *Proceedings of the National Academy of Sciences of the United States of America* 110, 531-536.
- Mordue, D.G., Desai, N., Dustin, M., Sibley, L.D., 1999. Invasion by *Toxoplasma gondii* establishes a moving junction that selectively excludes host cell plasma membrane proteins on the basis of their membrane anchoring. *The Journal of experimental medicine* 190, 1783-1792.
- Moris, P., Jongert, E., van der Most, R.G., 2018. Characterization of T-cell immune responses in clinical trials of the candidate RTS,S malaria vaccine. *Human vaccines & immunotherapeutics* 14, 17-27.
- Morita, M., Nagaoka, H., Ntege, E.H., Kanoi, B.N., Ito, D., Nakata, T., Lee, J.W., Tokunaga, K., Iimura, T., Torii, M., Tsuboi, T., Takashima, E., 2018. PV1, a novel *Plasmodium falciparum* merozoite dense granule protein, interacts with exported protein in infected erythrocytes. *Scientific reports* 8, 3696.
- Morita, M., Takashima, E., Ito, D., Miura, K., Thongkukiatkul, A., Diouf, A., Fairhurst, R.M., Diakite, M., Long, C.A., Torii, M., Tsuboi, T., 2017. Immunoscreening of *Plasmodium falciparum* proteins expressed in a wheat germ cell-free system reveals a novel malaria vaccine candidate. *Scientific reports* 7, 46086.
- Morriswood, B., Havlicek, K., Demmel, L., Yavuz, S., Sealey-Cardona, M., Vidilaseris, K., Anrather, D., Kostan, J., Djinic-Carugo, K., Roux, K.J., Warren, G., 2013. Novel bilobe components in *Trypanosoma brucei* identified using proximity-dependent biotinylation. *Eukaryotic cell* 12, 356-367.

- Mota, M.M., Pradel, G., Vanderberg, J.P., Hafalla, J.C., Frevert, U., Nussenzweig, R.S., Nussenzweig, V., Rodriguez, A., 2001. Migration of Plasmodium sporozoites through cells before infection. *Science* 291, 141-144.
- Mueller, A.K., Camargo, N., Kaiser, K., Andorfer, C., Frevert, U., Matuschewski, K., Kappe, S.H., 2005. Plasmodium liver stage developmental arrest by depletion of a protein at the parasite-host interface. *Proceedings of the National Academy of Sciences of the United States of America* 102, 3022-3027.
- Muller, I.B., Hyde, J.E., 2010. Antimalarial drugs: modes of action and mechanisms of parasite resistance. *Future microbiology* 5, 1857-1873.
- Mundwiler-Pachlatko, E., Beck, H.P., 2013. Maurer's clefts, the enigma of Plasmodium falciparum. *Proceedings of the National Academy of Sciences of the United States of America* 110, 19987-19994.
- Nasamu, A.S., Glushakova, S., Russo, I., Vaupel, B., Oksman, A., Kim, A.S., Fremont, D.H., Tolia, N., Beck, J.R., Meyers, M.J., Niles, J.C., Zimmerberg, J., Goldberg, D.E., 2017. Plasmepsins IX and X are essential and druggable mediators of malaria parasite egress and invasion. *Science* 358, 518-522.
- Nee, G., Kramer, K., Nakabayashi, K., Yuan, B., Xiang, Y., Miatton, E., Finkemeier, I., Soppe, W.J.J., 2017. DELAY OF GERMINATION1 requires PP2C phosphatases of the ABA signalling pathway to control seed dormancy. *Nature communications* 8, 72.
- Nguitragool, W., Bokhari, A.A., Pillai, A.D., Rayavara, K., Sharma, P., Turpin, B., Aravind, L., Desai, S.A., 2011. Malaria parasite clag3 genes determine channel-mediated nutrient uptake by infected red blood cells. *Cell* 145, 665-677.
- Nilsson, S., Angeletti, D., Wahlgren, M., Chen, Q., Moll, K., 2012. Plasmodium falciparum antigen 332 is a resident peripheral membrane protein of Maurer's clefts. *PLoS one* 7, e46980.
- Nyalwidhe, J., Lingelbach, K., 2006. Proteases and chaperones are the most abundant proteins in the parasitophorous vacuole of Plasmodium falciparum-infected erythrocytes. *Proteomics* 6, 1563-1573.
- O'Neill, M.T., Phuong, T., Healer, J., Richard, D., Cowman, A.F., 2011. Gene deletion from Plasmodium falciparum using FLP and Cre recombinases: implications for applied site-specific recombination. *International journal for parasitology* 41, 117-123.
- Oakley, M.S., Gerald, N., McCutchan, T.F., Aravind, L., Kumar, S., 2011. Clinical and molecular aspects of malaria fever. *Trends in parasitology* 27, 442-449.
- Oberli, A., Slater, L.M., Cutts, E., Brand, F., Mundwiler-Pachlatko, E., Rusch, S., Masik, M.F., Erat, M.C., Beck, H.P., Vakonakis, I., 2014. A Plasmodium falciparum PHIST protein binds the virulence factor PfEMP1 and comigrates to knobs on the host cell surface. *FASEB journal : official publication of the Federation of American Societies for Experimental Biology* 28, 4420-4433.
- Pachlatko, E., Rusch, S., Muller, A., Hemphill, A., Tilley, L., Hanssen, E., Beck, H.P., 2010. MAHRP2, an exported protein of Plasmodium falciparum, is an essential component of Maurer's cleft tethers. *Molecular microbiology* 77, 1136-1152.
- Pan, C., Liu, H.D., Gong, Z., Yu, X., Hou, X.B., Xie, D.D., Zhu, X.B., Li, H.W., Tang, J.Y., Xu, Y.F., Yu, J.Q., Zhang, L.Y., Fang, H., Xiao, K.H., Chen, Y.G., Wang, J.Y., Pang, Q., Chen, W., Sun, J.P., 2013. Cadmium is a potent inhibitor of PPM phosphatases and targets the M1 binding site. *Scientific reports* 3, 2333.
- Pan, C., Tang, J.Y., Xu, Y.F., Xiao, P., Liu, H.D., Wang, H.A., Wang, W.B., Meng, F.G., Yu, X., Sun, J.P., 2015. The catalytic role of the M2 metal ion in PP2C $\alpha$ . *Scientific reports* 5, 8560.
- Pandey, R., Mohammed, A., Pierrot, C., Khalife, J., Malhotra, P., Gupta, D., 2014. Genome wide in silico analysis of Plasmodium falciparum phosphatome. *BMC genomics* 15, 1024.
- Perrin, A.J., Collins, C.R., Russell, M.R.G., Collinson, L.M., Baker, D.A., Blackman, M.J., 2018. The Actinomyosin Motor Drives Malaria Parasite Red Blood Cell Invasion but Not Egress. *mBio* 9.
- Pinzon-Ortiz, C., Friedman, J., Esko, J., Sinnis, P., 2001. The binding of the circumsporozoite protein to cell surface heparan sulfate proteoglycans is required for

- plasmodium sporozoite attachment to target cells. *The Journal of biological chemistry* 276, 26784-26791.
- Prieur, E., Druilhe, P., 2009. The malaria candidate vaccine liver stage antigen-3 is highly conserved in *Plasmodium falciparum* isolates from diverse geographical areas. *Malaria journal* 8, 247.
- Rahimi, B.A., Thakkestian, A., White, N.J., Sirivichayakul, C., Dondorp, A.M., Chokeyindachai, W., 2014. Severe vivax malaria: a systematic review and meta-analysis of clinical studies since 1900. *Malaria journal* 13, 481.
- Ross, R., 1897.
- Roux, K.J., Kim, D.I., Raida, M., Burke, B., 2012. A promiscuous biotin ligase fusion protein identifies proximal and interacting proteins in mammalian cells. *The Journal of cell biology* 196, 801-810.
- Ruecker, A., Shea, M., Hackett, F., Suarez, C., Hirst, E.M., Milutinovic, K., Withers-Martinez, C., Blackman, M.J., 2012. Proteolytic activation of the essential parasitophorous vacuole cysteine protease SERA6 accompanies malaria parasite egress from its host erythrocyte. *The Journal of biological chemistry* 287, 37949-37963.
- Russo, I., Babbitt, S., Muralidharan, V., Butler, T., Oksman, A., Goldberg, D.E., 2010. Plasmeprin V licenses *Plasmodium* proteins for export into the host erythrocyte. *Nature* 463, 632-636.
- Sa, E.C.C., Nyboer, B., Heiss, K., Sanches-Vaz, M., Fontinha, D., Wiedtke, E., Grimm, D., Przyborski, J.M., Mota, M.M., Prudencio, M., Mueller, A.K., 2017. *Plasmodium berghei* EXP-1 interacts with host Apolipoprotein H during *Plasmodium* liver-stage development. *Proceedings of the National Academy of Sciences of the United States of America* 114, E1138-E1147.
- Sanders, P.R., Gilson, P.R., Cantin, G.T., Greenbaum, D.C., Nebl, T., Carucci, D.J., McConville, M.J., Schofield, L., Hodder, A.N., Yates, J.R., 3rd, Crabb, B.S., 2005. Distinct protein classes including novel merozoite surface antigens in Raft-like membranes of *Plasmodium falciparum*. *The Journal of biological chemistry* 280, 40169-40176.
- Sargeant, T.J., Marti, M., Caler, E., Carlton, J.M., Simpson, K., Speed, T.P., Cowman, A.F., 2006. Lineage-specific expansion of proteins exported to erythrocytes in malaria parasites. *Genome biology* 7, R12.
- Schnider, C.B., Bausch-Fluck, D., Bruhlmann, F., Heussler, V.T., Burda, P.C., 2018. BioID Reveals Novel Proteins of the *Plasmodium* Parasitophorous Vacuole Membrane. *mSphere* 3.
- Schwab, J.C., Beckers, C.J., Joiner, K.A., 1994. The parasitophorous vacuole membrane surrounding intracellular *Toxoplasma gondii* functions as a molecular sieve. *Proceedings of the National Academy of Sciences of the United States of America* 91, 509-513.
- Schweighofer, A., Hirt, H., Meskiene, I., 2004. Plant PP2C phosphatases: emerging functions in stress signaling. *Trends in plant science* 9, 236-243.
- Sharma, A., Yogavel, M., Akhouri, R.R., Gill, J., Sharma, A., 2008. Crystal structure of soluble domain of malaria sporozoite protein UIS3 in complex with lipid. *The Journal of biological chemistry* 283, 24077-24088.
- Sherling, E.S., Knuepfer, E., Brzostowski, J.A., Miller, L.H., Blackman, M.J., van Ooij, C., 2017. The *Plasmodium falciparum* rhoptry protein RhopH3 plays essential roles in host cell invasion and nutrient uptake. *eLife* 6.
- Shi, Y., 2009. Serine/threonine phosphatases: mechanism through structure. *Cell* 139, 468-484.
- Silmon de Monerri, N.C., Flynn, H.R., Campos, M.G., Hackett, F., Koussis, K., Withers-Martinez, C., Skehel, J.M., Blackman, M.J., 2011. Global identification of multiple substrates for *Plasmodium falciparum* SUB1, an essential malarial processing protease. *Infection and immunity* 79, 1086-1097.
- Simmons, D., Woollett, G., Bergin-Cartwright, M., Kay, D., Scaife, J., 1987. A malaria protein exported into a new compartment within the host erythrocyte. *The EMBO journal* 6, 485-491.
- Sloves, P.J., Delhay, S., Mouveaux, T., Werkmeister, E., Slomianny, C., Hovasse, A., Dilezitoko Alayi, T., Callebaut, I., Gaji, R.Y., Schaeffer-Reiss, C., Van Dorsselaar, A.,

- Carruthers, V.B., Tomavo, S., 2012. Toxoplasma sortilin-like receptor regulates protein transport and is essential for apical secretory organelle biogenesis and host infection. *Cell host & microbe* 11, 515-527.
- Spielmann, T., Ferguson, D.J., Beck, H.P., 2003. etramps, a new Plasmodium falciparum gene family coding for developmentally regulated and highly charged membrane proteins located at the parasite-host cell interface. *Molecular biology of the cell* 14, 1529-1544.
- Spielmann, T., Gardiner, D.L., Beck, H.P., Trenholme, K.R., Kemp, D.J., 2006. Organization of ETRAMPs and EXP-1 at the parasite-host cell interface of malaria parasites. *Molecular microbiology* 59, 779-794.
- Spielmann, T., Gilberger, T.W., 2015. Critical Steps in Protein Export of Plasmodium falciparum Blood Stages. *Trends in parasitology* 31, 514-525.
- Spielmann, T., Montagna, G.N., Hecht, L., Matuschewski, K., 2012. Molecular make-up of the Plasmodium parasitophorous vacuolar membrane. *International journal of medical microbiology : IJMM* 302, 179-186.
- Straimer, J., Lee, M.C., Lee, A.H., Zeitler, B., Williams, A.E., Pearl, J.R., Zhang, L., Rebar, E.J., Gregory, P.D., Llinas, M., Urnov, F.D., Fidock, D.A., 2012. Site-specific genome editing in Plasmodium falciparum using engineered zinc-finger nucleases. *Nature methods* 9, 993-998.
- Struck, N.S., de Souza Dias, S., Langer, C., Marti, M., Pearce, J.A., Cowman, A.F., Gilberger, T.W., 2005. Re-defining the Golgi complex in Plasmodium falciparum using the novel Golgi marker PfGRASP. *Journal of cell science* 118, 5603-5613.
- Sturm, A., Amino, R., van de Sand, C., Regen, T., Retzlaff, S., Rennenberg, A., Krueger, A., Pollok, J.M., Menard, R., Heussler, V.T., 2006. Manipulation of host hepatocytes by the malaria parasite for delivery into liver sinusoids. *Science* 313, 1287-1290.
- Sun, P., Sleat, D.E., Lecocq, M., Hayman, A.R., Jadot, M., Lobel, P., 2008. Acid phosphatase 5 is responsible for removing the mannose 6-phosphate recognition marker from lysosomal proteins. *Proceedings of the National Academy of Sciences of the United States of America* 105, 16590-16595.
- Taylor, H.M., McRobert, L., Grainger, M., Sicard, A., Dluzewski, A.R., Hopp, C.S., Holder, A.A., Baker, D.A., 2010. The malaria parasite cyclic GMP-dependent protein kinase plays a central role in blood-stage schizogony. *Eukaryotic cell* 9, 37-45.
- Thomas, J.A., Tan, M.S.Y., Bisson, C., Borg, A., Umrekar, T.R., Hackett, F., Hale, V.L., Vizcay-Barrena, G., Fleck, R.A., Snijders, A.P., Saibil, H.R., Blackman, M.J., 2018. A protease cascade regulates release of the human malaria parasite Plasmodium falciparum from host red blood cells. *Nature microbiology* 3, 447-455.
- Thwing, J., Eisele, T.P., Steketee, R.W., 2011. Protective efficacy of malaria case management and intermittent preventive treatment for preventing malaria mortality in children: a systematic review for the Lives Saved Tool. *BMC public health* 11 Suppl 3, S14.
- Tonkin, C.J., Pearce, J.A., McFadden, G.I., Cowman, A.F., 2006a. Protein targeting to destinations of the secretory pathway in the malaria parasite Plasmodium falciparum. *Current opinion in microbiology* 9, 381-387.
- Tonkin, C.J., Struck, N.S., Mullin, K.A., Stimmler, L.M., McFadden, G.I., 2006b. Evidence for Golgi-independent transport from the early secretory pathway to the plastid in malaria parasites. *Molecular microbiology* 61, 614-630.
- Tonkin, M.L., Roques, M., Lamarque, M.H., Pugniere, M., Douguet, D., Crawford, J., Lebrun, M., Boulanger, M.J., 2011. Host cell invasion by apicomplexan parasites: insights from the co-structure of AMA1 with a RON2 peptide. *Science* 333, 463-467.
- Toure-Balde, A., Perlaza, B.L., Sauzet, J.P., Ndiaye, M., Aribot, G., Tall, A., Sokhna, C., Rogier, C., Corradin, G., Roussillon, C., Druilhe, P., 2009. Evidence for multiple B- and T-cell epitopes in Plasmodium falciparum liver-stage antigen 3. *Infection and immunity* 77, 1189-1196.
- Trager, W., Jensen, J.B., 1976. Human malaria parasites in continuous culture. *Science* 193, 673-675.
- Trampuz, A., Jereb, M., Muzlovic, I., Prabhu, R.M., 2003. Clinical review: Severe malaria. *Critical care* 7, 315-323.

- Trelka, D.P., Schneider, T.G., Reeder, J.C., Taraschi, T.F., 2000. Evidence for vesicle-mediated trafficking of parasite proteins to the host cell cytosol and erythrocyte surface membrane in *Plasmodium falciparum* infected erythrocytes. *Molecular and biochemical parasitology* 106, 131-145.
- Tribensky, A., Graf, A.W., Diehl, M., Fleck, W., Przyborski, J.M., 2017. Trafficking of PfExp1 to the parasitophorous vacuolar membrane of *Plasmodium falciparum* is independent of protein folding and the PTEX translocon. *Cellular microbiology* 19.
- Van Itallie, C.M., Tietgens, A.J., Aponte, A., Fredriksson, K., Fanning, A.S., Gucek, M., Anderson, J.M., 2014. Biotin ligase tagging identifies proteins proximal to E-cadherin, including lipoma preferred partner, a regulator of epithelial cell-cell and cell-substrate adhesion. *Journal of cell science* 127, 885-895.
- Vera, I.M., Beatty, W.L., Sinnis, P., Kim, K., 2011. Plasmodium protease ROM1 is important for proper formation of the parasitophorous vacuole. *PLoS pathogens* 7, e1002197.
- Vial, H.J., Eldin, P., Tielens, A.G., van Hellemond, J.J., 2003. Phospholipids in parasitic protozoa. *Molecular and biochemical parasitology* 126, 143-154.
- Volz, J.C., Yap, A., Sisquella, X., Thompson, J.K., Lim, N.T., Whitehead, L.W., Chen, L., Lampe, M., Tham, W.H., Wilson, D., Nebl, T., Marapana, D., Triglia, T., Wong, W., Rogers, K.L., Cowman, A.F., 2016. Essential Role of the PfRh5/PfRipr/CyRPA Complex during *Plasmodium falciparum* Invasion of Erythrocytes. *Cell host & microbe* 20, 60-71.
- Wagner, J.C., Platt, R.J., Goldfless, S.J., Zhang, F., Niles, J.C., 2014. Efficient CRISPR-Cas9-mediated genome editing in *Plasmodium falciparum*. *Nature methods* 11, 915-918.
- Waller, R.F., Reed, M.B., Cowman, A.F., McFadden, G.I., 2000. Protein trafficking to the plastid of *Plasmodium falciparum* is via the secretory pathway. *The EMBO journal* 19, 1794-1802.
- Ward, G.E., Miller, L.H., Dvorak, J.A., 1993. The origin of parasitophorous vacuole membrane lipids in malaria-infected erythrocytes. *Journal of cell science* 106 ( Pt 1), 237-248.
- Ward, P., Equinet, L., Packer, J., Doerig, C., 2004. Protein kinases of the human malaria parasite *Plasmodium falciparum*: the kinome of a divergent eukaryote. *BMC genomics* 5, 79.
- Wassmer, S.C., Taylor, T.E., Rathod, P.K., Mishra, S.K., Mohanty, S., Arevalo-Herrera, M., Duraisingh, M.T., Smith, J.D., 2015. Investigating the Pathogenesis of Severe Malaria: A Multidisciplinary and Cross-Geographical Approach. *The American journal of tropical medicine and hygiene* 93, 42-56.
- Weber, J.L., Lyon, J.A., Wolff, R.H., Hall, T., Lowell, G.H., Chulay, J.D., 1988. Primary structure of a *Plasmodium falciparum* malaria antigen located at the merozoite surface and within the parasitophorous vacuole. *The Journal of biological chemistry* 263, 11421-11425.
- Webster, W.A., McFadden, G.I., 2014. From the genome to the phenome: tools to understand the basic biology of *Plasmodium falciparum*. *The Journal of eukaryotic microbiology* 61, 655-671.
- Weed, R.I., Reed, C.F., Berg, G., 1963. Is hemoglobin an essential structural component of human erythrocyte membranes? *The Journal of clinical investigation* 42, 581-588.
- Weiss, G.E., Gilson, P.R., Taechalertpaisarn, T., Tham, W.H., de Jong, N.W., Harvey, K.L., Fowkes, F.J., Barlow, P.N., Rayner, J.C., Wright, G.J., Cowman, A.F., Crabb, B.S., 2015. Revealing the sequence and resulting cellular morphology of receptor-ligand interactions during *Plasmodium falciparum* invasion of erythrocytes. *PLoS pathogens* 11, e1004670.
- Wellems, T.E., Plowe, C.V., 2001. Chloroquine-resistant malaria. *The Journal of infectious diseases* 184, 770-776.
- WHO, 2016. World malaria report 2016. World Health Organization, Geneva.
- WHO, 2017. World malaria report 2017. World Health Organization, Geneva.
- Wickham, M.E., Rug, M., Ralph, S.A., Klonis, N., McFadden, G.I., Tilley, L., Cowman, A.F., 2001. Trafficking and assembly of the cytoadherence complex in *Plasmodium falciparum*-infected human erythrocytes. *The EMBO journal* 20, 5636-5649.

- Wilkes, J.M., Doerig, C., 2008. The protein-phosphatome of the human malaria parasite *Plasmodium falciparum*. *BMC genomics* 9, 412.
- Wisniewski, J.R., Zougman, A., Nagaraj, N., Mann, M., 2009. Universal sample preparation method for proteome analysis. *Nature methods* 6, 359-362.
- Wu, B., Rambow, J., Bock, S., Holm-Bertelsen, J., Wiechert, M., Soares, A.B., Spielmann, T., Beitz, E., 2015. Identity of a *Plasmodium lactate/H(+)* symporter structurally unrelated to human transporters. *Nature communications* 6, 6284.
- Wu, Y., Sifri, C.D., Lei, H.H., Su, X.Z., Wellems, T.E., 1995. Transfection of *Plasmodium falciparum* within human red blood cells. *Proceedings of the National Academy of Sciences of the United States of America* 92, 973-977.
- Xue, T., Wang, D., Zhang, S., Ehrling, J., Ni, F., Jakab, S., Zheng, C., Zhong, Y., 2008. Genome-wide and expression analysis of protein phosphatase 2C in rice and *Arabidopsis*. *BMC genomics* 9, 550.
- Yang, C., Arrizabalaga, G., 2017. The serine/threonine phosphatases of apicomplexan parasites. *Molecular microbiology* 106, 1-21.
- Yap, A., Azevedo, M.F., Gilson, P.R., Weiss, G.E., O'Neill, M.T., Wilson, D.W., Crabb, B.S., Cowman, A.F., 2014. Conditional expression of apical membrane antigen 1 in *Plasmodium falciparum* shows it is required for erythrocyte invasion by merozoites. *Cellular microbiology* 16, 642-656.
- Yeh, E., DeRisi, J.L., 2011. Chemical rescue of malaria parasites lacking an apicoplast defines organelle function in blood-stage *Plasmodium falciparum*. *PLoS biology* 9, e1001138.
- Yeoh, S., O'Donnell, R.A., Koussis, K., Dluzewski, A.R., Ansell, K.H., Osborne, S.A., Hackett, F., Withers-Martinez, C., Mitchell, G.H., Bannister, L.H., Bryans, J.S., Kettleborough, C.A., Blackman, M.J., 2007. Subcellular discharge of a serine protease mediates release of invasive malaria parasites from host erythrocytes. *Cell* 131, 1072-1083.
- Zhang, M., Fennell, C., Ranford-Cartwright, L., Sakthivel, R., Gueirard, P., Meister, S., Caspi, A., Doerig, C., Nussenzweig, R.S., Tuteja, R., Sullivan, W.J., Jr., Roos, D.S., Fontoura, B.M., Menard, R., Winzeler, E.A., Nussenzweig, V., 2010. The *Plasmodium* eukaryotic initiation factor-2 $\alpha$  kinase IK2 controls the latency of sporozoites in the mosquito salivary glands. *The Journal of experimental medicine* 207, 1465-1474.
- Zhang, M., Mishra, S., Sakthivel, R., Fontoura, B.M., Nussenzweig, V., 2016. UIS2: A Unique Phosphatase Required for the Development of *Plasmodium* Liver Stages. *PLoS pathogens* 12, e1005370.
- Zhang, M., Wang, C., Otto, T.D., Oberstaller, J., Liao, X., Adapa, S.R., Udenze, K., Bronner, I.F., Casandra, D., Mayho, M., Brown, J., Li, S., Swanson, J., Rayner, J.C., Jiang, R.H.Y., Adams, J.H., 2018. Uncovering the essential genes of the human malaria parasite *Plasmodium falciparum* by saturation mutagenesis. *Science* 360.
- Zhuo, S., Clemens, J.C., Stone, R.L., Dixon, J.E., 1994. Mutational analysis of a Ser/Thr phosphatase. Identification of residues important in phosphoesterase substrate binding and catalysis. *The Journal of biological chemistry* 269, 26234-26238.
- Zuegge, J., Ralph, S., Schmuker, M., McFadden, G.I., Schneider, G., 2001. Deciphering apicoplast targeting signals--feature extraction from nuclear-encoded precursors of *Plasmodium falciparum* apicoplast proteins. *Gene* 280, 19-26.

## Appendix

### Mass spectrometry results

The following tables show the results from the mass spectrometry run for SP-GFP-BirA\* pellet and supernatant fraction and 3D7 control cells pellet and supernatant fraction. All proteins that were identified by only one unique peptide (UP) are shaded in grey.

**Table xviii: Mass spectrometry results for the SP-GFP-BirA\* pellet fraction**

#	Accession	Description	# UP
1	PF3D7_1149000	antigen 332, DBL-like protein (Pf332)	40
2	PF3D7_0500800	mature parasite-infected erythrocyte surface antigen,erythrocyte membrane protein 2 (MESA)	26
3	PF3D7_1436300	translocon component PTEX150 (PTEX150)	23
4	PF3D7_1464600	phosphatase, putative	17
5	PF3D7_1222300	endoplasmic, putative (GRP94)	16
6	PF3D7_0917900	heat shock protein 70 (HSP70-2)	15
7	PF3D7_0929400	high molecular weight rhoptry protein 2 (RhopH2)	14
8	PF3D7_1016300	glycophorin binding protein (GBP)	13
9	PF3D7_0818900	heat shock protein 70 (HSP70)	10
10	PF3D7_1420700	surface protein P113 (P113)	10
11	PF3D7_0608800	ornithine aminotransferase (OAT)	10
12	PF3D7_0626800	pyruvate kinase (PyrK)	9
13	PF3D7_1024800	conserved Plasmodium protein, unknown function	8
14	PF3D7_1462800	glyceraldehyde-3-phosphate dehydrogenase (GAPDH)	7
15	PF3D7_1035300	glutamate-rich protein (GLURP)	7
16	PF3D7_0708400	heat shock protein 90 (HSP90)	7
17	PF3D7_0922200	S-adenosylmethionine synthetase (SAMS)	7
18	PF3D7_1311800	M1-family alanyl aminopeptidase (M1AAP)	7
19	PF3D7_1116800	heat shock protein 101, chaperone protein ClpB2 (HSP101)	7
20	PF3D7_0922500	phosphoglycerate kinase (PGK)	6
21	PF3D7_1345700	isocitrate dehydrogenase (NADP), mitochondrial precursor (IDH)	6
22	PF3D7_1471100	exported protein 2 (EXP2)	6
23	PF3D7_0930300	merozoite surface protein 1 (MSP1)	6
24	PF3D7_1312700	probable protein, unknown function	6
25	PF3D7_1129100	parasitophorous vacuolar protein 1 (PV1)	5
26	PF3D7_0730900	EMP1-trafficking protein (PTP4)	5
27	PF3D7_1452500	SNARE protein, putative (BET1)	5
28	PF3D7_0827900	protein disulfide isomerase (PDI8)	5
29	PF3D7_0207600	serine repeat antigen 5 (SERA5)	5
30	PF3D7_1015900	enolase (ENO)	5
31	PF3D7_0831700	heat shock protein 70 (HSP70-x)	4
32	PF3D7_1343000	phosphoethanolamine N-methyltransferase (PMT)	4
33	PF3D7_1016400	serine/threonine protein kinase, FIKK family (FIKK10.1)	4
34	PF3D7_0813900	40S ribosomal protein S16, putative	4
35	PF3D7_0507100	60S ribosomal protein L4 (RPL4)	4
36	PF3D7_1229400	macrophage migration inhibitory factor (MIF)	4
37	PF3D7_0818200	14-3-3 protein (14-3-3I)	4
38	PF3D7_1134000	heat shock protein 70 (HSP70-3)	4
39	PF3D7_1451100	elongation factor 2	4
40	PF3D7_0511800	inositol-3-phosphate synthase (INO1)	4

41	PF3D7_0617200	conserved Plasmodium protein, unknown function	4
42	PF3D7_1317100	DNA replication licensing factor MCM4 (MCM4)	4
43	PF3D7_1308200	carbamoyl phosphate synthetase (cpsSII)	4
44	PF3D7_0801000	Plasmodium exported protein (PHISTc), unknown function	4
45	PF3D7_1357000	elongation factor 1-alpha	4
46	PF3D7_1105400	40S ribosomal protein S4, putative	4
47	PF3D7_1201000	Plasmodium exported protein (PHISTb), unknown function	4
48	PF3D7_1334500	MSP7-like protein (MSRP6)	3
49	PF3D7_0619400	cell division cycle protein 48 homologue, putative	3
50	PF3D7_1108600	endoplasmic reticulum-resident calcium binding protein (ERC)	3
51	PF3D7_0320300	T-complex protein 1 epsilon subunit, putative	3
52	PF3D7_1224300	polyadenylate-binding protein, putative (PABP)	3
53	PF3D7_0524000	karyopherin beta (KASbeta)	3
54	PF3D7_0220000	liver stage antigen 3 (LSA3)	3
55	PF3D7_1117700	GTP-binding nuclear protein RAN/TC4 (RAN)	3
56	PF3D7_1130200	60S ribosomal protein P0 (PfP0)	3
57	PF3D7_0520900	S-adenosyl-L-homocysteine hydrolase (SAHH)	3
58	PF3D7_1229500	T-complex protein 1, gamma subunit, putative	3
59	PF3D7_0212300	peptide chain release factor subunit 1, putative	3
60	PF3D7_0920800	inosine-5'-monophosphate dehydrogenase	3
61	PF3D7_1029600	adenosine deaminase (ADA)	3
62	PF3D7_1105600	translocon component PTEX88 (PTEX88)	3
63	PF3D7_1129200	26S proteasome regulatory subunit RPN7, putative (RPN7)	3
64	PF3D7_0915400	6-phosphofructokinase (PFK9)	3
65	PF3D7_0826700	receptor for activated c kinase (RACK)	3
66	PF3D7_1468700	eukaryotic initiation factor 4A (eIF4A)	3
67	PF3D7_1212700	eukaryotic translation initiation factor 3 subunit 10, putative	2
68	PF3D7_0307200	60S ribosomal protein L7, putative	2
69	PF3D7_0532100	early transcribed membrane protein 5 (ETRAMP5)	2
70	PF3D7_1033200	early transcribed membrane protein 10.2 (ETRAMP10.2)	2
71	PF3D7_1353200	membrane associated histidine-rich protein (MAHRP2)	2
72	PF3D7_0814200	DNA/RNA-binding protein Alba 1 (ALBA1)	2
73	PF3D7_0905400	high molecular weight rhoptry protein 3 (RhopH3)	2
74	PF3D7_0823200	RNA-binding protein, putative	2
75	PF3D7_1008700	tubulin beta chain	2
76	PF3D7_0501200	parasite-infected erythrocyte surface protein (PIESP2)	2
77	PF3D7_1012400	hypoxanthine-guanine phosphoribosyltransferase (HGPRT)	2
78	PF3D7_0728000	eukaryotic translation initiation factor 2 alpha subunit, putative	2
79	PF3D7_1310500	conserved protein, unknown function	2
80	PF3D7_1108700	heat shock protein DnaJ homologue Pfj2	2
81	PF3D7_1345100	thioredoxin 2 (TRX2)	2
82	PF3D7_0302200	cytoadherence linked asexual protein 3.2 (CLAG3.2)	2
83	PF3D7_0302500	cytoadherence linked asexual protein 3.1 (CLAG3.1)	2
84	PF3D7_0918000	secreted acid phosphatase (GAP50)	2
85	PF3D7_1420400	glycine--tRNA ligase (GlyRS)	2
86	PF3D7_1322000	adenosine-diphosphatase, putative	2
87	PF3D7_1428300	proliferation-associated protein 2g4, putative	2
88	PF3D7_1107300	polyadenylate-binding protein-interacting protein 1, putative (PAIP1)	2
89	PF3D7_1011800	PRE-binding protein (PREBP)	2
90	PF3D7_1001400	alpha/beta hydrolase, putative	2

91	PF3D7_0315100	translation initiation factor 4E (eIF4E)	2
92	PF3D7_1444800	fructose-bisphosphate aldolase (FBPA)	2
93	PF3D7_1334200	chaperone binding protein, putative	2
94	PF3D7_1015800	ribonucleotide reductase small subunit, putative	2
95	PF3D7_1235700	ATP synthase subunit beta, mitochondrial	2
96	PF3D7_0810600	RNA helicase, putative	2
97	PF3D7_1409800	RNA binding protein Bruno, putative (HoBo)	2
98	PF3D7_1116700	cathepsin C, homolog, dipeptidyl aminopeptidase 1 (DPAP1)	2
99	PF3D7_1123500	conserved Plasmodium protein, unknown function	2
100	PF3D7_1424400	60S ribosomal protein L7-3, putative	2
101	PF3D7_0629200	DnaJ protein, putative	2
102	PF3D7_1311900	vacuolar ATP synthase subunit a (vapA)	2
103	PF3D7_1341900	vacuolar ATP synthase subunit d, putative	2
104	PF3D7_1426100	basic transcription factor 3b, putative	2
105	PF3D7_1302800	40S ribosomal protein S7, putative	2
106	PF3D7_0418200	golgi organization and biogenesis factor, putative	2
107	PF3D7_1136300	tudor staphylococcal nuclease (TSN)	2
108	PF3D7_1304500	small heat shock protein, putative	2
109	PF3D7_0501300	skeleton-binding protein 1 (SBP1)	2
110	PF3D7_1460700	60S ribosomal protein L27 (RPL27)	2
111	PF3D7_1226900	conserved Plasmodium protein, unknown function	2
112	PF3D7_0106300	calcium-transporting ATPase (ATP6)	2
113	PF3D7_1206200	eukaryotic translation initiation factor 3 subunit 8, putative	2
114	PF3D7_0922100	ubiquitin-like protein, putative	2
115	PF3D7_1424100	60S ribosomal protein L5, putative	2
116	PF3D7_0614500	60S ribosomal protein L19 (RPL19)	2
117	PF3D7_1109900	60S ribosomal protein L36 (RPL36)	2
118	PF3D7_1352500	thioredoxin-related protein, putative	2
119	PF3D7_1219100	clathrin heavy chain, putative	2
120	PF3D7_1340600	RNA lariat debranching enzyme, putative (DBR1)	2
121	PF3D7_0731600	acyl-CoA synthetase (ACS5)	2
122	PF3D7_1462300	conserved Plasmodium protein, unknown function	2
123	PF3D7_1013300	conserved Plasmodium protein, unknown function	2
124	PF3D7_1360800	falcilysin (FLN)	2
125	PF3D7_0912400	conserved Plasmodium protein, unknown function	2
126	PF3D7_1132200	TCP-1/cpn60 chaperonin family, putative	2
127	PF3D7_1104400	conserved protein, unknown function	2
128	PF3D7_1037300	ADP/ATP transporter on adenylate translocase (ADT)	2
129	PF3D7_0424600	Plasmodium exported protein (PHISTb), unknown function	2
130	PF3D7_1338200	60S ribosomal protein L6-2, putative	2
131	PF3D7_1135400	conserved Plasmodium protein, unknown function	2
132	PF3D7_1323100	60S ribosomal protein L6, putative	2
133	PF3D7_0622800	leucine--tRNA ligase, putative	2
134	PF3D7_0919000	nucleosome assembly protein (NAPS)	2
135	PF3D7_0935800	cytoadherence linked asexual protein 9 (CLAG9)	2
136	PF3D7_0721100	conserved Plasmodium protein, unknown function	2
137	PF3D7_0610400	histone H3 (H3)	1
138	PF3D7_1124600	ethanolamine kinase (EK)	1
139	PF3D7_0815300	FAD-dependent monooxygenase, putative	1
140	PF3D7_0505700	conserved Plasmodium membrane protein, unknown function	1

141	PF3D7_0305600	AP endonuclease (DNA-[apurinic or apyrimidinic site] lyase), putative	1
142	PF3D7_1320800	dihydrolipoyllysine-residue succinyltransferase component of 2-oxoglutarate dehydrogenase complex	1
143	PF3D7_1323400	60S ribosomal protein L23 (RPL23)	1
144	PF3D7_0815600	eukaryotic translation initiation factor, putative	1
145	PF3D7_0617900	histone H3 variant, putative (H3.3)	1
146	PF3D7_1239600	hydroxyethylthiazole kinase, putative	1
147	PF3D7_0532300	Plasmodium exported protein (PHISTb), unknown function	1
148	PF3D7_0503400	actin-depolymerizing factor 1 (ADF1)	1
149	PF3D7_0109400	tubulin-specific chaperone a, putative	1
150	PF3D7_1036900	conserved Plasmodium protein, unknown function	1
151	PF3D7_0625400	conserved Plasmodium protein, unknown function	1
152	PF3D7_0211800	asparagine--tRNA ligase (AsnRS)	1
153	PF3D7_0802000	glutamate dehydrogenase, putative (GDH3)	1
154	PF3D7_0516200	40S ribosomal protein S11	1
155	PF3D7_1404900	conserved Plasmodium protein, unknown function	1
156	PF3D7_0416800	small GTP-binding protein sar1 (SAR1)	1
157	PF3D7_0207800	serine repeat antigen 3 (SERA3)	1
158	PF3D7_0628200	protein kinase PK4 (PK4)	1
159	PF3D7_1243000	syntaxin, Qa-SNARE family (SYN16)	1
160	PF3D7_1447900	multidrug resistance protein 2 (heavy metal transport family) (MDR2)	1
161	PF3D7_1004000	60S ribosomal protein L13, putative	1
162	PF3D7_0709000	chloroquine resistance transporter (CRT)	1
163	PF3D7_0912500	conserved Plasmodium protein, unknown function	1
164	PF3D7_0406100	vacuolar ATP synthase subunit b	1
165	PF3D7_0831400	Plasmodium exported protein, unknown function	1
166	PF3D7_1349200	glutamate--tRNA ligase, putative	1
167	PF3D7_0102900	aspartate--tRNA ligase	1
168	PF3D7_1325100	phosphoribosylpyrophosphate synthetase	1
169	PF3D7_1228600	merozoite surface protein 9 (MSP9)	1
170	PF3D7_0933600	mitochondrial-processing peptidase subunit beta, putative (MAS1)	1
171	PF3D7_1441400	FACT complex subunit SSRP1, putative (FACT-S)	1
172	PF3D7_1104100	syntaxin, Qa-SNARE family (SYN13)	1
173	PF3D7_1246800	signal recognition particle receptor, beta subunit (SRPR-beta)	1
174	PF3D7_1008100	conserved Plasmodium protein, unknown function	1
175	PF3D7_0711500	regulator of chromosome condensation, putative	1
176	PF3D7_1231100	ras-related protein Rab-2 (RAB2)	1
177	PF3D7_0703500	erythrocyte membrane-associated antigen	1
178	PF3D7_1465900	40S ribosomal protein S3	1
179	PF3D7_1033400	haloacid dehalogenase-like hydrolase (HAD1)	1
180	PF3D7_1362200	RuvB-like helicase 3 (RUVB3)	1
181	PF3D7_1204300	eukaryotic translation initiation factor 5A (EIF5A)	1
182	PF3D7_0206900.2	merozoite surface protein 5 (MSP5)	1
183	PF3D7_0206900.1	merozoite surface protein 5 (MSP5)	1
184	PF3D7_0513600	deoxyribodipyrimidine photo-lyase, putative	1
185	PF3D7_1120100	phosphoglycerate mutase, putative (PGM1)	1
186	PF3D7_1423700	conserved Plasmodium protein, unknown function	1
187	PF3D7_1246200	actin I (ACT1)	1
188	PF3D7_1468100	conserved Plasmodium protein, unknown function	1
189	PF3D7_0936800	Plasmodium exported protein (PHISTc), unknown function	1

190	PF3D7_1124000	endoplasmic reticulum oxidoreductin, putative (ERO1)	1
191	PF3D7_1225800	ubiquitin-activating enzyme E1 (UBA1)	1
192	PF3D7_1105000	histone H4 (H4)	1
193	PF3D7_0606700	coatomer alpha subunit, putative	1
194	PF3D7_1470100	conserved Plasmodium protein, unknown function	1
195	PF3D7_1355100	DNA replication licensing factor MCM6 (MCM6)	1
196	PF3D7_0822600	protein transport protein SEC23 (SEC23)	1
197	PF3D7_1251200	coronin	1
198	PF3D7_1144000	40S ribosomal protein S21 (RPS21)	1
199	PF3D7_0317600	40S ribosomal protein S11, putative (RPS11)	1
200	PF3D7_1023900	chromodomain-helicase-DNA-binding protein 1 homolog, putative (CHD1)	1
201	PF3D7_0914700	transporter, putative	1
202	PF3D7_1426000	60S ribosomal protein L21 (RPL21)	1
203	PF3D7_0202400	conserved Plasmodium protein, unknown function	1
204	PF3D7_0207900	serine repeat antigen 2 (SERA2)	1
205	PF3D7_1309100	60S ribosomal protein L24, putative	1
206	PF3D7_1236100	clustered-asparagine-rich protein	1
207	PF3D7_0627500	protein DJ-1 (DJ1)	1
208	PF3D7_1407100	fibrillarin, putative (NOP1)	1
209	PF3D7_0618000	conserved Plasmodium membrane protein, unknown function	1
210	PF3D7_1027300	peroxiredoxin (nPrx)	1
211	PF3D7_0716300	conserved Plasmodium protein, unknown function	1
212	PF3D7_1426200	arginine methyltransferase 1 (PRMT1)	1
213	PF3D7_1461900	valine--tRNA ligase, putative	1
214	PF3D7_0935900	ring-exported protein 1 (REX1)	1
215	PF3D7_1129000	spermidine synthase (SpdSyn)	1
216	PF3D7_1350100	lysine--tRNA ligase (KRS1)	1
217	PF3D7_1308800	tyrosine recombinase (INT)	1
218	PF3D7_1354500	adenylosuccinate synthetase (ADSS)	1
219	PF3D7_1002000	Plasmodium exported protein (hyp2), unknown function	1
220	PF3D7_1419000	conserved Plasmodium protein, unknown function	1
221	PF3D7_1015200.3	cysteine--tRNA ligase, putative (CysRS)	1
222	PF3D7_1015200.2	cysteine--tRNA ligase, putative (CysRS)	1
223	PF3D7_1015200.1	cysteine--tRNA ligase, putative (CysRS)	1
224	PF3D7_1007900	eukaryotic translation initiation factor 3 subunit 7, putative	1
225	PF3D7_0529000	conserved Plasmodium protein, unknown function	1
226	PF3D7_0532400	lysine-rich membrane-associated PHISTb protein (LyMP)	1
227	PF3D7_0904800	replication protein A1, small fragment (RPA1)	1
228	PF3D7_1474600	conserved Plasmodium membrane protein, unknown function	1
229	PF3D7_0513800	ras-related protein Rab-1A (RAB1a)	1
230	PF3D7_0512600	ras-related protein Rab-1B (RAB1b)	1
231	PF3D7_1144900	ras-related protein Rab-6 (RAB6)	1
232	PF3D7_0303000	N-ethylmaleimide-sensitive fusion protein (NSF)	1
233	PF3D7_0202000	knob-associated histidine-rich protein (KAHRP)	1
234	PF3D7_0217900	conserved Plasmodium protein, unknown function	1
235	PF3D7_0308500	activator of Hsp90 ATPase, putative	1
236	PF3D7_1408600	40S ribosomal protein S8e, putative	1
237	PF3D7_1002900	conserved Plasmodium protein, unknown function	1
238	PF3D7_1366900	conserved Plasmodium protein, unknown function	1
239	PF3D7_1027800	60S ribosomal protein L3 (RPL3)	1

240	PF3D7_1316600	choline-phosphate cytidyltransferase (CCT)	1
241	PF3D7_0807300	ras-related protein Rab-18 (RAB18)	1
242	PF3D7_1030500	26S proteasome regulatory subunit RPN9, putative (RPN9)	1
243	PF3D7_0402400	Plasmodium exported protein, unknown function (GEXP18)	1
244	PF3D7_0321100	conserved Plasmodium protein, unknown function	1
245	PF3D7_1410600	eukaryotic translation initiation factor 2 gamma subunit, putative	1
246	PF3D7_0802200	1-cys peroxiredoxin (1-CysPxn)	1
247	PF3D7_1121600	circumsporozoite-related antigen, exported protein 1 (EXP1)	1
248	PF3D7_0812400	karyopherin alpha (KARalpha)	1
249	PF3D7_1133800	RNA (uracil-5-)methyltransferase, putative	1
250	PF3D7_0925900	conserved Plasmodium protein, unknown function	1
251	PF3D7_1450400	zinc finger protein, putative	1
252	PF3D7_1416900	prefoldin subunit 2, putative	1
253	PF3D7_1234800	splicing factor 3B subunit 3, putative (SF3B3)	1
254	PF3D7_0903700	alpha tubulin 1	1
255	PF3D7_1130400	26S protease regulatory subunit 6a, putative (RPT5)	1
256	PF3D7_1358800	40S ribosomal protein S15 (RPS15)	1
257	PF3D7_1215100	conserved Plasmodium protein, unknown function	1
258	PF3D7_1411900	p1/s1 nuclease, putative	1
259	PF3D7_1318800	translocation protein SEC63 (SEC63)	1
260	PF3D7_1253400	acyl-CoA synthetase (ACS3)	1
261	PF3D7_1479000	acyl-CoA synthetase (ACS1a)	1
262	PF3D7_1372400	acyl-CoA synthetase (ACS4)	1
263	PF3D7_0401900	acyl-CoA synthetase (ACS6)	1
264	PF3D7_1421200	40S ribosomal protein S25 (RPS25)	1
265	PF3D7_0313000	conserved Plasmodium protein, unknown function	1
266	PF3D7_1417800	DNA replication licensing factor MCM2 (MCM2)	1
267	PF3D7_1441200	60S ribosomal protein L1, putative	1
268	PF3D7_0401800	Plasmodium exported protein (PHISTb), unknown function (PfD80)	1
269	PF3D7_1237700	conserved Plasmodium membrane protein, unknown function	1
270	PF3D7_1112900	conserved Plasmodium protein, unknown function	1
271	PF3D7_1243900	double C2-like domain-containing protein (DOC2)	1
272	PF3D7_1142600	60S ribosomal protein L35ae, putative	1
273	PF3D7_1021900	conserved Plasmodium protein (10b antigen), unknown function	1
274	PF3D7_0308200	TCP-1/cpn60 chaperonin family, putative	1
275	PF3D7_0516900	60S ribosomal protein L2 (RPL2)	1
276	PF3D7_1122900	dynein heavy chain, putative	1
277	PF3D7_0525100	acyl-CoA synthetase (ACS10)	1
278	PF3D7_0520000	40S ribosomal protein S9, putative	1
279	PF3D7_1034900	methionine--tRNA ligase, putative	1
280	PF3D7_1003500	40S ribosomal protein S20e, putative	1
281	PF3D7_1105100	histone H2B (H2B)	1
282	PF3D7_1104000	phenylalanyl-tRNA synthetase beta chain, putative	1
283	PF3D7_0525800	inner membrane complex protein 1g, putative (IMC1g)	1
284	PF3D7_1211400	heat shock protein DNAJ homologue Pfj4 (PfJ4)	1
285	PF3D7_0913200	elongation factor 1-beta (EF-1beta)	1
286	PF3D7_0618300	60S ribosomal protein L27a, putative	1
287	PF3D7_0112000	TatD-like deoxyribonuclease, putative	1
288	PF3D7_0422400	40S ribosomal protein S19 (RPS19)	1
289	PF3D7_1344200	heat shock protein 110, putative (HSP110)	1
290	PF3D7_1119900	conserved Plasmodium protein, unknown function	1

291	PF3D7_1320600	ras-related protein Rab-11A (RAB11a)	1
292	PF3D7_1456800	V-type H(+)-translocating pyrophosphatase, putative (VP1)	1
293	PF3D7_1116200.1	pyridoxine biosynthesis protein PDX2 (PDX2)	1
294	PF3D7_1236000	vesicle transport v-SNARE protein VT11, putative	1
295	PF3D7_0601900	conserved Plasmodium protein, unknown function	1
296	PF3D7_1216200	glycerol-3-phosphate dehydrogenase, putative	1
297	PF3D7_0617800	histone H2A (H2A)	1
298	PF3D7_0320900	histone H2A variant, putative (H2A.Z)	1
299	PF3D7_0320700	signal peptidase complex subunit 2, putative (SPC2)	1
300	PF3D7_1454700	6-phosphogluconate dehydrogenase, decarboxylating, putative	1
301	PF3D7_0713700	conserved Plasmodium protein, unknown function	1
302	PF3D7_1408000	plasmepsin II	1
303	PF3D7_1332900	isoleucine--tRNA ligase, putative	1
304	PF3D7_0523100	mitochondrial processing peptidase alpha subunit, putative	1
305	PF3D7_1324700	SNARE protein, putative (YKT6.2)	1
306	PF3D7_0719700	40S ribosomal protein S10, putative	1
307	PF3D7_0727800	cation transporting ATPase, putative	1
308	PF3D7_1211700	DNA replication licensing factor MCM5, putative (MCM5)	1
309	PF3D7_1466800	conserved Plasmodium protein, unknown function	1
310	PF3D7_1118200	heat shock protein 90, putative	1
311	PF3D7_1409400	conserved Plasmodium membrane protein, unknown function	1
312	PF3D7_0621200	pyridoxine biosynthesis protein PDX1 (PDX1)	1
313	PF3D7_1364200	conserved Plasmodium protein, unknown function	1
314	PF3D7_1331800	60S ribosomal protein L23, putative	1
315	PF3D7_0814000	60S ribosomal protein L13-2, putative	1
316	PF3D7_1252100	rhoptry neck protein 3 (RON3)	1
317	PF3D7_0807500	proteasome subunit alpha type-6, putative	1
318	PF3D7_0515700	glideosome-associated protein 40, putative (GAP40)	1
319	PF3D7_1456700	conserved Plasmodium protein, unknown function	1
320	PF3D7_1342600	myosin A (MyoA)	1
321	PF3D7_1211800	polyubiquitin (PfpUB)	1
322	PF3D7_1365900	ubiquitin-60S ribosomal protein L40	1
323	PF3D7_1138500	protein phosphatase 2C (PP2C)	1
324	PF3D7_0209800	ATP-dependent RNA helicase UAP56 (UAP56)	1
325	PF3D7_0217100	ATP synthase F1, alpha subunit	1
326	PF3D7_1402300	26S proteasome regulatory subunit RPN6 (RPN6)	1
327	PF3D7_0305500	conserved Plasmodium protein, unknown function	1
328	PF3D7_0109800	phenylalanine--tRNA ligase, putative	1
329	PF3D7_0721600	40S ribosomal protein S5, putative	1
330	PF3D7_1312000	malonyl CoA-acyl carrier protein transacylase precursor (MCAT)	1
331	PF3D7_1012600	GMP synthetase (GMPS)	1
332	PF3D7_1012800	conserved Plasmodium protein, unknown function	1
333	PF3D7_0209400	conserved protein, unknown function	1
334	PF3D7_0301700	Plasmodium exported protein, unknown function	1
335	PF3D7_1320000	rhoptry protein 2, putative (PRP2)	1
336	PF3D7_0214000	T-complex protein 1, putative	1
337	PF3D7_1405100	GTPase-activating protein, putative	1
338	PF3D7_1340700	ras-related protein Rab-11B (RAB11b)	1
339	PF3D7_0314400	serine/threonine protein phosphatase 6, putative (PPP6)	1
340	PF3D7_0722400	GTP-binding protein, putative	1
341	PF3D7_0409000	conserved Plasmodium protein, unknown function	1

342	PF3D7_0216400	vacuolar protein sorting-associated protein 45, putative (VPS45)	1
343	PF3D7_0105800	conserved Plasmodium protein, unknown function	1
344	PF3D7_0904300	conserved protein, unknown function	1
345	PF3D7_0714000	histone H2B variant (H2B.Z)	1

**Table xix: Mass spectrometry results for the 3D7 pellet fraction**

#	Accession	Description	# UP
1	PF3D7_0818900	heat shock protein 70 (HSP70)	14
2	PF3D7_0608800	ornithine aminotransferase (OAT)	12
3	PF3D7_0917900	heat shock protein 70 (HSP70-2)	11
4	PF3D7_1345700	isocitrate dehydrogenase (NADP), mitochondrial precursor (IDH)	10
5	PF3D7_1462800	glyceraldehyde-3-phosphate dehydrogenase (GAPDH)	9
6	PF3D7_0929400	high molecular weight rhostry protein 2 (RhopH2)	9
7	PF3D7_1311800	M1-family alanyl aminopeptidase (M1AAP)	9
8	PF3D7_1222300	endoplasmic, putative (GRP94)	9
9	PF3D7_1134000	heat shock protein 70 (HSP70-3)	8
10	PF3D7_0626800	pyruvate kinase (PyrK)	7
11	PF3D7_1015900	enolase (ENO)	7
12	PF3D7_0922200	S-adenosylmethionine synthetase (SAMS)	6
13	PF3D7_0500800	mature parasite-infected erythrocyte surface antigen, erythrocyte membrane protein 2 (MESA)	5
14	PF3D7_1357000	elongation factor 1-alpha	5
15	PF3D7_0922500	phosphoglycerate kinase (PGK)	5
16	PF3D7_0525800	inner membrane complex protein 1g, putative (IMC1g)	5
17	PF3D7_1451100	elongation factor 2	5
18	PF3D7_0617200	conserved Plasmodium protein, unknown function	5
19	PF3D7_1023900	chromodomain-helicase-DNA-binding protein 1 homolog, putative (CHD1)	5
20	PF3D7_0831700	heat shock protein 70 (HSP70-x)	4
21	PF3D7_1016300	glycophorin binding protein (GBP)	4
22	PF3D7_0905400	high molecular weight rhostry protein 3 (RhopH3)	4
23	PF3D7_0813900	40S ribosomal protein S16, putative	4
24	PF3D7_0818200	14-3-3 protein (14-3-3I)	4
25	PF3D7_0520900	S-adenosyl-L-homocysteine hydrolase (SAHH)	4
26	PF3D7_0826700	receptor for activated c kinase (RACK)	4
27	PF3D7_0621200	pyridoxine biosynthesis protein PDX1 (PDX1)	4
28	PF3D7_1343000	phosphoethanolamine N-methyltransferase (PMT)	4
29	PF3D7_1444800	fructose-bisphosphate aldolase (FBPA)	4
30	PF3D7_0211800	asparagine--tRNA ligase (AsnRS)	4
31	PF3D7_0827900	protein disulfide isomerase (PDI8)	3
32	PF3D7_1211400	heat shock protein DNAJ homologue Pfj4 (PfJ4)	3
33	PF3D7_0619400	cell division cycle protein 48 homologue, putative	3
34	PF3D7_0823200	RNA-binding protein, putative	3
35	PF3D7_1012400	hypoxanthine-guanine phosphoribosyltransferase (HGPRT)	3
36	PF3D7_1115800	conserved Plasmodium protein, unknown function	3
37	PF3D7_0207600	serine repeat antigen 5 (SERA5)	3
38	PF3D7_0810600	RNA helicase, putative	3
39	PF3D7_1224300	polyadenylate-binding protein, putative (PABP)	3
40	PF3D7_1229400	macrophage migration inhibitory factor (MIF)	3
41	PF3D7_0708400	heat shock protein 90 (HSP90)	3
42	PF3D7_1468700	eukaryotic initiation factor 4A (eIF4A)	3

43	PF3D7_1317100	DNA replication licensing factor MCM4 (MCM4)	3
44	PF3D7_1251200	coronin	3
45	PF3D7_1014900	conserved Plasmodium protein, unknown function	3
46	PF3D7_1308200	carbamoyl phosphate synthetase (cpsSII)	3
47	PF3D7_0106300	calcium-transporting ATPase (ATP6)	3
48	PF3D7_1235700	ATP synthase subunit beta, mitochondrial	3
49	PF3D7_1246200	actin I (ACT1)	3
50	PF3D7_1424400	60S ribosomal protein L7-3, putative	3
51	PF3D7_1105400	40S ribosomal protein S4, putative	3
52	PF3D7_1367000	suppressor of kinetochore protein 1, putative (SKP1)	2
53	PF3D7_1117700	GTP-binding nuclear protein RAN/TC4 (RAN)	2
54	PF3D7_0814200	DNA/RNA-binding protein Alba 1 (ALBA1)	2
55	PF3D7_1456800	V-type H(+)-translocating pyrophosphatase, putative (VP1)	2
56	PF3D7_1341900	vacuolar ATP synthase subunit d, putative	2
57	PF3D7_0106100	vacuolar ATP synthase subunit c, putative	2
58	PF3D7_1008700	tubulin beta chain	2
59	PF3D7_0315100	translation initiation factor 4E (eIF4E)	2
60	PF3D7_0320300	T-complex protein 1 epsilon subunit, putative	2
61	PF3D7_0112000	TatD-like deoxyribonuclease, putative	2
62	PF3D7_0501300	skeleton-binding protein 1 (SBP1)	2
63	PF3D7_1359400	rRNA associated RNA binding protein, putative	2
64	PF3D7_0711500	regulator of chromosome condensation, putative	2
65	PF3D7_0512600	ras-related protein Rab-1B (RAB1b)	2
66	PF3D7_0807300	ras-related protein Rab-18 (RAB18)	2
67	PF3D7_1116200.1	pyridoxine biosynthesis protein PDX2 (PDX2)	2
68	PF3D7_1428300	proliferation-associated protein 2g4, putative	2
69	PF3D7_1361900	proliferating cell nuclear antigen (PCNA)	2
70	PF3D7_0831400	Plasmodium exported protein, unknown function	2
71	PF3D7_1325100	phosphoribosylpyrophosphate synthetase	2
72	PF3D7_1211900	non-SERCA-type Ca <sup>2+</sup> -transporting P-ATPase (ATP4)	2
73	PF3D7_0930300	merozoite surface protein 1 (MSP1)	2
74	PF3D7_0622800	leucine--tRNA ligase, putative	2
75	PF3D7_0524000	karyopherin beta (KASbeta)	2
76	PF3D7_0511800	inositol-3-phosphate synthase (INO1)	2
77	PF3D7_0920800	inosine-5'-monophosphate dehydrogenase	2
78	PF3D7_1003600	inner membrane complex protein 1c, putative (IMC1c)	2
79	PF3D7_0320900	histone H2A variant, putative (H2A.Z)	2
80	PF3D7_1033400	haloacid dehalogenase-like hydrolase (HAD1)	2
81	PF3D7_0722400	GTP-binding protein, putative	2
82	PF3D7_1349200	glutamate--tRNA ligase, putative	2
83	PF3D7_1124600	ethanolamine kinase (EK)	2
84	PF3D7_1320800	dihydrolipoyllysine-residue succinyltransferase component of 2-oxoglutarate dehydrogenase complex	2
85	PF3D7_1364200	conserved Plasmodium protein, unknown function	2
86	PF3D7_1248700	conserved Plasmodium protein, unknown function	2
87	PF3D7_0706500	conserved Plasmodium protein, unknown function	2
88	PF3D7_1237700	conserved Plasmodium membrane protein, unknown function	2
89	PF3D7_1426200	arginine methyltransferase 1 (PRMT1)	2
90	PF3D7_1029600	adenosine deaminase (ADA)	2
91	PF3D7_0308500	activator of Hsp90 ATPase, putative	2
92	PF3D7_1130200	60S ribosomal protein P0 (PfP0)	2

93	PF3D7_1460700	60S ribosomal protein L27 (RPL27)	2
94	PF3D7_0614500	60S ribosomal protein L19 (RPL19)	2
95	PF3D7_1441200	60S ribosomal protein L1, putative	2
96	PF3D7_0721600	40S ribosomal protein S5, putative	2
97	PF3D7_1465900	40S ribosomal protein S3	2
98	PF3D7_1421200	40S ribosomal protein S25 (RPS25)	2
99	PF3D7_0422400	40S ribosomal protein S19 (RPS19)	2
100	PF3D7_0516200	40S ribosomal protein S11	2
101	PF3D7_1015800	ribonucleotide reductase small subunit, putative	1
102	PF3D7_0617900	histone H3 variant, putative (H3.3)	1
103	PF3D7_0610400	histone H3 (H3)	1
104	PF3D7_0918000	secreted acid phosphatase (GAP50)	1
105	PF3D7_0823300	histone acetyltransferase GCN5 (GCN5)	1
106	PF3D7_0815600	eukaryotic translation initiation factor, putative	1
107	PF3D7_0532100	early transcribed membrane protein 5 (ETRAMP5)	1
108	PF3D7_0806800	vacuolar proton translocating ATPase subunit A, putative	1
109	PF3D7_0406100	vacuolar ATP synthase subunit b	1
110	PF3D7_1225800	ubiquitin-activating enzyme E1 (UBA1)	1
111	PF3D7_1365900	ubiquitin-60S ribosomal protein L40	1
112	PF3D7_0516700	ubiquitin carboxyl-terminal hydrolase 2, putative	1
113	PF3D7_1349300	tyrosine kinase-like protein (TKL3)	1
114	PF3D7_0109400	tubulin-specific chaperone a, putative	1
115	PF3D7_1318800	translocation protein SEC63 (SEC63)	1
116	PF3D7_1132200	TCP-1/cpn60 chaperonin family, putative	1
117	PF3D7_0306800	T-complex protein beta subunit, putative	1
118	PF3D7_1129000	spermidine synthase (SpdSyn)	1
119	PF3D7_1304500	small heat shock protein, putative	1
120	PF3D7_1457000	signal peptide peptidase (SPP)	1
121	PF3D7_0320700	signal peptidase complex subunit 2, putative (SPC2)	1
122	PF3D7_1310700	RNA-binding protein, putative	1
123	PF3D7_0605100	RNA-binding protein, putative	1
124	PF3D7_0629400	RNA-binding protein, putative	1
125	PF3D7_0916700	RNA-binding protein musashi, putative (HoMu)	1
126	PF3D7_1340600	RNA lariat debranching enzyme, putative (DBR1)	1
127	PF3D7_1409800	RNA binding protein Bruno, putative (HoBo)	1
128	PF3D7_1133800	RNA (uracil-5-)methyltransferase, putative	1
129	PF3D7_1405600	ribonucleotide reductase small subunit (RNR)	1
130	PF3D7_1410400	rho-try-associated protein 1 (RAP1)	1
131	PF3D7_0722200	rho-try-associated leucine zipper-like protein 1 (RALP1)	1
132	PF3D7_0613300	rho-try protein (ROP14)	1
133	PF3D7_1144900	ras-related protein Rab-6 (RAB6)	1
134	PF3D7_0513800	ras-related protein Rab-1A (RAB1a)	1
135	PF3D7_1320600	ras-related protein Rab-11A (RAB11a)	1
136	PF3D7_1135100	protein phosphatase 2C, putative	1
137	PF3D7_0321400	protein kinase, putative	1
138	PF3D7_0627500	protein DJ-1 (DJ1)	1
139	PF3D7_1474000	probable protein, unknown function	1
140	PF3D7_1416900	prefoldin subunit 2, putative	1
141	PF3D7_1211800	polyubiquitin (PfpUB)	1
142	PF3D7_1107300	polyadenylate-binding protein-interacting protein 1, putative (PAIP1)	1
143	PF3D7_1353100	Plasmodium exported protein, unknown function	1

144	PF3D7_0936800	Plasmodium exported protein (PHISTc), unknown function	1
145	PF3D7_0801000	Plasmodium exported protein (PHISTc), unknown function	1
146	PF3D7_0532300	Plasmodium exported protein (PHISTb), unknown function	1
147	PF3D7_0424600	Plasmodium exported protein (PHISTb), unknown function	1
148	PF3D7_1120100	phosphoglycerate mutase, putative (PGM1)	1
149	PF3D7_0109800	phenylalanine--tRNA ligase, putative	1
150	PF3D7_0212300	peptide chain release factor subunit 1, putative	1
151	PF3D7_0919000	nucleosome assembly protein (NAPS)	1
152	PF3D7_1244100	N-alpha-acetyltransferase 15, NatA auxiliary subunit, putative	1
153	PF3D7_1342600	myosin A (MyoA)	1
154	PF3D7_1031200	MORN repeat-containing protein 1 (MORN1)	1
155	PF3D7_0702200	lysophospholipase, putative	1
156	PF3D7_1350100	lysine--tRNA ligase (KRS1)	1
157	PF3D7_0202000	knob-associated histidine-rich protein (KAHRP)	1
158	PF3D7_1239600	hydroxyethylthiazole kinase, putative	1
159	PF3D7_1105000	histone H4 (H4)	1
160	PF3D7_0714000	histone H2B variant (H2B.Z)	1
161	PF3D7_1105100	histone H2B (H2B)	1
162	PF3D7_0617800	histone H2A (H2A)	1
163	PF3D7_1118200	heat shock protein 90, putative	1
164	PF3D7_0409400	heat shock protein 40 (DnaJ)	1
165	PF3D7_0708800	heat shock protein 110 (HSP110c)	1
166	PF3D7_1116800	heat shock protein 101, chaperone protein ClpB2 (HSP101)	1
167	PF3D7_1420400	glycine--tRNA ligase (GlyRS)	1
168	PF3D7_1132900	glycine cleavage system H protein (GCVH)	1
169	PF3D7_0423500	glideosome associated protein with multiple membrane spans 2 (GAPM2)	1
170	PF3D7_1441400	FACT complex subunit SSRP1, putative (FACT-S)	1
171	PF3D7_1204300	eukaryotic translation initiation factor 5A (EIF5A)	1
172	PF3D7_0528200	eukaryotic translation initiation factor 3, subunit 6, putative	1
173	PF3D7_0612100	eukaryotic translation initiation factor 3 subunit L, putative	1
174	PF3D7_1007900	eukaryotic translation initiation factor 3 subunit 7, putative	1
175	PF3D7_1212700	eukaryotic translation initiation factor 3 subunit 10, putative	1
176	PF3D7_0728000	eukaryotic translation initiation factor 2 alpha subunit, putative	1
177	PF3D7_0102500	erythrocyte binding antigen-181 (EBA181)	1
178	PF3D7_0730900	EMP1-trafficking protein (PTP4)	1
179	PF3D7_1338300	elongation factor 1-gamma, putative	1
180	PF3D7_0202500	early transcribed membrane protein 2 (ETRAMP2)	1
181	PF3D7_1033200	early transcribed membrane protein 10.2 (ETRAMP10.2)	1
182	PF3D7_1426300	dynein-associated protein, putative	1
183	PF3D7_1347500	DNA/RNA-binding protein Alba 4 (ALBA4)	1
184	PF3D7_1227100	DNA helicase 60 (DH60)	1
185	PF3D7_1032500	DER1-like protein, putative (Der1-2)	1
186	PF3D7_1127100	deoxyuridine 5'-triphosphate nucleotidohydrolase (dUTPase)	1
187	PF3D7_0935800	cytoadherence linked asexual protein 9 (CLAG9)	1
188	PF3D7_0302500	cytoadherence linked asexual protein 3.1 (CLAG3.1)	1
189	PF3D7_1409900	cytidine diphosphate-diacylglycerol synthase (CDS)	1
190	PF3D7_1439000	copper transporter	1
191	PF3D7_1104400	conserved protein, unknown function	1
192	PF3D7_1402100	conserved Plasmodium protein, unknown function	1
193	PF3D7_1470100	conserved Plasmodium protein, unknown function	1

194	PF3D7_1445700	conserved Plasmodium protein, unknown function	1
195	PF3D7_1341500	conserved Plasmodium protein, unknown function	1
196	PF3D7_1336000	conserved Plasmodium protein, unknown function	1
197	PF3D7_1105800	conserved Plasmodium protein, unknown function	1
198	PF3D7_1125900	conserved Plasmodium protein, unknown function	1
199	PF3D7_1008100	conserved Plasmodium protein, unknown function	1
200	PF3D7_1004500	conserved Plasmodium protein, unknown function	1
201	PF3D7_1036900	conserved Plasmodium protein, unknown function	1
202	PF3D7_0925900	conserved Plasmodium protein, unknown function	1
203	PF3D7_0819600	conserved Plasmodium protein, unknown function	1
204	PF3D7_0813300	conserved Plasmodium protein, unknown function	1
205	PF3D7_0529000	conserved Plasmodium protein, unknown function	1
206	PF3D7_0415700	conserved Plasmodium protein, unknown function	1
207	PF3D7_0313000	conserved Plasmodium protein, unknown function	1
208	PF3D7_0305500	conserved Plasmodium protein, unknown function	1
209	PF3D7_0212100	conserved Plasmodium protein, unknown function	1
210	PF3D7_1409400	conserved Plasmodium membrane protein, unknown function	1
211	PF3D7_0618000	conserved Plasmodium membrane protein, unknown function	1
212	PF3D7_1236100	clustered-asparagine-rich protein	1
213	PF3D7_0608700	chaperone, putative	1
214	PF3D7_1446600	centrin-2 (CEN2)	1
215	PF3D7_1116700	cathepsin C, homolog,dipeptidyl aminopeptidase 1 (DPAP1)	1
216	PF3D7_1426100	basic transcription factor 3b, putative	1
217	PF3D7_0217100	ATP synthase F1, alpha subunit	1
218	PF3D7_1110400	asparagine-rich antigen	1
219	PF3D7_0528100	AP-1 complex subunit beta, putative	1
220	PF3D7_1149000	antigen 332, DBL-like protein (Pf332)	1
221	PF3D7_1454400	aminopeptidase P (APP)	1
222	PF3D7_0525100	acyl-CoA synthetase (ACS10)	1
223	PF3D7_0915400	6-phosphofructokinase (PFK9)	1
224	PF3D7_0307200	60S ribosomal protein L7, putative	1
225	PF3D7_1338200	60S ribosomal protein L6-2, putative	1
226	PF3D7_1424100	60S ribosomal protein L5, putative	1
227	PF3D7_1027800	60S ribosomal protein L3 (RPL3)	1
228	PF3D7_1460300	60S ribosomal protein L29, putative	1
229	PF3D7_1309100	60S ribosomal protein L24, putative	1
230	PF3D7_1323400	60S ribosomal protein L23 (RPL23)	1
231	PF3D7_1431700	60S ribosomal protein L14, putative	1
232	PF3D7_1004000	60S ribosomal protein L13, putative	1
233	PF3D7_0719600	60S ribosomal protein L11a, putative	1
234	PF3D7_1447000	40S ribosomal protein S5	1
235	PF3D7_0322900	40S ribosomal protein S3A, putative	1
236	PF3D7_1461300	40S ribosomal protein S28e, putative	1
237	PF3D7_1308300	40S ribosomal protein S27 (RPS27)	1
238	PF3D7_1003500	40S ribosomal protein S20e, putative	1
239	PF3D7_1317800	40S ribosomal protein S19 (RPS19)	1
240	PF3D7_0317600	40S ribosomal protein S11, putative (RPS11)	1
241	PF3D7_0719700	40S ribosomal protein S10, putative	1
242	PF3D7_1130400	26S protease regulatory subunit 6a, putative (RPT5)	1

**Table xx: Mass spectrometry results for the SP-GFP-BirA\* supernatant fraction**

#	Accession	Description	# UP
1	PF3D7_1016300	glycophorin binding protein (GBP)	17
2	PF3D7_0801000	Plasmodium exported protein (PHISTc), unknown function	17
3	PF3D7_0500800	mature parasite-infected erythrocyte surface antigen, erythrocyte membrane protein 2 (MESA)	10
4	PF3D7_0730900	EMP1-trafficking protein (PTP4)	8
5	PF3D7_1201000	Plasmodium exported protein (PHISTb), unknown function	7
6	PF3D7_1357000	elongation factor 1-alpha	7
7	PF3D7_0608800	ornithine aminotransferase (OAT)	6
8	PF3D7_0922200	S-adenosylmethionine synthetase (SAMS)	6
9	PF3D7_1149000	antigen 332, DBL-like protein (Pf332)	6
10	PF3D7_1129100	parasitophorous vacuolar protein 1 (PV1)	5
11	PF3D7_0207600	serine repeat antigen 5 (SERA5)	5
12	PF3D7_1311800	M1-family alanyl aminopeptidase (M1AAP)	5
13	PF3D7_1444800	fructose-bisphosphate aldolase (FBPA)	5
14	PF3D7_1462800	glyceraldehyde-3-phosphate dehydrogenase (GAPDH)	5
15	PF3D7_1229400	macrophage migration inhibitory factor (MIF)	4
16	PF3D7_1229500	T-complex protein 1, gamma subunit, putative	4
17	PF3D7_0626800	pyruvate kinase (PyrK)	4
18	PF3D7_1120100	phosphoglycerate mutase, putative (PGM1)	4
19	PF3D7_0708400	heat shock protein 90 (HSP90)	4
20	PF3D7_1246200	actin I (ACT1)	4
21	PF3D7_1451100	elongation factor 2	4
22	PF3D7_0818200	14-3-3 protein (14-3-3I)	3
23	PF3D7_0922500	phosphoglycerate kinase (PGK)	3
24	PF3D7_1228600	merozoite surface protein 9 (MSP9)	3
25	PF3D7_1124600	ethanolamine kinase (EK)	2
26	PF3D7_1117700	GTP-binding nuclear protein RAN/TC4 (RAN)	2
27	PF3D7_0831700	heat shock protein 70 (HSP70-x)	2
28	PF3D7_1343000	phosphoethanolamine N-methyltransferase (PMT)	2
29	PF3D7_1015900	enolase (ENO)	2
30	PF3D7_0935900	ring-exported protein 1 (REX1)	2
31	PF3D7_1012400	hypoxanthine-guanine phosphoribosyltransferase (HGPRT)	2
32	PF3D7_0524000	karyopherin beta (KASbeta)	2
33	PF3D7_1008700	tubulin beta chain	2
34	PF3D7_1222300	endoplasmic, putative (GRP94)	2
35	PF3D7_1454400	aminopeptidase P (APP)	2
36	PF3D7_0902800	serine repeat antigen 9 (SERA9)	2
37	PF3D7_0511800	inositol-3-phosphate synthase (INO1)	2
38	PF3D7_1253000	gametocyte erythrocyte cytosolic protein (GECO)	2
39	PF3D7_1012600	GMP synthetase (GMPS)	2
40	PF3D7_1116700	cathepsin C, homolog, dipeptidyl aminopeptidase 1 (DPAP1)	2
41	PF3D7_1302100	gamete antigen 27/25 (Pfg27)	2
42	PF3D7_0520900	S-adenosyl-L-homocysteine hydrolase (SAHH)	2
43	PF3D7_1109900	60S ribosomal protein L36 (RPL36)	2
44	PF3D7_0320900	histone H2A variant, putative (H2A.Z)	2
45	PF3D7_1464600	phosphatase, putative	2
46	PF3D7_1424100	60S ribosomal protein L5, putative	2
47	PF3D7_0532100	early transcribed membrane protein 5 (ETRAMP5)	1
48	PF3D7_1033200	early transcribed membrane protein 10.2 (ETRAMP10.2)	1

49	PF3D7_0731100	EMP1-trafficking protein (PTP2)	1
50	PF3D7_1323400	60S ribosomal protein L23 (RPL23)	1
51	PF3D7_0730800.2	Plasmodium exported protein, unknown function	1
52	PF3D7_0730800.1	Plasmodium exported protein, unknown function	1
53	PF3D7_0815600	eukaryotic translation initiation factor, putative	1
54	PF3D7_1350500	conserved Plasmodium protein, unknown function	1
55	PF3D7_0306300	glutaredoxin 1 (GRX1)	1
56	PF3D7_1353200	membrane associated histidine-rich protein (MAHRP2)	1
57	PF3D7_0532300	Plasmodium exported protein (PHISTb), unknown function	1
58	PF3D7_1015800	ribonucleotide reductase small subunit, putative	1
59	PF3D7_1465900	40S ribosomal protein S3	1
60	PF3D7_1404900	conserved Plasmodium protein, unknown function	1
61	PF3D7_0813300	conserved Plasmodium protein, unknown function	1
62	PF3D7_1035400	merozoite surface protein 3 (MSP3)	1
63	PF3D7_0818900	heat shock protein 70 (HSP70)	1
64	PF3D7_1204300	eukaryotic translation initiation factor 5A (EIF5A)	1
65	PF3D7_1016400	serine/threonine protein kinase, FIKK family (FIKK10.1)	1
66	PF3D7_0406100	vacuolar ATP synthase subunit b	1
67	PF3D7_0810600	RNA helicase, putative	1
68	PF3D7_0320300	T-complex protein 1 epsilon subunit, putative	1
69	PF3D7_1029600	adenosine deaminase (ADA)	1
70	PF3D7_0516200	40S ribosomal protein S11	1
71	PF3D7_1349200	glutamate--tRNA ligase, putative	1
72	PF3D7_1024800	conserved Plasmodium protein, unknown function	1
73	PF3D7_1416900	prefoldin subunit 2, putative	1
74	PF3D7_0416800	small GTP-binding protein sar1 (SAR1)	1
75	PF3D7_1104000	phenylalanyl-tRNA synthetase beta chain, putative	1
76	PF3D7_1235700	ATP synthase subunit beta, mitochondrial	1
77	PF3D7_0802200	1-cys peroxiredoxin (1-CysPxn)	1
78	PF3D7_1034900	methionine--tRNA ligase, putative	1
79	PF3D7_1130200	60S ribosomal protein P0 (PfP0)	1
80	PF3D7_1446200	M17 leucyl aminopeptidase (LAP)	1
81	PF3D7_1004000	60S ribosomal protein L13, putative	1
82	PF3D7_0106100	vacuolar ATP synthase subunit c, putative	1
83	PF3D7_0306800	T-complex protein beta subunit, putative	1
84	PF3D7_1426200	arginine methyltransferase 1 (PRMT1)	1
85	PF3D7_1426100	basic transcription factor 3b, putative	1
86	PF3D7_1334200	chaperone binding protein, putative	1
87	PF3D7_0922400	para-aminobenzoic acid synthetase (pBAS)	1
88	PF3D7_0608700	chaperone, putative	1
89	PF3D7_0627500	protein DJ-1 (DJ1)	1
90	PF3D7_0827900	protein disulfide isomerase (PDI8)	1
91	PF3D7_0102900	aspartate--tRNA ligase	1
92	PF3D7_1445900	ATP-dependent RNA helicase DDX5, putative (DDX5)	1
93	PF3D7_1350100	lysine--tRNA ligase (KRS1)	1
94	PF3D7_1436300	translocon component PTEX150 (PTEX150)	1
95	PF3D7_0929400	high molecular weight rhoptry protein 2 (RhopH2)	1
96	PF3D7_1468700	eukaryotic initiation factor 4A (eIF4A)	1
97	PF3D7_1015200.3	cysteine--tRNA ligase, putative (CysRS)	1
98	PF3D7_1015200.2	cysteine--tRNA ligase, putative (CysRS)	1
99	PF3D7_1015200.1	cysteine--tRNA ligase, putative (CysRS)	1

100	PF3D7_1461300	40S ribosomal protein S28e, putative	1
101	PF3D7_0920800	inosine-5'-monophosphate dehydrogenase	1
102	PF3D7_1446500	conserved Plasmodium protein, unknown function	1
103	PF3D7_1421200	40S ribosomal protein S25 (RPS25)	1
104	PF3D7_1030500	26S proteasome regulatory subunit RPN9, putative (RPN9)	1
105	PF3D7_1132200	TCP-1/cpn60 chaperonin family, putative	1
106	PF3D7_0919000	nucleosome assembly protein (NAPS)	1
107	PF3D7_1311900	vacuolar ATP synthase subunit a (vapA)	1
108	PF3D7_1309100	60S ribosomal protein L24, putative	1
109	PF3D7_0112000	TatD-like deoxyribonuclease, putative	1
110	PF3D7_1302800	40S ribosomal protein S7, putative	1
111	PF3D7_1354500	adenylosuccinate synthetase (ADSS)	1
112	PF3D7_0113000	glutamic acid-rich protein (GARP)	1
113	PF3D7_1304500	small heat shock protein, putative	1
114	PF3D7_0614500	60S ribosomal protein L19 (RPL19)	1
115	PF3D7_0520000	40S ribosomal protein S9, putative	1
116	PF3D7_0719700	40S ribosomal protein S10, putative	1
117	PF3D7_0617800	histone H2A (H2A)	1
118	PF3D7_0721100	conserved Plasmodium protein, unknown function	1
119	PF3D7_1460700	60S ribosomal protein L27 (RPL27)	1
120	PF3D7_1323100	60S ribosomal protein L6, putative	1
121	PF3D7_1441200	60S ribosomal protein L1, putative	1
122	PF3D7_0915400	6-phosphofructokinase (PFK9)	1
123	PF3D7_1414400	serine/threonine protein phosphatase PP1 (PP1)	1
124	PF3D7_1134800	coatmer delta subunit, putative	1
125	PF3D7_1458400	aminodeoxychorismate lyase (ADCL)	1
126	PF3D7_1105400	40S ribosomal protein S4, putative	1
127	PF3D7_0710600	60S ribosomal protein L34 (RPL34)	1
128	PF3D7_1226900	conserved Plasmodium protein, unknown function	1
129	PF3D7_1105600	translocon component PTEX88 (PTEX88)	1
130	PF3D7_1306500	MORN repeat protein, putative	1
131	PF3D7_1033100	S-adenosylmethionine decarboxylase/ornithine decarboxylase (AdoMetDC/ODC)	1
132	PF3D7_0826700	receptor for activated c kinase (RACK)	1
133	PF3D7_0913600	conserved Plasmodium protein, unknown function	1
134	PF3D7_1035300	glutamate-rich protein (GLURP)	1
135	PF3D7_0316200	conserved Plasmodium protein, unknown function	1
136	PF3D7_0201800	knob associated heat shock protein 40 (KAHsp40)	1

**Table xxi: Mass spectrometry results for the 3D7 supernatant fraction**

#	Accession	Description	# UP
1	PF3D7_1016300	glycophorin binding protein (GBP)	10
2	PF3D7_1462800	glyceraldehyde-3-phosphate dehydrogenase (GAPDH)	9
3	PF3D7_1015900	enolase (ENO)	8
4	PF3D7_1357000	elongation factor 1-alpha	8
5	PF3D7_0922200	S-adenosylmethionine synthetase (SAMS)	8
6	PF3D7_1246200	actin I (ACT1)	7
7	PF3D7_1444800	fructose-bisphosphate aldolase (FBPA)	7
8	PF3D7_0608800	ornithine aminotransferase (OAT)	7
9	PF3D7_1120100	phosphoglycerate mutase, putative (PGM1)	6
10	PF3D7_1129100	parasitophorous vacuolar protein 1 (PV1)	6

11	PF3D7_0922500	phosphoglycerate kinase (PGK)	6
12	PF3D7_0929400	high molecular weight rhoptry protein 2 (RhopH2)	6
13	PF3D7_1311800	M1-family alanyl aminopeptidase (M1AAP)	6
14	PF3D7_0511800	inositol-3-phosphate synthase (INO1)	6
15	PF3D7_1451100	elongation factor 2	5
16	PF3D7_0818200	14-3-3 protein (14-3-3I)	5
17	PF3D7_0626800	pyruvate kinase (PyrK)	5
18	PF3D7_1229400	macrophage migration inhibitory factor (MIF)	4
19	PF3D7_0818900	heat shock protein 70 (HSP70)	4
20	PF3D7_0211800	asparagine--tRNA ligase (AsnRS)	4
21	PF3D7_1426200	arginine methyltransferase 1 (PRMT1)	4
22	PF3D7_1117700	GTP-binding nuclear protein RAN/TC4 (RAN)	3
23	PF3D7_1343000	phosphoethanolamine N-methyltransferase (PMT)	3
24	PF3D7_0708400	heat shock protein 90 (HSP90)	3
25	PF3D7_1029600	adenosine deaminase (ADA)	3
26	PF3D7_1022400	serine/arginine-rich splicing factor 4 (SRSF4)	3
27	PF3D7_0801000	Plasmodium exported protein (PHISTc), unknown function	2
28	PF3D7_0500800	mature parasite-infected erythrocyte surface antigen,erythrocyte membrane protein 2 (MESA)	2
29	PF3D7_1012400	hypoxanthine-guanine phosphoribosyltransferase (HGPRT)	2
30	PF3D7_1465900	40S ribosomal protein S3	2
31	PF3D7_1308200	carbamoyl phosphate synthetase (cpsSII)	2
32	PF3D7_0728000	eukaryotic translation initiation factor 2 alpha subunit, putative	2
33	PF3D7_0503400	actin-depolymerizing factor 1 (ADF1)	2
34	PF3D7_1124600	ethanolamine kinase (EK)	2
35	PF3D7_1349200	glutamate--tRNA ligase, putative	2
36	PF3D7_0920800	inosine-5'-monophosphate dehydrogenase	2
37	PF3D7_1008700	tubulin beta chain	2
38	PF3D7_0507100	60S ribosomal protein L4 (RPL4)	2
39	PF3D7_1428300	proliferation-associated protein 2g4, putative	2
40	PF3D7_1015200.3	cysteine--tRNA ligase, putative (CysRS)	2
41	PF3D7_1015200.2	cysteine--tRNA ligase, putative (CysRS)	2
42	PF3D7_1015200.1	cysteine--tRNA ligase, putative (CysRS)	2
43	PF3D7_0320300	T-complex protein 1 epsilon subunit, putative	2
44	PF3D7_0813900	40S ribosomal protein S16, putative	2
45	PF3D7_1235700	ATP synthase subunit beta, mitochondrial	2
46	PF3D7_0320900	histone H2A variant, putative (H2A.Z)	2
47	PF3D7_1416900	prefoldin subunit 2, putative	2
48	PF3D7_0306300	glutaredoxin 1 (GRX1)	2
49	PF3D7_1426100	basic transcription factor 3b, putative	2
50	PF3D7_1012600	GMP synthetase (GMPS)	2
51	PF3D7_1110200	pre-mRNA-processing factor 6, putative (PRPF6)	2
52	PF3D7_0207600	serine repeat antigen 5 (SERA5)	2
53	PF3D7_1350100	lysine--tRNA ligase (KRS1)	2
54	PF3D7_1109900	60S ribosomal protein L36 (RPL36)	2
55	PF3D7_1338300	elongation factor 1-gamma, putative	2
56	PF3D7_0826700	receptor for activated c kinase (RACK)	2
57	PF3D7_0520900	S-adenosyl-L-homocysteine hydrolase (SAHH)	2
58	PF3D7_1460700	60S ribosomal protein L27 (RPL27)	2
59	PF3D7_1035400	merozoite surface protein 3 (MSP3)	2
60	PF3D7_1323400	60S ribosomal protein L23 (RPL23)	1

61	PF3D7_1467600	conserved Plasmodium protein, unknown function	1
62	PF3D7_1010200	DNA2/NAM7 helicase, putative	1
63	PF3D7_0730900	EMP1-trafficking protein (PTP4)	1
64	PF3D7_0516200	40S ribosomal protein S11	1
65	PF3D7_1361900	proliferating cell nuclear antigen (PCNA)	1
66	PF3D7_0401800	Plasmodium exported protein (PHISTb), unknown function (PfD80)	1
67	PF3D7_1368100	26S proteasome regulatory subunit RPN11, putative (RPN11)	1
68	PF3D7_0312800	60S ribosomal protein L26, putative	1
69	PF3D7_0831700	heat shock protein 70 (HSP70-x)	1
70	PF3D7_1308300	40S ribosomal protein S27 (RPS27)	1
71	PF3D7_0802200	1-cys peroxiredoxin (1-CysPxn)	1
72	PF3D7_0706000	importin-7, putative	1
73	PF3D7_1317100	DNA replication licensing factor MCM4 (MCM4)	1
74	PF3D7_1033400	haloacid dehalogenase-like hydrolase (HAD1)	1
75	PF3D7_0617800	histone H2A (H2A)	1
76	PF3D7_1446200	M17 leucyl aminopeptidase (LAP)	1
77	PF3D7_1204300	eukaryotic translation initiation factor 5A (EIF5A)	1
78	PF3D7_1026800	40S ribosomal protein S2 (RPS2)	1
79	PF3D7_0813300	conserved Plasmodium protein, unknown function	1
80	PF3D7_1015800	ribonucleotide reductase small subunit, putative	1
81	PF3D7_1132200	TCP-1/cpn60 chaperonin family, putative	1
82	PF3D7_1206200	eukaryotic translation initiation factor 3 subunit 8, putative	1
83	PF3D7_0627500	protein DJ-1 (DJ1)	1
84	PF3D7_0608700	chaperone, putative	1
85	PF3D7_0619400	cell division cycle protein 48 homologue, putative	1
86	PF3D7_1454400	aminopeptidase P (APP)	1
87	PF3D7_0307200	60S ribosomal protein L7, putative	1
88	PF3D7_0525100	acyl-CoA synthetase (ACS10)	1
89	PF3D7_0926700	glutamine-dependent NAD(+) synthetase, putative (NADSYN)	1
90	PF3D7_0406100	vacuolar ATP synthase subunit b	1
91	PF3D7_1125900	conserved Plasmodium protein, unknown function	1
92	PF3D7_0308500	activator of Hsp90 ATPase, putative	1
93	PF3D7_0302500	cytoadherence linked asexual protein 3.1 (CLAG3.1)	1
94	PF3D7_1421200	40S ribosomal protein S25 (RPS25)	1
95	PF3D7_0622800	leucine--tRNA ligase, putative	1
96	PF3D7_0105800	conserved Plasmodium protein, unknown function	1
97	PF3D7_1105000	histone H4 (H4)	1
98	PF3D7_1468700	eukaryotic initiation factor 4A (eIF4A)	1
99	PF3D7_0321100	conserved Plasmodium protein, unknown function	1
100	PF3D7_0520000	40S ribosomal protein S9, putative	1
101	PF3D7_1229500	T-complex protein 1, gamma subunit, putative	1
102	PF3D7_0621200	pyridoxine biosynthesis protein PDX1 (PDX1)	1
103	PF3D7_1116700	cathepsin C, homolog,dipeptidyl aminopeptidase 1 (DPAP1)	1
104	PF3D7_0919000	nucleosome assembly protein (NAPS)	1
105	PF3D7_0719700	40S ribosomal protein S10, putative	1
106	PF3D7_0614500	60S ribosomal protein L19 (RPL19)	1
107	PF3D7_0106100	vacuolar ATP synthase subunit c, putative	1
108	PF3D7_1447000	40S ribosomal protein S5	1
109	PF3D7_1144000	40S ribosomal protein S21 (RPS21)	1
110	PF3D7_1126200	40S ribosomal protein S18, putative	1
111	PF3D7_1027800	60S ribosomal protein L3 (RPL3)	1

112	PF3D7_0112000	TatD-like deoxyribonuclease, putative	1
113	PF3D7_0413600	26S proteasome AAA-ATPase subunit RPT3, putative	1
114	PF3D7_1458400	aminodeoxychorismate lyase (ADCL)	1
115	PF3D7_1331800	60S ribosomal protein L23, putative	1
116	PF3D7_1332900	isoleucine--tRNA ligase, putative	1
117	PF3D7_1105400	40S ribosomal protein S4, putative	1
118	PF3D7_0212300	peptide chain release factor subunit 1, putative	1
119	PF3D7_0915400	6-phosphofructokinase (PFK9)	1
120	PF3D7_1441200	60S ribosomal protein L1, putative	1
121	PF3D7_1130400	26S protease regulatory subunit 6a, putative (RPT5)	1
122	PF3D7_0708800	heat shock protein 110 (HSP110c)	1
123	PF3D7_0710600	60S ribosomal protein L34 (RPL34)	1
124	PF3D7_1202600	conserved protein, unknown function	1
125	PF3D7_1224300	polyadenylate-binding protein, putative (PABP)	1
126	PF3D7_1029400	conserved Plasmodium protein, unknown function	1
127	PF3D7_0115700	erythrocyte membrane protein 1, PfEMP1 (VAR)	1
128	PF3D7_1016400	serine/threonine protein kinase, FIKK family (FIKK10.1)	1
129	PF3D7_0814000	60S ribosomal protein L13-2, putative	1
130	PF3D7_1244100	N-alpha-acetyltransferase 15, NatA auxiliary subunit, putative	1
131	PF3D7_0516700	ubiquitin carboxyl-terminal hydrolase 2, putative	1
132	PF3D7_1215400	conserved Plasmodium protein, unknown function	1
133	PF3D7_0719600	60S ribosomal protein L11a, putative	1
134	PF3D7_1453800	glucose-6-phosphate dehydrogenase-6-phosphogluconolactonase (G6PDH)	1
135	PF3D7_1020300	cytoplasmic dynein intermediate chain, putative	1
136	PF3D7_0702200	lysophospholipase, putative	1
137	PF3D7_1139600	conserved Plasmodium protein, unknown function	1
138	PF3D7_0709300	Cg2 protein (CG2)	1
139	PF3D7_1314500	cop-coated vesicle membrane protein p24 precursor, putative	1

**Table xxii: Mass spectrometry hit list for the supernatant fraction**SP-GFP-BirA\* - 3D7, threshold  $\geq 1$  unique peptide (UP)

#	Accession	Description	# UP
1	PF3D7_0730900	EMP1-trafficking protein (PTP4)	8
2	PF3D7_1201000	Plasmodium exported protein (PHISTb), unknown function	7
3	PF3D7_1149000	antigen 332, DBL-like protein (Pf332)	6
4	PF3D7_1229500	T-complex protein 1, gamma subunit, putative	4
5	PF3D7_1228600	merozoite surface protein 9 (MSP9)	3
6	PF3D7_0831700	heat shock protein 70 (HSP70-x)	2
7	PF3D7_1222300	endoplasmic reticulum chaperone, putative (GRP94)	2
8	PF3D7_1253000	gametocyte erythrocyte cytosolic protein (GECO)	2
9	PF3D7_1116700	cathepsin C, homolog, dipeptidyl aminopeptidase 1 (DPAP1)	2
10	PF3D7_1424100	60S ribosomal protein L5, putative	2
11	PF3D7_0935900	ring-exported protein 1 (REX1)	2
12	PF3D7_0524000	karyopherin beta (KASbeta)	2
13	PF3D7_1454400	aminopeptidase P (APP)	2
14	PF3D7_0902800	serine repeat antigen 9 (SERA9)	2
15	PF3D7_1302100	gamete antigen 27/25 (Pfg27)	2
16	PF3D7_1464600	phosphatase, putative	2

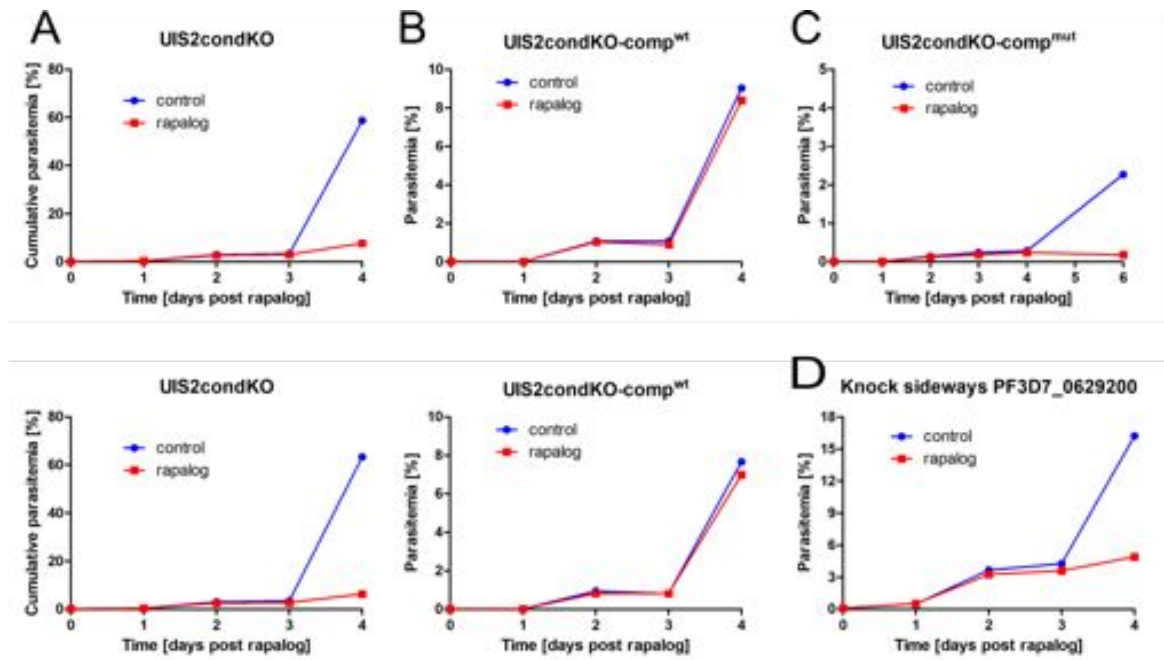
## Extended data for SLI-TGD, integration checks and FACS assay

Table xxiii: Attempts for SLI-TGD

Accession #	PlasmoDB	SLI-TGD	Attempts for integration*
PF3D7_0220000	liver stage antigen 3	important for growth	6 (incorrect integration in 1 of 6)
PF3D7_0629200	DnaJ protein, putative	important for growth	6
PF3D7_0731600	acyl-CoA synthetase	not essential	correct integration
PF3D7_0912400	alkaline phosphatase, putative	not essential	correct integration
PF3D7_1013300	conserved Plasmodium protein, unknown function	important for growth	6 (incorrect integration in 2 of 6)
PF3D7_1024800	conserved Plasmodium protein, unknown function (EXP3)	not essential	correct integration
PF3D7_1123500	conserved Plasmodium protein, unknown function (GP2)	not essential	correct integration
PF3D7_1135400	conserved Plasmodium protein, unknown function	not essential/important for growth	correct integration/ 6 (incorrect integration in 2 of 6)
PF3D7_1226900	conserved Plasmodium protein, unknown function (PV2)	important for growth	9
PF3D7_1310500	conserved protein, unknown function	important for growth	6
PF3D7_1350500	conserved Plasmodium protein, unknown function	important for growth	6 (incorrect integration in 1 of 6)
PF3D7_1462300	conserved Plasmodium protein, unknown function	important for growth	6
PF3D7_1464600	serine/threonine protein phosphatase UIS2, putative	important for growth	6 (incorrect integration in 1 of 6)

**Table xxiv: Expected sizes for integration check PCR**

<b>Accession #</b>	<b>Integration</b>	<b>ori [bp]</b>	<b>5' [bp]</b>	<b>3' [bp]</b>
PF3D7_0220000	SLI	852	1697	804
PF3D7_0629200	SLI	1000	1698	1048
PF3D7_0731600	SLI	1039	1838	864
	SLI-TGD	1390	1014	1062
PF3D7_0912400	SLI	762	1502	842
	SLI-TGD	1593	993	1241
PF3D7_1013300	SLI	884	1681	914
PF3D7_1024800	SLI	1336	2130	1392
	SLI-TGD	2007	1157	1104
PF3D7_1123500	SLI	1559	2276	1403
	SLI-TGD	1163	657	760
PF3D7_1135400	SLI	844	1601	894
	SLI-TGD	1444	1025	952
PF3D7_1226900	SLI	855	1661	906
PF3D7_1310500	SLI	694	1524	773
PF3D7_1350500	SLI	426	1113	1318
PF3D7_1462300	SLI	1260	1974	1290
PF3D7_1464600	SLI	889	1659	964
	SLI-TGD loxP	1707	840	1439



**Figure xxx: Flow cytometry growth curves**

Extended data files for the flow cytometry growth assay for A) UIS2condKO (n=2,3), B) UIS2cond KO-comp<sup>wt</sup> (n=2,3), C) UIS2cond KO-comp<sup>mut</sup> (n=2) and D) knock sideways with the ER mislocalizer for PF3D7\_0629200 (n=2).

## **Safety and sanitation**

Experiments that included genetically modified organisms were conducted in laboratories assigned as safety level 2. Chemicals were handled according to their safety data sheets provided by the Bernhard-Nocht-Institute for tropical medicine.

Materials that were exposed to genetically modified organisms were autoclaved before sanitation. Professionals of the Bernhard-Nocht-Institute for tropical medicine safeguarded appropriate sanitation of chemicals.

## Publications

### **Identification of novel parasitophorous vacuole proteins in *P. falciparum* parasites using BioID**

Melissa Khosh-Naucke<sup>1</sup>, Johanna Becker<sup>1</sup>, Paolo Mesén-Ramírez<sup>1</sup>, Parnian Kiani<sup>2</sup>, Jakob Birnbaum<sup>1</sup>, Ulrike Fröhlke<sup>1</sup>, Ernst Jonscher<sup>1</sup>, Hartmut Schlüter<sup>2</sup> and Tobias Spielmann<sup>1</sup>

(Published on the 27<sup>th</sup> of July 2017 in the International journal of medical microbiology (IJMM), doi: 10.1016/j.ijmm.2017.07.007)

1) Bernhard Nocht Institute for Tropical Medicine, Parasitology Section, Bernhard-Nocht-Straße 74, 20359 Hamburg, Germany.

2) Core Facility Mass Spectrometric Proteomics, Institute of Clinical Chemistry, University Medical Center Hamburg-Eppendorf, 20246 Hamburg, Germany.

## Acknowledgements

Mein größter Dank geht an Dr. Tobias Spielmann für die gute Projektidee und deren Beantragung, die wertvolle Betreuung und das verständnisvolle Miteinander. Danke!

Ich danke Prof. Dr. Hartmut Schlüter und Dr. Parnian Kiani für die Möglichkeit und die Hilfe die massenspektrometrischen Analysen am UKE durchzuführen.

Für die Co-Betreuung am BNITM möchte ich Prof. Dr. Iris Bruchhaus und PD Dr. Thomas Jacobs herzlich danken.

Ich danke Dr. Tobias Spielmann und Prof. Dr. Tim Gilberger für die Übernahme des Dissertationsgutachtens. Auch möchte ich mich an dieser Stelle bei Prof. Dr. Julia Kehr, Prof. Dr. Jörg Ganzhorn und Prof. Dr. Iris Bruchhaus für die Aufstellung als Prüfungskommission bedanken.

Johanna Becker hat im Rahmen des Projektes ihre Masterarbeit durchgeführt. Ich danke ihr vor allem für die Unterstützung in der Zellkultur, welche ich aufgrund meiner Schwangerschaft nicht ausüben durfte.

Weiterhin möchte ich dem Schwerpunktprogramm 1580 für die Bereitstellung von Chancengleichheitsmitteln danken, die mir die Anstellung von Tuyen Tran als studentische Hilfswissenschaftlerin ermöglichte. Tuyen, vielen Dank für deine Unterstützung.

Mein Dank gilt auch der gesamten Spielmann Arbeitsgruppe sowie der AG Gilberger für die angenehme Arbeitsatmosphäre, die schönen gemeinsamen Stunden und die Unterstützung.

Im besonderen möchte ich Louisa Wilcke, Sarah Scharf und Mateo Naucke für das Korrekturlesen von Teilen meiner Doktorarbeit danken.

Mein großer Dank gilt auch meiner Großfamilie, die mich tatkräftig während der Doktorarbeit unterstützt hat. Ohne den guten Familienzusammenhalt hätte ich dieses Familienprojekt „Doktorarbeit“ schwer abschließen können. Abschließend möchte ich meinem Mann Mateo Naucke und meiner Tochter Mara Naucke meinen Dank und meine Anerkennung ausdrücken: Wir sind ein wundervolles Team und ich bin dankbar, dass ihr mich in dieser Zeit begleitet und unterstützt habt. Ich bin gespannt auf die Zukunft.